

**Mechanisms Underlying Direct Cardiac Sarcomere Modulators
That Target Troponin**

by
Fangze Cai

A thesis submitted in partial fulfillment of the requirements for the degree of

Doctor of Philosophy

Department of Biochemistry
University of Alberta

© Fangze Cai, 2020

Abstract

Heart muscle contraction is regulated by calcium binding to cardiac troponin C. This induces troponin I (cTnI) switch region binding to the regulatory domain of troponin C (cNTnC). Compounds that directly modulate the interface of cNTnC and cTnI switch region have potential for treating heart diseases.

In chapter 2, we identified that some small molecules bind tightly to cNTnC-cTnI chimera (cChimera) with $K_D \sim 10 \mu\text{M}$. NMR structure of cChimera faithfully represents the native interface between cNTnC and cTnI, making cChimera a great tool for structure, dynamics, and drug binding studies. NMR structure of cChimera-3-mDPA reveals that the small molecule binds deeply in the hydrophobic pocket of cNTnC and minimal structural perturbation is observed.

In chapter 3, we determined the structure of sarcomere inhibitor W7 bound to cChimera. The structure shows that W7 does not perturb the overall structure of the cNTnC-cTnI interface. The naphthalene ring of W7 sits in the hydrophobic pocket of cNTnC, while the positively charged amine tail extends into the solvent. We characterized the role of electrostatics and the precise location of the charged amino group in the mechanism of sarcomere inhibitor W7 in chapters 4 and 5. A7, where the amino group of W7 was replaced with a carboxyl group, decreased the binding affinity of cTnI to cNTnC significantly less than W7 and has a much weaker negative inotropic effect than W7 on ventricular trabeculae. The short negatively charged A6 and positively charged W6 do not change the calcium sensitivity of ventricular trabeculae. The structures show that naphthalene rings of W7, W6 and A7 sit in the same hydrophobic pocket, but the tails of W7 and W6 go to the same rout while the tail of

A7 takes a different route to the surface of the complex. These results indicate that both electrostatic repulsion and the precise location of the charged amino group are important in the negative inotropic effect of W7.

In chapter 6, we reported a strong cardiac sarcomere inhibitor, DN-F01, targeting the cTnC-cTnI interface. ATPase activity studies show that DN-F01 has a strong inhibiting effect on cardiomyofibrils. The NMR titrations reveal that the binding position of DN-F01 bound covalently or non-covalently to the cTnC-cTnI chimera might be different.

In chapter 7, we found that the cardiac-specific N-terminal extension of cTnI (residues 1–37) remains largely disordered while it interacts electrostatically with cTnC. This interaction does not directly affect the calcium binding affinity of cTnC, but indirectly increases calcium affinity by positioning cTnC to bind the cTnI switch peptide.

Preface

The literature review in chapter 1 and the final conclusions in chapter 8 are my original work. Most of the remaining chapters have been published previously, with exceptions of chapters 4 and 5 which are still in preparation. In the following paragraphs I detail the author's contributions to each chapter.

Chapter 2 has been published as Cai, F., Li, M.X., Pineda-Sanabria, S.E., Gelozia, S., Lindert, S., West, F., Sykes, B.D. & Hwang, P.M. Structures reveal details of small molecule binding to cardiac troponin. *J. Mol. Cell. Cardiol.* 101, 134–144 (2016). FC and MXL performed drug titrations for screening. FC and PMH acquired the NMR spectra for structure determination. FC purified the protein, assigned the protein chemical shift, analyzed the data and solved the structures with help of SEPS and PMH. SG and FW synthesized all SHG-compounds. SL performed virtual screening. FC wrote the manuscript with help of PMH and BDS. PMH led the research.

Chapter 3 has been published as Cai, F., Hwang, P. M. & Sykes, B. D. Structural Changes Induced by the Binding of the Calcium Desensitizer W7 to Cardiac Troponin. *Biochemistry* 57, 6461–6469 (2018). FC purified the protein, performed all experiments, analyzed the data and solved the structure. FC wrote the manuscript with help of BDS and PMH. BDS directed the research.

Chapter 4 has been published as Cai, F., Robertson, I. M., Kampourakis, T., Klein, B. A. & Sykes, B. D. The Role of Electrostatics in the Mechanism of Cardiac Thin Filament Based Sensitizers. *ACS Chem. Biol.* 15, 2289–2298 (2020). IMR designed and synthesized the A-series compounds. FC acquired the NMR spectra for structure determination, dynamics study, analyzed the data and solved the structure. FC and IMR performed drug and peptide titrations, wrote the manuscript. TK prepared the ventricular trabeculae and performed force-calcium titrations. All authors helped review and edit the manuscript. BDS guided the research.

Chapter 5 is in preparation. Cai, F., Kampourakis, T., Klein, B. A., Cockburn, K. T. & Sykes, B. D. The Mechanism of Cardiac Thin Filament Inhibition: the Precision of W7. FC and BAK performed drug titration. TK prepared the ventricular trabeculae and performed force-calcium titrations. KTC and BAK synthesized

compound A4. FC acquired the NMR spectra for structure determination and wrote the manuscript. BDS guided the research.

Chapter 6 is in preparation. Cai, F., Kampourakis, T. Klein, B. A., & Sykes, B. D. A Fluorescent Reversible-covalent Cardiac Muscle Inhibitor. TK prepared the cardiac myofibril and performed the ATPase measurement. BAK performed the fluorescence experiments. FC performed the NMR titration, analyzed the data and wrote the manuscript. All authors helped review and edit the manuscript. BDS directed the research.

Chapter 7 has been published as Hwang, P. M., Cai, F., Pineda-Sanabria, S. E., Corson, D. C. & Sykes, B. D. The cardiac-specific N-terminal region of troponin I positions the regulatory domain of troponin C. *Proc. Natl. Acad. Sci. U. S. A.* 111, 14412–7 (2014). FC performed the fluorescence experiments with help of SEPS. PMH acquired the NMR experiments, analyzed the results and wrote the manuscript. DCC purified the protein. PMH and BDS directed the research.

“It is the time you spent on your rose
that makes your rose so important.”

-Antoine de Saint-Exupéry,
The Little Prince

Acknowledgements

This page is dedicated to those who, with their compassion, encouragement, support, and kindness helped me traverse through this unforgettable journey.

Firstly, I would like to express my sincerest gratitude to my supervisor Dr. Brian Sykes for his continued mentorship and for being an amazing source of inspiration. His extraordinary ability to lead by providing the perfect amount of guidance while still challenging you to find solutions to your problems in your own way have made the past six years of graduate studies a very rewarding learning experience. To me, he is not only a mentor, but also a great friend. We have shared so many wonderful memories throughout this time, including attending several international conferences, winning the Sykes lab golf tournament and enjoying Christmas dinners at his home. I would also like to thank my co-supervisor Dr. Peter Hwang for all of his guidance and his incredible patience throughout my time at the lab. His endless enthusiasm for science and pursuit of new discoveries have significantly motivated me.

Next, I want to thank the current and past members of Sykes and Hwang's labs who have helped and supported me. Thanks to Dr. Sandra Pineda-Sanabria for showing me the ropes when I first came to the lab as an undergrad by teaching me how to prepare samples and perform titrations, for inviting me to soccer and hockey games and for showing me what real Mexican food tastes like. Thanks to Dr. Monica Li for all of the support she has provided and for being someone that I can always rely on. Thanks to Phillip Liu for helping me grow and purify proteins. Thanks to Dr. Zelin Fu for being a good friend that I could always talk to when the work gets tough. Thanks to Brittney Klein for all of her valuable input towards my research and her cheerful smile. I would like to thank Dr. Peter Holmes, Kieran Cockburn, Dr. Somaya Zahran, Gaddaffi Ibrahim Dammaliki, Zabed Mahmud for their on-going support. I would also like to thank summer students Esther Joo-Young Lee and Elizabeth Chao for all of their assistance.

Thanks to Dr. Ian Roberson for always being available to answer my questions either in person or via e-mail even with his busy schedule. Thanks to Dr. Thomas

Kampourakis, our collaborator from King's College London for providing the crucial physiological studies. Thank to Dr. Howard Young for being part of my supervisory committee who have always brought insightful suggestions to every meeting. Thanks to Dr. Leo Spyrapoulos for always being willing to help when needed. Thanks to Dean Schieve for always helping me solve software problems.

Thanks to my dear friend Lisha Cao who has always being so caring, kind and supportive. We have shared many joyous and wonderful memories together that I will always cherish. Thanks to my dear friend Gia Xu who no longer lives in Edmonton, but continues to support me from afar and for always cheering me up.

My deep and sincerest gratitude to my parents for their continuous and unconditional love and support. I am very grateful for the strength and opportunities they have provided me and for instilling in me the attitude that I could accomplish anything if I was determined enough to do so and have encouraged me every step of the way. Thanks to my dear husband Henry Di for being so loving, caring, understanding and encouraging. I am truly grateful to him for all of his tireless support and all the little things he did to make my life easier. Lastly, I would like to thank my son Raymond Di for being such a loving and understanding child with such a beautiful and warm smile that always brightens my day.

Finally, I am thankful to University of Alberta Faculty of Medicine and Dentistry for supporting my graduate research through the Motyl Graduate Studentship in Cardiac Sciences, the 75th Anniversary Graduate Studentship Award, and the Queen Elisabeth II Graduate Studentship.

Table of Contents

Chapter 1 Introduction	1
Cardiac physiology	1
Cardiac cycle	1
Electrical conduction system	3
Cardiomyocyte structure and function	5
Cardiomyocyte	5
The thick filament	7
The thin filament	8
The cross-bridge cycle	10
Troponin structure and function	10
Troponin C	11
Troponin I	13
Troponin T	15
“Drag and release” mechanism	16
Inotropic therapy for heart failure	18
Heart failure	18
Pharmaceutical compounds for heart failure	18
Direct sarcomere modulators targeting troponin C	22
Bepridil	23
Levosimendan	24
W7	26
NMR spectroscopy in drug discovery	27
Small molecule binding	28
Structure determination	30
cNTnC-cTnI chimera as drug target	31
References	33
Chapter 2 Structures Reveal Details of Small Molecule Binding to Cardiac Troponin	43
Summary	43
Introduction	44
Material and methods	46

cChimera design, expression, and purification	46
Chemicals	48
NMR spectroscopy	48
Drug titrations	48
NMR experiments for structure calculation	49
Structure calculation	50
Virtual screening of DPA-like Compounds	51
Results and discussion	52
Structure of cChimera	52
Selection of diphenylamine as starting compound	54
Interaction of cChimera with 3-mDPA	55
Solution structure of the cChimera-3-mDPA complex	58
Small molecule binding	63
Conclusion	68
Acknowledgments	69
References	70

Chapter 3 Structural Changes Induced by the Binding of the Calcium

Desensitizer W7 to Cardiac Troponin 74

Summary	74
Introduction	75
Material and methods	78
Materials and sample preparation	78
NMR spectroscopy	79
Drug titrations and lineshape analysis	79
Structure calculations	80
Results and discussion	81
Binding of W7 to cChimera	81
Secondary structure assessment of cChimera-W7 complex:	83
Solution structure of the cChimera-W7 complex	84
Structure of cChimera in cChimera-W7 complex	86
cChimera dynamics	90
Conclusions	92
Acknowledgments	92
References	93

Chapter 4 The Role of Electrostatics in the Mechanism of Cardiac Thin

Filament Based Sensitizers	97
Summary	97
Introduction	98
Material and methods	101
Protein expression, and purification	101
Chemicals	101
NMR spectroscopy	103
Drug titrations and lineshape analysis	103
Structure calculations	104
Preparation of ventricular trabeculae and force-calcium titrations	105
Results and Discussion	106
Design and synthesis of A-series compounds	106
Binding of W7 and A7 to cNTnC-cTnI switch cChimera	108
cChimera dynamics	110
Structural insight of cChimera-A7 complex	112
Binding of W7 and A7 to cNTnC-cTnI switch gChimera	114
Interaction of cNTnC, cTnI and A7	116
Titrations with A8 and A6	116
Effects of compounds on calcium sensitivity of force of ventricular trabeculae	117
Conclusions	119
Acknowledgements	121
References	122
Chapter 5 The Mechanism of Cardiac Thin Filament Inhibition: the Precision of	
W7	125
Summary	125
Introduction	126
Material and methods	128
Protein expression, and purification	128
Chemicals	129
NMR spectroscopy	129
Small molecule titrations	130
Structure calculations	130
Preparation of ventricular trabeculae and force-calcium titrations	131

Results and Discussion	132
W-series and A-series compounds	132
Binding of W-series compounds to cNTnC-cTnI chimera	133
Binding of A-series compounds to cNTnC-cTnI cChimera	135
Effects of compounds on ventricular trabeculae	136
Structural insight of cChimera-W6 complex	138
Conclusions	141
Acknowledgements	141
References	142
Chapter 6 A Fluorescent Reversible-Covalent Cardiac Muscle Inhibitor	145
Summary	145
Introduction	146
Material and methods	147
Material	147
Fluorescence spectroscopy	147
NMR spectroscopy	148
ATPase activity measurements	149
Results and discussion	150
DN-F01 chemical structure	150
Effect of DN-F01 on ATPase activity	151
The use of cNTnC-cTnI chimera	152
Fluorescence study of DN-F01	153
NMR study of DN-F01 to cNTnC-cTnI chimera	154
Stability of DN-F01	159
Conclusions	162
Acknowledgements	162
References	163
Chapter 7 The cardiac-specific N-terminal region of cardiac troponin I electrostatically positions the regulatory domain of troponin C despite remaining in an intrinsically disordered state	165
Summary	165
Introduction	166
Materials and Methods	167
Protein production and purification	167

NMR spectroscopy sample preparation	168
NMR spectroscopy and data analysis	169
Fluorescence spectroscopy	170
Results	170
Chemical shift assignment and secondary structure of cTnI[1–73] free and in complex with cTnC.	170
¹ H- ¹ H NOE analysis of the cTnC–cTnI[1–73] complex	173
¹⁵ N relaxation of cTnI[1–73] free and in complex with cTnC	178
Calcium titration of cTnI[1–73]–cTnC.	181
Discussion	182
Acknowledgements	184
References	185
Chapter 8 Conclusions	190
References	196
Bibliography	198

List of Tables

Table 2.1. Structure statistics of cChimera-3-mDPA structures.	59
Table 2.2. Dissociation constant (K_D) of DPA-like compounds for cChimera.	65
Table 3.1. Structural statistics of cChimera-W7 structures.	85
Table 4.1. Structural statistics of the chimera-A7 complex.	114
Table 4.2. Binding of W7, A7 and A6 to troponin.	117
Table 4.3. Effect of W7, A7 or A6 on trabeculae.	119
Table 5.1. Binding of W7-derivatives to cChimera.	136

List of Figures

Figure 1.1. The heart and circulation system.	2
Figure 1.2. The cardiac cycle.	4
Figure 1.3. Cardiac muscle.	6
Figure 1.4. Structure of the cardiac sarcomere.	7
Figure 1.5. Actin-myosin cross-bridge cycle.	9
Figure 1.6. Closed-to-open differences between cTnC and sTnC.	11
Figure 1.7. X-ray structure of cardiac troponin core complex.	12
Figure 1.8. Interaction between troponin and other thin filament components.	15
Figure 1.9. Structural changes of the troponin complex upon calcium binding.	17
Figure 1.10. Mechanism of calcium mobilizer increasing intracellular calcium.	19
Figure 1.11. Chemical structures of direct sarcomere modulators.	22
Figure 1.12. Effect of bepridil and cTnI switch peptide on cTnC.	24
Figure 1.13. Overview of applications of NMR in drug discovery.	29
Figure 2.1. Sequence of cTnC-cTnI switch region cChimera.	47
Figure 2.2. Structure of cChimera.	53
Figure 2.3. Chemical structure of Bepridil and derivatives.	55
Figure 2.4. 3-mDPA binding to cChimera monitored by $^1\text{H}, ^{15}\text{N}$ -HSQC.	56
Figure 2.5. cChimera CSP induced by 3-mDPA binding.	57
Figure 2.6. 3-mDPA binding to cChimera monitored by $^1\text{H}, ^{13}\text{C}$ -HSQC.	58
Figure 2.7. Binding site of unsubstituted aryl ring of 3-mDPA.	60
Figure 2.8. Binding sites of methyl-substituted ring of 3-mDPA.	61
Figure 2.9. Structures of 3-mDPA bound to cChimera.	63
Figure 3.1. W7 binding to cChimera monitored by $^1\text{H}, ^{15}\text{N}$ -HSQC.	82
Figure 3.2. W7 binding to cChimera monitored by $^1\text{H}, ^{13}\text{C}$ -HSQC.	82
Figure 3.3 Secondary structure of cChimera-W7.	83
Figure 3.4. Structures of W7 bound to cChimera.	85
Figure 3.5. Structure comparison of cChimera-W7.	87
Figure 3.6. W7 binding pocket.	89
Figure 3.7. cChimera dynamics upon W7 binding.	91

Figure 4.1. The reaction scheme used in the synthesis of A series compounds.	102
Figure 4.2. Chemical structures of dfbp-o, W7, A7, A6 and A8.	107
Figure 4.3. W7 and A7 binding to cChimera monitored by $^1\text{H},^{15}\text{N}$ -HSQC.	109
Figure 4.4. W7 and A7 binding to cChimera monitored by ^1H NMR.	109
Figure 4.5. W7 and A7 binding to cChimera and gChimera.	110
Figure 4.6. Fitting of the A7 titration of cChimera to extract kinetic information.	111
Figure 4.7. the cChimera-A7 complex solution structures.	113
Figure 4.8. Interaction of cNTnC, cTnI and A7.	115
Figure 4.9. Effect of W7, A7 or A6 on trabeculae.	118
Figure 4.10. Overlay of the structures of A7, W7, bepridil, dfbp-o and 3-mDPA.	121
Figure 5.1. Chemical structures of W7, W6, W4, A7, A6 and A4.	133
Figure 5.2. Small molecule titrations into the cNTnC-cTnI chimera.	134
Figure 5.3. Effect of A4, W6 and W4 on ventricular trabeculae force.	137
Figure 5.4. Intramolecular NOEs between cChimera and W7 or W6.	139
Figure 5.5 The solution structure of the cChimea-W6 complex.	140
Figure 6.1. Structures of Levosimendan, 3-mDPA, 3-CIDPA, and DN-F01.	150
Figure 6.2. Malachite green assay is not affected by DN-F01 fluorescence.	151
Figure 6.3. Effect of DN-F01 on ATPase Activity.	152
Figure 6.4. DN-F01 fluorescence scan and titration.	153
Figure 6.5. DN-F01 solubility test.	155
Figure 6.6. DN-F01 titration to C35S and A-cys chimera.	156
Figure 6.7. Mass spectra of C35S chimera and DN-F01.	157
Figure 6.8. DN-F01 titration to C35S, A-cys and C35S C84-BME chimera.	158
Figure 6.9. Stability of DN-F01 in the absence and presence of DTT.	160
Figure 6.10. Mass spectra of C35S chimera and degraded DN-F01.	161
Figure 7.1. Chemical shift analysis of cTnI[1-73].	171
Figure 7.2. Predicted secondary structure for cTnI[1-73].	173
Figure 7.3. Structural changes in C35S,C84S-cTnC induced by binding of cTnI.	175
Figure 7.4. Localization of NOEs between cTnC and cTnI[1-73].	176
Figure 7.5. Intermolecular ^1H - ^1H NOEs from cTnC to cTnI[1-73].	177
Figure 7.6. ^{15}N backbone relaxation data for cTnI[1-73].	180

Figure 7.7. Calcium binding to C35S-cTnC bound to cTnI[1-73] or cTnI[34-71].	181
Figure 8.1. ^{13}C labelled compounds for future studies.	194
Figure 8.2. Dfbp-o amine series compounds.	194

Chapter 1

Introduction

Cardiac physiology

The heart is one of the most hardworking organs. The human heart beats approximately 100,000 times a day and ejects over 10,000 liters of blood daily. With each heartbeat, blood is pumped throughout the body, supplying the entire body with oxygen and nutrients. The heart has four chambers: two upper chambers called atria, and two lower chambers called ventricles. The right atrium and the right ventricle make up the right heart, which is responsible for the pulmonary circulation. The left atrium and left ventricle make up the left heart, which is responsible for the systemic circulation. The right heart receives oxygen-deficient, carbon dioxide-rich blood from the body via the superior and inferior vena cava. The blood is then pumped through the pulmonary arteries to the lungs, where the blood exchanges carbon dioxide for oxygen in the lung and then travels to the left heart via the pulmonary veins. The left heart pumps the blood to the rest of the body to deliver oxygen and collect waste, which returns to the right atrium, and the cycle repeats^{1,2} (Figure 1.1).

Cardiac cycle

It is essential that all components of the heart are carefully coordinated to ensure the body is supplied with a sufficient amount of blood. The cardiac cycle is used to describe a sequence of events that occur and repeat with every heartbeat. It includes two major phases: diastole and systole. Diastole occurs when the heart muscle relaxes and fills with blood, while systole occurs when the heart muscle contracts and pumps blood. The key principle of the cardiac cycle is that blood flows from a higher pressure area to a lower pressure area. The cycle begins with the atria and ventricles in relaxed state, and blood flows freely into the atria, increasing the atrial pressure. The atrioventricular (AV, tricuspid for the right heart and mitral for the left heart) valves open when atrial pressures are higher than ventricular pressures, allowing blood to partially fill the ventricles. Atrial contractions push the blood from the atria into the ventricles, completing the ventricle filling. Next, the ventricles contract and the atria

relax, which causes the AV valves to close, preventing blood from flowing back to the atria. The closing of the AV valves produces the first heart sound (S_1). The ventricles continue to contract, rapidly building up the ventricular pressure. This isovolumetric contraction causes the ventricular pressure to exceed the blood pressure and opens the semilunar (pulmonary for the right heart and aortic for the left heart) valves, allowing blood to enter the aorta and pulmonary arteries. After the contraction, the ventricles relax and the intraventricular pressure drops, causing blood reverse flow. This also forces the semilunar valves to close and prevents the blood from re-entering the ventricles. The semilunar valves shut producing the second heart sound (S_2)^{1,2}.

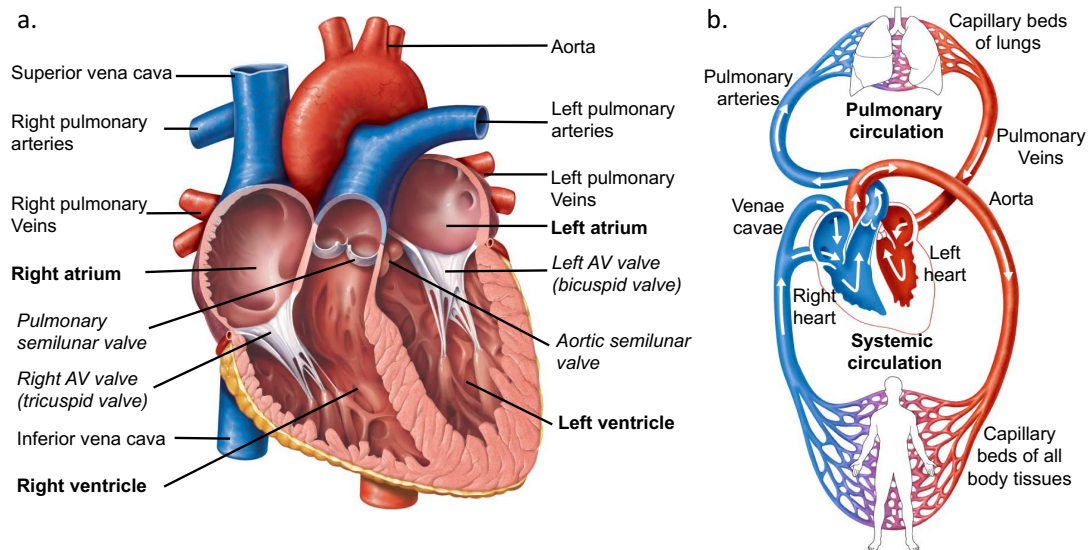


Figure 1.1. The heart and circulation system.

a. The structural anatomy of the heart. The labels for the four heart chambers are bold and for the four valves are italic. b. The pulmonary and systemic circulations. Red blood is rich in oxygen and blue blood is low in oxygen. Arrows indicate the path of blood flow. The figures are adapted from Marieb, E. N. & Hoehn, K. *Pearson Education*. 2013.²

Electrical conduction system

The electrical conduction system of the heart facilitates the simultaneous contraction of the left and right side of the heart, and the sequential contraction of the atria and ventricles. The two primary types of cardiac muscle cells are myocardial contractile cells and myocardial conducting cells. Contractile cardiomyocytes are responsible for the cardiac contractions while conducting cardiomyocytes carry the electrical signal to coordinate contraction and maintain the rhythm. The specialized conducting cells carry electrical signal more quickly than the contractile cells, but action potentials spread through all heart muscle cells to trigger contraction. The specialized myocardial conducting cells, also referred to as pacemaker cells, including sinoatrial (SA) node, atrioventricular (AV) node, bundle of His, bundle branches, and Purkinje fibers, account for one percent of all cardiomyocytes. The pacemaker cells undergo automaticity, which indicates they generate an action potential and depolarize by themselves, and have their inherent rate of depolarization. In normal human hearts, the SA node has the fastest rate of depolarization and tends to outpace all other cardiac myocytes, making it responsible for the heart rate in a healthy heart. When the SA node fails in the disease state, the AV node, bundle of His, bundle branches and Purkinje fibers could also take over as pacemakers to function according to their speed of depolarization³.

The cardiac electrical conduction system starts with the depolarization of the SA node, located in the right atrium near the entrance of the superior vena cava. The action potential initiated by the SA node spreads through the muscle cells of the atria, represented by the P-wave on the electrocardiogram (Figure 1.2), causing the right and left atria to contract at the same time. The electrical signal generated in the SA node spreads through the atrium and down to the AV node, located at the base of the right atrium. The AV node causes a small delay on the action potential propagation, which allows the atrial contraction to be completed before ventricular contraction. The action potential travels through the AV node down into the bundle of His, through bundle branches and into Purkinje fibers. Purkinje fibers rapidly distribute the impulse throughout the ventricle, causing a simultaneous depolarization of the right and left ventricles, represented by the QRS complex, and ensures both ventricles contract in

coordination. As ventricular repolarization reflected by the T wave begins, the ventricles start to relax^{2,4}.

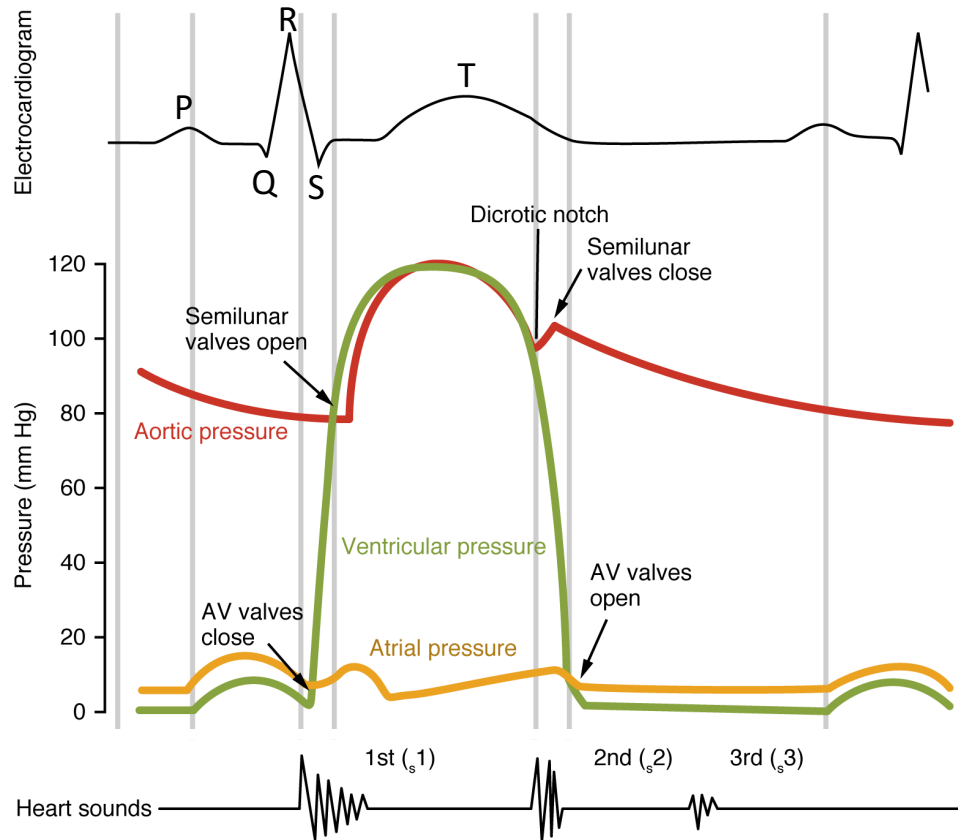


Figure 1.2. The cardiac cycle.

Aortic, atrial and ventricular pressure, phonocardiogram, and electrocardiogram as a function of time. Figure is adapted from <https://open.oregonstate.edu/aandp/chapter/19-3-cardiac-cycle/>

Cardiomyocyte structure and function

Cardiomyocyte

Cardiomyocytes (also called cardiac myocytes) are cells that make up the cardiac muscle (or myocardium). These cells are responsible for pumping blood through the body. Each cardiomyocyte is surrounded by a cell membrane called the sarcolemma and usually contains only one nucleus located in the center of the cell. Cardiomyocytes are often branched and are tightly connected to adjacent myocytes by intercalated discs, which mainly contain gap junctions and desmosomes (Figure 1.3a). Gap junctions are channels that allow cations to flow from one cell to the next to facilitate quick transmission of the depolarization wave and the coordinated contraction of the heart muscles. Desmosomes hold the ends of adjacent cardiomyocytes together, so the cells do not pull apart during the contraction. The main components of the cardiomyocyte inside the sarcolemma are the sarcomeres, nucleus, mitochondria, sarcoplasmic reticulum (SR), and the cytosol. Cardiac myocytes are loaded with mitochondria to provide sufficient ATP required for cardiac muscle contraction. SR is a network of tubules wrapping around the myofibrils, and its primary function is to store calcium. Upon depolarization, extracellular calcium enters the cytoplasm across T-tubules through the L-type calcium channel, activating the calcium release channels in the SR membrane. This causes SR to release a much larger amount of calcium into the cytoplasm and triggers the myofibril contraction. After contraction, calcium is pumped back into the SR by the ATP-dependent calcium pump, causing the myofibrils to relax^{2,5}.

A sarcomere is the basic contractile unit of the contractile cardiomyocyte, defined as the structure between two neighboring Z-discs (Figure 1.4a). Sarcomeres mainly consist of thick filaments and thin filaments, such that each central thick filament is surrounded by six parallel thin filaments that bond to Z-disc at both ends of the sarcomere. The sarcomeres appear striated under the microscope and features alternating dark A bands corresponding to thick filaments along with light I bands spanned by thin filaments and titin only. Muscle contraction occurs when the thick filament pulls the thin filaments, sliding the two filaments across each other to shorten the sarcomere length⁶.

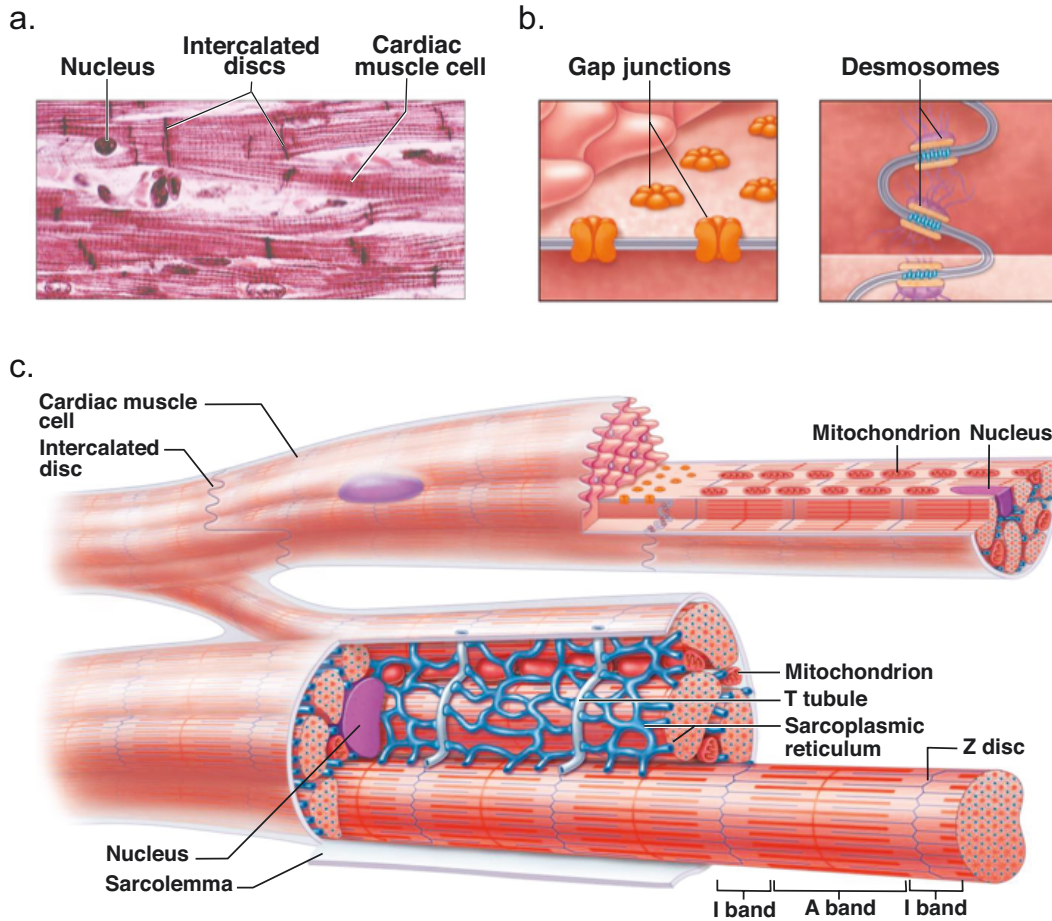


Figure 1.3. Cardiac muscle.

a. Light micrograph of cardiac muscle tissue. The cardiac muscle has a striated appearance. b. Diagram of intercalated discs containing gap junctions and desmosomes. c. Diagram of the cardiac muscle unit. The main components of the cardiomyocyte are the sarcolemma, nucleus, mitochondria, sarcomeres, sarcoplasmic reticulum (SR), and the cytosol. Figures are adapted from Marieb, E. N. & Hoehn, K. *Pearson Education*. 2013.²

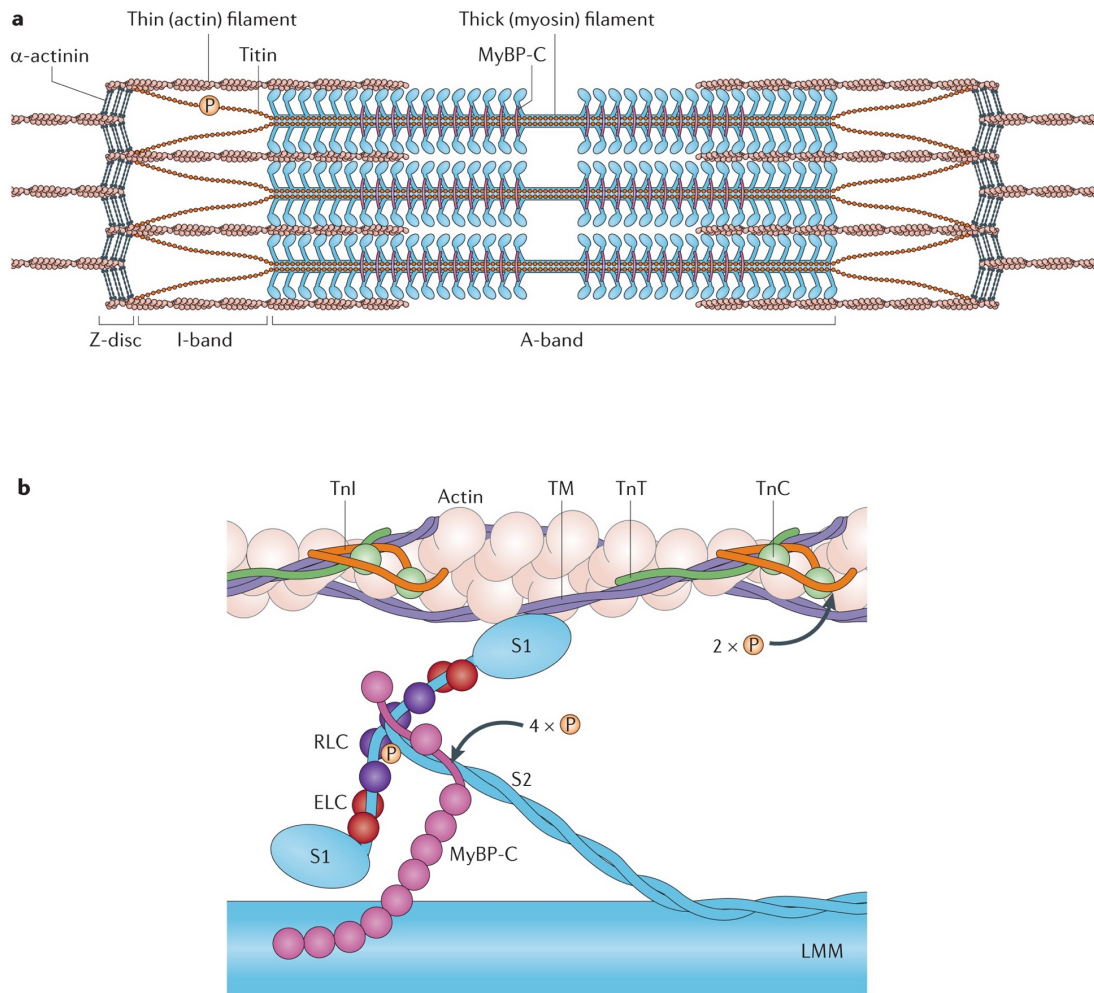


Figure 1.4. Structure of the cardiac sarcomere.

a. Sarcomere structure. b. Thick and thin filament substructure. TnI: troponin I, TnT: troponin T, TnC: troponin C, TM: tropomyosin, RLC: myosin regulatory light chain, ELC: myosin essential light chain, LMM: light meromyosin, MyBP-C: myosin binding protein C. Figure is adapted from Hwang, P. M. & Sykes, B. D. *Nat Rev Drug Discov.* 2015.⁷

The thick filament

Thick myofilaments are mainly composed of myosin protein complexes. Myosin is an elongated molecule consisting of two identical heavy chains and two pairs of light chains (Figure 1.4b)⁸. Each heavy chain consists of an N-terminal globular head

region and a C-terminal α -helical tail domain. The head (S1) contains a motor domain which binds actin and hydrolyses ATP to generate force, and a neck region which binds to one essential light chain (ELC) and one regulatory light chain (RLC) to regulate the activity of the head domain⁹. The long tails consist of S2, a soluble linker to the head region, and light meromyosin (LMM), which forms rod-like thick filaments. The tails of the two heavy chains intertwine and form a coiled-coil structure, holding the two heavy chains together. Hundreds of myosin proteins are assembled on a titin scaffold along the length of the thick filament, with tails towards the M-line and heads towards the Z-line on both sides. As a result, the bipolar myosin thick filament creates a bare zone free of myosin heads at the filament center¹⁰.

Another important thick filament protein is myosin binding protein-C (MyBP-C). MyBP-C is anchored to the thick filament through its strong binding to LMM and titin. The N-terminal domains of MyBP-C interacts with myosin S2 and actin, and regulates actomyosin interaction¹¹. A recent study reveals that MyBP-C activates thin filaments and inhibits thick filaments in cardiac muscle cells¹².

The thin filament

Thin filaments are primarily made of actin with bound regulatory proteins troponin and tropomyosin (Figure 1.4b). Actin monomers, also referred to as globular actin (G-actin), polymerize into a double helix to form filamentous actin (F-actin). Each G-actin monomer contains an active site that can bind either to the myosin head during contraction or to tropomyosin in the resting state. Tropomyosin (Tm) is a long double stranded α -helical coiled coil that polymerizes in a head-to-tail manner along the surface of F-actin molecules. Each Tm binds to one troponin complex, as well as seven consecutive actin monomers on each side of the F-actin, thereby forming a repeating pattern of the thin filament¹³. Troponin is a regulatory protein that links muscle activation to cellular calcium concentration. Under resting calcium concentration, Tm is pinned in place by calcium-free troponin complex such that Tm covers the myosin binding site on actin and blocks the actin-myosin interaction¹⁴. During systole, calcium is released from the sarcoplasmic reticulum (SR) into the cytosol, and the intracellular calcium concentration increases over 10-fold, from sub

The cross-bridge cycle

At micromolar calcium concentration, calcium binds to troponin inducing conformational changes that allow tropomyosin to move away from the myosin binding sites on actin. This allows myosin and actin to interact, causing the cross-bridge cycle to start (Figure 1.5). In the absence of ATP, myosin will strongly bind to actin in the rigor state. Binding of ATP to the myosin head rapidly dissociates it from actin and the head then shifts to the pre-power stroke position. ATP hydrolyzes to ADP-Pi (inorganic phosphate) that remains bound to myosin, and the released energy converts the myosin head to the high energy conformation. If the active site of actin is covered by tropomyosin, the myosin will remain in this high energy conformation. The myosin-ADP-Pi complex binds weakly to actin when the myosin binding site is exposed on actin. A conformational change of myosin leads to a strongly bound state of the myosin-actin-ADP complex, release of Pi, and a force-generating power stroke. After the power stroke, myosin will go into the lower energy state and ADP is released, but the cross-bridge formed is still in place. ATP binding to myosin completes the cycle, releasing actin and resetting the myosin head to its pre-power stroke position. Interaction between actin and myosin pulls the two Z lines toward each other, shortening the muscle and generating force. Contraction continues until calcium dissociates from troponin, and tropomyosin blocks the myosin binding site on actin^{9,16}.

Troponin structure and function

The troponin complex is the key protein that turns muscle contraction on and off in a calcium-dependent manner. Troponin is a heterotrimeric complex formed by the calcium-binding subunit troponin C (TnC), the inhibitory subunit troponin I (TnI), and the tropomyosin-binding subunit troponin T (TnT)¹⁷. TnC responds to the changes of calcium concentration by interacting with TnI. TnI is an elongated protein that forms numerous contacts with TnC, TnT, and actin, which inhibits the ATPase activity of the actomyosin complex at a low calcium level. TnT binds to tropomyosin and anchors the troponin complex onto the thin filaments¹⁸.

Troponin C

Troponin C, in both skeletal and cardiac isoforms, consists of two globular domains, and each domain has two EF-hand helix-loop-helix motif divalent metal binding sites. Sites I/II are located in the regulatory N-terminal domain (NTnC) and sites III/IV are located in the structural C-terminal domain (CTnC), where the two domains are connected by a linker. This linker is a long α -helix in the crystal structures of sTnC^{19–22}, but it is flexible in NMR solution structure of sTnC²³. In contrast, both NMR solution structure of cTnC²⁴ and crystal structure of cTnC-cTnI-cTnT complex¹⁷ shows that the linker between cardiac NTnC (cNTnC) and cardiac CTnC (cCTnC) is flexible.

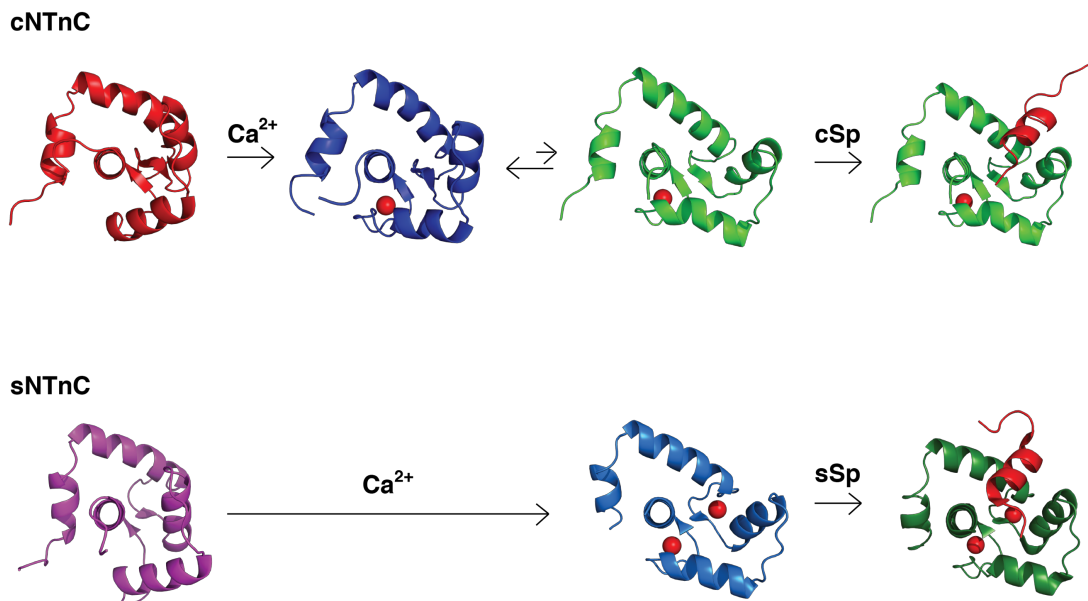


Figure 1.6. Closed-to-open differences between cNTnC and sNTnC.

The structure of cNTnC remains relatively unchanged whether free (1spy.pdb²⁵) or bound (1ap4.pdb²⁵) to calcium, and changes to open conformation upon cTnI switch peptide binding (1mxl.pdb²⁶). The structure of sNTnC is in the closed conformation without calcium (1tnp.pdb²⁷), and in the open conformation in the presence of calcium (1avs.pdb²⁸) or both calcium and sTnI switch peptide (1ytz.pdb²²). Figure adapted from Li, M. X. & Hwang, P. M. *Gene*. 2015.²⁹

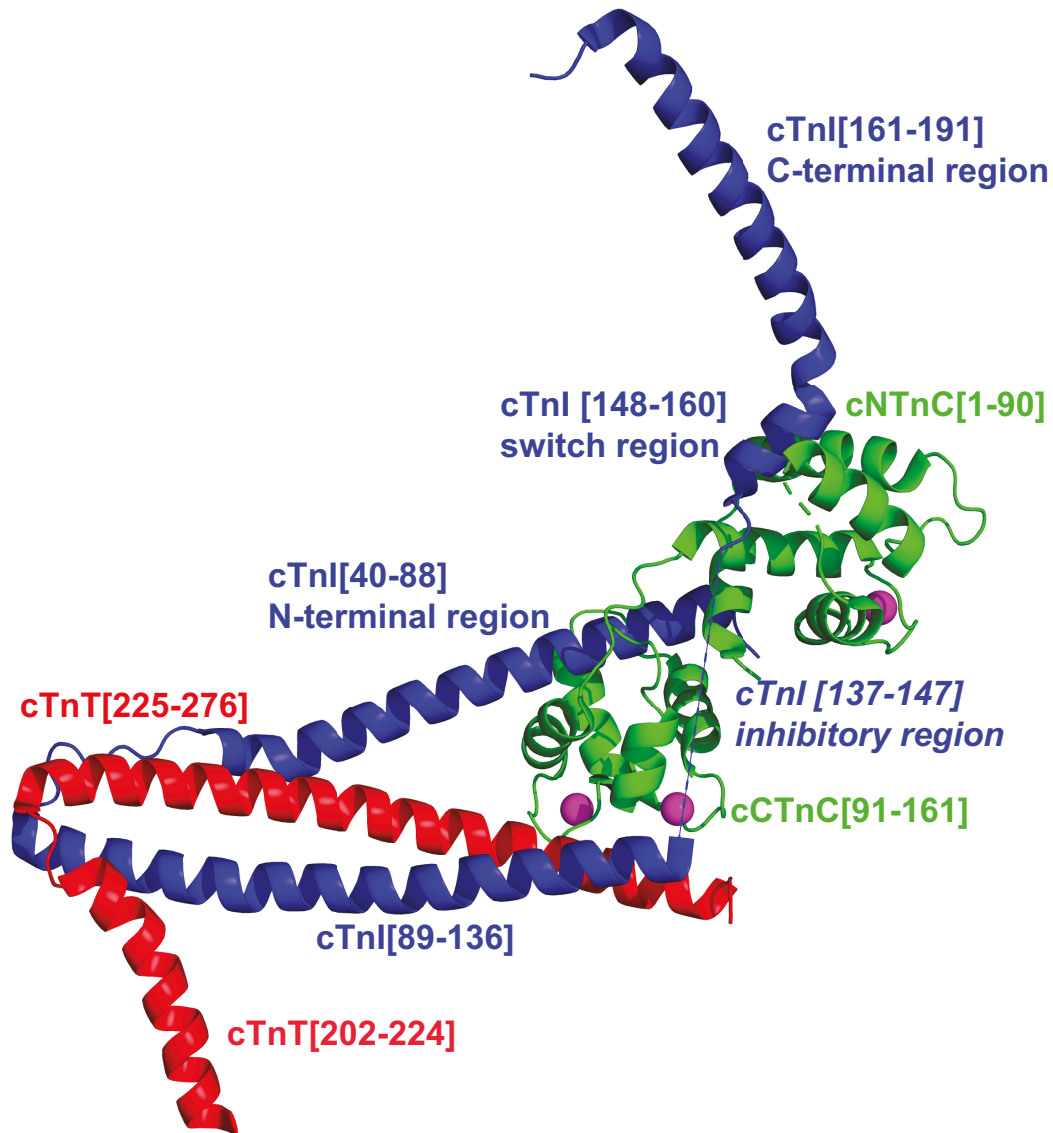


Figure 1.7. X-ray structure of cardiac troponin core complex.

Calcium-saturated cTnC-cTnI₃₄₋₂₁₀-cTnT₁₈₂₋₂₈₈ complex (1j1e.pdb)¹⁷. cTnC is colored in green and the 3 bound calcium ions are represented by magenta spheres, cTnI is colored in blue, and cTnT is colored in red. cTnI inhibitory region structure is unknown shown as blue dash lines.

Sites III and IV in CTnC are high affinity calcium and magnesium binding sites, and are always saturated by calcium or magnesium under physiological conditions³⁰, whereas sites I and II in NTnC are calcium specific sites. Site I in cNTnC is inactive due to several key amino acid substitutions³¹ compared to skeletal NTnC (sNTnC). The structural changes of troponin C upon calcium binding is different for cardiac and skeletal isoforms. Calcium binding to sites I and II of sNTnC triggers a closed-to-open conformational transition, opening the hydrophobic cleft for skeletal TnI (sTnI) binding^{27,28,32}. Calcium binding to site II of cNTnC does not induce the opening of the hydrophobic pocket²⁵, and binding of cardiac cTnI (cTnI) is required to stabilize the open conformation of cNTnC²⁶ (Figure 1.6). On the other hand, the calcium or magnesium saturated C-domain of both sTnC and cTnC are having similar structures, whether free or bound to TnI^{24,33-35}.

Troponin I

TnI is an extended molecule that binds to TnC, TnT, and actin-tropomyosin. The structure of TnI can be divided into six structural regions: the N-terminal cardiac-specific extension (cTnI₁₋₃₁), the N-terminal region (cTnI₃₄₋₇₉ and sTnI₁₋₄₇) that binds to the CTnC, the TnT binding region (cTnI₈₀₋₁₃₆ and sTnI₅₀₋₁₀₆), the inhibitory region (cTnI₁₂₈₋₁₄₇ and sTnI₉₆₋₁₁₅) that binds to both TnC and actin-tropomyosin, the switch region (cTnI₁₄₇₋₁₆₃ and sTnI₁₁₅₋₁₃₁) that binds to the NTnC, and the C-terminal region (cTnI₁₆₄₋₂₁₀ and sTnI₁₃₂₋₁₈₀) that binds to actin-tropomyosin¹⁸.

The cardiac-specific N-terminal extension contains two phosphorylation sites (Ser 22/23)³⁶, and phosphorylation at cTnI Ser22/23 decreases the calcium sensitivity of the cardiac sarcomere. Although there is no high-resolution structure for this region, NMR studies have shown that the cardiac-specific N-terminal extension maintains an extended³⁷ or disordered³⁸ state.

The structure of calcium-saturated sTnC-sTnI₁₋₄₇ shows that the N-terminal region of sTnI forms an α -helix, stretching on the surface of the sCTnC and making contact with sNTnC³⁹. The corresponding region of cTnI was found to bind the hydrophobic cleft of cCTnC with similar conformation and orientation³³. The structures of calcium-saturated CTnC (sCTnC and cCTnC) are similar whether free or

bound to the N-terminal region of TnI^{24,33-35}. The crystal structures of calcium-saturated core domain of skeletal sTnC-sTnI₁₋₁₈₂-sTnT₁₅₆₋₂₆₂²² and cardiac troponin complex cTnC-cTnI₃₄₋₂₁₀-cTnT₁₈₂₋₂₈₈¹⁷ (Figure 1.7) reveal the structures of the full-length sTnI and cTnI (except for the cardiac-specific N-terminal extension and cardiac inhibitory region). The N-terminal region cTnI₄₃₋₇₉ forms an α -helix, which binds to the hydrophobic cleft of cCTnC (residues 41-60), in agreement with the binary complex³³, and the α -helix continues beyond cCTnC until residue 80. cTnI₈₀₋₈₇ forms a loop that interacts with cTnT, followed by another long α -helix (residues 90-135), which proceeds back towards cTnC forming a coiled coil with the C-terminal region of cTnT. The next region is the cTnI inhibitory region (residues 137-148), which is not defined in the cTnC-cTnI-cTnT complex structure, but it is thought to be in an extended conformation based on the distance between Arg 136 and Thr 149. The NMR structure of calcium-saturated cCTnC-cTnI₁₂₈₋₁₄₇ shows that residues 134-139 form a helix interacting with cCTnC and C-terminal residues 140-147 adopt an extended conformation, making potential electrostatic contact with the linker region (beginning of E-helix)³⁵.

The inhibitory region of sTnI (residues 104-115) is well defined in the sTnC-sTnI-sTnT complex, displaying an ordered loop structure with the C-terminal sTnI inhibitory segments (residues 111-115) stretched along the sTnC central helix²², similar to the structure of cTnI inhibitory region in the binary complex³⁵. The inhibitory region is followed by an α -helical switch region, cTnI₁₄₇₋₁₆₃. The NMR structure of the calcium-saturated cTnC-cTnI₁₄₇₋₁₆₃ complex revealed that cTnI switch peptide adopts a α -helical conformation spanning residues 150-159 that binds to the hydrophobic pocket of cTnC stabilizing its open conformation. The NMR structure of cTnC-cTnI₁₄₇₋₁₆₃ complex adopts a similar structure with the corresponding regions in the crystal structure of cTnC-cTnI-cTnT complex¹⁷. The corresponding sTnI switch region (residues 115-131) shares a similar structure and a similar interaction with the sTnC compared to the cardiac isoforms, observed in the NMR structure of sTnC(rhodamine)-sTnI switch peptide complex and the crystal structure of sTnC-sTnI-sTnT complex. The last component of TnI is the C-terminal region cTnI₁₆₄₋₁₈₈ that forms an α -helical structure free of contact with cTnC or cTnT.

“Drag and release” mechanism

The overall cardiac troponin core domain structure is dominated by α -helices that can be divided into two structurally distinct subdomains, the regulatory head (cNTnC and cTnI switch region for cTn; sNTnC and sTnI switch region for sTn) and the IT arm (cCTnC, cTnI₄₂₋₁₃₆ and cTnT₂₀₃₋₂₇₁ for cTn, sCTnC, sTnI₈₋₁₀₆ and sTnT₂₀₀₋₂₄₄ for sTn), which are connected by flexible linkers. The cNTnC-cCTnC linker and the inhibitory region of cTnI form a flexible joint allowing the regulatory head and IT arm to rotate and change their relative orientations. The most widely accepted mechanism of calcium regulatory switch activation is the “drag and release” model (Figure 1.8)¹⁷. Calcium binding to the regulatory N-domain of TnC induces the association of the switch region of TnI. The movement of the switch region of TnI towards NTnC drags the adjoining inhibitory region off the actin-tropomyosin and the C-terminal of TnI is carried along with this motion. As a result, the C-terminal half of cTnI toggles between cNTnC and actin-tropomyosin in the regulatory head during the contraction and relaxation cycle.

The recent cryo-EM structures of the thin filament in calcium free and bound states further demonstrate the “drag and release” model of troponin activation⁴⁰. In the calcium free state, the EF hand of cNTnC is closed and cTnI is tightly bound to actin and Tm. The entire troponin structure is highly elongated over seven actin subunits, of which the upper four are bound to C-terminal region of TnI and TnC core, and the bottom three of the opposite strand are bound to N-terminal region of TnT (Figure 1.9e). The inhibitory region (residues 137-148), switch region (residues 149-160), and mobile region (residues 163-210) extend along and between actin and Tm, stabilizing the Tm coiled coil in the “off” position that blocks the myosin head access to actin filament (Figure 1.9a and c). The N-terminal region of TnT starting from G199 crosses the actin strands down towards the Tm on the opposite actin strand, with residues 87-150 forming an α -helix extending down along and across the Tm coiled coil near Tm-Tm head-to-tail junction. Upon calcium binding to cNTnC, the EF hand is in an open conformation that binds to the regulatory switch region of TnI, dragging the inhibitory region and eventually the entire C-terminal region of TnI off actin and Tm (Figure 1.9b and d). The overall structures are very similar between calcium bound and calcium free

states, except cNTnC is in an open conformation bound to the cTnI switch region, and the C-terminal region of TnI is missing in the calcium bound state (Figure 1.9c and d)⁴⁰. The dissociation of C-terminal region of TnI promotes Tm shifting along the surface of the actin filament to “on” position, making the myosin binding site of actin accessible to the myosin head, and the binding of myosin head to actin causes Tm to further shift to the “fully on” position^{40,41}.

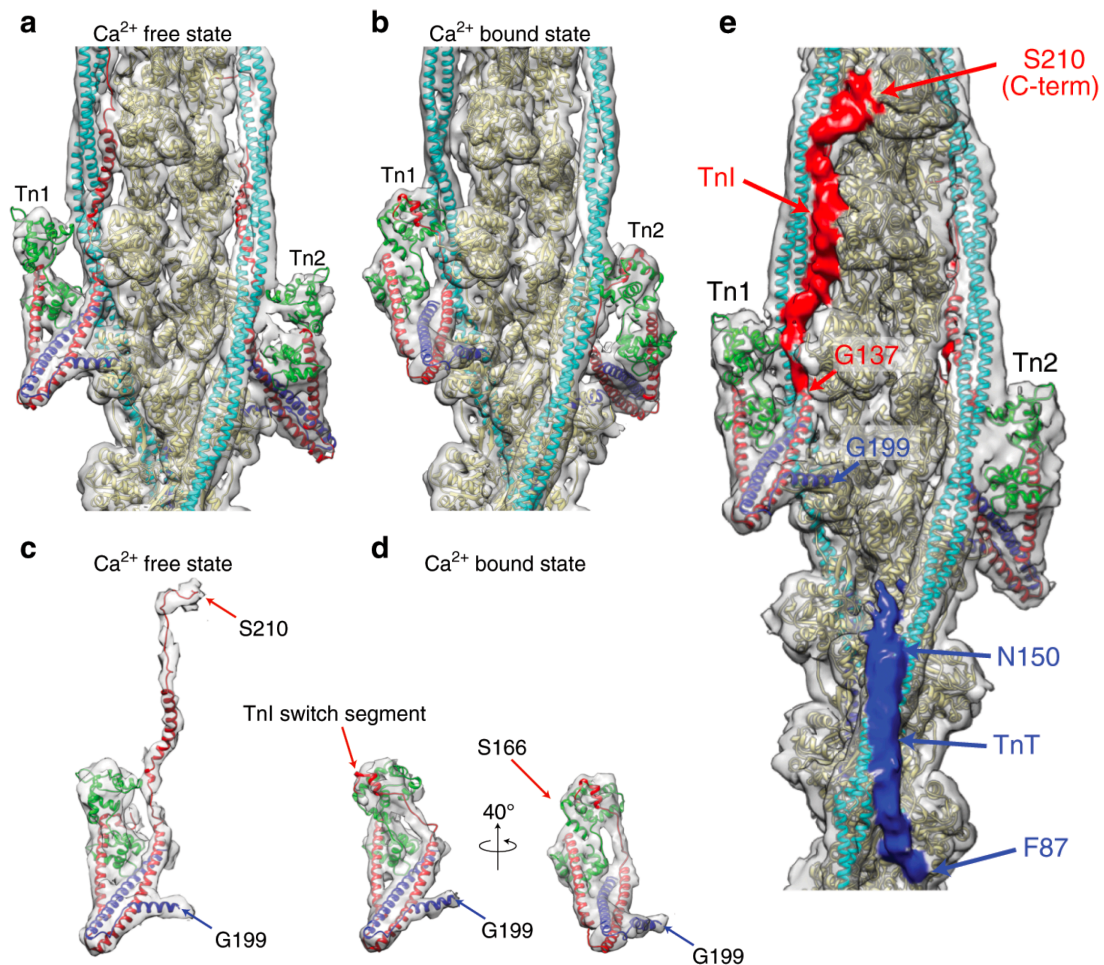


Figure 1.9. Structural changes of the troponin complex upon calcium binding.

a, c, e. Calcium free state. b, d. Calcium bound state. e. The entire structure of the Tn ternary complex is shown for each of the Tn pair, labeled Tn1 and Tn2, in the front and back of the thin filament. Models are colored as: actin, beige; Tm, light blue; TnI, red; TnT, dark blue; and TnC, green. Figure is adapted from Yamada, Y., Namba, K. & Fujii, T. *Nat. Commun.* 2020.⁴⁰

Inotropic therapy for heart failure

Heart failure

Cardiovascular diseases are the leading cause of death worldwide⁴², and heart failure is the end stage of almost all heart diseases. Heart failure, also referred to as congestive heart failure, occurs when the heart is unable to pump a sufficient amount of blood to meet the needs of the body. It is a long-term chronic condition that often gets worse over time. Heart failure can occur in both systolic and diastolic stages. Systolic heart failure is caused by impaired cardiac muscle contraction, also called heart failure with reduced ejection fraction (HFrEF). Under this condition, the heart muscle becomes weak and dilated, losing its ability to generate enough force. Over time, the inefficient contraction leads to volume overload, which causes the heart muscle to further dilate and enlarge, making it even more difficult to contract. Diastolic heart failure, also referred to as heart failure with preserved ejection fraction (HFpEF), is characterized by inadequate diastolic filling. In diastolic heart failure, the muscle becomes thick and stiff, losing its ability to expand and preventing the heart from filling enough blood during the relaxation period⁷.

Pharmaceutical compounds for heart failure

The treatment of systolic or diastolic heart failure would be positive or negative inotropes, which increase or decrease heart muscle contractility to enhance cardiac output. Digoxin, a derivative of the foxglove plant, is the oldest drug for heart failure, first described by William Withering in 1785⁴³. Digoxin inhibits the sodium-potassium adenosine triphosphatase (ATPase) pump, leading to an increase in sarcoplasmic sodium. High sodium concentration drives sodium-calcium exchanger to pump calcium into the cell and increases the intracellular calcium concentration (Figure 1.10). This results in an increase in contraction and a positive inotropic effect. Large clinical trials on digoxin did not identify a significant benefit pertaining to mortality rate, and the use of digoxin for heart failure treatment has generally declined over time⁴⁴.

Two commonly used inotropes in clinical practice are dobutamine and milrinone, both of which increase cardiac output by upregulating signaling pathways⁴⁵.

Dobutamine activates the β_1 -adrenergic receptor and stimulates adenylyl cyclase to convert ATP to cAMP. Milrinone inhibits phosphodiesterases 3 and 4 (PDE3 and PDE4), which prevents the conversion of cAMP to AMP. In both cases, the rise in cAMP activates the protein kinase A (PKA), and in turn increases the intracellular calcium concentration (Figure 1.10). These drugs are similar in terms of the mechanisms behind their inotropic effects, and have been described as indirect sarcomere modulators⁷.

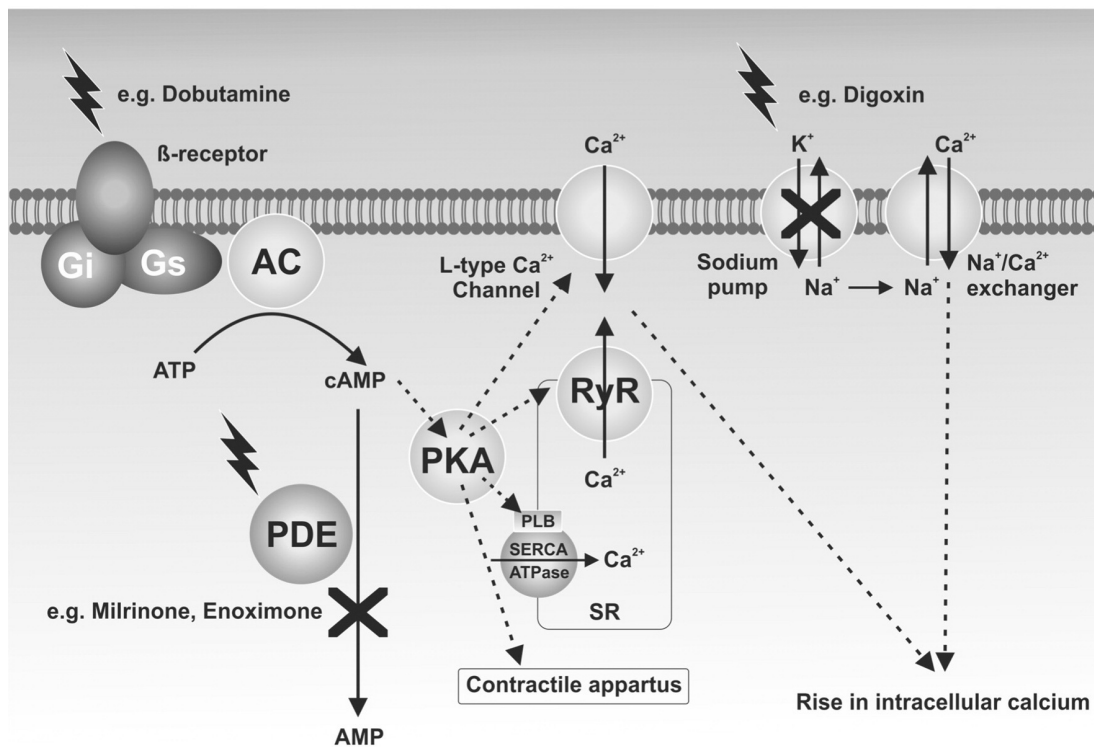


Figure 1.10. Mechanism of calcium mobilizer increasing intracellular calcium.

AC, adenylate cyclase; PDE, phosphodiesterase; PKA, protein kinase A; RyR, ryanodine receptor; SERCA ATPase, sarcoplasmic endoplasmic ATPase; PLB, phospholamban; SR, sarcoplasmic reticulum. Figure adapted from Pollesello, P., Papp, Z. & Papp, J. G. *Int. J. Cardiol.* 2016⁴⁶.

Indirect sarcomere modulators alter the contractility of cardiac muscle by regulating the upstream signaling pathways; however, they also affect other downstream effectors such as ion channels and cross-react with other targets such as smooth muscle⁴⁷. Indirect sarcomere modulators raise the oxygen demand of the heart and further increase mortality by precipitating life-threatening arrhythmias and systemic hypotension. Compounds that directly alter the response of the cardiac sarcomere without altering cytosolic calcium homeostasis have therapeutic potential for the treatment of heart failure. A different class of inotropes is direct sarcomere modulators, which directly change the contractile response of the heart to calcium without altering the calcium transient. Several of these compounds have entered into clinical trials, including pimobendan and levosimendan targeting the troponin complex and omecamtiv mecarbil targeting myosin⁴⁶.

Pimobendan was the first direct sarcomere activator to reach clinical trial for human use, with a dual mechanism of action consisting of calcium sensitization of myocardial contractile proteins and phosphodiesterase 3 (PDE3) inhibition. It was discovered in 1984⁴⁸ and the first clinical trial was reported in 1988⁴⁹. The myofilament calcium sensitizing ability of pimobendane is from the interaction with cTnC and subsequent increased calcium affinity⁵⁰. Pimobendan is available for the treatment of systolic heart failure only in Japan⁵¹, since it showed a strong trend towards an increase in mortality in another study⁵². Currently, pimobendan is one of the most common treatments for congestive heart failure in dogs⁵³. Study also showed that cats with heart failure receiving pimobendane saw a significant improvement in survival time⁵⁴.

Levosimendan (marketed as SimDaX) was discovered in 1994⁵⁵ and was first approved for clinical use in early 2000⁵⁶. It has been approved in more than 60 countries mainly in Europe and Latin America, and is in active clinical trials in the US⁵⁷. Levosimendan has been shown to increase cardiac output without an increase in oxygen demand⁵⁸ and reduces symptoms of acute heart failure. Levosimendan binds to the calcium-saturated cardiac troponin C (cTnC), which could be the primary mechanism responsible for its calcium sensitizing effect⁵⁹. Like pimobendane, levosimendan can also increase calcium sensitivity by selectively inhibiting PDE3⁶⁰. In addition to calcium sensitization, levosimendan promotes vasodilatation by opening

of ATP-dependent potassium channels on vascular smooth muscle cells. Levosimendan has been evaluated in more than 200 clinical trials during the past 20 years, in a wide range of therapeutic areas. Many clinical trials showed an improved survival rate in the treatment of acute decompensated systolic heart failure, although larger phase III trials did not show a mortality benefit^{56,61}. Most recent trials in the past few years provided indications of benefit from levosimendan therapy⁵⁷.

Omecamtiv mecarbil (originally CK-1827452), first reported in 2010⁶², was the first cardiac myosin activator to enter clinical trials. Omecamtiv mecarbil is a selective cardiac myosin activator, which binds to myosin at an allosteric site and stabilizes the pre-powerstroke state of myosin, resulting in an increase in the number of myosin heads involved in the force generation process⁶³. Omecamtiv mecarbil enhanced cardiac muscle contraction by directly interacting with myosin without changing the calcium transient. Unlike pimobendane and levosimendan, which are also PDE3 inhibitors in addition to directly activating the sarcomere, omecamtiv mecarbil is thought to be a pure myosin activator. Early phase I⁶⁴ and II⁶⁵ clinical trials showed Omecamtiv mecarbil dose-dependently enhances the systolic function of the left ventricle and has a favorable effect on systolic function both in healthy volunteers and in patients with systolic heart failure. A later phase II trial for intravenous Omecamtiv mecarbil showed that the drug did not have a significant impact on improvement in dyspnea compared to placebo⁶⁶. However, another Phase II trial for oral therapy has shown that omecamtiv mecarbil was associated with decreased ventricular diameter and improvement in cardiac function⁶⁷. A large phase III trial for oral therapy is still ongoing, and results will be available in 2021⁶⁸.

The development of small molecules targeting the heart presents difficulties beyond common concerns in therapeutics such as toxicity and bioavailability. A more important concern would be the determination of optimal efficacy. A drug targeting cancer would intend to completely stop the cancer; however, a drug targeting the heart would only try to make minor changes instead of stopping the heart completely. It is also difficult to design a drug with specificity to cardiac muscle because the structure of sarcomere proteins in striated muscle are similar. These issues are a major reason why there is a lack of existing drugs targeting troponin⁶⁹.

Direct sarcomere modulators targeting troponin C

The key calcium-dependent switch for contraction and relaxation in cardiac muscle is the association and dissociation of the N-domain of cTnC and the cTnI switch region. The interface of cTnC-cTnI is the logical target for the development of troponin activators or inhibitors. A number of small molecules are known to bind to this interface and modulate muscle contraction. Several structure studies of small molecule bound to cTnC-cTnI have provide structural insights into the mechanisms of calcium modulating. Although there are a few small molecules that alter the calcium sensitivity by binding to the C-domain of cTnC (EMD 57033, resveratrol and EGCg), only the ones targeting the interface of cTnC and cTnI switch region (bepridil, levosimendan, and W7) will be reviewed here (Figure 1.11).

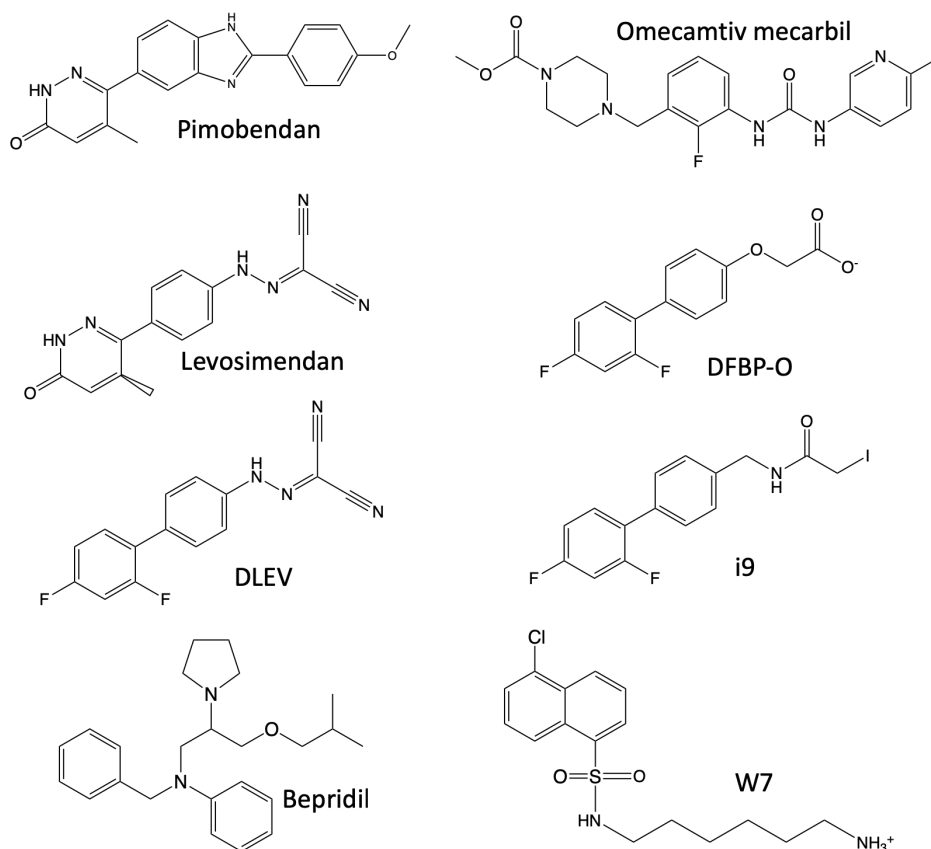


Figure 1.11. Chemical structures of direct sarcomere modulators.

Bepridil

Bepridil (N-benzyl-N-[3-(2-methylpropoxy)-2-(pyrrolidin-1-yl)propyl]aniline) is a calcium channel blocker that was previously marketed as a treatment for angina. It is also a calmodulin antagonist that inhibits the calcium/calmodulin-dependent activities⁷⁰. As an off-target effect, bepridil has been shown to bind to cTnC with a K_D of $\sim 10 \mu\text{M}$ and enhance calcium binding to the regulatory site of cTnC⁷¹. An NMR study using Met methyl groups as structural markers identified three bepridil binding sites on cTnC⁷². In the crystal structure of the calcium-saturated cTnC-3bepridil complex, two bepridil molecules pull the N- domain and C-domain of cTnC close together to produce a compact structure of cTnC, while a third bepridil binds to the hydrophobic patch of cTnC stabilizing the calcium-bound open conformation⁷³. Subsequent NMR studies revealed that only one bepridil binds to the cTnC in the presence of cTnI, with a K_D of $\sim 140 \mu\text{M}$ ⁷⁴. Bepridil binds to the hydrophobic patch located in the cTnC, much like the binding of the cTnI switch region. Both bepridil and cTnI switch region mediate an increase in calcium binding affinity by interacting with and stabilizing the open conformation of calcium-saturated cTnC.

NMR spectroscopy was used to investigate the effect of bepridil on cTnI switch region binding when binding to calcium-saturated cTnC. The results indicate that bepridil and cTnI switch peptide bind to cTnC simultaneously, but with negative cooperativity. Bepridil decreases the affinity of cTnI switch peptide for cTnC by 3.5-fold (K_D from $154 \mu\text{M}$ to $550 \mu\text{M}$), and vice versa (K_D from $23 \mu\text{M}$ to $80 \mu\text{M}$)⁷⁵. The solution structure of calcium-saturated cTnC-cTnI switch peptide-bepridil complex reveals that bepridil binds in the hydrophobic core of cTnC (Figure 1.12). The N-terminus of the cTnI switch peptide clashes with part of the bepridil molecule, which would explain the negative cooperativity between cTnI switch peptide and bepridil for cTnC. The results of these observations indicate that bepridil binding stabilizes the calcium-bound open state of cTnC, but also destabilizes the complex by displacing the cTnI switch peptide. Ideally, an activator would increase the calcium binding affinity of cTnC and enhance the interaction between cTnC and cTnI switch region as well.

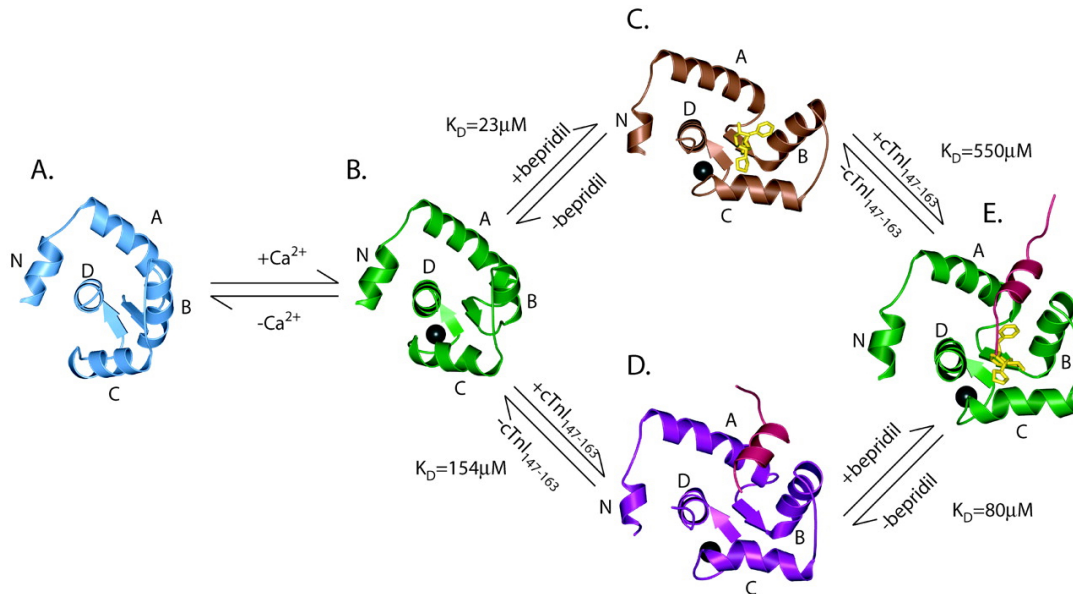


Figure 1.12. Effect of bepridil and cTnI switch peptide on cNTnC.

a. The cNTnC (apo). b. cNTnC-Ca. c. cNTnC-Ca-bepridil. d. cNTnC-Ca-cTnI switch peptide. E. cNTnC-Ca-cTnI switch peptide-bepridil. For the corresponding equilibria, the dissociation constants K_D are also shown. Figure adapted from Wang, X., Li, M. X. & Sykes, B. D. *J. Biol. Chem.* 2002.⁷⁵

Levosimendan

Levosimendan (4-(1,4,5,6-tetrahydro-4-methyl-6-oxo-3-pyridazinyl)phenyl)-hydrazono)propanedinitrile) is one of the most extensively studied direct sarcomere activators. It was demonstrated that levosimendan and its active metabolite OR-1896, selectively bind to phosphodiesterase 3 (PDE3), inhibiting its enzymatic activity and upregulating cAMP-mediated signaling⁷⁶. However, it appears that levosimendan does not cause a significant increase in intracellular cAMP at therapeutic dose⁶⁰. The positive inotropic effect of levosimendan is primarily due to its interaction with cTnC. Study shows that levosimendan binds to calcium-saturated human cTnC in the hydrophobic patch of the N-terminal domain⁵⁵. NMR studies show that levosimendan binds both domains of calcium-saturated cTnC (C35S) in the absence of cTnI. Slow conformational exchange is observed due to the binding of levosimendan to the

primary site in the N-domain, and fast exchange for a secondary binding site in the C-domain⁷⁷. It is apparent that Cys 84 is necessary for the association of levosimendan and the cNTnC, since no binding of levosimendan to the N-domain region of calcium-saturated A-cys cTnC (C35S C84S) was observed⁷⁷. Subsequent study of levosimendan binding to calcium-saturated C35S cNTnC-cTnI₃₂₋₇₉-cTnI₁₂₈₋₁₈₀ complex revealed that levosimendan only binds to the regulatory N-domain (estimated K_D of 200 μ M) in the presence of cTnI. cTnI₃₂₋₇₉ blocked the levosimendan binding site on the C-domain, but cTnI₁₂₈₋₁₈₀ did not compete with levosimendan for the binding site on the N-domain⁵⁹. The exact binding site of levosimendan on cNTnC remains unclear due to the lack of a high resolution cNTnC-levosimendan complex structure caused by levosimendan's instability.

Dfbp-o (2',4'-difluoro(1,1'-biphenyl)-4-yloxy acetic acid) is an analogue of levosimendan, which was found to increase the calcium sensitivity of cardiac trabeculae in a manner similar to levosimendan⁷⁸. Dfbp-o increases the binding of cTnI switch peptide (residues 147-163) to cTnC from 130 μ M to 60 μ M, and the binding of dfbp-o to cNTnC was increased by the presence of cTnI switch peptide from 820 μ M to 380 μ M. The solution structure of cTnC-cTnI-dfbp-o complex shows that dfbp-o binds to the hydrophobic pocket formed between cNTnC and the cTnI switch peptide, and stabilizes the open conformation of cNTnC⁷⁸. The interaction between the negative carboxylate group of dfbp-o and the positively charged side chain of Arg 147 of cTnI could be an explanation for the enhanced binding of cTnI to cNTnC.

I9 is another analogue of levosimendan, which was designed to form a covalent bond with Cys 84 of cNTnC. I9 has been shown to bind in the hydrophobic pocket of cNTnC and slightly reduces the cTnI affinity to cNTnC. An increase calcium sensitivity of cardiac muscle is observed after an exchange of native cTnC for cTnC (C35S)-i9 in ventricular trabeculae⁷⁹. The possible explanation is that i9 enhances calcium sensitivity by stabilizing the open conformation despite slightly reducing cTnI binding.

Recent study using NMR spectroscopy and mass spectrometry has shown that levosimendan reacts specifically with Cys 84 of cTnC by forming a reversible covalent thioimidate bond, but only reacts with the calcium bound form of cNTnC⁸⁰. This

suggests that levosimendan enhances the calcium sensitivity by stabilizing the calcium-bound conformation of cTnC. Subsequent *in situ* experiments by mass spectrometry showed that the covalent complex between levosimendan and cTnC is observed when cTnC is anchored within the myofibril⁶⁹. An levosimendan analogue DLEV (((4-(2,4-difluorophenyl)phenyl)-hydrazono)propanedinitrile) was reported to form a reversible covalent bond with Cys 84 of cTnC and increase ATPase activity of bovine cardiac muscle myofibrils⁸¹. Therefore, targeting this unique cTnC C84 reactivity could be a promising way to discover calcium modulating drugs for heart failure.

W7

The calmodulin antagonist W7 (N-(6-aminohexyl)-5-chloro-1-naphthalenesulfonamide) is a well-studied direct sarcomere inhibitor. W7 was initially discovered to inhibit vascular smooth muscle actomyosin in a dose-dependent fashion⁸². W7 was found to be a calmodulin antagonist, inhibiting calcium/calmodulin-regulated protein kinase and ATPase⁸³. Other than calmodulin, W7 binds specifically to TnC, but not to any other muscle protein⁸³. A study investigating the interplay of troponin- and myosin-based pathways of calcium activation showed that W7 inhibits ATPase activity and tension development in both skeletal and cardiac muscle⁸⁴. NMR study has shown that W7 binds to both domains of calcium-saturated cTnC, with a dissociation constant K_D of 0.85-0.91 mM and 3.40-3.65 mM for two sites binding to cCTnC, and 0.15-0.3 mM for single site binding to cNTnC⁸⁵. To investigate whether multiple-site binding is relevant within the troponin complex, W7 was titrated into a calcium-saturated cTnC-cTnI₃₄₋₇₁-cTnI₁₂₈₋₁₆₃ complex. In the presence of cTnI, W7 only binds to cNTnC with K_D of ~ 0.5 mM and no longer binds to cCTnC⁸⁶. Both W7 and cTnI switch peptide binding to cNTnC suggests that W7 may directly modulate the calcium sensitivity by interacting with cNTnC and cTnI switch region.

The NMR structures of W7 bound to calcium-saturated cNTnC⁸⁷ and cNTnC-cTnI switch peptide complex⁸⁸ revealed that W7 binds to the hydrophobic groove of cNTnC, with similar position in both structures and other small molecules such as bepridil and levosimendan. However, in the presence of W7, the binding of cTnI switch peptide to cNTnC decreased by 13-fold, from K_D of 150 μ M to 2000 μ M. The cTnI

switch region shifted away from its preferred binding site and some helical structure of cTnI diminished as well⁸⁸. Like bepridil, the competition of W7 and cTnI switch region is likely caused by steric clashing. In addition, the positively charged amino group of W7 also could have electrostatic repulsion to the positively charged side chain of cTnI switch region Arg 147.

Recent physiology study has shown that W7 had a rapid effect in correcting contractile dysfunction in hyper-sensitive states at the myocyte level and whole heart levels⁸⁹. W7 was shown to decrease intact cardiac myocyte contractility in a calcium transient amplitude-independent manner, indicating the main target of W7 is the sarcomere protein cTnC. The negative inotropic effect of W7 may present a novel treatment for hypertrophic cardiomyopathy and diastolic heart failure.

NMR spectroscopy in drug discovery

NMR is a powerful technique to study protein structure, dynamics and interactions. Over the past few decades, NMR has been extensively used in drug discovery, including pharmacophore identification, hit validation, hit optimization, structure-based drug design, and fragment-based drug design (Figure 1.13)⁹⁰. Unlike X-ray crystallography, NMR does not require proteins to form crystal, and this greatly broadens the range of protein that can be studied, especially for proteins that are small and flexible. The protein NMR sample is usually prepared in solution, so that protein structures and dynamics can be studied in conditions that are very close to physiological state. The binding studies on small molecules to the target protein are useful for understanding drug action, screening small libraries and discovering new drug lead. The solution structures of protein-ligand complex are frequently used to locate the ligand binding site on the target protein, which is crucial for structure-based drug discovery and development.

Small molecule binding

Ligand titration monitored by two-dimensional correlation spectra of the target protein is the most commonly used approach to identify small molecules by NMR. Ligand-induced chemical shift perturbation is used to confirm the identified hits, determine ligand binding affinity and locate the ligand binding site⁹¹. The ¹H-¹⁵N-heteronuclear single quantum correlation (HSQC) spectrum is frequently used since this experiment has high sensitivity and the peaks are generally well resolved. The chemical shift is sensitive to the environment of a nucleus, and the chemical shift will be perturbed if the ligand binds to the target protein. When the cross peaks of the ¹H-¹⁵N-HSQC spectrum are assigned, the ligand binding site on the target protein could be determined by the chemical shift perturbation on each residue, which is referred to as chemical-shift mapping⁹². This method can rapidly provide information on which part of the protein is interacting with the ligand without a high-resolution protein-ligand complex structure. In the absence of chemical shift assignment, although the binding site cannot be identified, the association constant of the protein-ligand interaction can still be measured.

The chemical shift perturbations of residues are affected by not only directly interacting with the ligand, but other changes in the environment as well. Widespread chemical shift perturbations, including the residues far away from the binding site, may be observed if a protein undergoes substantial structural changes upon ligand binding⁹². The chemical shift perturbation of the target protein upon small molecule binding can map the ligand binding site, as well as reveal the changes of protein secondary structure⁹³. The chemical shift index 3.0 (CSI 3.0)⁹⁴ can be used to predict the secondary structure by comparing the chemical shift to the reference values. The chemical shift can be used to directly derive the backbone ϕ and ψ dihedral angle restraints by TALOS+⁹⁵, which can also be used to identify the secondary structure. An example of using CSI 3.0 and TALOS+ to predict protein secondary structure in the absence and presence of direct sarcomere inhibitor W7 is shown in Chapter 3.

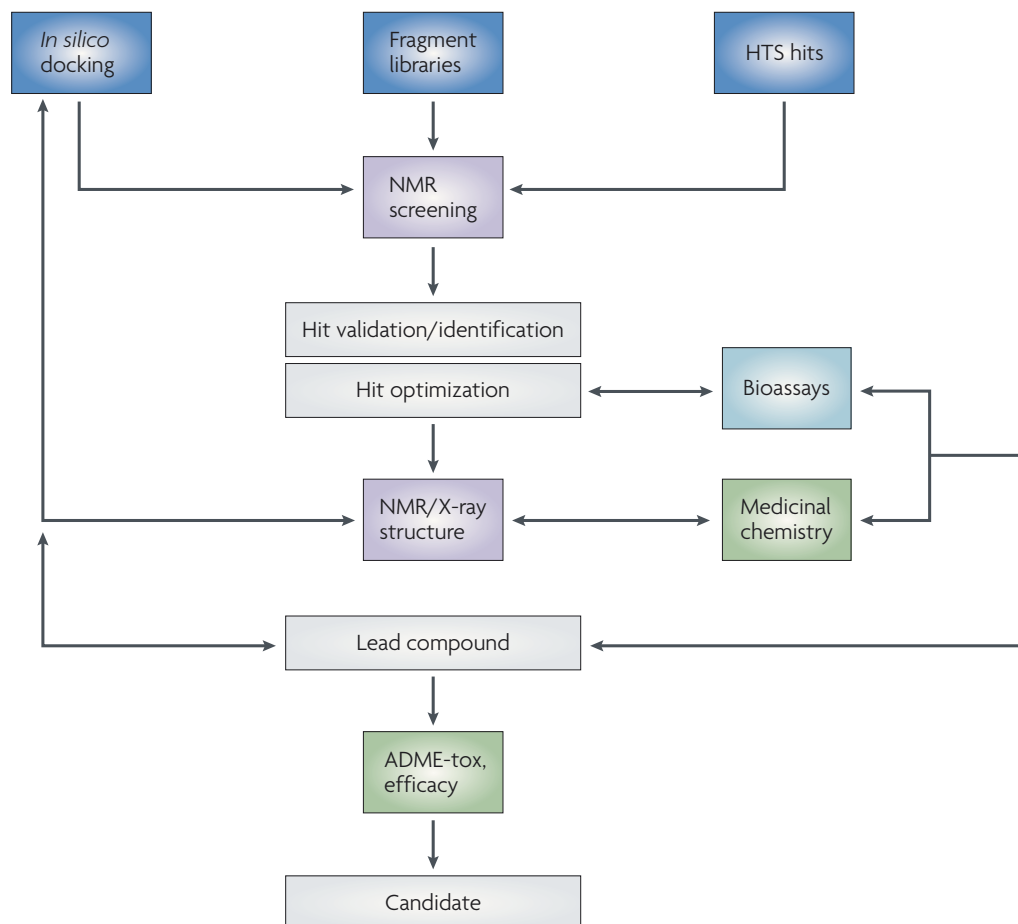


Figure 1.13. Overview of applications of NMR in drug discovery.

NMR spectroscopy can provide critical information in drug discovery. NMR measurements for binding studies can represent a key step to eliminate false positives from high-throughput (HTS) campaigns, to validate putative hits from in silico screens or to identify novel scaffolds in fragment-based programs. NMR and X-ray crystallography can also provide unique information to subsequently guide hit-to-lead. Figure adapted from Pellecchia, M. *et al. Nat. Rev. Drug Discov.* 2008.⁹⁰

Structure determination

NMR Spectroscopy plays a critical role in protein and protein-ligand structure determination. The atomic level structures of protein-ligand complex can provide in-depth information about the orientation and interaction between the ligand and the target protein. The first protein solution structure solved by NMR, proteinase inhibitor IIA, is reported in 1985 by Wüthrich's group. However, the NMR technique for structure determination was not accepted by well-established crystallography community until several structures initially determined by NMR were solved again using crystallography⁹⁶. The reliability of NMR as a tool for structure determination of proteins has since improved over the past few decades as new technologies and methods were developed. The improvement of protein isotopic labeling strategies, the development of three- and four-dimensional spectroscopy, and increases in magnetic field strength with sensitive probes have made NMR applicable to investigate the structures of larger proteins⁹⁷.

To determine a protein structure using solution NMR, the following steps are required: protein purification, sample preparation, data collection, resonance assignment, distance restraint assignment, and structure determination⁹⁸. The resonance and distant restraints assignment are usually derived from the heteronuclear experiments using ¹⁵N and ¹³C isotope labeled sample. Data acquisition and analysis are time-consuming, although new data acquisition strategies and automatic data analysis can be used to shorten the process^{91,99}. For protein-ligand complex structure, distance restraints (NOEs) between the ligand and the target protein are the key factor with respect to acquiring a detailed ligand binding site¹⁰⁰.

The NMR solution structure of protein-drug complex can be used to investigate the underlying mechanism of the protein-ligand interaction. In chapter 2, the lead compound diphenylamine (DPA), which has a significantly higher affinity to cTn in comparison to other compounds from screening, was derived from the NMR structure of cNTnC-cTnI-bepridil complex. We determined the structure of 3-methylDPA bound to cNTnC-cTnI chimera and revealed the small molecule binding pocket and interaction with the target protein. A subsequent study has found that one of the compounds from our NMR screening based on DPA is a sarcomere activator¹⁰¹. The

structure of sarcomere inhibitor W7 bound to cNTnC-cTnI chimera is determined in chapter 3, revealing the small molecule binding position and suggesting the positively charged tail of W7 being the reason of the inhibitory effect. In chapter 4 and 5, we investigated the role of electrostatics and the precise location of the positively charged tail of W7, by comparing the structure of the W7 derivatives (A7 and W6) bound to cNTnC-cTnI chimera.

Physiological and functional testing for the compound of interest is an important addition to the NMR structural work. We are working in close collaboration with physiologists to investigate the positive or negative inotropic effect of small molecules on cardiac muscle fibres. In chapter 4 and 5, calcium-dependent force development of ventricular trabeculae was measured in the absence or presence of W-series (W7, W6, and W4) and A-series (A7, A6, and A4) compounds. The results of physiological experiments indicate that only W7 has a strong inhibitory effect on force development and calcium sensitivity of trabeculae, which aligns with the NMR titration and structural studies. In chapter 6, DN-F01 has been found to bind tightly to cTnC by NMR and fluorescence studies. Furthermore, physiological studies show that DN-F01 strongly inhibits the cardiac myofibril ATPase activity. These results prompted us to focus and investigate more on this direct sarcomere inhibitor. The physiological studies and NMR binding and structural studies complimented each other and helped direct the research.

cNTnC-cTnI chimera as drug target

A number of small molecules are known to bind to the interface between the regulatory cNTnC and the cTnI switch region and alter the calcium binding to cTnC^{75,78,88,102}. The structural studies commonly use samples containing isotope labeled cNTnC, unlabeled cTnI switch peptide, and the small molecules. It is difficult to produce isotope labeled cTnI peptide and the proton resonance of the peptide was always not fully assigned due to signal overlap.

Hybrid proteins have been used to simplify systems with complex protein–protein interactions, including both skeletal and cardiac isoforms of troponin^{103,104}. Since the interface between cNTnC and cTnI switch region is the target for potential

direct sarcomere modulating drugs, cNTnC-cTnI switch region chimeras (cChimera) are constructed for structure, dynamics and small molecule binding studies. cChimera consists of human cNTnC, a linker region, and cTnI switch region. The first cChimera is Thm_cChimera, which the cNTnC and cTnI switch region are attached by a thrombin-protease cleavable linker¹⁰³. Another usage for this chimera is that it is able to produce isotope labeled cTnI switch peptide by protease cleavage for NMR structural studies.

The chimera used for structure study in this thesis is TnI_cChimera, based on the previous design of Thm_cChimera. TnI_cChimera consists of human cNTnC (C35S, C84S), followed by residues 136–163 of cTnI (comprising the inhibitory region residues 136–147 and switch region residues 147–163) and ending with a C-terminal Gly and His-tag. The inhibitory region acts as a linker between cNTnC and the cTnI switch region, and all of the amino acid residues in the TnI_cChimera are derived from the native cTnC or cTnI sequence (except the C-terminal Gly and His-tag). In Chapter 2, the NMR solution structure shows that cChimera faithfully reproduces the native interface between cNTnC and cTnI switch region, with the cNTnC in an open conformation. Solution structures of cChimera bound to several small molecules, including i9⁷⁹, 3-mDPA¹⁰⁵ (Chapter 2), W7¹⁰⁶ (Chapter 3), A7¹⁰⁷ (Chapter 4) and W6 (Chapter 5) have been determined, and cChimera has been proved to be a great tool to investigate the small molecules targeting the interface of cNTnC and cTnI switch region.

The structural and functional studies of small molecules targeting the interface of cNTnC-cTnI switch region have acknowledged the critical role of the cNTnC and cTnI interaction in modulating calcium sensitivity. We proposed that the interface of cNTnC and cTnI switch region within the thin filament is a potential site for the development of drugs that modulate the performance of the heart. Our approach is to directly target the sarcomere without altering the calcium homeostasis in the heart. This thesis aims to provide a more thorough understanding on the underlying mechanisms of several positive and negative direct cardiac sarcomere modulators that target the cNTnC-cTnI interface to aid in drug discovery.

References

1. Opie, L. H. *Heart Physiology: From Cell to Circulation Fourth Edition*. (Lippincott Williams & Wilkins, 2003).
2. Marieb, E. N. & Hoehn, K. *Human Anatomy and Physiology Ninth Edition*. (Pearson Education, 2013).
3. Olson, C. B. & Waud, D. R. On Looking at Electrical Activity of Heart Muscle. *Anesthesiology* **33**, 520–533 (1970).
4. van Weerd, J. H. & Christoffels, V. M. The formation and function of the cardiac conduction system. *Development* **143**, 197–210 (2016).
5. Severs, N. J. The cardiac muscle cell. *BioEssays* **22**, 188–199 (2000).
6. HUXLEY, H. & HANSON, J. Changes in the Cross-Striations of Muscle during Contraction and Stretch and their Structural Interpretation. *Nature* **173**, 973–976 (1954).
7. Hwang, P. M. & Sykes, B. D. Targeting the sarcomere to correct muscle function. *Nat Rev Drug Discov* **14**, 313–28 (2015).
8. Craig, R. & Woodhead, J. L. Structure and function of myosin filaments. *Curr. Opin. Struct. Biol.* **16**, 204–212 (2006).
9. Geeves, M. A. & Holmes, K. C. The molecular mechanism of muscle contraction. *Adv. Protein Chem.* **71**, 161–193 (2005).
10. Agarkova, I. & Perriard, J. C. The M-band: An elastic web that crosslinks thick filaments in the center of the sarcomere. *Trends Cell Biol.* **15**, 477–485 (2005).
11. Flashman, E., Redwood, C., Moolman-Smook, J. & Watkins, H. Cardiac myosin binding protein C: Its role in physiology and disease. *Circ. Res.* **94**, 1279–1289 (2004).
12. Kampourakis, T., Yan, Z., Gautel, M., Sun, Y.-B. & Irving, M. Myosin binding protein-C activates thin filaments and inhibits thick filaments in heart muscle cells. *Proc. Natl. Acad. Sci. U. S. A.* **111**, 18763–8 (2014).
13. Kobayashi, T., Jin, L. & de Tombe, P. P. Cardiac thin filament regulation. *Pflügers Arch. - Eur. J. Physiol.* **457**, 37–46 (2008).
14. Parry, D. A. D. & Squire, J. M. Structural role of tropomyosin in muscle

- regulation: Analysis of the X-ray diffraction patterns from relaxed and contracting muscles. *J. Mol. Biol.* **75**, 33–55 (1973).
15. Narita, A., Yasunaga, T., Ishikawa, T., Mayanagi, K. & Wakabayashi, T. Ca²⁺-induced switching of troponin and tropomyosin on actin filaments as revealed by electron cryo-microscopy¹ Edited by A. Klug. *J. Mol. Biol.* **308**, 241–261 (2001).
 16. Gordon, A. M., Homsher, E. & Regnier, M. Regulation of contraction in striated muscle. *Physiol. Rev.* **80**, 853–924 (2000).
 17. Takeda, S., Yamashita, A., Maeda, K. & Maéda, Y. Structure of the core domain of human cardiac troponin in the Ca(2+)-saturated form. *Nature* **424**, 35–41 (2003).
 18. Li, M. X., Wang, X. & Sykes, B. D. Structural based insights into the role of troponin in cardiac muscle pathophysiology. *J. Muscle Res. Cell Motil.* **25**, 559–79 (2004).
 19. Satyshur, K. A. *et al.* Refined structure of chicken skeletal muscle troponin C in the two-calcium state at 2-Å resolution. *J. Biol. Chem.* **263**, 1628–47 (1988).
 20. Sundaralingam, M. *et al.* Molecular structure of troponin C from chicken skeletal muscle at 3-angstrom resolution. *Science* **227**, 945–8 (1985).
 21. Houdusse, A., Love, M. L., Dominguez, R., Grabarek, Z. & Cohen, C. Structures of four Ca²⁺-bound troponin C at 2.0 Å resolution: further insights into the Ca²⁺-switch in the calmodulin superfamily. *Structure* **5**, 1695–1711 (1997).
 22. Vinogradova, M. V *et al.* Ca(2+)-regulated structural changes in troponin. *Proc. Natl. Acad. Sci. U. S. A.* **102**, 5038–43 (2005).
 23. Slupsky, C. M. & Sykes, B. D. NMR solution structure of calcium-saturated skeletal muscle troponin C. *Biochemistry* **34**, 15953–15964 (1995).
 24. Sia, S. K. *et al.* Structure of Cardiac Muscle Troponin C Unexpectedly Reveals a Closed Regulatory Domain. *J. Biol. Chem.* **272**, 18216–18221 (1997).
 25. Spyropoulos, L. *et al.* Calcium-induced structural transition in the regulatory domain of human cardiac troponin C. *Biochemistry* **36**, 12138–46 (1997).
 26. Li, M. X., Spyropoulos, L. & Sykes, B. D. Binding of cardiac troponin-I147-

- 163 induces a structural opening in human cardiac troponin-C. *Biochemistry* **38**, 8289–98 (1999).
27. Gagné, S. M., Tsuda, S., Li, M. X., Smillie, L. B. & Sykes, B. D. Structures of the troponin C regulatory domains in the apo and calcium-saturated states. *Nat. Struct. Mol. Biol.* **2**, 784–789 (1995).
 28. Strynadka, N. C. *et al.* Structural details of a calcium-induced molecular switch: X-ray crystallographic analysis of the calcium-saturated N-terminal domain of troponin C at 1.75 Å resolution. *J. Mol. Biol.* **273**, 238–55 (1997).
 29. Li, M. X. & Hwang, P. M. Structure and function of cardiac troponin C (TNNC1): Implications for heart failure, cardiomyopathies, and troponin modulating drugs. *Gene* **571**, 153–66 (2015).
 30. Potter, J. D. & Gergely, J. The calcium and magnesium binding sites on troponin and their role in the regulation of myofibrillar adenosine triphosphatase. *J. Biol. Chem.* **250**, 4628–33 (1975).
 31. van Eerd, J.-P. & Takahashi, K. The amino acid sequence of bovine cardiac troponin-C. Comparison with rabbit skeletal troponin-C. *Biochem. Biophys. Res. Commun.* **64**, 122–127 (1975).
 32. McKay, R. T., Tripet, B. P., Hodges, R. S. & Sykes, B. D. Interaction of the Second Binding Region of Troponin I with the Regulatory Domain of Skeletal Muscle Troponin C as Determined by NMR Spectroscopy. *J. Biol. Chem.* **272**, 28494–28500 (1997).
 33. Gasmi-Seabrook, G. M. C. *et al.* Solution Structures of the C-Terminal Domain of Cardiac Troponin C Free and Bound to the N-Terminal Domain of Cardiac Troponin I^{†,‡}. *Biochemistry* **38**, 8313–8322 (1999).
 34. Finley, N. L., Howarth, J. W. & Rosevear, P. R. Structure of the Mg²⁺-Loaded C-Lobe of Cardiac Troponin C Bound to the N-Domain of Cardiac Troponin I: Comparison with the Ca²⁺-Loaded Structure^{†,‡}. *Biochemistry* **43**, 11371–11379 (2004).
 35. Lindhout, D. A. & Sykes, B. D. Structure and Dynamics of the C-domain of Human Cardiac Troponin C in Complex with the Inhibitory Region of Human

- Cardiac Troponin I. *J. Biol. Chem.* **278**, 27024–27034 (2003).
36. Solaro, R. J., Henze, M. & Kobayashi, T. Integration of troponin I phosphorylation with cardiac regulatory networks. *Circ. Res.* **112**, 355–66 (2013).
 37. Howarth, J. W., Meller, J., Solaro, R. J., Trewhella, J. & Rosevear, P. R. Phosphorylation-dependent conformational transition of the cardiac specific N-extension of troponin I in cardiac troponin. *J. Mol. Biol.* **373**, 706–22 (2007).
 38. Hwang, P. M., Cai, F., Pineda-Sanabria, S. E., Corson, D. C. & Sykes, B. D. The cardiac-specific N-terminal region of troponin I positions the regulatory domain of troponin C. *Proc. Natl. Acad. Sci. U. S. A.* **111**, 14412–7 (2014).
 39. Vassylyev, D. G., Takeda, S., Wakatsuki, S., Maeda, K. & Maeda, Y. Crystal structure of troponin C in complex with troponin I fragment at 2.3-Å resolution. *Proc. Natl. Acad. Sci.* **95**, 4847–4852 (1998).
 40. Yamada, Y., Namba, K. & Fujii, T. Cardiac muscle thin filament structures reveal calcium regulatory mechanism. *Nat. Commun.* **11**, 153 (2020).
 41. McKillop, D. F. & Geeves, M. A. Regulation of the interaction between actin and myosin subfragment 1: evidence for three states of the thin filament. *Biophys. J.* **65**, 693–701 (1993).
 42. WHO. *World Health Statistics 2017: Monitoring health for the SDGs.* (2017).
 43. An Account of the Fox Glove, and Some of Its Medical Uses; with Practical Remarks on Dropsy, and Other Diseases. *L. Med J.* (1785).
 44. Ahmed, A. *et al.* Effects of Digoxin on Morbidity and Mortality in Diastolic Heart Failure. *Circulation* **114**, 397–403 (2006).
 45. Sonnenblick, E. H., Frishman, W. H. & LeJemtel, T. H. Dobutamine: a new synthetic cardioactive sympathetic amine. *N. Engl. J. Med.* **300**, 17–22 (1979).
 46. Pollesello, P., Papp, Z. & Papp, J. G. Calcium sensitizers: What have we learned over the last 25 years? *Int. J. Cardiol.* **203**, 543–548 (2016).
 47. Boswell-Smith, V., Spina, D. & Page, C. P. Phosphodiesterase inhibitors. *Br. J. Pharmacol.* **147**, S252–S257 (2006).
 48. Rüegg, J. C., Pfitzer, G., Eubler, D. & Zeugner, C. Effect on contractility of

- skinned fibres from mammalian heart and smooth muscle by a new benzimidazole derivative, 4,5-dihydro-6-[2-(4-methoxyphenyl)-1H-benzimidazol-5-yl]-5-methyl-3(2H)-pyridazinone. *Arzneimittelforschung*. **34**, 1736–8 (1984).
49. Walter, M. *et al.* Pimobendane (UD-CG 115 BS) in the treatment of severe congestive heart failure. An acute haemodynamic cross-over and double-blind study with two different doses. *Br. J. Clin. Pharmacol.* **25**, 323–329 (1988).
 50. Solaro, R. J., Fujino, K. & Sperelakis, N. The positive inotropic effect of pimobendan involves stereospecific increases in the calcium sensitivity of cardiac myofilaments. *J. Cardiovasc. Pharmacol.* **14 Suppl 2**, S7-12 (1989).
 51. Kato, K. Clinical Efficacy and Safety of Pimobendan in Treatment of Heart Failure – Experience in Japan. *Cardiology* **88**, 28–36 (1997).
 52. Lubsen, J. *et al.* Effect of pimobendan on exercise capacity in patients with heart failure: main results from the Pimobendan in Congestive Heart Failure (PICO) trial. *Heart* **76**, 223–231 (1996).
 53. Boyle, K. L. & Leech, E. A review of the pharmacology and clinical uses of pimobendan. *J. Vet. Emerg. Crit. Care* **22**, 398–408 (2012).
 54. Reina-Doreste, Y. *et al.* Case-control study of the effects of pimobendan on survival time in cats with hypertrophic cardiomyopathy and congestive heart failure. *J. Am. Vet. Med. Assoc.* **245**, 534–539 (2014).
 55. Pollesello, P. *et al.* Binding of a new Ca²⁺ sensitizer, levosimendan, to recombinant human cardiac troponin C. *J. Biol. Chem.* **269**, 28584–90 (1994).
 56. Nieminen, M. S. *et al.* Levosimendan: current data, clinical use and future development. *Hear. lung Vessel.* **5**, 227–45 (2013).
 57. Papp, Z. *et al.* Pharmacological Therapy Levosimendan Efficacy and Safety : 20 years of SIMDAX in Clinical Use Pharmacological Therapy. (2020).
 58. Michaels, A. D. *et al.* Effects of Intravenous Levosimendan on Human Coronary Vasomotor Regulation, Left Ventricular Wall Stress, and Myocardial Oxygen Uptake. *Circulation* **111**, 1504–1509 (2005).
 59. Sorsa, T., Pollesello, P., Permi, P., Drakenberg, T. & Kilpeläinen, I. Interaction

- of levosimendan with cardiac troponin C in the presence of cardiac troponin I peptides. *J. Mol. Cell. Cardiol.* **35**, 1055–61 (2003).
60. Papp, Z. *et al.* Levosimendan: molecular mechanisms and clinical implications: consensus of experts on the mechanisms of action of levosimendan. *Int. J. Cardiol.* **159**, 82–7 (2012).
 61. Mebazaa, A. *et al.* Levosimendan vs Dobutamine for Patients With Acute Decompensated Heart Failure. *JAMA* **297**, 1883 (2007).
 62. Morgan, B. P. *et al.* Discovery of omecamtiv mecarbil the first, selective, small molecule activator of cardiac myosin. *ACS Med. Chem. Lett.* **1**, 472–477 (2010).
 63. Malik, F. I. *et al.* Cardiac Myosin Activation: A Potential Therapeutic Approach for Systolic Heart Failure. *Science (80-.).* **331**, 1439–1443 (2011).
 64. Teerlink, J. R. *et al.* Dose-dependent augmentation of cardiac systolic function with the selective cardiac myosin activator, omecamtiv mecarbil: A first-in-man study. *Lancet* **378**, 667–675 (2011).
 65. Cleland, J. G. F. *et al.* The effects of the cardiac myosin activator, omecamtiv mecarbil, on cardiac function in systolic heart failure: A double-blind, placebo-controlled, crossover, dose-ranging phase 2 trial. *Lancet* **378**, 676–683 (2011).
 66. Teerlink, J. R. *et al.* Acute Treatment with Omecamtiv Mecarbil to Increase Contractility in Acute Heart Failure: The ATOMIC-AHF Study. *J. Am. Coll. Cardiol.* **67**, 1444–1455 (2016).
 67. Teerlink, J. R. *et al.* Chronic Oral Study of Myosin Activation to Increase Contractility in Heart Failure (COSMIC-HF): a phase 2, pharmacokinetic, randomised, placebo-controlled trial. *Lancet* **388**, 2895–2903 (2016).
 68. Teerlink, J. R. *et al.* Omecamtiv Mecarbil in Chronic Heart Failure With Reduced Ejection Fraction: Rationale and Design of GALACTIC-HF. *JACC Hear. Fail.* **8**, 329–340 (2020).
 69. Klein, B. A. *et al.* Reversible Covalent Reaction of Levosimendan with Cardiac Troponin C in Vitro and in Situ. *Biochemistry* **57**, 2256–2265 (2018).
 70. Lugnier, C., Follenius, A., Gerard, D. & Stoclet, J. C. Bepridil and flunarizine as calmodulin inhibitors. *Eur. J. Pharmacol.* **98**, 157–158 (1984).

71. Solaro, R. J., Bousquet, P. & Johnson, J. D. Stimulation of cardiac myofilament force, ATPase activity and troponin C Ca⁺⁺ binding by bepridil. *J. Pharmacol. Exp. Ther.* **238**, 502–7 (1986).
72. Kleerekoper, Q., Liu, W., Choi, D. & Putkey, J. A. Identification of binding sites for bepridil and trifluoperazine on cardiac troponin C. *J. Biol. Chem.* **273**, 8153–8160 (1998).
73. Li, Y., Love, M. L., Putkey, J. A. & Cohen, C. Bepridil opens the regulatory N-terminal lobe of cardiac troponin C. *Proc. Natl. Acad. Sci. U. S. A.* **97**, 5140–5 (2000).
74. Abusamhadneh, E. *et al.* Interaction of bepridil with the cardiac troponin C/troponin I complex. *FEBS Lett.* **506**, 51–54 (2001).
75. Wang, X., Li, M. X. & Sykes, B. D. Structure of the regulatory N-domain of human cardiac troponin C in complex with human cardiac troponin I147-163 and bepridil. *J. Biol. Chem.* **277**, 31124–33 (2002).
76. Szilágyi, S. *et al.* The effects of levosimendan and OR-1896 on isolated hearts, myocyte-sized preparations and phosphodiesterase enzymes of the guinea pig. *Eur. J. Pharmacol.* **486**, 67–74 (2004).
77. Sorsa, T. *et al.* Binding of Levosimendan, a Calcium Sensitizer, to Cardiac Troponin C. *J. Biol. Chem.* **276**, 9337–9343 (2001).
78. Robertson, I. M., Sun, Y.-B., Li, M. X. & Sykes, B. D. A structural and functional perspective into the mechanism of Ca²⁺-sensitizers that target the cardiac troponin complex. *J. Mol. Cell. Cardiol.* **49**, 1031–1041 (2010).
79. Pineda-Sanabria, S. E., Robertson, I. M., Sun, Y.-B. B., Irving, M. & Sykes, B. D. Probing the mechanism of cardiovascular drugs using a covalent levosimendan analog. *J. Mol. Cell. Cardiol.* **92**, 174–184 (2016).
80. Robertson, I. M. *et al.* Reversible Covalent Binding to Cardiac Troponin C by the Ca²⁺-Sensitizer Levosimendan. *Biochemistry* **55**, 6032–6045 (2016).
81. Klein, B. A. *et al.* Thioimidate Bond Formation between Cardiac Troponin C and Nitrile-containing Compounds. *ACS Med. Chem. Lett.* **10**, 1007–1012 (2019).

82. Hidaka, H. *et al.* A Novel Vascular Relaxing Agent, N-(6-Aminohexyl)-5-Chloro-1-Naphthalenesulfonamide Which Affects Vascular Smooth Muscle Actomyosin. *J. Pharmacol. Exp. Ther.* **207**, 8–15 (1978).
83. Hidaka, H. *et al.* Calcium-regulated modulator protein interacting agents inhibit smooth muscle calcium-stimulated protein kinase and ATPase. *Mol. Pharmacol.* **17**, 66–72 (1980).
84. Adhikari, B. B. & Wang, K. Interplay of Troponin- and Myosin-Based Pathways of Calcium Activation in Skeletal and Cardiac Muscle: The Use of W7 as an Inhibitor of Thin Filament Activation. *Biophys. J.* **86**, 359–370 (2004).
85. Hoffman, R. M. B., Li, M. X. & Sykes, B. D. The binding of W7, an inhibitor of striated muscle contraction, to cardiac troponin C. *Biochemistry* **44**, 15750–15759 (2005).
86. Li, M. X., Hoffman, R. M. B. & Sykes, B. D. Interaction of Cardiac Troponin C and Troponin I with W7 in the Presence of Three Functional Regions of Cardiac Troponin I †. *Biochemistry* **45**, 9833–9840 (2006).
87. Hoffman, R. M. B. & Sykes, B. D. Structure of the Inhibitor W7 Bound to the Regulatory Domain of Cardiac Troponin C. *Biochemistry* **48**, 5541–5552 (2009).
88. Oleszczuk, M., Robertson, I. M., Li, M. X. & Sykes, B. D. Solution structure of the regulatory domain of human cardiac troponin C in complex with the switch region of cardiac troponin I and W7: The basis of W7 as an inhibitor of cardiac muscle contraction. *J. Mol. Cell. Cardiol.* **48**, 925–933 (2010).
89. Thompson, B. R., Martindale, J. & Metzger, J. M. Sarcomere neutralization in inherited cardiomyopathy: small-molecule proof-of-concept to correct hyper-Ca²⁺-sensitive myofilaments. *Am. J. Physiol. Heart Circ. Physiol.* **311**, H36-43 (2016).
90. Pellecchia, M. *et al.* Perspectives on NMR in drug discovery: a technique comes of age. *Nat. Rev. Drug Discov.* **7**, 738–745 (2008).
91. Becker, W., Bhattiprolu, K. C., Gubensäk, N. & Zangger, K. Investigating Protein–Ligand Interactions by Solution Nuclear Magnetic Resonance

- Spectroscopy. *ChemPhysChem* **19**, 895–906 (2018).
92. Williamson, M. P. Using chemical shift perturbation to characterise ligand binding. *Prog. Nucl. Magn. Reson. Spectrosc.* **73**, 1–16 (2013).
 93. Wishart, D. S., Sykes, B. D. & Richards, F. M. Relationship between nuclear magnetic resonance chemical shift and protein secondary structure. *J. Mol. Biol.* **222**, 311–333 (1991).
 94. Hafsa, N. E., Arndt, D. & Wishart, D. S. CSI 3.0: A web server for identifying secondary and super-secondary structure in proteins using NMR chemical shifts. *Nucleic Acids Res.* **43**, W370–W377 (2015).
 95. Shen, Y., Delaglio, F., Cornilescu, G. & Bax, A. TALOS+: A hybrid method for predicting protein backbone torsion angles from NMR chemical shifts. *J. Biomol. NMR* **44**, 213–23 (2009).
 96. Marion, D. An introduction to biological NMR spectroscopy. *Mol. Cell. Proteomics* **12**, 3006–3025 (2013).
 97. Doerr, A. Solution for solution structures. *Nat. Phys.* **4**, S15–S15 (2008).
 98. Li, Q. & Kang, C. B. A practical perspective on the roles of solution NMR spectroscopy in drug discovery. *Molecules* **25**, 1–19 (2020).
 99. Hyberts, S. G., Arthanari, H. & Wagner, G. Applications of Non-Uniform Sampling and Processing. in *Topics in Current Chemistry* **316**, 125–148 (2011).
 100. Orts, J. & Gossert, A. D. Structure determination of protein-ligand complexes by NMR in solution. *Methods* **138–139**, 3–25 (2018).
 101. Tikunova, S. B. *et al.* 3-Chlorodiphenylamine activates cardiac troponin by a mechanism distinct from bepridil or TFP. *J. Gen. Physiol.* **151**, 9–17 (2019).
 102. Robertson, I. M., Baryshnikova, O. K., Li, M. X. & Sykes, B. D. Defining the binding site of levosimendan and its analogues in a regulatory cardiac troponin C-troponin I complex. *Biochemistry* **47**, 7485–95 (2008).
 103. Pineda-Sanabria, S. E., Julien, O. & Sykes, B. D. Versatile Cardiac Troponin Chimera for Muscle Protein Structural Biology and Drug Discovery. *ACS Chem. Biol.* **9**, 2121–2130 (2014).
 104. Julien, O. *et al.* Is there nascent structure in the intrinsically disordered region

- of troponin I? *Proteins* **79**, 1240–1250 (2011).
105. Cai, F. *et al.* Structures reveal details of small molecule binding to cardiac troponin. *J. Mol. Cell. Cardiol.* **101**, 134–144 (2016).
 106. Cai, F., Hwang, P. M. & Sykes, B. D. Structural Changes Induced by the Binding of the Calcium Desensitizer W7 to Cardiac Troponin. *Biochemistry* **57**, 6461–6469 (2018).
 107. Cai, F., Robertson, I. M., Kampourakis, T., Klein, B. A. & Sykes, B. D. The Role of Electrostatics in the Mechanism of Cardiac Thin Filament Based Sensitizers. *ACS Chem. Biol.* **15**, 2289–2298 (2020).

Chapter 2

Structures Reveal Details of Small Molecule Binding to Cardiac Troponin

Fangze Cai¹, Monica X. Li², Sandra E. Pineda-Sanabria¹, Shorena Gelozia³,
Steffen Lindert⁴, Frederick West³, Brian D. Sykes¹, Peter M. Hwang^{1,2}

¹Department of Biochemistry, University of Alberta, Edmonton, AB, Canada.

²Department of Medicine, University of Alberta, Edmonton, AB, Canada.

³Department of Chemistry, University of Alberta, Edmonton, AB, Canada.

⁴Department of Chemistry and Biochemistry, Ohio State University, Columbus, OH, USA.

A version of this chapter has been previously published: Cai, F., Li, M.X., Pineda-Sanabria, S.E., Gelozia, S., Lindert, S., West, F., Sykes, B.D. & Hwang, P.M. Structures reveal details of small molecule binding to cardiac troponin. *J. Mol. Cell. Cardiol.* **101**, 134–144 (2016).

Contribution: FC and MXL performed drug titrations for screening. FC and PMH acquired the NMR spectra for structure determination. FC purified the protein, assigned the protein chemical shift, analyzed the data and solved the structures with help of SEPS and PMH. SG and FW synthesized all SHG-compounds. SL performed virtual screening. FC wrote the manuscript with help of PMH and BDS. PMH led the research.

Summary

In cardiac and skeletal muscle, the troponin complex turns muscle contraction on and off in a calcium-dependent manner. Many small molecules are known to bind to the troponin complex to modulate its calcium binding affinity, and this may be useful in a broad range of conditions in which striated muscle function is compromised, such as congestive heart failure. As a tool for developing drugs specific for the cardiac isoform of troponin, we have designed a chimeric construct (cChimera) consisting of

the regulatory N-terminal domain of cardiac troponin C (cNTnC) fused to the switch region of cardiac troponin I (cTnI), mimicking the key binding event that turns on muscle contraction. We demonstrate by solution NMR spectroscopy that cChimera faithfully reproduces the native interface between cTnI and cNTnC.

We determined that small molecules based on diphenylamine can bind to cChimera with a K_D as low as 10 μM . Solution NMR structures show that minimal structural perturbations in cChimera are needed to accommodate 3-methyldiphenylamine (3-mDPA), which is probably why it binds with higher affinity than previously studied compounds like bepridil, despite its significantly smaller size. The unsubstituted aromatic ring of 3-mDPA binds to an inner hydrophobic pocket adjacent to the central beta sheet of cNTnC. However, the methyl-substituted ring is able to bind in two different orientations, either inserting into the cNTnC-cTnI interface or “flipping out” to form contacts primarily with helix C of cNTnC. Our work suggests that preservation of the native interaction between cNTnC and cTnI is key to the development of a high affinity cardiac troponin-specific drug.

Introduction

Cardiovascular disease is the number one cause of death worldwide¹, and heart failure is the end stage of almost all heart disease. Heart failure occurs when the heart is unable to pump sufficient blood to satisfy the needs of the body. Impaired cardiac muscle contraction results in systolic heart failure, also referred to as heart failure with reduced ejection fraction (HFrEF). By far, the most common cause of HFrEF is ischemic cardiomyopathy. However, in the absence of atherosclerotic coronary disease or valvular abnormalities, a wide range of etiologies encompassing infiltrative, infectious, autoimmune, toxic, hormonal, and genetic causes, can give rise to dilated cardiomyopathy (DCM)². Over time, the volume overload that develops in HFrEF causes the heart muscle to further dilate, thin, and scar, making it even more difficult to generate force.

Positive inotropes, which increase the contractility of heart muscle to enhance cardiac output, should theoretically be useful in the treatment of systolic heart failure. Two inotropes used in acute decompensated heart failure are dobutamine and

milrinone, both of which upregulate sympathetic β_1 -adrenergic stimulated pathways to increase heart rate and stroke volume³. However, inotropes acting on these pathways increase the oxygen demand of the heart and further increase mortality by precipitating life-threatening arrhythmias and systemic hypotension. A different class of positive inotropes is the calcium sensitizers, which increase the contractile response of the heart to calcium, in contrast to calcium mobilizers like dobutamine and milrinone. The first calcium sensitizer to reach large-scale clinical trials is levosimendan⁴. It was found to increase cardiac output without increasing oxygen demand⁵. Earlier trials showed an improved survival in the treatment of acute decompensated systolic heart failure, but larger phase III trials did not show a mortality benefit^{6,7}.

Levosimendan and its active metabolite, OR-1896, bind to cardiac troponin (cTn)^{8,9}. The protein switch that turns contraction on and off in a calcium-dependent manner. The heterotrimeric cTn complex is composed of the calcium-binding subunit troponin C (cTnC), the inhibitory subunit troponin I (cTnI), and the tropomyosin-binding subunit troponin T (cTnT)¹⁰. Under resting calcium concentrations, the troponin complex maintains tropomyosin in a position that blocks actin–myosin interaction¹¹. When the intracellular calcium concentration increases, calcium binding to the N-terminal regulatory domain of cTnC (cNTnC) induces binding of the switch region of cTnI (residues 147-163)¹². This in turn promotes the dissociation of the cTnI inhibitory region (residues 135-147) from actin, shifting tropomyosin to expose the myosin-binding sites on actin and allowing cardiac contraction to proceed. Since cNTnC is the calcium-dependent switch for contraction and relaxation in cardiac muscle, it is a prime target for developing calcium sensitizing drugs.

While levosimendan has been shown to bind to cNTnC^{13,14}, it has been shown to impact the activity of other proteins as well, including type 3 phosphodiesterase¹⁵ and ATP-sensitive potassium channels^{16,17}. It is possible that off-target binding could potentially give rise to unintended adverse effects, like hypotension. We aim to develop calcium sensitizers that are more specific for cardiac troponin. In this regard, it is interesting to note that tirasemtiv (CK-2017357) is a drug that binds to skeletal troponin, though it shows no activity towards the cardiac isoform¹⁸.

In the current study, we demonstrate that compounds based on the small molecule diphenylamine are able to bind to cardiac troponin with reasonably high affinity ($K_D \sim 10 \mu\text{M}$) given their small size. Our solution NMR structures reveal how one of these compounds, 3-methyldiphenylamine, binds to a deep but narrow hydrophobic cavity in the troponin C-I complex. Optimizing the fit to this tight cavity will be essential to developing high affinity cardiac troponin-modulating compounds.

Material and methods

cChimera design, expression, and purification

Hybrid proteins have been used to simplify systems with complex protein-protein interactions^{19,20}, including both skeletal and cardiac muscle isoforms of troponin^{21,22}. Since dfbp-o and other compounds are known to bind to the interface between NTnC and TnI switch peptide²³, we developed a cardiac troponin C-troponin I chimera, cChimera, in which the switch region of cTnI is fused to the C terminus of cNTnC, building upon the previous design cNTnC-linker-switch peptide 144-173²¹. cChimera begins with residues 1 to 90 of human cNTnC (C35S, C84S), followed by residues 136-163 of cTnI (comprising the inhibitory 136-147 and switch 147-163 regions) and ending with a C-terminal Gly and His-tag (see Figure 2.1). The inhibitory region acts as linker between cNTnC and the cTnI switch region, and residues 136 and 137 of the cTnI inhibitory region are coincidentally the same as residues 91 and 92 of cTnC. Unlike the previous chimera, in which the engineered linker region contains a protease cleavage site²¹, all of the amino acids residues in our new cNTnC-cTnI chimera are derived from the native cTnC or cTnI sequence, with the exception of the C-terminal Gly and His-tag. Our new 125-amino acid 14.2 kDa cChimera construct has the following advantages over the previous construct²¹: native N-terminus of cTnC, switch region of cTnI extended N-terminally to include the inhibitory region (residues 136-147), which also serves as the linker to cNTnC, C35S and C84S double mutation to avoid issues with cysteine oxidation, and shortened C-terminal tail of cTnI, limiting the number of disordered residues contributing to NMR spectral overlap.

```

1    MDDIYKAAVE QLTEEQKNEF KAAFDIFVLG AEDGSISTKE LGKVMRMLGQ
51   NPTPEELQEM IDEVDEDGSG TVDFDEFLVM MVRSMKDDSK GKFKRPTLRR
                                     136
101  VRISADAMMQ ALLGARAKGH HHHHH 125
                                     163

```

Figure 2.1. Sequence of cNTnC-cTnI switch region cChimera.

cChimera sequence: residues 1-90 of cNTnC (C35S and C84S are shown in bold), followed by residues 136-163 of cTnI (shown in grey, overlapping residues are shown underlined), and ending with a C-terminal His-tag.

The expression plasmid for the cChimera was produced by DNA 2.0, with a high copy number origin of replication, ampicillin selection, and IPTG-inducible T5 RNA polymerase (which uses native *Escherichia coli* RNA polymerase) promoter. Isotope-enriched [¹⁵N, ¹³C]-cNTnC-cTnI [136-163] chimera were expressed in *E. coli* BL21(DE3) as previously described²⁴. The expression of cChimera was carried out in 1 L of minimal M9 medium, containing 9 g Na₂HPO₄ and 2.5 g KH₂PO₄ at pH 7.3-7.4. To the autoclaved phosphate solution was added a filter-sterilized solution containing 1 mL of 1 M MgSO₄, 1 mL of 100 mM CaCl₂, 1 mg of biotin, 200 mg of thiamine, 1 g [¹⁵N] NH₄SO₄ (99.9 atom %), 3 g [¹³C] glucose (99.0 atom %) dissolved in 20 mL ddH₂O, and 1 mL of 10% ampicillin. Cells from a 2 L culture were grown to a cell density between A₆₀₀ 0.7 and 1.0 and then induced for 6 h with 1 mM IPTG. Cells were harvested by centrifugation at 5000 rpm (4420 ×g) for 15 min and then resuspended in 20 mL buffer containing 50 mM Tris (pH 8.0), 10 mM MgSO₄, 10 µg/mL DNase and 1 mM CaCl₂. Cells were lysed by adding 20 mg of lysozyme and 200 mg of deoxycholic acid, with mechanical homogenization to break cell clumps. The cell lysate was clarified by centrifugation at 15,000 rpm (27,200 ×g) and then syringe-filtered using a 0.8 µm filter. The supernatant was applied to a Ni-NTA column equilibrated with binding buffer (20 mM Tris-HCl, 0.3 M NaCl, 10 mM imidazole, 1 mM CaCl₂), washed with the same buffer containing 80 mM imidazole, and then eluted with the same buffer with 250 mM Imidazole. Purified fractions were dialyzed against 5 mM ammonium bicarbonate and 10 µM CaCl₂ for three days and then lyophilized.

Protein identity and purity >95% were confirmed by gel electrophoresis and mass spectrometry. Yield was ~ 60-100 mg purified protein per liter of growth culture.

Chemicals

Bepridil (N-benzyl-N-[3-(2-methylpropoxy)-2-(pyrrolidin-1-yl)propyl]aniline) and 3-methyldiphenylamine were purchased from Sigma-Aldrich. 3-Chlorodiphenylamine was purchased from Toronto Research Chemicals Inc. All “NCI” compounds in the study were provided by the Developmental Therapeutics Program (DTP) at the National Cancer Institute (NCI). All “Chembridge” compounds were provided by ChemBridge Corp. All “SHG” compounds were synthesized in-house, with the identity and purity confirmed by NMR spectroscopy.

NMR spectroscopy

NMR samples contained 0.1-0.6 mM cChimera in 100 mM KCl, 10 mM imidazole buffer pH ~6.8, 5-10 mM CaCl₂, and 0.25 mM 2,2-dimethyl-2-silapentane-5-sulfonate-d₆ sodium salt (DSS-d₆) as an NMR internal reference in 95/5% H₂O/ D₂O or 100% D₂O. Stock solutions of 10 to 50 mM of small compounds were prepared in DMSO-d₆ (Cambridge Isotopes Inc.) and added independently in aliquots to the protein sample. By the end of each titration, the addition of DMSO-d₆ did not exceed 10% of the sample volume. NMR data were acquired on a Varian Inova 500 MHz or 800 MHz spectrometer at 30 °C. Both spectrometers are equipped with triple resonance probes with pulsed field gradients.

Drug titrations

The binding of 3-methyl diphenylamine (3-mDPA) to cChimera was monitored using 2D-¹H,¹⁵N-HSQC and 2D-¹H,¹³C-HSQC NMR spectra. We titrated 0.15 mM ¹⁵N-cChimera with 0.01, 0.03, 0.06, 0.1, 0.2, 0.4 and 0.7 mM of 3-mDPA while acquiring 2D-¹H,¹⁵N-HSQC spectrum. We titrated 0.25 mM ¹³C,¹⁵N-cChimera with 0.05, 0.1, 0.25, 0.5 and 0.8 mM of 3-mDPA while acquiring 2D-¹H,¹³C-HSQC spectrum. The solubility of 3-mDPA in NMR buffer is ~0.15 mM, so precipitation became increasingly apparent towards the end of the titration, a phenomenon that

complicated the calculation of K_D in most of our drug titrations. Dilution by addition of drug stock solution was taken into consideration. Chemical shift changes at each titration point were used by our in-house software, *xcrvfit* (www.bionmr.ualberta.ca/bds/software/xcrvfit), to calculate dissociation constants, K_D .

For drug screening purposes, we used a 3-point titration to estimate K_D . 2D- ^1H , ^{15}N -HSQC spectra were acquired to monitor the titration of 0.2 mM ^{15}N -cChimera with 0, 0.1, and 1 mM drug, yielding 3 points with [drug]/ [protein] ratios with 0, 0.5, and 5 equivalents. In the event of drug compound precipitation during the titration, K_D would be underestimated because the observed chemical shift changes plateau early due to precipitation instead of protein saturation. Thus, the 3-point titration provides a lower bound estimate of K_D . To provide an upper bound estimate for K_D for insoluble compounds, the last titration point was removed and replaced by chemical shifts corresponding to cChimera fully saturated with 3-chlorodiphenylamine, the compound with the highest affinity in this study, displaying some of the largest chemical shift changes. This seemed to be a reasonable approximation, given that the observed chemical shift change patterns were similar in all titrations of DPA-based compounds.

NMR experiments for structure calculation

The backbone ^1H , ^{15}N , and ^{13}C chemical shift assignments for cChimera (both with and without 3-mDPA) were obtained by analyzing 3D CBCA(CO)NH, 3D HNCACB, 3D HN(CA)CO and 3D HNCO experiments. 3D (H)C(CO)NH-TOCSY (total correlation spectroscopy) and H(C)(CO)NH-TOCSY experiments were used to obtain side-chain ^1H and ^{13}C chemical shift assignments. Moreover, 3D HNHB and 3D HN(CO)HB experiments were used in combination with 3D ^{15}N -edited NOESY (75 ms mixing time) to obtain stereospecific assignment for β methylene protons and χ_1 dihedral angles. However, this strategy worked reliably only for residues with trans χ_1 dihedral angle (C γ and N at 180°) due to the low inherent sensitivity of the HN(CO)HB experiment, so that we were unable to distinguish between gauche+ and gauche- conformations. Stereospecific assignments of Val, Leu methyl groups were derived from 2D constant time ^1H , ^{13}C -HSQC of [^{15}N , 10% ^{13}C]-cChimera (pro-R methyl

groups were in phase with alanine methyl groups)²⁵. Aromatic side-chain resonances were assigned using an aromatic 3D ¹³C-edited NOESY-HSQC.

3D ¹⁵N-edited NOESY-HSQC (mixing time 75 ms), and 3D ¹³C-edited NOESY (mixing time 100 ms) were obtained to provide intramolecular (within the protein cChimera) distance restraints. 2D ¹³C,¹⁵N-double-filtered NOESY (150 ms mixing time) experiments were obtained on 3-mDPA in complex with ¹³C,¹⁵N-labeled cChimera to obtain chemical shift assignments and intramolecular distance restraints for bound 3-mDPA. Intermolecular distance restraints between 3-mDPA and cChimera were derived from a 3D ¹³C-filtered/edited NOESY-HSQC (mixing times: 75 ms) experiment. Protons from the methyl-containing aromatic ring could not be observed (though the methyl group itself was observable), because of broadening of 3-mDPA resonances. These resonances could still be observed in the 3D ¹³C-edited NOESY-HSQC, due to the shorter pulse sequence employed. Intermolecular restraints between 3-mDPA and cChimera could be easily identified in this unfiltered experiment (containing both intra- and intermolecular NOEs) by comparing the spectrum derived from cChimera bound to 3-mDPA with that from cChimera alone. This was the most sensitive method for obtaining intermolecular NOEs. VNMRJ v.2.21B (Varian, Inc.) was used for the analysis of one-dimensional NMR spectra, and all 2D and 3D NMR data were processed with NMRPipe²⁶ and analyzed with NMRViewJ²⁷, using scripts written in-house.

Structure calculation

Backbone ϕ - and ψ -dihedral angle restraints were obtained using TALOS+²⁸, which makes predictions based on backbone chemical shifts (¹H α , ¹³C', ¹³C α , ¹³C β , ¹⁵N, and ¹HN). Restraints were used only for those residues for which there was complete agreement from all 10 nearest database hits with a chemical shift-derived backbone order parameter >0.65²⁹.

NOE-derived distance restraints for the cChimera protein were generated using ARIA 2.3^{30,31}, using default settings. ARIA automatically generates distance restraints based on peak tables derived from NOESY spectra. Initially, most restraints are ambiguous due to chemical shift degeneracy. With each successive cycle of restrained

molecular dynamics with simulated annealing using CNS 1.21³², generated structures are used to resolve ambiguities, and the proportion of unambiguous distance restraints increases with each cycle (eight in total). The frequency window tolerances for assigning NOEs were 0.02 and 0.03 ppm for direct and indirect proton dimensions, respectively, and 0.2 ppm for nitrogen and carbon dimensions. Fairly narrow tolerance ranges could be employed because the chemical shift assignments were adjusted to exactly match signals in the NOESY spectra. Dihedral angle restraints derived from TALOS+ were incorporated in the calculation. We found that two spectral artifacts created problems for the ARIA program – diagonal peaks needed to be removed (as specified in the ARIA graphical user interface), and sinc wiggles also had to be manually removed from the NOESY peak lists. Moreover, in our experience, mobile regions of the protein would give rise to high intensity peaks that ARIA erroneously assigns to cause structural distortions if chemical shift assignments are not 100% complete. Thus, NOE cross-peaks involving unstructured regions of the protein were also removed from peak lists after manual inspection confirmed that there was no long range NOEs that could contribute to protein folding.

The web-based server, PRODRG³³, was used to generate topology and parameter files for 3-mDPA. Calcium was not included in the ARIA structure calculations, but 3-mDPA was included. Intermolecular NOEs between 3-mDPA and cChimera were not included in the peak lists. Instead, these NOE peaks were manually assigned and used to generate distance restraints that were added to the ARIA structure calculations. All intramolecular protein NOEs were calibrated automatically and assigned iteratively by ARIA; the final assignments were checked manually for errors. 80 conformers with lowest energy were calculated for each iteration; after the eighth iteration, 40 conformers with the lowest restraint energies were refined in a shell of water, and 8 conformers with the lowest total energies were selected.

Virtual screening of DPA-like Compounds

DPA-like compounds (based on diphenylmethylene, diphenylether, and diphenylamine) were extracted from the NCI database. For this the NCI substructure search was used for SMILES strings c2ccc(Nc1cccc1)cc2, c2ccc(Cc1cccc1)cc2, and

c2ccc(Oc1ccccc1)cc2. A total of 15,876 compounds were retrieved. Those were prepared for docking using LigPrep with the protocol described previously³⁴. This generated 23,438 compounds. Those compounds were docked into the hydrophobic pocket of the cardiac troponin complex using Glide XP³⁵. The compounds were subsequently ordered by predicted docking score and ligand efficiency. Lastly, NCI compounds with every possible single substitution at the 3 (meta) position (based on diphenylmethylen, diphenylether, and diphenylamine) were identified using the NCI substructure search tool. A total of 61 compounds were identified which were again prepared for docking using LigPrep, generating a total of 72 compounds. After Glide XP docking, those 72 compounds were ranked by docking score. Compounds were selected for NMR binding studies if they scored well, were predicted to be soluble, had a molecular weight <300 Da, and were available from NCI.

Results and discussion

Structure of cChimera

The NMR solution structure of the cTnC₁₋₉₀-cTnI₁₃₆₋₁₆₃ chimera (cChimera) was determined in the absence of any drug (Figure 2.2a). As shown in Figure 2.2b, the NMR structure of cChimera superimposes well to the corresponding regions in the X-ray crystal structure of the cardiac troponin complex (1J1E.pdb)¹⁰, with a root-mean-square deviation (RMSD) of 1.2 Å for the backbone heavy atoms of residues 3-85 of cNTnC. The linker region between cNTnC and cTnI switch region is highly mobile by NMR, as indicated by random coil chemical shifts and lack of NOE contacts to the rest of the protein. Val146 is the first structured residue in cTnI immediately following the linker, showing NOEs to Pro52, Glu56 and Met60 of cNTnC (Figure 2.2c). This is the first time these contacts have been observed in an NMR structure, though they are also present in a single asymmetric unit of the crystal structure, showing that Val146 is actually part of the switch region of cTnI that binds to cNTnC. The conformation and interactions of the rest of the switch region of cTnI are similar in the X-ray and NMR structures, with residues 146-149 in an extended conformation and residues 150-159 forming an alpha helix. Residues C-terminal to Leu159 are flexible according to the X-

ray structure (different conformations observed within the asymmetric unit) and as indicated by NMR chemical shifts.

In many EF-hand proteins, calcium binding triggers a closed-to-open conformational transition³⁶. However, in cNTnC, the closed conformation predominates still upon calcium binding, though the open form is still populated to a small degree³⁷. Binding of the cTnI 146-158 switch region locks cNTnC into the open conformation, characterized by a rotation of the B-C helical unit away from helices N-A-D. The cTnI switch region binds between the outer C-terminus of helix B and helices A-D (Figure 2.2a), analogous to wedging a wastebasket between a door and its frame to keep it open. Importantly, this leaves a sizeable cavity between the hinge of the protein (the central β sheet) and the cTnI peptide, where drug binding can occur. The size and configuration of this cavity is virtually identical between cChimera and the X-ray structure.

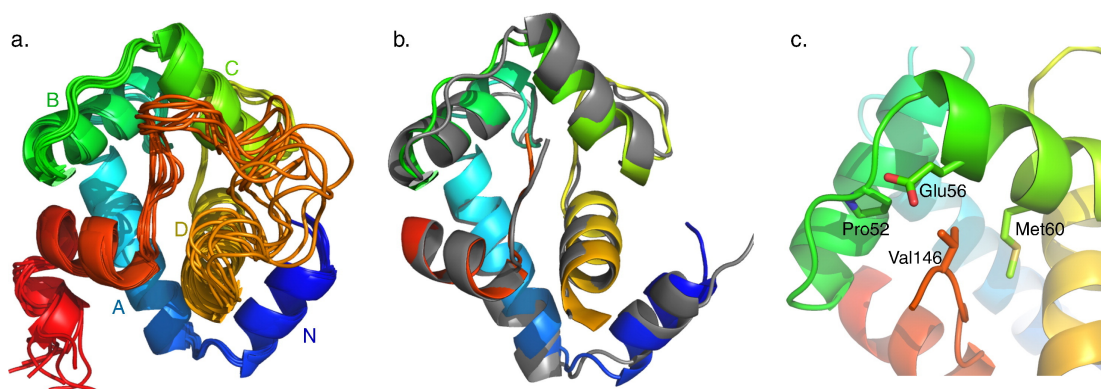


Figure 2.2. Structure of cChimera.

a. The eight lowest energy solution NMR structures of cChimera (cTnI switch region shown in red). b. The x-ray structure cNTnC-cTnI derived from the cardiac troponin complex (1J1E.pdb, grey) was aligned by secondary structural elements (residues 3-85) to cChimera (cNTnC region: blue, cyan, green, and yellow spectrum, cTnI inhibitory region linker: orange, cTnI switch region: red). c. Residue Val146 of cTnI (red) forms contacts with Pro52, Glu56 and Met60 (green) of cNTnC, shown in sticks.

Selection of diphenylamine as starting compound

Bepridil is a calcium channel blocker that was previously marketed as a treatment for angina. As an off-target effect, it was previously found to bind to the troponin complex to act as a calcium sensitizer³⁸. A crystal structure showed that in the absence of cTnI, bepridil binds to the hydrophobic patch of cNTnC and stabilizes its calcium-bound open state, though its binding site overlaps with where the cTnI switch region normally binds³⁹. NMR studies showed that bepridil and cTnI switch region bind to calcium-saturated cNTnC simultaneously but with negative cooperativity⁴⁰. Thus, bepridil binding stabilizes the calcium-bound open state of cNTnC (with a K_D of 20 μM), but also destabilizes the complex by displacing the cTnI switch peptide. In the presence of switch peptide, bepridil binds with an affinity of 80 μM ⁴⁰. We tested the binding of bepridil to cChimera, but were unable to obtain a binding constant due to signal broadening, consistent with competitive binding of bepridil against the switch peptide. Since the binding affinity of bepridil for cNTnC was the highest of any compound published to date, we decided that it would be a good starting point for drug design.

In the NMR-based structure determination of bepridil bound to cNTnC-cTnI switch peptide, it was evident that most NOE-derived distance restraints localized to the two aromatic rings of bepridil⁴⁰. Therefore, we tested a series of small compounds mimicking the two aromatic rings of bepridil. Of these, benzyaniline is a fragment of bepridil that binds with a K_D of 150 μM (Figure 2.3). Removing the methylene carbon to yield diphenylamine (DPA) improved binding to K_D of 120 μM , while addition of a methylene carbon (dibenzylamine) completely abolished binding. The effect of adding methylene carbons is at least two-fold, increasing the length of the molecule and increasing the partial positive charge on the central nitrogen atom (increasing $\text{p}K_a$), and both of these factors likely contribute to decreased binding to cChimera. While DPA bound to cChimera with slightly lower affinity than what was previously found for bepridil, we noted that the molecular weight of DPA was less than half that of bepridil, making it an excellent starting scaffold for drug development. We initially added single methyl or chloro substituents and found that 3-chlorodiphenylamine (3-CIDPA) bound with the highest affinity with a K_D of 10 μM . We decided to pursue the structure of 3-

methyldiphenylamine (3-mDPA) by NMR because the methyl group would provide an additional signal for structure determination.

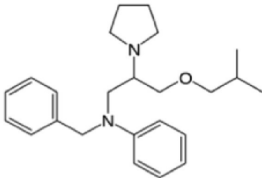
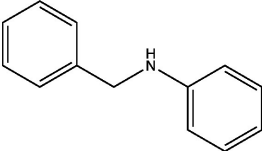
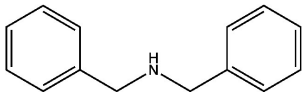
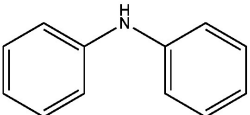
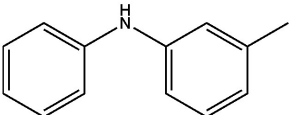
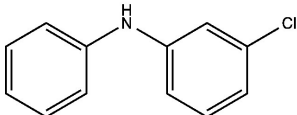
<p>Bepridil K_D* 80 μM</p> 	<p>Benzylaniline K_D 150 μM</p> 	<p>Dibenzylamine No binding</p> 
<p>Diphenylamine (DPA) K_D 120 μM</p> 	<p>3-Methyldiphenylamine K_D 30 μM</p> 	<p>3-Chlorodiphenylamine K_D 10 μM</p> 

Figure 2.3. Chemical structure of Bepridil and derivatives.

Chemical structures and cChimera binding affinity (K_D) of N-benzyl-N-(3-isobutoxy-2-pyrrolidin-1-yl-propyl)aniline (bepridil), benzylaniline, dibenzylamine, diphenylamine (DPA), 3-methyldiphenylamine (3-mDPA) and 3-chlorodiphenylamine (3-CIDPA). For bepridil, K_D* is binding affinity to cTnC-switch cTnI peptide complex (binding to cChimera could not be accurately measured).

Interaction of cChimera with 3-mDPA

To characterize its interaction with cChimera, 3-mDPA was titrated into ¹⁵N-labeled cChimera and monitored by ¹H, ¹⁵N-HSQC NMR spectra (Figure 2.4a). Backbone chemical shifts migrated in a linear fashion, indicating a 1:1 stoichiometry. Since 3-mDPA interacts with cChimera on a fast exchange timescale, almost all resonances could be easily followed throughout the titration. Chemical shift changes of the backbone amides of Phe27, Ser37, Ile61, Val64, Asp65, Glu66, Phe77, Val79,

and Ala150 were plotted as a function of 3-mDPA-to-cChimera concentrations; a global dissociation constant (K_D) of 29 μM was determined (Figure 2.4b). Chemical shift changes in cChimera upon titration with 3-mDPA are shown in Figure 2.5. Chemical shift mapping of ^1H and ^{15}N signals do not seem to accurately delineate the small molecule binding site in cNTnC. Instead, they are sensitive markers of conformational changes in the protein⁴¹ that are needed to accommodate drug binding. The largest ^{15}N chemical shift changes are seen in Val64 and Met81 in cNTnC, and Ala150 in cTnI, highlighting hotspots of conformational change that occur upon 3-mDPA binding.

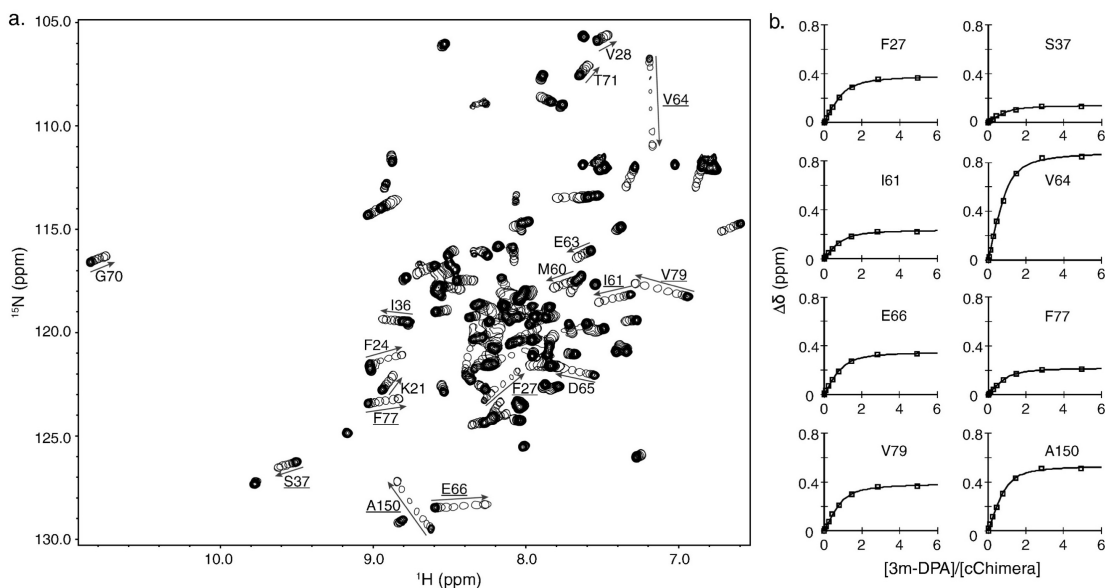


Figure 2.4. 3-mDPA binding to cChimera monitored by ^1H , ^{15}N -HSQC.

a. Overlay of 2D ^1H , ^{15}N -HSQC spectra of cChimera acquired during titration with 3-mDPA. The first point of each titration is represented with multiple contours and subsequent titration points for the drug are represented by single contours. Residues that experienced large chemical shift changes are labeled. b. Global fit for residues in cChimera that experienced large chemical shift perturbations upon addition of 3-mDPA. $K_D \sim 30\mu\text{M}$.

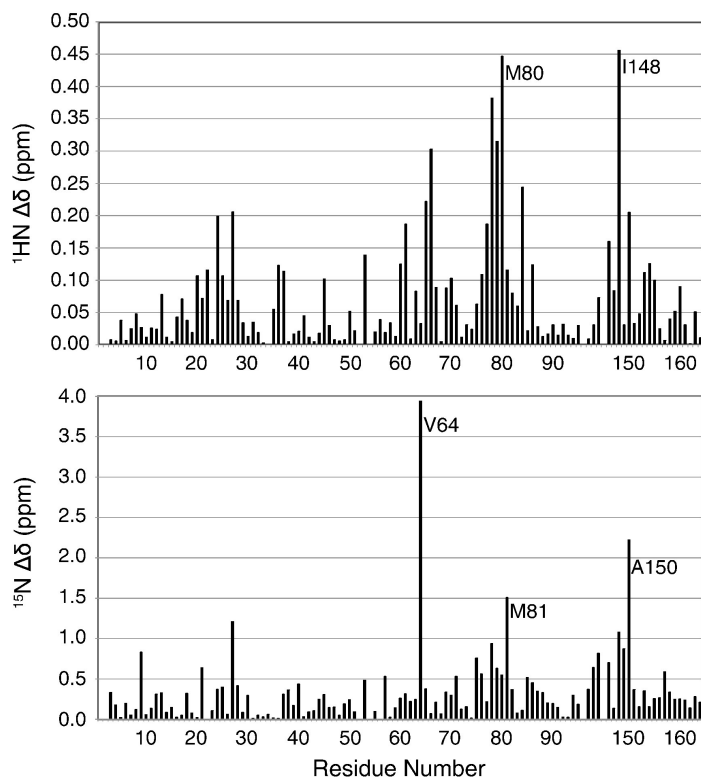


Figure 2.5. cChimera CSP induced by 3-mDPA binding.

The backbone $^1\text{H N}$ and ^{15}N chemical shift perturbation (CSP, $\Delta\delta$) between cChimera and cChimera-3-mDPA as a function of sequence.

^{13}C chemical shift changes upon 3-mDPA titration were also tracked using $^1\text{H}, ^{13}\text{C}$ -HSQC NMR spectra. The chemical shift changes of the methyl groups of Ile61, Val64, Met80, and Met153 were plotted as a function of 3-mDPA-to-cChimera concentrations; a global dissociation constant (K_D) of 25 μM was determined (Figure 2.6a and 2.6b). The largest chemical shift changes observed in methyl groups seems to map more consistently to the binding site than the backbone amide chemical shift changes.

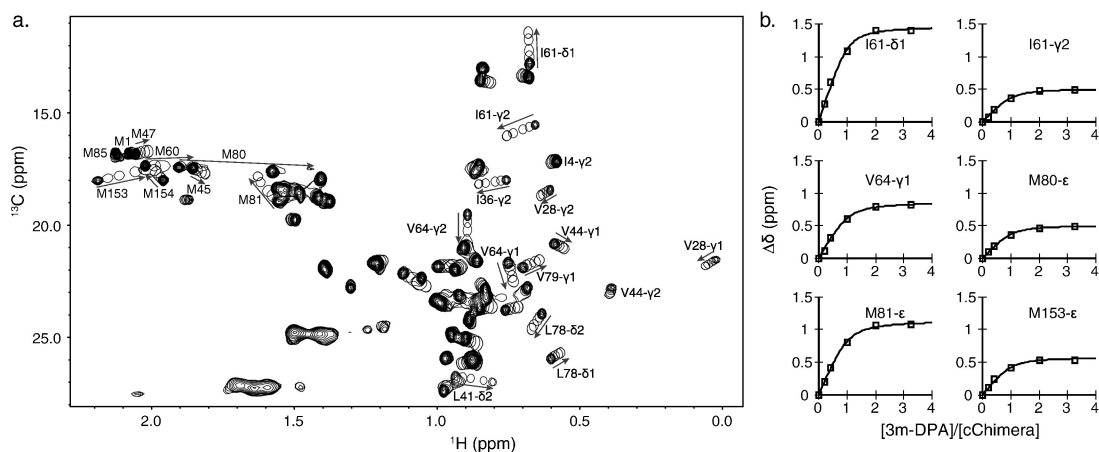


Figure 2.6. 3-mDPA binding to cChimera monitored by ^1H , ^{13}C -HSQC.

a. Overlay of 2D ^1H , ^{13}C -HSQC spectra of cChimera acquired during the titration of 3-mDPA. b. Global fit for residues in cChimera that experienced large chemical shift perturbations upon addition of 3-mDPA. $K_D \sim 25\mu\text{M}$.

Solution structure of the cChimera-3-mDPA complex

Accurate determination of the drug binding site of cChimera requires a complete solution structure determination of the protein-drug complex, complete with a full set of NOE-derived distance restraints and chemical shift-derived dihedral angle restraints (see Table 2.1). NOEs from the cChimera protein to the methyl substituted ring of 3-mDPA clustered into two groups, with one set of NOEs to a solvent-exposed site in cNTnC (to Met60 and Val64) and another set localizing to the cNTnC-cTnI interface (Val44, Met45, Leu48 of cNTnC and Ile148 and Met153 of cTnI). Both sets could not be simultaneously satisfied within a single structure. Since the two sets of NOEs indicated that 3-mDPA was able to bind in two different orientations, two separate structure calculations were performed for each set. Coincidentally, both NOE distance restraint sets contained 30 out of the 43 total 3-mDPA-cChimera intermolecular restraints (17 restraints common to both sets, 13 restraints unique to each set).

Table 2.1. Structure statistics of cChimera-3-mDPA structures.

Total numbers of structural restraints used in the final round of ARIA calculations.

	cChimera	cChimera+ 3-mDPA _{peptide}	cChimera+ 3-mDPA _{solvent} exposed
Backbone dihedral angles	192	192	192
Sidechain dihedral angles	6	6	6
Unambiguous distance restraints	1730	1630	1630
Ambiguous distance restraints	420	370	370
Intermolecular drug-protein distance restraints	-	30	30

Unlike the methyl-substituted ring of 3-mDPA, NOEs to the unsubstituted aryl ring unambiguously position it into a deep pocket, with its para-position (furthest from the central nitrogen) making contacts with the central β -sheet core of cNTnC, centered about Ile36 and Val72 (Figure 2.7a). This deep binding subsite must be sterically tight, since the presence of a single methyl group on the meta-substituted ring precludes binding in this location. The positioning of the deep binding site corresponds exactly to the binding site of the phenyl ring of bepridil in both the X-ray and NMR structures of the cNTnC-bepridil complex^{39,40}. Remarkably, this deep binding pocket is present even in the absence of small molecule binding, as seen in the structure of cChimera alone and in the X-ray structure of the cardiac troponin complex¹⁰. However, it is occupied by Met80, though its sidechain is too small to perfectly fill the cavity. We postulate that binding of any sizeable molecule to the central cavity of cNTnC requires displacement of the Met80 sidechain, making this the minimal conformational change necessary to support drug binding. Displacement of Met80 is achieved through sidechain χ dihedral angle rotations, with the backbone of Met80 relatively fixed within helix D (Figure 2.7b). The linear nature of the methionine sidechain makes it the amino acid most able to adapt to a wide range of binding partners, a phenomenon that has been well characterized in calmodulin, a versatile signaling protein homologous to TnC

that is able to interact with a plethora of protein targets through its methionine-rich binding surfaces⁴². The importance of Met80 sidechain displacement in cNTnC for drug binding is supported by the fact that NMR signal from the ϵ CH₃ group of Met80 moves and broadens more than any other ¹H-¹³C group in the ¹H,¹³C-HSQC spectrum of cChimera as 3-mDPA is added (Figure 2.6a). The conformational change of the Met80 sidechain likely accounts for the large chemical shift changes that occur in its vicinity upon drug binding, including the backbone ¹⁵N chemical shift of Met81 (Figure 2.5).

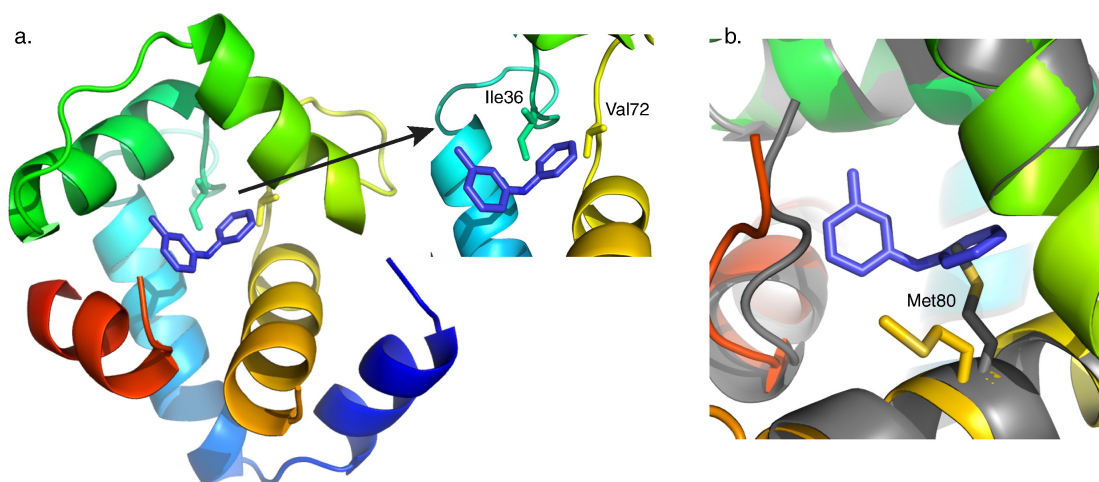


Figure 2.7. Binding site of unsubstituted aryl ring of 3-mDPA.

a. Deep binding site of 3-mDPA bound to cChimera. The main contact residues Ile36 and Val72 are shown in sticks. b. The sidechain of Met80 is displaced in the presence of 3-mDPA. X-ray troponin complex (Grey), cChimera-3-mDPA (yellow).

In contrast to the unsubstituted aryl ring, NOEs observed for the methyl-substituted ring of 3-mDPA cluster into two distinct groups that can only be satisfied by two distinct modes of 3-mDPA binding (Figure 2.8a). One set of NOEs localizes to the cNTnC-cTnI interface, with the methyl group of 3-mDPA nestled between residues Val44, Met45, and Leu48 in helix B, and the rest of the ring making contacts with

Ile148, Ala150, and Met153 of the cTnI switch peptide. The ring is also spatially close to the sidechains of Met80 and Ser84, but intermolecular NOEs could not be observed due to exchange-induced broadening of these residues. The hydrophobic burial of the 3-mDPA methyl group explains its favorable effect on cChimera binding.

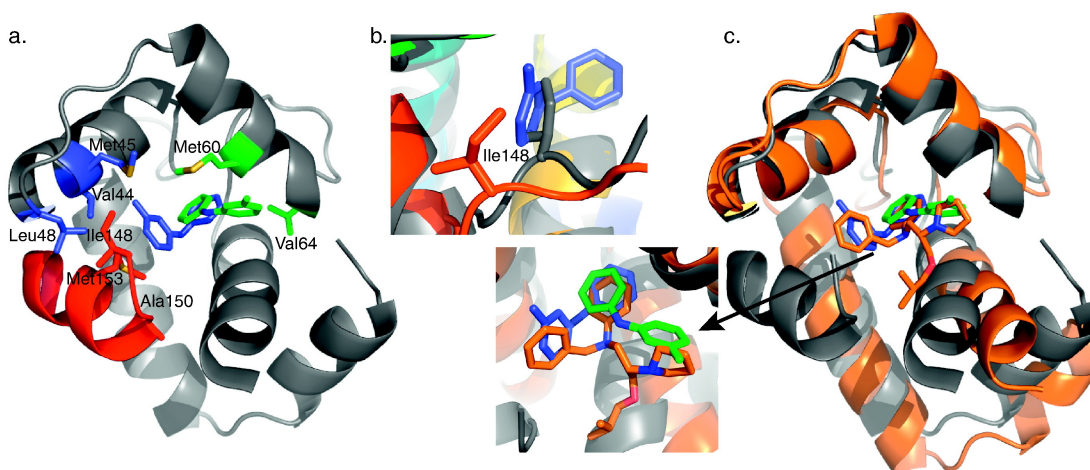


Figure 2.8. Binding sites of methyl-substituted ring of 3-mDPA.

a. cChimera residues with observed NOEs to the methyl-substituted ring of 3-mDPA. cChimera-3-mDPA_{peptide} drug binding site, contacting Val44, Met45, and Leu48 of cNTnC are shown in blue, Ile148 and Met153 of cTnI are shown in blue. cChimera-3-mDPA_{solvent exposed} drug binding site, contacting Val64 and Met60, are shown in green. b. The sidechain of Ile148 is displaced when 3-mDPA binds at the peptide binding site (cChimera: grey, cChimera-3-mDPA_{peptide}: red). c. The drug binding site of the cTnC-bepridil complex x-ray structure (orange), cChimera-3-mDPA_{peptide} (cChimera: grey, 3-mDPA: blue) and cChimera-3-mDPA_{solvent exposed} (cChimera: grey, 3-mDPA: green). Note how steric clash of the bepridil isopropyl group pushes helices N and A away from the rest of the protein, increasing the size of the central cNTnC cavity in order to accommodate bepridil.

The sidechain of Ile148 is the most deeply inserted element of cTnI relative to the hydrophobic cavity of cNTnC (Figure 2.8a). Although the sidechain does not extend deeply enough to fill the cavity, it does need to be displaced to allow insertion of the 3-mDPA methyl-substituted ring. Ile148 is a β -branched amino acid, and displacement of its sidechain by 3-mDPA requires a rotation of the extended backbone around Ile 148 along its long axis (Figure 2.8b). This accounts for the large changes in chemical shift that occur in this region upon titration with 3-mDPA (Figure 2.5).

In the alternative mode of 3-mDPA binding to cChimera, the methyl-substituted ring is flipped out of the switch peptide interface into a solvent-exposed space adjacent to helix C, resulting in NOEs to Met60 and Val64 of helix C (Figure 2.8a). Val64 is in an opposite corner of the drug binding site, spatially distant from the interface between cTnI switch peptide and cNTnC helix B. This solvent-exposed binding site corresponds well with the location of the pyrrolidine ring in the cNTnC-bepridil X-ray crystal structure (Figure 2.8c). It has fewer hydrophobic contacts than the interfacial site, mainly Met60, Val64, and Met80, suggesting that binding here would not be as favorable. However, the intensity of NOEs to Met60 and Val64 suggest that this mode of binding is as favorable as the interfacial mode, likely because it does not require any displacement of the switch peptide. The solvent-exposed subsite has some proximity to charged sidechains from cNTnC: Glu63 from helix B and Arg83 from helix D, which form an ion pair, but there are no groups in 3-mDPA that are available for hydrogen bonding to these.

The eight lowest energy structures of the cChimera-drug complex for both interfacial and solvent-exposed binding modes are shown in Figures 2.9a and b, respectively. Both drug-bound models were aligned to cChimera without drug (Figure 2.9c) and the backbone RMSDs of residues 3-85 were 1.3 Å and 1.3 Å for interfacial binding modes and the solvent-exposed, respectively, similar to the RMSD between the cChimera alone and the X-ray structure of the troponin complex (1J1E.pdb). The binding of 3-mDPA does not impart a large-scale structural perturbation to the backbone of cChimera, contrasting with the considerable opening of cNTnC structure needed to accommodate the large bepridil molecule, particularly its isopropyl group (See Figure 2.8c).

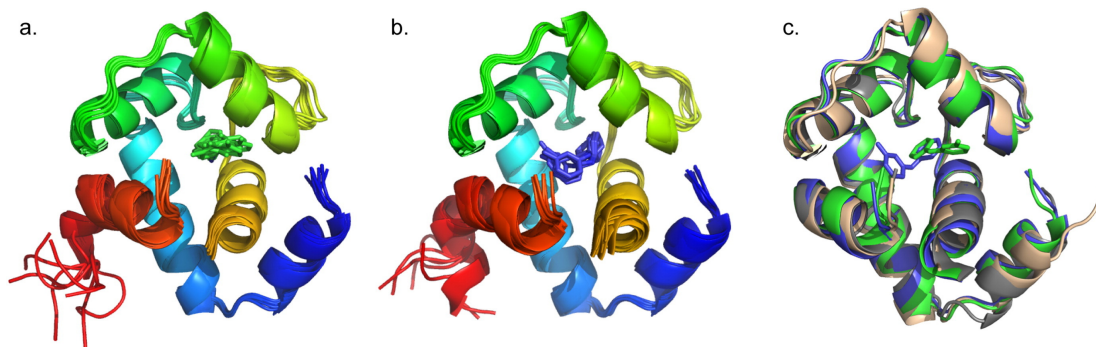


Figure 2.9. Structures of 3-mDPA bound to cChimera.

a. The eight lowest energy structures of cChimera-3-mDPA_{peptide}. b. 8 lowest energy structures of cChimera-3-mDPA_{solvent exposed}. c. The x-ray structure cNTnC-cTnI derived from the cardiac troponin complex (1J1E.pdb, wheat) was aligned by the secondary structural elements (residues 3-85) to the structure of cChimera (grey), cChimera-3-mDPA_{peptide} (blue) and cChimera-3-mDPA_{solvent exposed} (green). Linker regions are hidden.

Small molecule binding

We screened many compounds based on DPA for cChimera binding in order to explore its potential as a base structure for drug development (see Table 2.2). 3-mDPA binds to cChimera through entirely hydrophobic interactions. The choice of compounds to be tested was guided, in part, by the compounds suggested using *in silico* screening. Based on our structures, it appears that the central nitrogen atom of 3-mDPA does not participate in polar interactions with cChimera. DPA tolerates hydrophobic burial reasonably well because it does not carry appreciable positive charge. The central nitrogen is important for imparting some water solubility to the DPA base structure, but it is replaceable with –O- or –CH₂- without a major influence on cChimera binding, even though this changes the central geometry from trigonal planar to tetrahedral.

Strategically placed polar groups are important for the design of highly specific and tightly binding drugs. To date, all charged substituents added to the DPA base structure that we have tested have had an unfavorable effect on binding. Furthermore,

attachment of charged amino groups to the DPA backbone via flexible linkers also increased the K_D . The addition of polar but uncharged substituents to the DPA base structure was better tolerated than the addition of charged groups. It is interesting that $-F$ and $-Cl$ have a favorable effect on binding, with 2-chloro-DPA and 3-chloro-DPA having the tightest affinity of all compounds studied to-date. It is possible that van der Waals interactions between chlorine and protein hydrophobic groups are very favorable. Addition of a hydroxyl substituent to DPA slightly decreases affinity, and addition of an amine is less favorable than a hydroxyl. In the immediate vicinity of an aromatic ring, the amine has a slight positive charge (aniline pKa 4.6), while the hydroxyl has a slight negative charge (phenol pKa 10.0). The preference for $-OH$ over $-NH$ may be related more to the lesser partial charge on OH at the acidic pH (6-7) of the NMR samples, rather than any particular charge preference in the drug binding cavity.

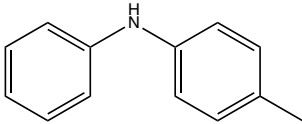
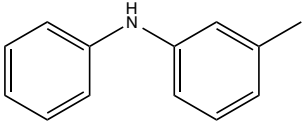
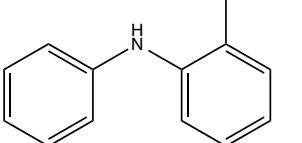
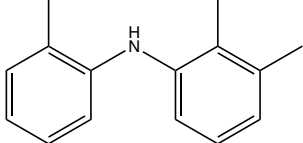
One particularly informative series of compounds is that employing single methyl substitutions to DPA. 4-mDPA, 3-mDPA and 2-mDPA all bind more tightly than unsubstituted DPA itself (K_D 60 μ M, 30 μ M, 15 μ M respectively). Much of this is likely due to enhanced hydrophobic interaction to cChimera and decreased water solubility. Nevertheless, the series points toward some important steric effects. The favorable binding of 3-mDPA relative to DPA can be rationalized in terms of the favorable burying of the 3-methyl group in between hydrophobic sidechains of helix B, though this would be partially offset by the loss of interchangeable binding to the deep pocket afforded by the unsubstituted symmetry of DPA. The lowest affinity compound is 4-mDPA, suggesting that a methyl group in the para position is not particularly favorable in any of the three binding subsites highlighted in this study. The best compound of this series is in fact 2-mDPA and not 3-mDPA, perhaps because the 2-methyl-substituted aryl ring is able to bind to any of the three binding subsites. The addition of multiple single atom substituents to the DPA base structure did not appear to increase binding affinity beyond what is observed for a single substituent, though not every possible combination was tested.

Placement of larger substituents on DPA is desirable from a drug development standpoint. Bulky substituents at the para position are not well tolerated, which is not

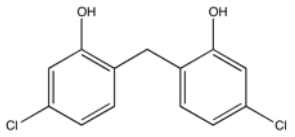
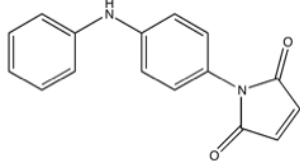
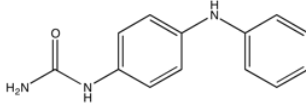
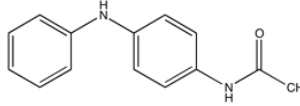
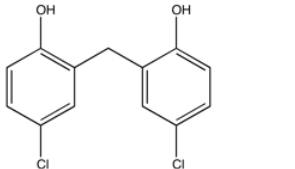
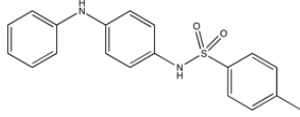
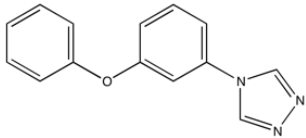
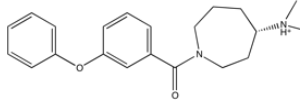
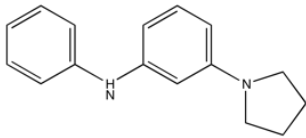
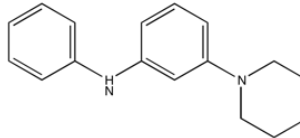
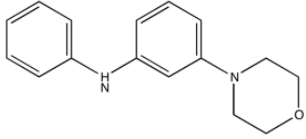
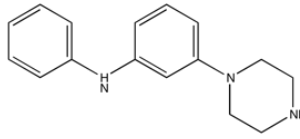
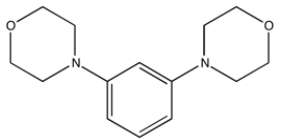
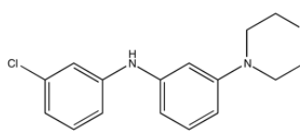
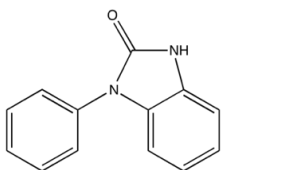
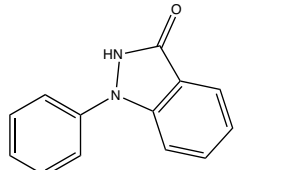
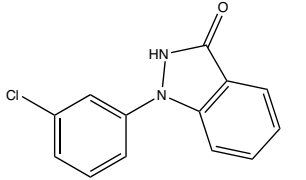
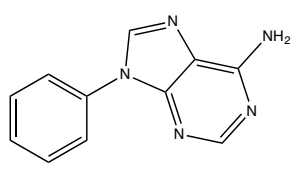
surprising, given that this was the least favorable position for single atom and methyl substituents. Bulky substituents at the meta ring position were better tolerated, but did not improve binding affinity. With the cChimera-3-mDPA structures in hand, it is possible to rationalize why substituents at these positions were not favorable in terms of the three binding sub-sites. Space is very limited in the deep binding pocket, even for single atom substituents. At the switch peptide interface, larger substituents in the meta position cannot fit into the helix B groove like the single methyl group of 3-mDPA, and substituents at the other meta position on the ring would further displace the switch peptide. The solvent-exposed subsite could accommodate bulky substituents at the meta and para positions, but these would be oriented out towards solvent and would thus not significantly improve the free energy of binding.

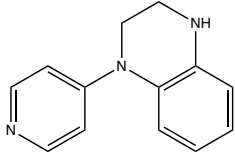
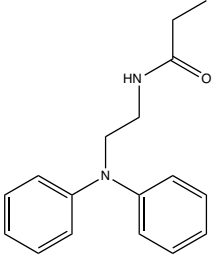
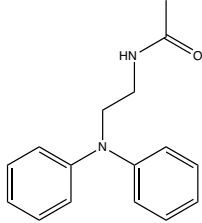
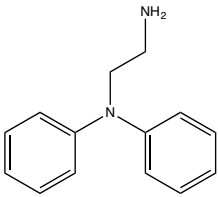
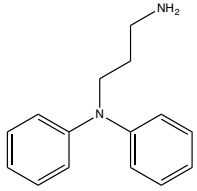
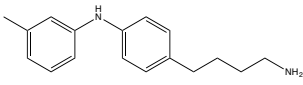
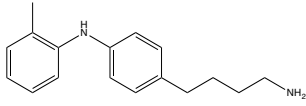
Table 2.2. Dissociation constant (K_D) of DPA-like compounds for cChimera.

K_D is the affinity constant calculated from small molecule titration, with the proviso that it provides a lower bound estimate (that is, a K_D that is too low) when the compound precipitates out before the final point in the titration. K_D^* is calculated based on the assumption that if solubility of the compound were not a limiting factor, saturation with the compound would cause chemical shift perturbations similar to 3-CIDPA. “Weak binding” denotes when titration with a compound led to very small chemical shift changes that could not be fit to a saturating curve, indicating a $K_D > 2$ mM.

	4-methyl diphenylamine K_D 60 μ M K_D^* 120 μ M		3-methyl diphenylamine K_D 30 μ M K_D^* 50 μ M
	2-methyl diphenylamine K_D 15 μ M K_D^* 25 μ M		2,2',3'- trimethyl diphenylamine K_D 5 μ M K_D^* 100 μ M

	2,2',5'- trimethyl diphenylamine K_D 3 μ M K_D^* 30 μ M		NSC18731 K_D 330 μ M K_D^* 320 μ M
	NSC215211 K_D 400 μ M K_D^* 800 μ M		NSC25027 K_D 80 μ M K_D^* 100 μ M
	2-chloro diphenylamine K_D 10 μ M		3-chloro diphenylamine K_D 10 μ M
	NSC50696 K_D 40 μ M K_D^* 30 μ M		NSC50453 K_D 20 μ M K_D^* 30 μ M
	NSC59989 K_D 20 μ M K_D^* 10 μ M		NSC56930 K_D 300 μ M K_D^* 220 μ M
	NSC11182 K_D 10 μ M K_D^* 10 μ M		NSC11184 K_D 60 μ M K_D^* 70 μ M
	NSC17285 Weak binding		NSC11177 K_D 60 μ M K_D^* 100 μ M
	NSC71607 K_D 180 μ M K_D^* 190 μ M		NSC75183 K_D 80 μ M K_D^* 60 μ M
	NSC167798 Weak binding		NSC89784 Weak binding

	NSC3947 K_D 180 μ M K_D^* 90 μ M		NSC39744 K_D 140 μ M K_D^* 500 μ M
	NSC24035 K_D 600 μ M K_D^* 1340 μ M		NSC40576 K_D 1400 μ M K_D^* 2000 μ M
	NSC38642 K_D 270 μ M K_D^* 120 μ M		NSC41053 Weak binding
	ChemBridge 54451398 Weak binding		ChemBridge 58784194 No binding
	SHG70 Weak binding		SHG72 Weak binding
	SHG74 K_D 210 μ M K_D^* 340 μ M		SHG78 Weak binding
	SHG82 No binding		SHG83 K_D 60 μ M K_D^* 360 μ M
	SHG102 K_D 270 μ M K_D^* 340 μ M		SHG115 K_D 26 μ M K_D^* 460 μ M
	SHG116 Weak binding		SHG118 No binding

	SHG123 No binding		SHG_DPA1: K_D 280 μ M
	SHG_DPA2: K_D 130 μ M		SHG_DPA3: K_D 1600 μ M
	SHG_DPA4: K_D 1200 μ M		SHG_DPA8 No binding
	SHG_DPA9 No binding		

Conclusion

Our solution NMR structures of cChimera bound to 3-mDPA show that DPA-based compounds bind well to cardiac troponin compared to much larger compounds like bepridil. Binding to the DPA base structure is less perturbing to the troponin C-I complex, requiring only minimal re-positioning of sidechains (Met80 in cTnC, Ile148 in cTnI). Previous cTnC-cTnI-small molecule structures show more extensive opening of cNTnC and more extensive displacement of the cTnI switch peptide, creating a large drug binding cavity. The cavity in the current study is much smaller, explaining the restrictive pattern of binding seen in our collection of DPA-like molecules. This better-defined binding site will facilitate *in silico* screening of potential high affinity compounds.

The flexibility of cNTnC itself and the adaptability of its interface with the cTnI switch region explains why the cNTnC-cTnI complex is able to bind to many

structurally unrelated small molecules, albeit with low affinity. Preservation of its preferred native conformation of the troponin complex appears to be critical in designing high affinity cardiac troponin modulators.

Acknowledgments

This study was supported by grants from Heart and Stroke foundation of Canada (B.D.S., G-14-0005884) and Canadian Institutes of Health Research (CIHR) (B.D.S., 37769). The authors also acknowledge support from the Hwang Professional Corporation and startup funds (to PMH) from the University of Alberta Faculty of Medicine & Dentistry and the Department of Medicine. This work was supported by the National Institutes of Health, the National Science Foundation, the Howard Hughes Medical Institute, the National Biomedical Computation Resource, and the NSF Supercomputer Centers. The authors would like to thank Dr. J. Andrew McCammon for helpful discussions.

References

1. WHO. Global status report on noncommunicable diseases. *World Health* 176 (2014). doi:ISBN 9789241564854
2. Sisakian, H. Cardiomyopathies: Evolution of pathogenesis concepts and potential for new therapies. *World J. Cardiol.* **6**, 478–494 (2014).
3. Sonnenblick, E. H., Frishman, W. H. & LeJemtel, T. H. Dobutamine: a new synthetic cardioactive sympathetic amine. *N. Engl. J. Med.* **300**, 17–22 (1979).
4. Cleland, J. G. F., Freemantle, N., Coletta, A. P. & Clark, A. L. Clinical trials update from the American Heart Association: REPAIR-AMI, ASTAMI, JELIS, MEGA, REVIVE-II, SURVIVE, and PROACTIVE. *Eur. J. Heart Fail.* **8**, 105–110 (2006).
5. Michaels, A. D. *et al.* Effects of Intravenous Levosimendan on Human Coronary Vasomotor Regulation, Left Ventricular Wall Stress, and Myocardial Oxygen Uptake. *Circulation* **111**, 1504–1509 (2005).
6. Mebazaa, A. *et al.* Levosimendan vs Dobutamine for Patients With Acute Decompensated Heart Failure. *JAMA* **297**, 1883 (2007).
7. Nieminen, M. S. *et al.* Levosimendan: current data, clinical use and future development. *Hear. lung Vessel.* **5**, 227–45 (2013).
8. Haikala, H. *et al.* Cardiac troponin C as a target protein for a novel calcium sensitizing drug, levosimendan. *J. Mol. Cell. Cardiol.* **27**, 1859–1866 (1995).
9. Pollesello, P. *et al.* Binding of a new Ca²⁺ sensitizer, levosimendan, to recombinant human cardiac troponin C. *J. Biol. Chem.* **269**, 28584–90 (1994).
10. Takeda, S., Yamashita, A., Maeda, K. & Maéda, Y. Structure of the core domain of human cardiac troponin in the Ca(2+)-saturated form. *Nature* **424**, 35–41 (2003).
11. Parry, D. A. D. & Squire, J. M. Structural role of tropomyosin in muscle regulation: Analysis of the X-ray diffraction patterns from relaxed and contracting muscles. *J. Mol. Biol.* **75**, 33–55 (1973).
12. Li, M. X., Spyropoulos, L. & Sykes, B. D. Binding of Cardiac Troponin-I 147-163 Induces a Structural Opening in Human Cardiac Troponin-C † , ‡. *Biochemistry* **38**, 8289–8298 (1999).

13. Sorsa, T., Pollesello, P., Permi, P., Drakenberg, T. & Kilpeläinen, I. Interaction of levosimendan with cardiac troponin C in the presence of cardiac troponin I peptides. *J. Mol. Cell. Cardiol.* **35**, 1055–61 (2003).
14. Robertson, I. M., Baryshnikova, O. K., Li, M. X. & Sykes, B. D. Defining the binding site of levosimendan and its analogues in a regulatory cardiac troponin C-troponin I complex. *Biochemistry* **47**, 7485–95 (2008).
15. Szilágyi, S. *et al.* The effects of levosimendan and OR-1896 on isolated hearts, myocyte-sized preparations and phosphodiesterase enzymes of the guinea pig. *Eur. J. Pharmacol.* **486**, 67–74 (2004).
16. Farmakis, D. *et al.* Levosimendan beyond inotropy and acute heart failure: Evidence of pleiotropic effects on the heart and other organs: An expert panel position paper. *International Journal of Cardiology* **222**, 303–312 (2016).
17. Grossini, E., Molinari, C., Caimmi, P. P., Uberti, F. & Vacca, G. Levosimendan induces NO production through p38 MAPK, ERK and Akt in porcine coronary endothelial cells: role for mitochondrial K(ATP) channel. *Br. J. Pharmacol.* **156**, 250–61 (2009).
18. Russell, A. J. *et al.* Activation of fast skeletal muscle troponin as a potential therapeutic approach for treating neuromuscular diseases. *Nat. Med.* **18**, 452–455 (2012).
19. Rezvanpour, A., Phillips, J. M. & Shaw, G. S. Design of high-affinity S100-target hybrid proteins. *Protein Sci.* **18**, 2528–36 (2009).
20. Porumb, T., Yau, P., Harvey, T. S. & Ikura, M. A calmodulin-target peptide hybrid molecule with unique calcium-binding properties. *Protein Eng.* **7**, 109–15 (1994).
21. Pineda-Sanabria, S. E., Julien, O. & Sykes, B. D. Versatile Cardiac Troponin Chimera for Muscle Protein Structural Biology and Drug Discovery. *ACS Chem. Biol.* **9**, 2121–2130 (2014).
22. Julien, O. *et al.* Is there nascent structure in the intrinsically disordered region of troponin I? *Proteins* **79**, 1240–1250 (2011).
23. Li, M. X. & Hwang, P. M. Structure and function of cardiac troponin C (TNNC1): Implications for heart failure, cardiomyopathies, and troponin

- modulating drugs. *Gene* **571**, 153–66 (2015).
24. Gagné, S. M. *et al.* Quantification of the calcium-induced secondary structural changes in the regulatory domain of troponin-C. *Protein Sci.* **3**, 1961–74 (1994).
 25. Neri, D., Szyperski, T., Otting, G., Senn, H. & Wüthrich, K. Stereospecific Nuclear Magnetic Resonance Assignments of the Methyl Groups of Valine and Leucine in the DNA-Binding Domain of the 434 Repressor by Biosynthetically Directed Fractional ¹³C Labeling. *Biochemistry* **28**, 7510–6 (1989).
 26. Delaglio, F. *et al.* NMRPipe: A multidimensional spectral processing system based on UNIX pipes. *J. Biomol. NMR* **6**, 277–293 (1995).
 27. Johnson, B. A. & Blevins, R. A. NMR View: A computer program for the visualization and analysis of NMR data. *J. Biomol. NMR* **4**, 603–614 (1994).
 28. Shen, Y., Delaglio, F., Cornilescu, G. & Bax, A. TALOS+: A hybrid method for predicting protein backbone torsion angles from NMR chemical shifts. *J. Biomol. NMR* **44**, 213–23 (2009).
 29. Berjanskii, M. V. & Wishart, D. S. A Simple Method To Predict Protein Flexibility Using Secondary Chemical Shifts. *J. Am. Chem. Soc.* **127**, 14970–14971 (2005).
 30. Linge, J. P., Habeck, M., Rieping, W. & Nilges, M. ARIA: automated NOE assignment and NMR structure calculation. *Bioinformatics* **19**, 315–6 (2003).
 31. Rieping, W. *et al.* ARIA2: Automated NOE assignment and data integration in NMR structure calculation. *Bioinformatics* **23**, 381–382 (2007).
 32. Brunger, A. T. Version 1.2 of the Crystallography and NMR system. *Nat. Protoc.* **2**, 2728–33 (2007).
 33. Schüttelkopf, A. W. & van Aalten, D. M. F. PRODRG: a tool for high-throughput crystallography of protein-ligand complexes. *Acta Crystallogr. D. Biol. Crystallogr.* **60**, 1355–63 (2004).
 34. Lindert, S. *et al.* Farnesyl diphosphate synthase inhibitors from in silico screening. *Chem. Biol. Drug Des.* **81**, 742–8 (2013).
 35. Friesner, R. A. *et al.* Extra precision glide: Docking and scoring incorporating a model of hydrophobic enclosure for protein-ligand complexes. *J. Med. Chem.* **49**, 6177–6196 (2006).

36. Gifford, J. L., Walsh, M. P. & Vogel, H. J. H. J. *Structures and metal-ion-binding properties of the Ca²⁺-binding helix-loop-helix EF-hand motifs. The Biochemical journal* **405**, 199–221 (Portland Press Limited, 2007).
37. Eichmüller, C. & Skrynnikov, N. R. A new amide proton R1rho experiment permits accurate characterization of microsecond time-scale conformational exchange. *J. Biomol. NMR* **32**, 281–93 (2005).
38. Solaro, R. J., Bousquet, P. & Johnson, J. D. Stimulation of cardiac myofilament force, ATPase activity and troponin C Ca⁺⁺ binding by bepridil. *J. Pharmacol. Exp. Ther.* **238**, 502–7 (1986).
39. Li, Y., Love, M. L., Putkey, J. A. & Cohen, C. Bepridil opens the regulatory N-terminal lobe of cardiac troponin C. *Proc. Natl. Acad. Sci. U. S. A.* **97**, 5140–5 (2000).
40. Wang, X., Li, M. X. & Sykes, B. D. Structure of the regulatory N-domain of human cardiac troponin C in complex with human cardiac troponin I147-163 and bepridil. *J. Biol. Chem.* **277**, 31124–33 (2002).
41. Robertson, I. M., Boyko, R. F. & Sykes, B. D. Visualizing the principal component of ¹H, ¹⁵N-HSQC NMR spectral changes that reflect protein structural or functional properties: application to troponin C. *J. Biomol. NMR* **51**, 115–22 (2011).
42. Yuan, T., Ouyang, H. & Vogel, H. J. Surface Exposure of the Methionine Side Chains of Calmodulin. *J. Biol. Chem.* **274**, 8411–20 (1999).

Chapter 3

Structural Changes Induced by the Binding of the Calcium Desensitizer W7 to Cardiac Troponin

Fangze Cai¹, Peter M. Hwang² and Brian D. Sykes¹

¹Department of Biochemistry, University of Alberta, Edmonton, AB, Canada.

²Department of Medicine, University of Alberta, Edmonton, AB, Canada.

A version of this chapter has been previously published: Cai, F., Hwang, P. M. & Sykes, B. D. Structural Changes Induced by the Binding of the Calcium Desensitizer W7 to Cardiac Troponin. *Biochemistry* **57**, 6461–6469 (2018).

Contribution: FC purified the protein, performed all experiments, analyzed the data and solved the structure. FC wrote the manuscript with help of BDS and PMH. BDS directed the research.

Summary

Compounds that directly modulate the affinity of the thin filament calcium regulatory proteins in cardiac muscle have potential for treating heart disease. A recent “proof of concept” study showed that the desensitizer W7 can correct hyper-calcium-sensitive sarcomeres from RCM R193H cTnI transgenic mice. We have determined the high-resolution NMR solution structure of W7 bound to a cNTnC-cTnI cChimera designed to represent the key aspects of the cTnC:cTnI interface. The structure shows that W7 does not perturb the overall structure of the cTnC:cTnI interface, with the helical structure and position of the cTnI switch region remaining intact upon W7 binding. The naphthalene ring of W7 sits in the hydrophobic pocket created by the cNTnC-cTnI switch peptide interface, while the positively charged amine tail extends into the solvent. The positively charged tail of the W7 is in close proximity of Arg147 of cTnI switch region, supporting the suggestion that electrostatic repulsion is an aspect

underlying the mechanism of desensitization. Ser84 (replacing the unique Cys84 in cTnC reported to make a reversible covalent bond with levosimendan) also contacts W7.

Introduction

Hypertrophic cardiomyopathy (HCM) is a common monogenic disease, with an estimated phenotypic prevalence of 1:500. It is essentially a disease of the sarcomere, the basic contractile unit of the heart. Mutations in a sarcomeric protein are identified in about half of all cases, with thick filament cardiac myosin and cardiac myosin binding protein-3, and thin filament cardiac troponin I or T being the most commonly implicated. Like HCM, restrictive cardiomyopathy (RCM) is a genetic disorder of sarcomere, but with a more severe disease phenotype. HCM and RCM mutations have been shown to increase the calcium sensitivity of the myofilament¹ and lead to diastolic dysfunction (especially in RCM)²⁻⁴. Diastolic dysfunction occurs when there is insufficient relaxation during diastole (the relaxation phase of the cardiac cycle); the left ventricle becomes stiff, losing its ability to expand and to fill properly during diastole. By comparison, systolic dysfunction is caused by impaired cardiac muscle contraction during systole, leading to a weak and dilated heart. Molecules that increase or decrease the contractility of cardiac muscle could potentially be useful treatments for cardiomyopathy and heart failure, especially those that correct underlying genetic defects. The common treatment for cardiac dysfunction alters calcium transients by regulating the calcium based signaling pathway, but this can also affect other signaling systems. Although beneficial in the short term, this can lead over time to arrhythmias and hypotension⁵. The ideal drug would directly alter the response of the cardiac sarcomere without changing calcium homeostasis. Molecules that sensitize or desensitize the response of the cardiac muscle to calcium would have therapeutic potential in treating cardiac dysfunction.

The thin filament is an attractive and logical target for calcium sensitizing and desensitizing drugs, since it regulates the muscle contractile cycle. The thin filaments are composed of actin, tropomyosin and troponin. Heart muscle contraction is regulated by calcium binding to the heterotrimeric troponin complex (cTn). cTn complex is

composed of three components: the calcium binding subunit troponin C (cTnC), the inhibitory subunit troponin I (cTnI), and tropomyosin-binding subunit troponin T (cTnT)⁶. Under resting calcium concentration, cTnI is bound to actin, maintaining the position of tropomyosin and blocking myosin binding sites on actin⁷. When the cytoplasmic calcium concentration increases during systole, calcium binds to the regulatory domain of cTnC (cNTnC), causing conformational changes that promote binding of the switch region of cTnI (residues 147-163)⁸. This in-turn causes dissociation of the cTnI inhibitory region from actin, triggering muscle contraction through the formation of actin-myosin cross-bridges^{9,10}. Fine-tuning the critical cTnC-cTnI interaction by drugs represents a plausible therapeutic strategy for both cardiomyopathies and heart failure.

A few drugs are known to bind to cNTnC and act as calcium sensitizers or desensitizers. (Note: These compounds (including W7) have in the past been referred to as sensitizers or desensitizers. However, inasmuch as cTnC acts in part as a Ca buffer in the cell¹¹, changing the pCa₅₀ of cTnC directly would change the calcium concentration in the cell. The desired compound would alter the contractile response to calcium but not impact the calcium pumps or channels that transport calcium across cellular membranes.) The calcium channel blocker bepridil was found to bind to the troponin complex to act as a calcium sensitizer¹². The NMR structure of the cNTnC-cTnI switch-bepridil complex revealed that bepridil and cTnI switch region simultaneously bind to calcium-saturated cNTnC but do so with negative cooperativity¹³. One of the most widely studied calcium sensitizers, levosimendan, has shown binding to the interface of cTnC and cTnI^{14,15}. The levosimendan analog dfbp-o has also been shown to bind to this interface, with positive switch peptide/drug cooperativity¹⁶. The levosimendan analog i9 was developed to covalently react with the unique C84 in the active site of cNTnC, and the structure of cNTnC-cTnI chimera bound to i9 showed that i9 binds to the interface between cNTnC and cTnI switch peptide. Physiological studies have shown greatly enhanced contractility of cardiac trabeculae when cTnC-i9 was exchanged in the fibers, proving that targeting cTnC can be effective¹⁷. It has also been demonstrated that levosimendan can make a reversible covalent thioimidate bond *in situ* with cTnC¹⁸. Recent computational studies have

discovered three novel compounds NSC147866, NSC600285 and NSC611817 that exhibit positive switch peptide-drug binding cooperativity^{19,20}.

The calmodulin antagonist W7 has been used to explore a wide range of physiological processes involving calcium signaling. W7 was initially discovered to inhibit vascular smooth muscle actomyosin²¹. W7 was then found to be a calmodulin antagonist, inhibiting calcium/calmodulin-regulated protein kinase and ATPase²². Other than calmodulin, W7 binds specifically to TnC, and not to any other muscle protein, such as tropomyosin, actin, or myosin²². A study investigating the interplay of troponin- and myosin-based pathways of calcium activation showed that W7 inhibits ATPase and decreases calcium sensitivity during calcium activation in both skeletal and cardiac muscle²³. A remarkable recent “proof-of-concept” study showed that W7 corrects the hyper-calcium sensitive sarcomere disease state. W7 decreased intact cardiac myocyte contractility in a Ca²⁺ transient amplitude-independent manner, indicating the main target of W7 is the sarcomere protein cTnC. They showed that W7 had a rapid effect in correcting contractile dysfunction in both acquired (alkalosis-induced) and inherited (RCM R193H cTnI gene mutation) forms of hyper-Ca²⁺-sensitive states at the myocyte level and whole heart levels²⁴. NMR studies have shown that W7 reduces the affinity of the cardiac troponin I switch peptide to cNTnC by 13-fold²⁵. The NMR structure of cNTnC-cTnI switch peptide-W7 complex revealed that W7 bound to the hydrophobic pocket formed by cNTnC-cTnI switch region, perturbing the structure of cNTnC and shifting the cTnI switch region from its preferred binding site, and diminishing some of its helical structure as well²⁵. The series of papers described above strengthen the hypothesis that modulating the cTnC-cTnI interface can be effective in regulating the balance between contraction and relaxation in the heart.

Although the NMR solution structure of cNTnC-cTnI-W7 has been presented, the details of interaction between the cNTnC and cTnI switch peptide could not be determined at high resolution because the binding of the switch peptide was so weak ($K_D \sim 2\text{mM}$) that saturation was not achieved, and the NMR data was acquired using unlabeled cTnI switch peptide²⁵. The cTnI switch peptide proton resonances were only partially assigned due to signal overlap and low binding affinity. Hybrid proteins have been used to study protein-protein interactions, including both skeletal and cardiac

muscle isoforms of troponin^{26,27}. We have used cardiac TnC-TnI chimeric proteins in which the switch region of cTnI is fused to the C terminus of cNTnC to determine the structure of the i9 compound covalently bound to cTnC¹⁷, and to delineate the binding determinants of small molecules such as 3-mDPA²⁸. The structure of cChimera showed that the cChimera faithfully represent the structure of the cNTnC-cTnI switch complex that triggers the systolic state²⁸. Since the cTnI switch peptide is covalently linked to cNTnC in the cChimera construct, cTnI peptide is labeled along with cNTnC, which allows the use of heteronuclear NMR experiments to fully assign the peptide. Herein, we use cChimera for W7 binding, solution structure, and dynamics studies using NMR spectroscopy.

Material and methods

Materials and sample preparation

The recombinant cNTnC-cTnI cChimera used in this study contains residues 1-90 of human cNTnC (C35S, C84S) fused to residues 136–163 of cTnI (containing the inhibitory region 136–147 and switch region 147–163), followed by a histidine tag. ¹⁵N- and ¹⁵N,¹³C-labeled cChimera was expressed in *Escherichia coli* and purified as previously described²⁸. Protein identity and purity were confirmed by gel electrophoresis and mass spectrometry. W7 (N-(6-aminohexyl)-5-chloro-1-naphthalenesulfonamide) was purchased from Sigma-Aldrich. Stock solutions of 100 mM W7 in DMSO-d₆ (Cambridge Isotopes) were prepared and wrapped in aluminum foil.

The NMR samples were prepared in 5 mm NMR tubes to a final volume of 500 μ l. The sample for structural studies contained 0.5 mM ¹⁵N- or ¹⁵N,¹³C- labeled cChimera with 2.5 mM W7 in 100 mM KCl, 10 mM imidazole, 5-10 mM CaCl₂, and 0.25 mM 2,2-dimethyl-2-silapentane-5-sulfonate-d₆ sodium salt (DSS-d₆) as an NMR internal reference in 95% H₂O/5% D₂O or 100% D₂O, and the pH was maintained at 6.7-6.8. Samples for the W7 titration monitored with ¹⁵N HSQC used 0.15 mM or 0.5 mM ¹⁵N- labeled cChimera, and titrations monitored with ¹³C HSQC used 0.5 mM ¹⁵N,¹³C- labeled cChimera.

NMR spectroscopy

NMR data were collected at 30 °C on Varian Inova 500 and 600 MHz spectrometers equipped with a triple resonance probe with pulsed field gradients. One-dimensional NMR spectra were processed with VNMRJ v.3.2 A (Varian, Inc.), two-dimensional and three-dimensional NMR spectra were processed with NMRPipe²⁹ and analyzed with NMRViewJ³⁰, using scripts written in-house.

The backbone ¹H, ¹⁵N, and ¹³C chemical shift assignments for cChimera-W7 complex were obtained by analyzing the W7 to ¹⁵N-labeled cChimera titration monitored by 2D-¹H,¹⁵N HSQC. The side chain ¹H, ¹³C chemical shift assignments for cChimera-W7 complex were obtained by analyzing the W7 to ¹⁵N, ¹³C-labeled cChimera titration monitored by 2D-¹H,¹³C HSQC NMR spectra. ¹⁵N T₂ relaxation experiments were acquired with recycle delay of 3 s, and variable relaxation delays of 10, 30, 50, 70, 90 110 ms at [W7]:[cChimera] ratios of 0, 1 and 5.

3D ¹⁵N-edited NOESY-HSQC (mixing time 75 ms), and 3D ¹³C-edited NOESY-HSQC (mixing time 100 ms) were used to complete the chemical shift assignments and obtain intramolecular (within the protein cChimera) distance restraints. The chemical shift assignment of W7 in cChimera-W7 complex was achieved using 2D ¹³C,¹⁵N-double-filtered TOCSY (60 ms mixing time) experiment. Intermolecular distance restraints between W7 and cChimera were derived from a 3D ¹³C-filtered/edited NOESY-HSQC (mixing time: 75 ms) experiment. Most of those distance restraints could be identified and confirmed in the 3D ¹³C-edited NOESY-HSQC (containing both intramolecular and intermolecular NOEs).

Drug titrations and lineshape analysis

The binding of W7 to cChimera was monitored using 2D-¹H,¹⁵N HSQC and 2D-¹H,¹³C HSQC NMR spectra. 0.015, 0.045, 0.1, 0.2, 0.5 and 1.1 mM of W7 was titrated into 0.15 mM ¹⁵N-labeled cChimera, or 0.1, 0.25, 0.5, 0.9, 1.5 and 2.5 mM of W7 into 0.5mM ¹⁵N- or ¹⁵N,¹³C- labeled cChimera. 100 mM W7 stock solution is added independently in aliquots to the protein sample. By the end of the titration, the addition of DMSO-d₆ did not exceed 5% of the sample volume. Dilution by each W7 solution addition was taken into consideration when calculating the concentration of protein at

each titration point. Chemical shift perturbations at each titration point were fit by our in-house software, xcrvfit (www.bionmr.ualberta.ca/bds/software/xcrvfit), to calculate dissociation constants, K_D . We acquired ^{15}N - T_2 relaxation experiments at W7 concentrations of 0, 0.5 and 2.5 mM ($[\text{W7}]/[\text{cChimera}] = 0, 1$ and 5). Relaxation data were fit to a two-parameter exponential decay curve using the Rate Analysis module of NMRViewJ³⁰.

The titration of W7 to cChimera monitored by 2D- ^1H , ^{15}N HSQC spectra was also analyzed by the 2D lineshape analysis software TITAN³¹. The two-state binding model is selected since W7 binds to cChimera with 1:1 stoichiometry. Protein and small molecule concentrations as well as NMR acquisition parameters were provided as inputs for the data fitting. Several peaks with significant chemical shift perturbation were selected for fitting to calculate dissociation constant, K_D , and dissociation rate, k_{off} . An error analysis was performed using 200 repeats to determine the uncertainties of the fitting.

Structure calculations

Backbone ϕ - and ψ -dihedral angle restraints were derived using TALOS+³² based on backbone chemical shifts (HN, $\text{H}\alpha$, $\text{C}\alpha$, $\text{C}\beta$ and N). TALOS+ identifies secondary structure by using artificial neural network (ANNs) to match chemical shift patterns against a large database. The Chemical Shift Index (CSI) 3.0 (<http://csi3.wishartlab.com>) was also used to confirm the secondary structure prediction obtained by TALOS+. CSI 3.0 can identify 11 types of the secondary structures using backbone chemical shifts³³.

NOE-derived intramolecular distance restraints within the cChimera protein were generated using ARIA 2.3³⁴. Protein dihedral angle restraints derived from TALOS+ were incorporated in the calculation. The frequency window tolerances for assigning NOEs were 0.03 ppm for the proton dimension and 0.3 ppm for nitrogen and carbon dimensions. All assignments were checked manually for errors. Parameter and topology files for W7 was generated using the web-based server PRODRG³⁵ (<http://davapc1.bioch.dundee.ac.uk/cgi-bin/prodrg/>) and xplo2d³⁶ (<ftp://xray.bmc.uu.se/pub/gerard/xutil/>) and were checked manually. Intermolecular

NOEs between W7 and cChimera were manually assigned and were used to generate distance restraints that were added to the XPLOR-NIH structure calculations³⁷. Intermolecular NOEs between the cNTnC region of cChimera and Ca²⁺ were derived from crystallographic data of the cardiac troponin complex⁶. The distance and dihedral constraints were used in the simulated annealing module of Xplor-NIH, version 2.46. 300 structures were calculated, from which the lowest-energy structure was used as the starting point for refinement. The final ensemble consisted of the 20 lowest-energy structures generated from the refinement step with no NOE or dihedral violations greater than 0.5 Å and 5°, respectively. This ensemble was validated with PROCHECK using the Protein Structure Validation Suite (PSVS 1.5) server at http://psvs-1_5-dev.nesg.org/.

Results and discussion

Binding of W7 to cChimera

To characterize the interaction of W7 with cChimera protein, W7 was titrated into ¹⁵N-labeled cChimera. The 2D ¹H-¹⁵N HSQC NMR spectrum of cChimera was assigned previously and was used to monitor the titration. Figure 3.1A shows the W7-induced backbone amide resonance shifts in cChimera as [W7]:[cChimera] increased from 0 to 7. Virtually all of the backbone amide signals shifted in a linear fashion, indicating a 1:1 stoichiometry. The residues that experienced the largest chemical shifts perturbations, Ile61, Val64, Asp65, Glu66, Phe77, Val79, Met81, Ala150 and Leu157, are plotted as a function of W7 to cChimera concentration in Figure 3.1B. A global dissociation constant K_D of 470±50 μM was determined, which is consistent with the previous reported W7 binding affinity to cNTnC-cTnI switch peptide complex (K_D= 500±100 μM)³⁸, validating the use of the cChimera for structural studies²⁸. The titration of W7 to cChimera was also monitored by 2D ¹H-¹³C HSQC NMR spectra, and most methyl groups show large linear chemical shift changes (Figure 3.2). The last points in the titration for a few residues deviated from linearity when the W7 concentration was around 2.5 mM ([W7]:[cChimera]=5:1), including V28 in the ¹H, ¹⁵N-HSQC, and V64, M81 and M154 in the ¹H, ¹³C-HSQC NMR spectra. This indicates that W7 can bind weakly to cChimera with >1:1 stoichiometry³⁹.

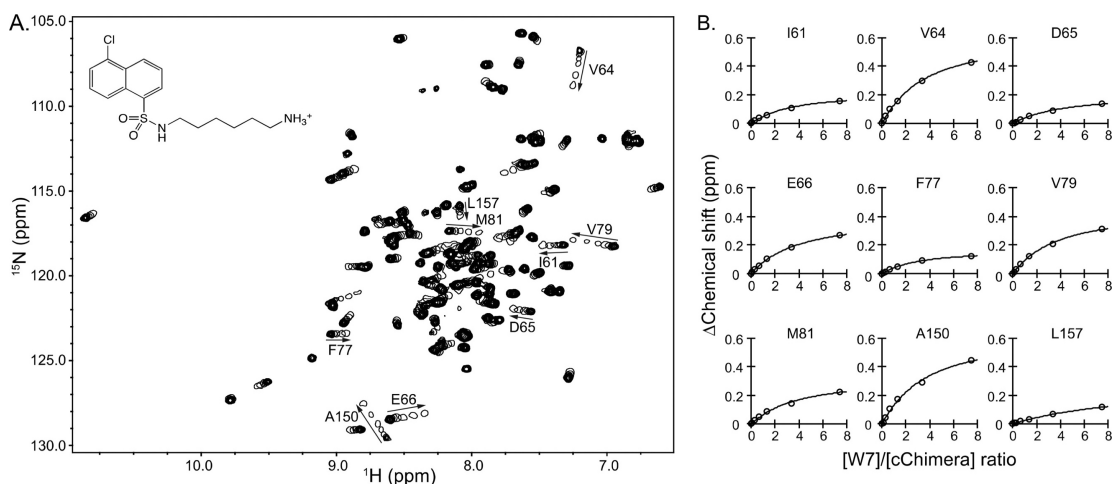


Figure 3.1. W7 binding to cChimera monitored by ^1H , ^{15}N -HSQC.

A. Overlay of 2D ^1H , ^{15}N -HSQC NMR spectra of cChimera acquired during the titration of W7. The first point of each titration represented with multiple contours and subsequent titration points for the W7 are represented by single contours and the arrows indicate direction of induced change. B. Global fit of the nine residues in cChimera that experienced the largest chemical shift perturbations in the titration to determine K_D .

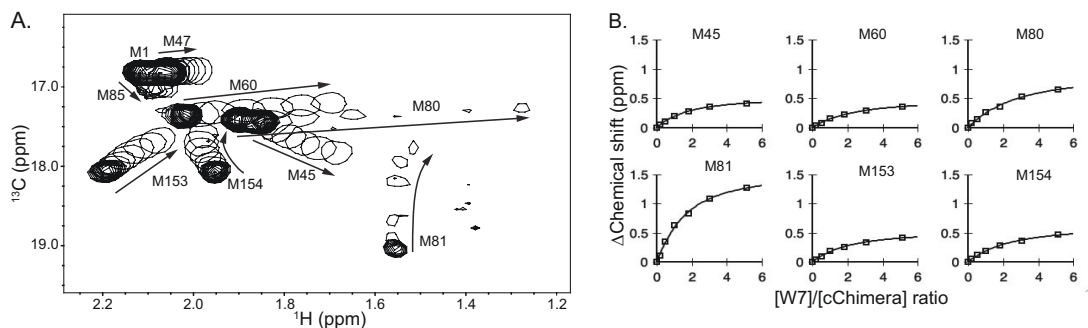


Figure 3.2. W7 binding to cChimera monitored by ^1H , ^{13}C -HSQC.

A. Overlay of 2D ^1H , ^{13}C -HSQC NMR spectra of cChimera acquired during the titration of W7 showing the methionine methyl group region. The first point of each titration represented with multiple contours and subsequent titration points for the W7 are represented by single contours and the arrows indicate direction of induced change. B. Global fit of titration for M45, M60, M80, M81, M153 and M154 to determine $K_D = 750 \pm 200 \mu\text{M}$.

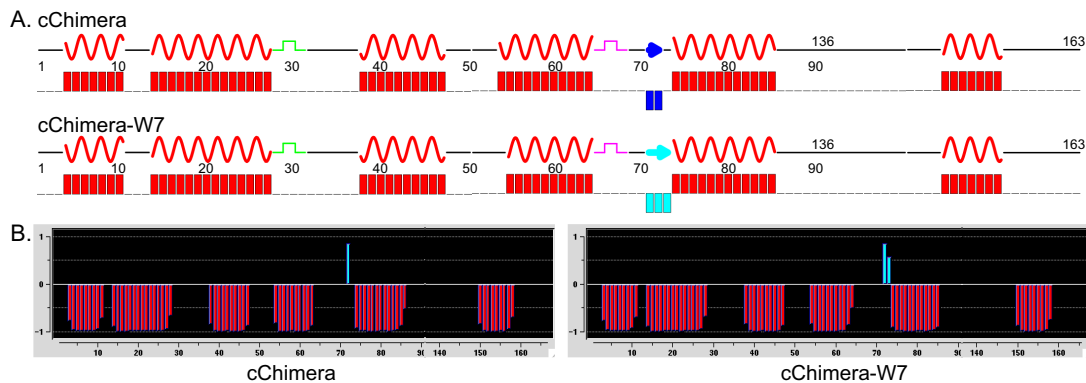


Figure 3.3 Secondary structure of cChimera-W7.

Secondary structure of cChimera and the cChimera-W7 complex predicted from backbone chemical shifts using: A. Chemical shift Index (CSI 3.0) and B. TALOS+. Predicted α helices are shown in red, β sheets are shown in blue.

Secondary structure assessment of cChimera-W7 complex:

The NMR spectra of cChimera are well resolved, allowing us to assign the backbone and sidechain chemical shift of cChimera-W7 complex by simply following the titration of W7 to ^{15}N - and $^{15}\text{N}/^{13}\text{C}$ -labeled cChimera monitored by $^1\text{H}, ^{15}\text{N}$ -HSQC and 2D $^1\text{H}, ^{13}\text{C}$ -HSQC NMR spectra respectively. Based on the chemical shift assignments of cChimera and the cChimera-W7 complex, secondary structures were predicted by chemical shift index (CSI) analysis (Figure 3.3A). We used CSI3.0 and the backbone ^1H , ^{15}N , $^{13}\text{C}\alpha$, $^1\text{H}\alpha$, $^{13}\text{C}\beta$, and $^1\text{H}\beta$ chemical shifts of the cChimera and cChimera-W7 complex to predict secondary structures, demonstrating that cChimera and cChimera-W7 complex have very similar secondary structures, with 5 helices from cNTnC (N, A, B, C, D helix), and one helix from cTnI switch region. The cTnI switch region of both structures starts from residue Ala 150 and ends with residue Ala 156. We also used TALOS+ to predict the secondary structure of cChimera and cChimera-W7 complex, and it shows similar results, but helical region of cTnI for both structures are from residue Ala 150 to Leu 158 (Figure 3.3B). Although the helical region predicted from both programs are different, they both suggest that the structure of the switch region does not change with W7 binding. The titration of W7 to cChimera

monitored by $^1\text{H},^{13}\text{C}$ -HSQC NMR did not show any significant ^{13}C chemical shift perturbations in the cTnI switch region, indicating no major structural changes, in contrast to the previous cNTnC-cTnI-W7 complex structure, which suggested that the helical structure of cTnI switch peptide is diminished upon W7 binding²⁵.

Solution structure of the cChimera-W7 complex

We determined a high-resolution solution NMR structural ensemble of the cChimera-W7 complex to characterize the structure of cTnI switch regions as well as the interactions between the calcium desensitizer W7 and cChimera (Figure 3.4). A total of 1584 NOE-derived distance restraints were used for structure calculations. There were 1526 intramolecular cChimera distance restraints (~ 12 restraints per residue), including 1323 within cNTnC, 156 within cTnI, and 47 between cNTnC and the cTnI switch region. There were 54 intermolecular contacts between cChimera and W7, including 40 between cNTnC and W7, and 12 between cTnI and W7. We added 6 distance restraints between cChimera and Ca^{2+} -derived from the X-ray crystal structure of the cardiac troponin complex⁶ (see Table 3.1). These restraints do not affect the global structure of cChimera, but they properly position the calcium ion, which is not directly observed in NMR experiments, within the calcium EF hand binding loop. The intermolecular restraints between W7 and cChimera derived from 3D ^{13}C -filtered/edited NOESY-HSQC experiment were checked and confirmed using 3D $^1\text{H},^{13}\text{C}$ -edited NOESY-HSQC NMR experiment. The ensemble of the 20 lowest energy structures of cChimera-W7 complex is shown in Figure 3.4B, with RMSD of backbone heavy atoms of core structure residues 3-85 and 146-160 around 0.6 Å compared to the average structure. In the structure, both cNTnC and cTnI switch peptide regions of the cChimera protein are well defined, as well as the small molecule W7 (Figure 3.4C). The linker region between cNTnC and the cTnI switch region is highly flexible, which is consistent with previous cChimera structures. The structure has been deposited in the Protein Data Bank (PDB) and the Biological Magnetic Resonance Data Bank (BMRB) under the ID 6MV3 and 30529, respectively.

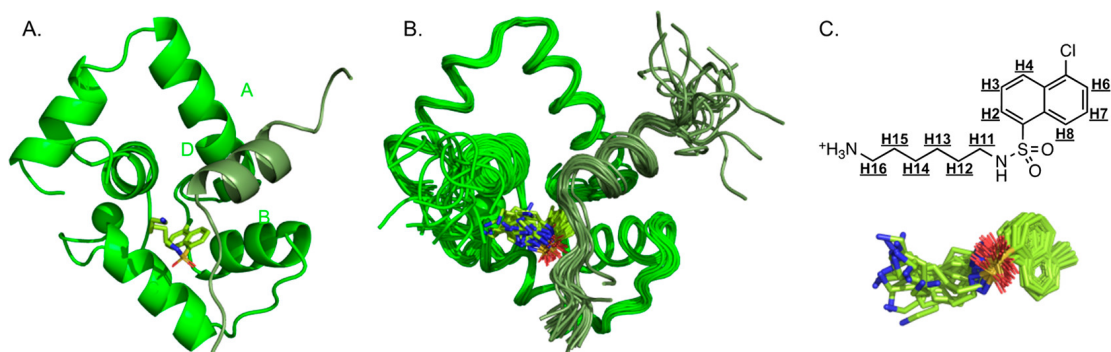


Figure 3.4. Structures of W7 bound to cChimera.

A. The solution structure of the cChimera-W7 complex. B. Top 20 structures as determined by xplor-nih are shown in green (linkers are removed for clarity). (cNTnC: light green, cTnI switch peptide: dark green, W7: lemon green, and Ca^{2+} ions: green spheres.) C. W7 chemical structure and superposition of W7 structures shown in sticks.

Table 3.1. Structural statistics of cChimera-W7 structures.

Structural statistics of the ensemble of the 20 structures of the cChimera-W7 complex.

Intramolecular distance restraints	
Total	1526
Within cNTnC region	1323
Within cTnI switch region	156
Between cNTnC and cTnI switch	47
Intermolecular distance restraints	
W7 and cChimera	52
W7 and cNTnC region	40
W7 and cTnI switch region	12
Artificial restraints to Ca^{2+}	6
Total distance restraints	1584
Backbone dihedral angle	192

Structure of cChimera in cChimera-W7 complex

We have previously determined that the structure of the cChimera in the absence of any ligands exhibits an open conformation, indicated by the movement of the B-C helix unit away from helices N-A-D²⁸, consistent with previous structures of cNTnC in the presence of cTnI switch region. The solution structure of cChimera-W7 complex is similar to the corresponding regions in the x-ray structure of cTn complex (1j1e.pdb)⁶ with an RMSD of 1.1 Å for backbone heavy atoms (used throughout) (Figure 3.5A); the NMR structure of cNTnC-cTnI switch peptide complex (1mxl.pdb)⁸ with an RMSD of 1.4 Å (Figure 3.5B); and the NMR solution structure of the unliganded cChimera (5vln.pdb)²⁸ with a RMSD of 1.1 Å (excluding linker region) (Figure 3.5C). The NMR solution structure of cChimera-W7 complex contains cNTnC, formed by five well-defined helices from N, A, B, C, D, and the cTnI switch region, which contains an additional α -helix. The helical position and length of the cTnI switch region in cChimera-W7 complex is the same as that observed in cChimera, with the helix starting at residue A150 and ending at residue L158/G159, which is also consistent with the cTnI switch region in x-ray crystal structure of the troponin complex. The helix of cTnI switch region sits between the A-B-D helices of cNTnC, making contacts with hydrophobic amino acids of A23, I26, F27 in the A-helix, V44, M45, M47, L48 in the B-helix and M81, S84 in the D-helix.

When cChimera-W7 complex structure is compared to the previously determined cNTnC-cTnI switch-W7 complex structure (2krd.pdb)²⁵ (Figure 3.5D), the RMSD is 2.1 Å for all residues and 1.7 Å for cNTnC. The C/D pair of EF hand in cNTnC-cTnI switch-W7 complex structure is more open than in the cChimera-W7 complex structure. The switch peptide helical structure in cNTnC-cTnI switch-W7 complex starts at D151 and ends at A156, compared to the longer helical structure of A150-L158/G159 in cChimera-W7 complex. However, although the structure shows that part of the helical structure of cTnI switch peptide is diminished in cNTnC-cTnI switch-W7, the overall orientation and position of cTnI switch is still similar for both of the structures. The backbone atoms of the cTnI switch region 17 residues (cTnI 147-163) in cChimera-W7 complex structure superimpose on to the average peptide structure with an RMSD of 0.7 Å, compared with an RMSD of 1.9 Å in the cNTnC-

cTnI switch-W7 complex structure. This indicates that the cTnI switch region in cChimera-W7 complex structure is well resolved, taking advantage of the isotope labeled cTnI switch peptide of cChimera protein. We note that in the structure of cNTnC- cTnI switch-W7 complex, most of the switch peptide (in excess of cNTnC) is in the free state, not bound to cNTnC. Thus, it is not surprising that the switch peptide has less secondary structure. However, in the current study using cChimera, we demonstrate that the cTnI switch region is actually able to adopt its fully folded conformation in binding to the cNTnC domain, undisturbed by binding of W7.

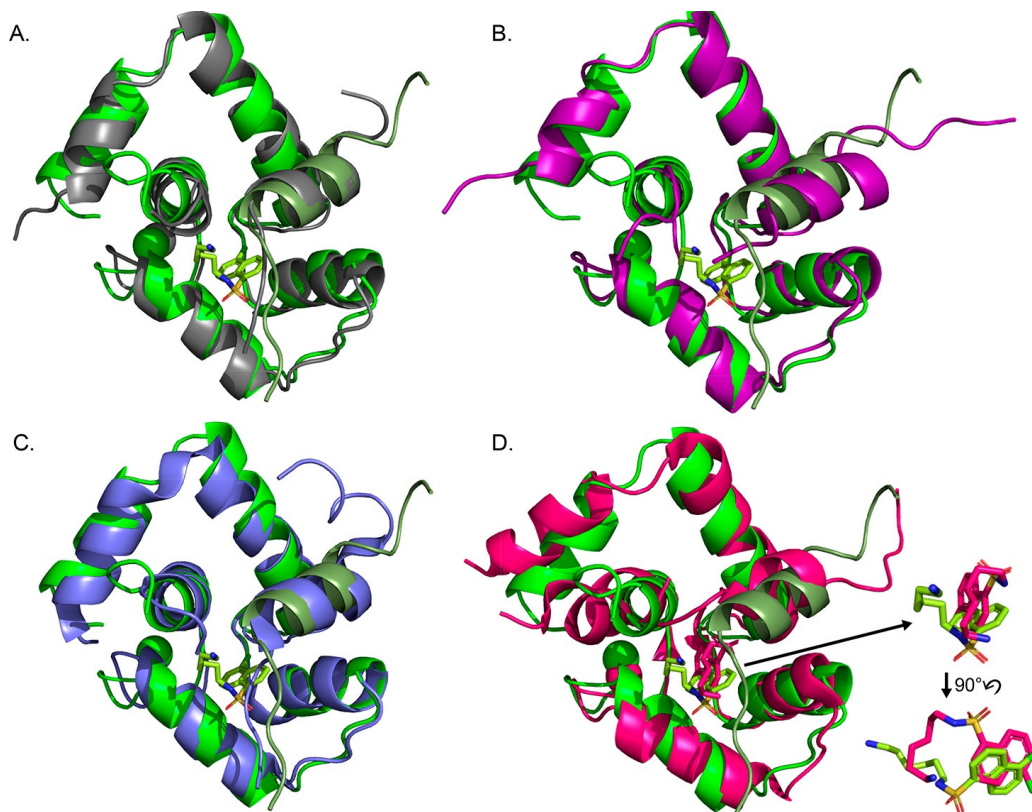


Figure 3.5. Structure comparison of cChimera-W7.

Comparison of the structure of the cChimera-W7 complex (green) with A. the X-ray structure cNTnC-cTnI derived from the cardiac troponin complex (1j1e.pdb, grey); B. the NMR structure of the cNTnC-cTnI[147–163] complex (1mxl.pdb, purple); C. the NMR structure of cChimera (5vln.pdb, blue); and D. the NMR structure of the cNTnC-cTnI[147–163]-W7 complex (2krd.pdb, pink), insert shows position of W7.

Structure of W7 in cChimera-W7 complex

W7 consists of a hydrophobic naphthalene group and a positively charged N-(6-aminohexyl) tail. 52 NOE-derived distance restraints define the position of W7 between the interface of cNTnC and cTnI switch region. The binding site of W7 in the cChimera-W7 complex is similar as in the structure of cNTnC-cTnI switch-W7 complex, but the orientation is flipped. All residues contacting W7 are colored in red shown in Figure 3.6A. The chlorine containing ring of W7 naphthalene ring contacts I61 on helix C and V72 from central β -sheet of cNTnC, indicating its deep binding position in the hydrophobic cleft (Figure 3.6B). The naphthalene ring of W7 contacts L41 and M45 on helix B, M60, I61 and V64 on helix C, M80 and M81 on helix D, as well as I148, A150 and M153 of cTnI switch region (Figure 3.6C). This hydrophobic binding site of W7 is comparable to that of other compounds that interact with cTnC such as bepridil¹³, dfbp-o¹⁶, and W7²⁵, and that interact with cChimera such as i9¹⁷ and 3-mDPA²⁸. A number of hydrophobic residues located in middle region of the W7 binding pocket, contacting both of the naphthalene rings and the hydrophobic hexyl part of the tail. M45, M80 and I148 also contact H11 of the proximal tail, while V64 and M81 contact more of the tail, H11, H12/H15 and H13/H14. (Note: H12 and H15 have very similar chemical shifts, as do H13 and H14.)

We observed close proximity between R147 and H13/14 of W7 (Figure 3.6B), supporting the previous hypothesis that the positively charged $-\text{NH}^{3+}$ tail of W7 repels the positively charged R147 of the cTnI switch region. Binding of W7 partially displaces cTnI I148 from its binding pocket in cNTnC. This rotates the extended backbone of R147-I148 in such a way that R147 is brought into closer proximity to the W7 tail. It is possible that the flexible tail of W7 is able to accommodate cTnI switch region binding, but when cTnI switch region is not bound, the flexible tail of W7 is able to bind to surfaces on cNTnC that obstruct cTnI binding.

An NOE contact was observed between W7 tail (H13/H14 and H12/15) and S84 (Figure 3.6B). Serine 84 was a C84S mutation introduced into the cChimera protein to avoid issues with cysteine oxidation. It has been shown that C84 forms reversible covalently thioimidate bond with a calcium sensitizer levosimendan. In our cChimera-W7 complex structure, we observe relatively strong NOEs between W7 tail

atoms and both H α and H β of S84, indicating that the S84 is in the binding pocket and Cysteine in this position might be important even for non-covalent drug. A concern about the proximity to S84 is that previous fluorescence studies usually attach the fluorophore on C84 position, might be present a caveat for drug screening.

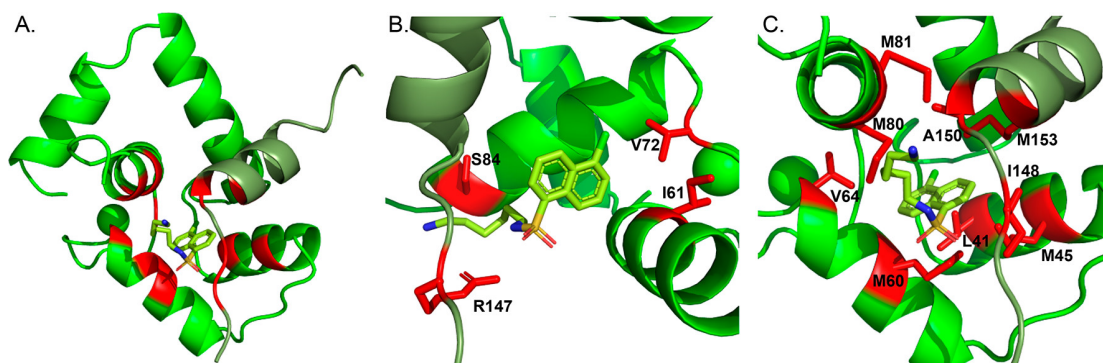


Figure 3.6. W7 binding pocket.

A. Structure of cChimera-W7 complex with residues contacting W7 shown in red; B. W7 deep binding ring contact with V72 and I61, and W7 tail contact with R147 and S84; and C. close-up view of the hydrophobic pocket of W7 binding showing residues lining pocket. The main contacts are shown in sticks.

All carbon protons of W7 except H16, which is the methylene group on the tail adjacent to the positively charged amide, are observed making contact to cChimera in the NMR experiments. One possible explanation for the absence of H16 contacts would be that the positively charged tail is flexible and goes out into the solvent, making it difficult to detect a specific NOE contact. When comparing the W7 binding position of cChimera-W7 complex and cNTnC-cTnI switch-W7 complex, the naphthalene ring is at a similar position, but the orientation is flipped with the chlorine pointing at a different direction (Figure 3.5D insert). The tail in the present structure is extended into the solvent, in contrast of the W7 in the cNTnC-cTnI switch-W7 complex structure, in which the tail is curled back into the protein against the W7 naphthalene ring. The

current structure seems more compatible with simultaneous binding of W7 and the cTnI switch peptide, given the favorable energy associated with solvating the amino group of W7, along with the greater conformational entropy of a solvent-exposed tail. We note that in the previous structure of cNTnC- cTnI switch-W7 complex, W7 is bound in an orientation that is more disruptive of switch peptide binding, whereas in the current structure, it is more accommodating.

cChimera dynamics

We carried out 2D NMR lineshape (TITAN) analyses to extract the dissociation rates k_{off} and the binding constant K_D of W7 binding for cChimera. The K_D calculated from TITAN is $450 \mu\text{M} \pm 100 \mu\text{M}$, which is consistent with the chemical shift perturbation-based fitting results using xcrvfit. The k_{off} of W7 to cChimera is about 10^4 s^{-1} (Figure 3.7A). These rates indicate a k_{on} of approximately $2 \times 10^7 \text{ M}^{-1} \text{ s}^{-1}$, which is near the diffusion-controlled limit with no limiting conformational exchange.

To evaluate changes in the dynamics of cChimera upon W7 binding, we determined the T_2 relaxation time for backbone amide of cChimera in the absence and presence of W7. R_2 values ($1/T_2$) for most of the cChimera residues in the absence of W7 are around 10 s^{-1} , with a few spikes (grey in Figure 3.7B). We noticed that cChimera is in a rapid conformational change even before small molecule binding, characterized by large R_2 values for F27, V28 (the last few residues of A helix), and V64 (the last residue of C helix), indicating an exchange between open and closed conformations. The R_2 of A150 and L157, the first and the last residues of the helical part of the cTnI switch region, experiencing large R_2 value as well consistent with conformational exchange. After W7 is added to $[\text{W7}]:[\text{cChimera}]=1:1$ (light green in Figure 3.7B), the R_2 profiles of cChimera in the absence and presence of W7 were very similar, though consistently slightly higher after addition of W7. When the W7 is added to $[\text{W7}]: [\text{cChimera}]= 5:1$ (dark green in Figure 3.7B), the R_2 profiles of cChimera:5X-W7 did not change significantly but become consistently higher when more W7 is added into the NMR sample, with R_2 increased from 10 to 12 s^{-1} . One possible explanation is that cChimera has a slight tendency to aggregate as more W7 is added. The R_2 value of F27, V64 and A150 higher at $[\text{W7}]: [\text{cChimera}]=1:1$ than $[\text{W7}]:$

[cChimera]=5:1, consistent with the expected behavior of exchange broadening as a function of fraction bound⁴⁰.

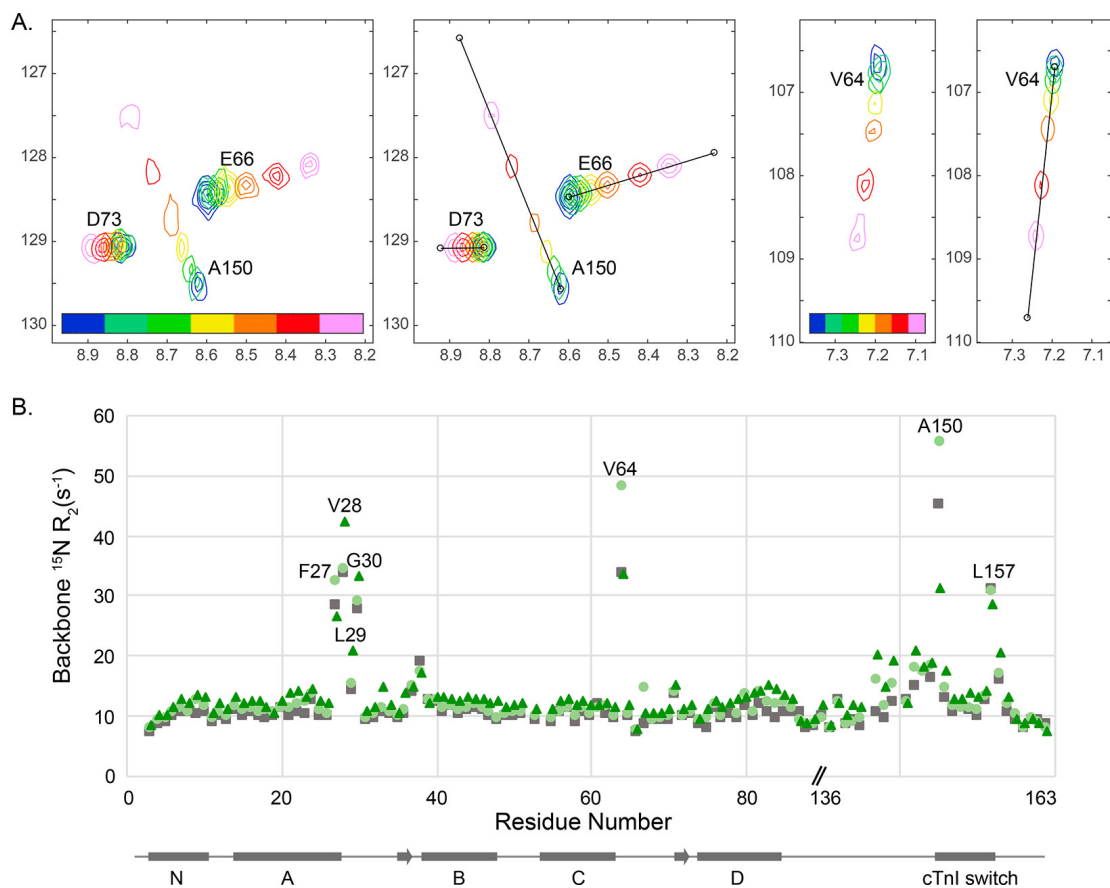


Figure 3.7. cChimera dynamics upon W7 binding.

Fitting of the W7 titration of cChimera monitored by $^1\text{H},^{15}\text{N}$ -2D HSQC NMR spectroscopy to extract kinetic information. A. The observed and fitted $^1\text{H},^{15}\text{N}$ -HSQC spectra are shown in the left and right panels for residues A150, E66, and V64. The cross peaks are color-ramped from blue to pink with increasing W7 concentration. B. ^{15}N backbone R_2 NMR relaxation for cChimera with 0 μM (grey), 500 μM (light green), and 2500 μM (dark green) W7.

Conclusions

In general, while mutations in thin filament sarcomere proteins can lead to large scale remodeling of the heart in the long term, little change can be observed in the structures or dynamics of these proteins (see L29Q⁴¹, L48Q⁴², and trout proteins⁴³). Cardiac DCM, HCM, and RCM mutations very often involve changes in charge^{3,4}. The situation is similar for drugs. This paper demonstrates that W7 is able to bind in a manner that is not perturbing to the cTnI switch peptide, which is different from the expectation that it displaces the switch peptide from its favored site, thus accounting for the drastic decrease in switch peptide affinity. Our structure of the cTnC-cTnI chimera W7 complex presented herein shows small changes such as the movement of residues in cTnI, caused by either electrostatic repulsion or steric clash, and contacts with S84 (replacing C84). Do these structural changes, or changes induced in the thermodynamics and kinetics of the complex formation, lead to the alterations of the performance of the heart?

Acknowledgments

This study was supported by grants from Heart and Stroke Foundation of Canada (B.D.S., G-14-0005884) and Canadian Institutes of Health Research (CIHR) (B.D.S., 37769). The authors would like to thank Philip Liu for assistance with protein purification.

References

1. Davis, J., Wen, H., Edwards, T. & Metzger, J. M. Allele and species dependent contractile defects by restrictive and hypertrophic cardiomyopathy-linked troponin I mutants. *J. Mol. Cell. Cardiol.* **44**, 891–904 (2008).
2. Wexler, R., Elton, T., Pleister, A. & Feldman, D. Cardiomyopathy: An overview. *Am. Fam. Physician* **79**, 778–784 (2009).
3. Willott, R. H. *et al.* Mutations in Troponin that cause HCM, DCM AND RCM: What can we learn about thin filament function? *J. Mol. Cell. Cardiol.* **48**, 882–892 (2010).
4. Parvatiyar, M. S., Pinto, J. R., Dweck, D. & Potter, J. D. Cardiac Troponin Mutations and Restrictive Cardiomyopathy. *J. Biomed. Biotechnol.* **2010**, 1–9 (2010).
5. Kass, D. A. & Solaro, R. J. Mechanisms and use of calcium-sensitizing agents in the failing heart. *Circulation* **113**, 305–315 (2006).
6. Takeda, S., Yamashita, A., Maeda, K. & Maéda, Y. Structure of the core domain of human cardiac troponin in the Ca(2+)-saturated form. *Nature* **424**, 35–41 (2003).
7. Parry, D. A. D. & Squire, J. M. Structural role of tropomyosin in muscle regulation: Analysis of the X-ray diffraction patterns from relaxed and contracting muscles. *J. Mol. Biol.* **75**, 33–55 (1973).
8. Li, M. X., Spyropoulos, L. & Sykes, B. D. Binding of cardiac troponin-I147-163 induces a structural opening in human cardiac troponin-C. *Biochemistry* **38**, 8289–98 (1999).
9. Kobayashi, T., Jin, L. & de Tombe, P. P. Cardiac thin filament regulation. *Pflügers Arch. - Eur. J. Physiol.* **457**, 37–46 (2008).
10. Li, M. X., Wang, X. & Sykes, B. D. Structural based insights into the role of troponin in cardiac muscle pathophysiology. *J. Muscle Res. Cell Motil.* **25**, 559–79 (2004).
11. Berlin, J. R., Bassani, J. W. & Bers, D. M. Intrinsic cytosolic calcium buffering properties of single rat cardiac myocytes. *Biophys. J.* **67**, 1775–1787 (1994).
12. Solaro, R. J., Bousquet, P. & Johnson, J. D. Stimulation of cardiac myofilament

- force, ATPase activity and troponin C Ca⁺⁺ binding by bepridil. *J. Pharmacol. Exp. Ther.* **238**, 502–7 (1986).
13. Wang, X., Li, M. X. & Sykes, B. D. Structure of the regulatory N-domain of human cardiac troponin C in complex with human cardiac troponin I147-163 and bepridil. *J. Biol. Chem.* **277**, 31124–33 (2002).
 14. Sorsa, T., Pollesello, P., Permi, P., Drakenberg, T. & Kilpeläinen, I. Interaction of levosimendan with cardiac troponin C in the presence of cardiac troponin I peptides. *J. Mol. Cell. Cardiol.* **35**, 1055–61 (2003).
 15. Robertson, I. M., Baryshnikova, O. K., Li, M. X. & Sykes, B. D. Defining the binding site of levosimendan and its analogues in a regulatory cardiac troponin C-troponin I complex. *Biochemistry* **47**, 7485–95 (2008).
 16. Robertson, I. M., Sun, Y.-B. B., Li, M. X. & Sykes, B. D. A structural and functional perspective into the mechanism of Ca²⁺-sensitizers that target the cardiac troponin complex. *J. Mol. Cell. Cardiol.* **49**, 1031–41 (2010).
 17. Pineda-Sanabria, S. E., Robertson, I. M., Sun, Y.-B. B., Irving, M. & Sykes, B. D. Probing the mechanism of cardiovascular drugs using a covalent levosimendan analog. *J. Mol. Cell. Cardiol.* **92**, 174–84 (2016).
 18. Robertson, I. M. *et al.* Reversible Covalent Binding to Cardiac Troponin C by the Ca²⁺-Sensitizer Levosimendan. *Biochemistry* **55**, 6032–6045 (2016).
 19. Lindert, S., Li, M. X., Sykes, B. D. & McCammon, J. A. Computer-Aided Drug Discovery Approach Finds Calcium Sensitizer of Cardiac Troponin. *Chem. Biol. Drug Des.* **85**, 99–106 (2015).
 20. Aprahamian, M. L. *et al.* Successful Identification of Cardiac Troponin Calcium Sensitizers Using a Combination of Virtual Screening and ROC Analysis of Known Troponin C Binders. *J. Chem. Inf. Model.* **57**, 3056–3069 (2017).
 21. Hidaka, H. *et al.* A Novel Vascular Relaxing Agent, N-(6-Aminohexyl)-5-Chloro-1-Naphthalenesulfonamide Which Affects Vascular Smooth Muscle Actomyosin. *J. Pharmacol. Exp. Ther.* **207**, 8–15 (1978).
 22. Hidaka, H. *et al.* Calcium-regulated modulator protein interacting agents inhibit smooth muscle calcium-stimulated protein kinase and ATPase. *Mol. Pharmacol.* **17**, 66–72 (1980).

23. Adhikari, B. B. & Wang, K. Interplay of Troponin- and Myosin-Based Pathways of Calcium Activation in Skeletal and Cardiac Muscle: The Use of W7 as an Inhibitor of Thin Filament Activation. *Biophys. J.* **86**, 359–370 (2004).
24. Thompson, B. R., Martindale, J. & Metzger, J. M. Sarcomere neutralization in inherited cardiomyopathy: small-molecule proof-of-concept to correct hyper-Ca²⁺-sensitive myofilaments. *Am. J. Physiol. Heart Circ. Physiol.* **311**, H36-43 (2016).
25. Oleszczuk, M., Robertson, I. M., Li, M. X. & Sykes, B. D. Solution structure of the regulatory domain of human cardiac troponin C in complex with the switch region of cardiac troponin I and W7: The basis of W7 as an inhibitor of cardiac muscle contraction. *J. Mol. Cell. Cardiol.* **48**, 925–933 (2010).
26. Julien, O. *et al.* Is there nascent structure in the intrinsically disordered region of troponin I? *Proteins* **79**, 1240–1250 (2011).
27. Pineda-Sanabria, S. E., Julien, O. & Sykes, B. D. Versatile Cardiac Troponin Chimera for Muscle Protein Structural Biology and Drug Discovery. *ACS Chem. Biol.* **9**, 2121–2130 (2014).
28. Cai, F. *et al.* Structures reveal details of small molecule binding to cardiac troponin. *J. Mol. Cell. Cardiol.* **101**, 134–144 (2016).
29. Delaglio, F. *et al.* NMRPipe: A multidimensional spectral processing system based on UNIX pipes. *J. Biomol. NMR* **6**, 277–293 (1995).
30. Johnson, B. A. & Blevins, R. A. NMR View: A computer program for the visualization and analysis of NMR data. *J. Biomol. NMR* **4**, 603–614 (1994).
31. Waudby, C. A., Ramos, A., Cabrita, L. D. & Christodoulou, J. Two-Dimensional NMR Lineshape Analysis. *Sci. Rep.* **6**, 24826 (2016).
32. Shen, Y., Delaglio, F., Cornilescu, G. & Bax, A. TALOS+: A hybrid method for predicting protein backbone torsion angles from NMR chemical shifts. *J. Biomol. NMR* **44**, 213–23 (2009).
33. Hafsa, N. E., Arndt, D. & Wishart, D. S. CSI 3.0: A web server for identifying secondary and super-secondary structure in proteins using NMR chemical shifts. *Nucleic Acids Res.* **43**, W370–W377 (2015).
34. Rieping, W. *et al.* ARIA2: Automated NOE assignment and data integration in

- NMR structure calculation. *Bioinformatics* **23**, 381–382 (2007).
35. Schüttelkopf, A. W. & van Aalten, D. M. F. *PRODRG*: a tool for high-throughput crystallography of protein–ligand complexes. *Acta Crystallogr. Sect. D Biol. Crystallogr.* **60**, 1355–63 (2004).
 36. Kleywegt, G. J. Dictionaries for Heteros. *CCP4/ESF- EACBM Newsl. Protein Crystallogr.* **31**, 45–50. (1995).
 37. Schwieters, C. D., Kuszewski, J. J., Tjandra, N. & Clore, G. M. The Xplor-NIH NMR molecular structure determination package. *J. Magn. Reson.* **160**, 65–73 (2003).
 38. Li, M. X., Hoffman, R. M. B. & Sykes, B. D. Interaction of Cardiac Troponin C and Troponin I with W7 in the Presence of Three Functional Regions of Cardiac Troponin I †. *Biochemistry* **45**, 9833–9840 (2006).
 39. Hoffman, R. M. B., Li, M. X. & Sykes, B. D. The binding of W7, an inhibitor of striated muscle contraction, to cardiac troponin C. *Biochemistry* **44**, 15750–15759 (2005).
 40. Baldo, J. H., Halford, S. E., Patt, S. L. & Sykes, B. D. The Stepwise Binding of Small Molecules to Proteins. Nuclear Magnetic Resonance and Temperature Jump Studies of the Binding of 4-(N-Acetylamino-glucosyl)-N-acetylglucosamine to Lysozyme. *Biochemistry* **14**, 1893–1899 (1975).
 41. Robertson, I. M. *et al.* The structural and functional effects of the familial hypertrophic cardiomyopathy-linked cardiac troponin C mutation, L29Q. *J. Mol. Cell. Cardiol.* **87**, 257–269 (2015).
 42. Wang, D. *et al.* Structural and Functional Consequences of the Cardiac Troponin C L48Q Ca²⁺-Sensitizing Mutation. *Biochemistry* **51**, 4473–4487 (2012).
 43. Gillis, T. E., Blumenschein, A., T. M., Sykes, B. D. & Tibbits, G. F. Effect of Temperature and the F27W Mutation on the Ca²⁺ Activated Structural Transition of Trout Cardiac Troponin C †. *Biochemistry* **42**, 6418–6426 (2003).

Chapter 4

The Role of Electrostatics in the Mechanism of Cardiac Thin Filament Based Sensitizers

Fangze Cai¹, Ian M. Robertson², Thomas Kampourakis³,
Brittney A. Klein¹, Brian D. Sykes¹

¹Department of Biochemistry, University of Alberta, Edmonton, AB, Canada.

²Ministry of Health, Government of Alberta, Edmonton, AB, Canada

³Randall Centre for Cell and Molecular Biophysics, King's College London, London, United Kingdom.

A version of this chapter has been previously published: Cai, F., Robertson, I. M., Kampourakis, T., Klein, B. A. & Sykes, B. D. The Role of Electrostatics in the Mechanism of Cardiac Thin Filament Based Sensitizers. *ACS Chem. Biol.* **15**, 2289–2298 (2020).

Contribution: IMR designed and synthesized the A-series compounds. FC acquired the NMR spectra for structure determination, dynamics study, analyzed the data and solved the structure. FC and IMR performed drug and peptide titrations, wrote the manuscript. TK prepared the ventricular trabeculae and performed force-calcium titrations. All authors helped review and edit the manuscript. BDS guided the research.

Summary

Heart muscle contraction is regulated by calcium binding to cardiac troponin C. This induces troponin I (cTnI) switch region binding to the regulatory domain of troponin C (cTnC), pulling the cTnI inhibitory region off actin and triggering muscle contraction. Small molecules targeting this cTnC–cTnI interface have potential in the treatment of heart disease. Most of these have an aromatic core which binds to the hydrophobic core of cTnC, and a polar and often charged ‘tail’. The calmodulin

antagonist W7 is unique in that it acts as calcium desensitizer. W7 binds to the interface of cNTnC and cTnI switch region and weakens cTnI binding, possibly by electrostatic repulsion between the positively charged terminal amino group of W7 and the positively charged RRVR₁₄₄₋₁₄₇ region of cTnI. To evaluate the role of electrostatics, we synthesized A7, where the amino group of W7 was replaced with a carboxyl group. We determined the high-resolution solution NMR structure of A7 bound to a cNTnC–cTnI chimera. The structure shows that A7 does not change the overall conformation of the cNTnC–cTnI interface, and the naphthalene ring of A7 sits in the same hydrophobic pocket as that of W7, but the charged tail takes a different route to the surface of the complex, especially with respect to the position of the switch region of cTnI. We measured the affinities of A7 for cNTnC and the cNTnC–cTnI complex and that of the cTnI switch peptide for the cNTnC–A7 complex. We also compared the binding of W7 and A7 for two cNTnC–cTnI chimeras, differing in the presence or absence of the RRVR region of cTnI. A7 decreased the binding affinity of cTnI to cNTnC substantially less than W7 and bound more tightly to the more positively charged chimera. We tested the effects of W7 and A7 on the force-calcium relation of demembrated rat right ventricular trabeculae and demonstrated that A7 has a much weaker desensitization effect than W7. We also synthesized A6, which has one less methylene group on the hydrocarbon chain than A7. A6 did not affect binding of cTnI switch peptide nor change the calcium sensitivity of ventricular trabeculae. These results suggest that the negative inotropic effect of W7 may result from a combination of electrostatic repulsion and steric hindrance with cTnI.

Introduction

Heart muscle contraction is regulated by the binding of calcium to the heterotrimeric thin filament protein troponin. The thin filament is made up of the double helical F-actin filament, tropomyosin, and troponin. Troponin is a complex of three proteins: the calcium binding subunit troponin C (cTnC), the inhibitory subunit troponin I (cTnI) and the tropomyosin binding subunit troponin T (cTnT)^{1,2}. cTnT is an elongated molecule that binds both cTnC and cTnI, as well as anchors the complex to the thin filament by interactions with tropomyosin. At resting calcium concentration,

the inhibitory region of cTnI (residues 135-147) is bound to actin, causing tropomyosin to be reoriented into a position that blocks myosin binding sites on actin, inhibiting muscle contraction³. When the cytosolic calcium concentration increases during systole, calcium binds to the regulatory domain of cTnC (cNTnC), causing conformational changes to promote association with the switch region of cTnI (residues 147-163)⁴. The binding of cTnI switch region drags cTnI off actin and triggers muscle contraction by the formation of actin-myosin cross-bridges (reviewed in ⁵⁻⁷). The calcium-sensitive cNTnC-cTnI switch region interaction therefore triggers contraction, and pharmacological fine-tuning of either calcium binding to cNTnC or the formation of the cNTnC-cTnI complex represent a rationale for the development of novel heart failure therapeutics.

A number of small molecules have been found to bind to cTnC and modulate the calcium sensitivity of muscle contraction. Our hypothesis is that the interaction of cTnI with cTnC following calcium binding is a major regulatory element and that many compounds influence force by perturbing this interaction. Most of these small molecules have a common motif including an aromatic core that binds to the hydrophobic core of cNTnC, which is exposed upon calcium binding, and a polar and often charged 'tail' positioned at or near the cNTnC-cTnI interface, which contains many charged residues from the acidic cTnC and the basic cTnI proteins. The calmodulin antagonist, W7 (N-(6-aminohexyl)-5-chloro-1-naphthalenesulfonamide), is a negative inotrope, which decreases muscle contractility^{8,9}. W7 binds to the interface of cNTnC and cTnI switch region and weakens cTnI binding to cNTnC¹⁰. The calcium channel blocker, bepridil, was found to be a calcium sensitizer¹¹ by binding to the hydrophobic pocket of cNTnC and stabilizing its calcium-bound open conformation¹². Despite acting as a calcium sensitizer, the NMR structure showed that bepridil partially clashed with the cTnI switch peptide, possibly by the repulsion between the positively charged nitrogen in the pyrrolidine ring and positively charged cTnI¹³. dfbp-o (2',4'-difluoro(1,1'-biphenyl)-4-yloxy acetic acid) was shown to be a positive inotrope that increased cardiac muscle contractility. This compound binds to the same interface and increases the binding affinity of cTnI switch peptide¹⁴. The NMR solution structures revealed that bepridil, W7 and dfbp-o all bind to the

hydrophobic pocket formed by cNTnC-cTnI switch peptide yet the overall structures of cNTnC-cTnI switch peptide-drug complex were not significantly different^{14,15}. The structure and position of cTnI switch region is not significantly perturbed in the presence of these compounds when compared to the solution structure of cNTnC-cTnI switch peptide⁴ or X-ray structure of the core troponin complex¹⁶. The binding affinity of cTnI switch peptide is markedly reduced in the presence of W7, but enhanced in the presence of dfbp-o. Comparisons of the structures revealed that the positively charged terminal amino group of W7 appears to repel the guanidinium group of R147 of cTnI switch region whereas the negatively charged carboxyl group of dfbp-o appears to attract it. The functional distinctions between these two compounds were rationalized to result from the differences in the charge of the two molecules^{10,14,15}.

The chemical structures of dfbp-o and W7 have differences other than the charge (Figure 4.2), and other issues such as the degree of opening of cNTnC are involved in the perturbation of the calcium sensitization of force development. For example, although bepridil inhibits cTnI binding to cNTnC¹³, it still acts as a calcium sensitizer, presumably through its enhancement of calcium binding to cTnC¹¹ by stabilizing the N-domain's open state¹². In order to evaluate how important electrostatics are in tuning the cNTnC-cTnI interface and the development of small molecules that perturb this interaction, we synthesized a new compound N-(6-carboxylhexyl)-5-chloro-1-naphthalenesulfonamide (A7) which has a carboxyl group in place of the amino group of W7. We determined the high-resolution solution NMR structure of A7 bound to cNTnC-cTnI chimera. The structure shows that A7 does not change the overall structure of the cNTnC-cTnI interface, and that the naphthalene ring of A7 sits in the same hydrophobic pocket as W7. However, the charged tail takes a different route to the surface of the complex, especially with respect to the position of the switch region of cTnI. We measured the affinities of A7 for cNTnC and the cNTnC-cTnI complex, and that of the cTnI switch peptide for the cNTnC-A7 complex. A7 was found to decrease the binding affinity of cTnI much less than W7. We compared the binding of W7 and A7 to two cNTnC-cTnI chimeras, which differ in the presence or absence of the RRVR region of cTnI. We tested the effect of W7 and A7 on the force-calcium relation of demembrated rat right ventricular trabeculae showing that A7 has

a much weaker desensitization effect than W7. We also synthesized and tested N-(7-carboxylhexyl)-5-chloro-1-naphthalenesulfonamide (A8) and N-(5-carboxylhexyl)-5-chloro-1-naphthalenesulfonamide (A6), which have one more (A8) and one less (A6) methylene group on the hydrocarbon chain compared to A7. A8 turned out to be very hydrophobic and was not soluble under our experimental conditions. A6 did not affect binding of cTnI switch peptide, nor change the calcium sensitivity of trabeculae. These results suggest that electrostatics play an important role in the balance of interactions that regulate calcium sensitivity.

Material and methods

Protein expression, and purification

Recombinant cChimera, gChimera, and cNTnC (residues 1-89) were used in this study. cChimera contains cNTnC (residue 1-90), cTnI (residue 136-163), and a histidine tag. gChimera contains cNTnC (residue 1-89), a linker (SGGSSGGSSGG), cTnI (residue 145-168), and a histidine tag. Both chimeras have C35 and C84 substituted with serine. The [¹⁵N, ¹³C] and [¹⁵N] cChimera and [¹⁵N]-gChimera proteins were expressed in *E. coli* BL21(DE3) and purified by Ni-NTA affinity chromatography followed by dialysis and lyophilization as previously described¹⁷. Protein identity and purity were confirmed by gel electrophoresis and mass spectrometry. ¹⁵N- and ¹³C,¹⁵N-labeled cNTnC (residue 1-89) was purified as described previously¹⁸. The synthetic peptide cTnI (residues 147-163, acetyl-RISADAMMQALLGARAK-amide) was obtained from GL Biochem Ltd. (Shanghai, China), and its quality was assessed by HPLC, NMR spectroscopy, and ESI-Mass Spectrometry.

Chemicals

W7 (N-(6-aminoethyl)-5-chloro-1-naphthalenesulfonamide) was purchased from Sigma-Aldrich. A7 (N-(6-carboxylhexyl)-5-chloro-1-naphthalenesulfonamide), A8 (N-(7-carboxylhexyl)-5-chloro-1-naphthalenesulfonamide) and A6 (N-(5-carboxylhexyl)-5-chloro-1-naphthalenesulfonamide) were synthesized in-house. The reaction scheme is shown in Figure 4.1, the reaction procedure is similar to that outlined previously¹⁹.

Synthesis of A7: 7-aminoheptanoic acid (Sigma-Aldrich) was dissolved in 0.5 M $\text{Na}_2\text{CO}_3/\text{NaHCO}_3$ buffer (pH 9.4), and heated to 60 °C. 5-chloro-naphthalene-1-sulfonyl chloride (Toronto Research Chemicals) was dissolved in acetonitrile. A 10:1 molar excess of 7-aminoheptanoic acid to 5-chloro-naphthalene-1-sulfonyl chloride was used in these reactions. The 5-chloro-naphthalene-1-sulfonyl chloride solution was added dropwise to the stirring carbonate solution. The reaction was refluxed for 2 hours. The progress of the reaction was monitored using ^1H NMR spectroscopy. The solution was acidified using 6M $\text{HCl}_{(\text{aq})}$ (pH 4) and extracted with ethyl acetate and a brine solution. The organic solution was dried using NaSO_4 and the product was collected using vacuum filtration. The product was verified by Liquid Chromatography-Mass Spectrometry (LC-MS). Signals were observed at 370.09 (M+H) and 352.07 (M-H $_2\text{O}$ +H) m/z (Theoretical molecular weight = 369.86 g/mol). Synthesis of A6 and A8 were carried out as described above (Figure 4.1). The products were verified using ^1H NMR spectroscopy and LC-MS.

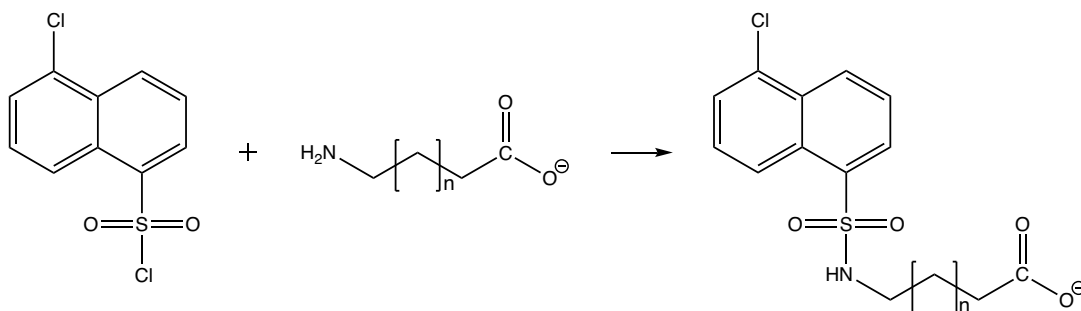


Figure 4.1. The reaction scheme used in the synthesis of A series compounds.

5-chloro-naphthalene-1-sulfonyl chloride (CNSC) was reacted with 8-aminooctanoic acid ($n=5$ for A8), 7-aminoheptanoic acid ($n=4$ for A7) and ϵ -aminocaproic acid ($n=3$ for A6).

NMR spectroscopy

The NMR samples were prepared in 5 mm NMR tubes to a final volume of 500 μ l. The protein samples were solubilized in 100 mM KCl, 10 mM imidazole, and 2-10 mM CaCl₂ in 95% H₂O/5% D₂O or 100% D₂O, using 0.25 mM 2,2-dimethyl-2-silapentane-5-sulfonate-d₆ sodium salt (DSS-d₆) as an NMR internal reference. The pH was maintained at 6.7-6.8. NMR data were collected at 30 °C on a Varian Inova 600 MHz spectrometer equipped with a triple resonance probe with pulsed field gradients. 1D NMR spectra were processed with VNMRJ v.3.2 A (Varian, Inc.), 2D and 3D NMR spectra were processed with NMRPipe²⁰ and analyzed with NMRViewJ²¹, using scripts written in-house.

Drug titrations and lineshape analysis

Peptide and drug stocks were prepared in DMSO-d₆ (Cambridge Isotopes) and concentrations were determined by 1D ¹H NMR spectroscopy, using DSS as an internal standard. The binding of small molecules or peptide to protein was monitored by NMR spectroscopy; at each aliquot, a ¹H,¹⁵N-HSQC NMR spectrum was acquired. All samples contained 2mM CaCl₂, and proteins were saturated with calcium. A7 was titrated into 0.15mM cChimera to final concentration of 0.01, 0.03, 0.06, 0.1, 0.15, 0.25, 0.35, 0.5 and 0.7 mM. W7 and A7 were titrated into 0.15mM gChimera to final concentration of 0.01, 0.03, 0.06, 0.1, 0.15, 0.25, 0.35, 0.5 and 0.7 mM. W7 was titrated into 0.15 mM cChimera to final concentrations of 0.015, 0.045, 0.1, 0.2, 0.5 and 1.1 mM. A7 was titrated into 0.14 mM of cNTnC to final concentration of 0.07, 0.14, 0.21, 0.28, 0.37, 0.56, and 0.84 mM. A7 was titrated into 0.3 mM of cNTnC-cTnI switch peptide to final concentrations of 0.08, 0.15, 0.23, 0.30, 0.38, 0.45, and 0.60 mM. cTnI switch peptide was titrated into a sample containing 0.13 mM of cNTnC-A7 to final concentrations of 0.03, 0.06, 0.09, 0.13, 0.17, 0.23, 0.28, 0.35, 0.48 mM. A6 was titrated into 0.2 mM of cNTnC to final concentrations of 0.05, 0.10, 0.20, 0.30, 0.35, 0.40, and 0.50 mM. A6 was titrated into 0.2 mM of cNTnC-cTnI switch peptide to final concentrations of 0.10, 0.20, 0.30, 0.40, 0.6, 0.70, 0.90 1.1 and 1.3 mM. cTnI switch peptide was titrated into 0.15 mM of cNTnC-A6 to final concentrations of 0.03, 0.06, 0.09, 0.11, 0.15, 0.19, 0.23, 0.28, 0.35 mM. By the end of the titration, the addition of

DMSO-d₆ did not exceed 5% of the sample volume. Dilution by each drug solution addition was taken into consideration when calculating the concentration of protein at each titration point. Chemical shift perturbation at each titration point were used by our in-house data fitting program, xcrvfit (www.bionmr.ualberta.ca/bds/software/xcrvfit), to calculate dissociation constants, K_D .

The ¹⁵N- T2 relaxation experiments were acquired at A7 concentrations of 0, 0.25 and 0.75mM ([A7]/[cChimera]=0, 0.5 and 1.5). The relaxation data were fitted to a two-parameter exponential decay curve using the Rate Analysis module of NMRViewJ²¹. ¹⁵N T2 relaxation experiments were acquired with recycle delay of 3 s, and variable relaxation delays of 10, 30, 50, 70, 90 and 110 ms. The titration of A7 to cChimera monitored by 2D-¹H,¹⁵N HSQC spectra was also analyzed by the 2D lineshape analysis software TITAN²². The two-state binding model is selected since A7 binding to cChimera is 1:1 stoichiometry. Protein and A7 concentrations, and NMR acquisition parameters were provided as inputs for the data fitting. Several peaks with significant chemical shift perturbation were chosen to be fitted to calculate dissociation constant, K_D , and dissociation rate, k_{off} . An error analysis was performed using 200 repeats to determine the uncertainties of the fitting.

Structure calculations

The sample for cChimera-A7 complex structural studies contained 0.5 mM ¹⁵N,¹³C- labeled cChimera with 0 - 0.7 mM A7. The backbone and side chain ¹H, ¹⁵N, and ¹³C chemical shift assignments for cChimera-A7 complex were obtained by analyzing the A7 to cChimera titration monitored by 2D-¹H,¹⁵N HSQC and 2D-¹H,¹³C HSQC NMR spectra. 3D ¹³C-edited NOESY (mixing time 100 ms) was used to complete the chemical shift assignment and obtain intramolecular (within the protein cChimera) distance restraints. The assignment of A7 in cChimera-A7 complex was obtained by following cChimera to A7 titration monitored by 1D spectra. Intermolecular distance restraints between A7 and cChimera were derived from 3D ¹³C-edited NOESY and 2D NOESY (mixing time:100ms) experiments.

Backbone ϕ - and ψ -dihedral angle restraints were predicted using TALOS+ based on backbone chemical shifts ($H\alpha$, $C\alpha$, $C\beta$, N, and HN)²³. Intramolecular distance

restraints within the protein were generated using ARIA 2.3²⁴, and all assignments were checked manually for errors. Parameter and topology files for A7 was generated using PRODRG²⁵ and xplor2d²⁶, and were modified manually. Intermolecular NOEs between A7 and cChimera were manually assigned, used to generate distance restraints that were added to the XPLOR-NIH structure calculations²⁷. Intermolecular NOEs between cNTnC region of the cChimera and Ca²⁺ were derived from crystallographic data of the cardiac troponin complex. The distance and dihedrals constraints were used in the simulated annealing module of Xplor-NIH, version 2.46. The weight is set to be 3 for NOE between A7 and cChimera, and 1 for all other NOEs. 300 structures were calculated, from which the lowest-energy structure was used as the starting point for refinement. 300 structures were calculated using the water refinement protocol. The final ensemble consists of the 10 lowest-energy structures generated in the refinement step with no NOE violations > 0.5 Å or dihedral violation > 5°.

Preparation of ventricular trabeculae and force-calcium titrations

All animals were treated in accordance with the guidelines approved by the UK Animal Scientific procedures Act (1986) and European Union Directive 2010/63/EU. Wistar rats (male, 200-250 g) were sacrificed by cervical dislocation without the use of anesthetics (Schedule 1 procedure in accordance with UK Animal Scientific Procedure Act, 1986) and demembrated right ventricular trabeculae were prepared as described previously²⁸.

Trabeculae were mounted between a force transducer (KRONEX, model A-801, resonance frequency ~2 kHz) and length controller (Aurora Scientific, Model 312C) in relaxing solution (composition in mmol/L: 25 Imidazole, 15 Na₂CrP, 78.4 KPr, 5.65 Na₂ATP, 6.8 MgCl₂, 10 K₂EGTA, 1 DTT, pH 7.1). Each activation was preceded by a 2-min incubation in pre-activating solution (composition in mmol/L: 25 imidazole, 15 Na₂CrP, 108.2 KPr, 5.65 Na₂ATP, 6.3 MgCl₂, 0.2 K₂EGTA, 1 DTT, pH 7.1). Solutions with varying concentrations of free [Ca²⁺] were prepared by mixing relaxing and activating solutions (in mmol/L: 25 imidazole, 15 Na₂CrP, 58.7 KPr, 5.65 Na₂ATP, 6.3 MgCl₂, 10 CaCl₂, 10 K₂EGTA, 1 DTT, pH 7.1) using MAXCHELATOR software (maxchelator.stanford.edu). The dependence of force on free calcium

concentration was fitted to data from individual trabeculae using non-linear least-squares regression to the modified Hill equation:

$$F = T + T_0 * \frac{1}{1 + 10^{n_H(pCa - pCa_{50})}}$$

where T is the resting tension, T₀ is the maximal calcium activated force, pCa₅₀ is the negative logarithm of [Ca²⁺] corresponding to half-maximal change in F and n_H is the Hill coefficient. Trabeculae which showed a decline in maximal calcium activated force of more than 15% after the pCa titrations were discarded.

The rate of force re-development was measured by a fast release and re-stretch protocol²⁹. Briefly, isometrically contracting trabeculae were released by 20% of their initial length (~500 μs step response), held at the new length for ~30 ms, and re-stretched to the original length. The time-course of force redevelopment was fitted to a single exponential, yielding the rate constant k_{tr}.

Stock solutions of W7, A7 and A6 were prepared in DMSO (molecular biology grade, Sigma, D8418). Compound stocks were directly diluted in physiological buffers used for trabeculae experiments. The DMSO concentration was typically not more than 0.2% (v/v) and control experiments showed that addition of 0.2% (v/v) DMSO had no effect on calcium sensitivity or cooperativity of force. Prior to the experiments, demembrated rat ventricular trabeculae were incubated in relaxing solution containing the appropriate concentration of either W7, A7 or A6 for 15-20 min at 22°C.

Results and Discussion

Design and synthesis of A-series compounds

A number of small molecules have been found to act as either calcium sensitizers or desensitizers through their binding at the cNTnC-cTnI interface. The overall solution structures of cNTnC-cTnI switch in complex with these small molecules are highly similar. The small molecules bind to the hydrophobic pocket formed by the cNTnC and cTnI switch region and cause little perturbation to the overall protein structure. The calcium desensitizer, W7, consists of a hydrophobic naphthalene group and an aliphatic “tail” with an amino moiety at its terminal end that is positively charged at physiological pH. The positively charged terminal amino group of W7

appeared to repel the positively charged guanidinium group of R147 of cTnI switch region, thereby significantly reducing the affinity of cTnI switch peptide to cNTnC¹⁰. On the other hand, the calcium sensitizer dfbp-o consists of a hydrophobic biphenyl moiety linked to a negatively charged carboxyl group. It has been suggested that the negatively charged carboxyl group of dfbp-o enhances the cTnI switch binding affinity by attracting the side chain of R147¹⁴. The functional distinctions between these two compounds were rationalized to be primarily the result of differences in the charge of the two molecules.

The chemical structures of dfbp-o and W7 have differences other than the charges at the end of the tail. In order to test our postulate that electrostatics are important in tuning the cNTnC-cTnI association, we have synthesized a new compound A7 (N-(6-carboxyl-hexyl)-5-chloro-1-naphthalenesulfonamide), with a carboxyl group in place of the amino group of W7. We also synthesized A8 (N-(7-carboxylhexyl)-5-chloro-1-naphthalene-sulfonamide) and A6 (N-(5-carboxylhexyl)-5-chloro-1-naphthalenesulfonamide), which have one more (A8) and one less (A6) methylene group on the aliphatic linker compared to A7. The chemical structures are shown in Figure 4.2.

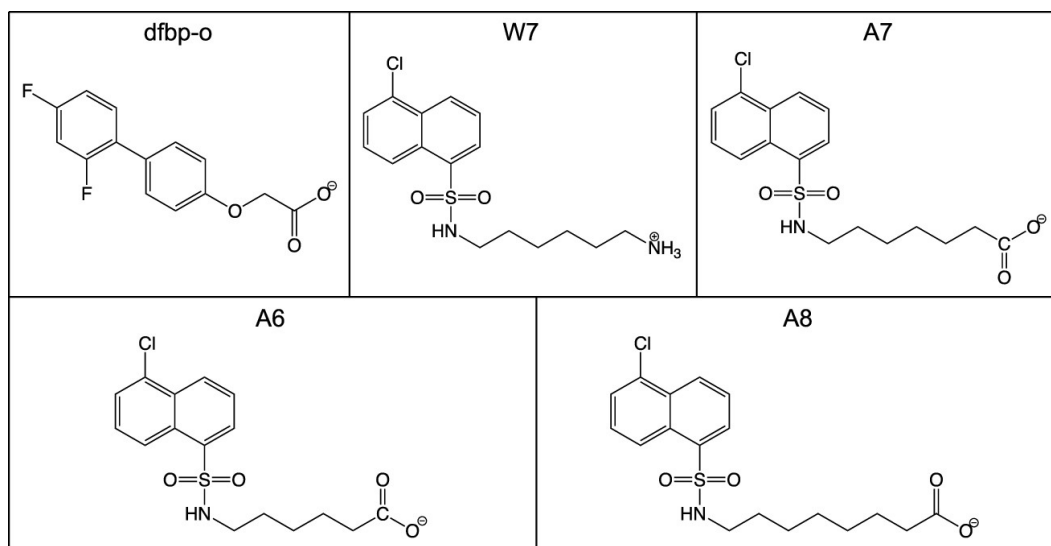


Figure 4.2. Chemical structures of dfbp-o, W7, A7, A6 and A8.

Binding of W7 and A7 to cNTnC-cTnI switch cChimera

A7 and W7 were titrated into calcium saturated ^{15}N -labeled cNTnC-cTnI switch chimera (cChimera). The linker of cChimera is comprised of residues from cTnI inhibitory region cTnI [136-144], and cChimera was shown to fully represent the cNTnC-cTnI switch complex¹⁷. The 2D ^1H - ^{15}N HSQC NMR spectrum of cChimera has been assigned previously¹⁷ and was used to monitor the A7 titration. Backbone amide resonance shift in cChimera induced by A7 titration is shown in Figure 4.3b, comparing to the W7 titration shown in Figure 4.3a. In both A7 and W7 titrations, all of the backbone amide signals shifted in a linear fashion, indicating a 1:1 stoichiometric binding of the compounds to cChimera. The residues that experienced the largest chemical shifts perturbation are plotted as a function of A7 to cChimera concentration in Figure 4.5b, and the global dissociation constant K_D is $120 \pm 30 \mu\text{M}$. The binding affinity of W7 to cChimera is 4 times weaker than A7. Many of the peaks are experiencing fast exchange in the W7 titration are undergoing intermediate exchange in the A7 titration. The peaks move in almost the same directions between the two titrations, suggesting that the binding pockets for A7 and W7 are similar.

The titrations of W7 and A7 to cChimera were also monitored by 1D ^1H NMR spectra. The ^1H chemical shifts corresponding to W7 and A7 rings are assigned and labeled in Figure 4.4. W7 peaks rise and sharpen up with excess W7, whereas the A7 peaks are much broader in the range $[\text{W7}]$ or $[\text{A7}]/[\text{cChimera}]$ ratio from 0 to 3.

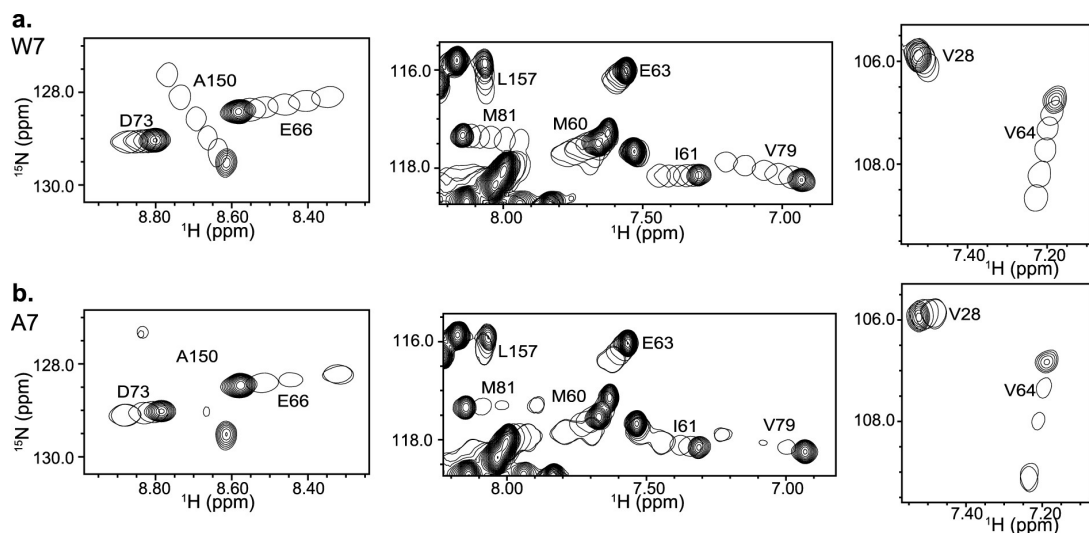


Figure 4.3. W7 and A7 binding to cChimera monitored by ^1H , ^{15}N -HSQC.

Comparison of regions of the ^1H , ^{15}N HSQC NMR spectra of cChimera during titrations with a. W7 and b. A7. [cChimera] \sim 500 μM ; [W7] \sim 0, 100, 250, 500, 900, 1500 μM ; and [A7] \sim 0, 100, 250, 750, 1500 μM .

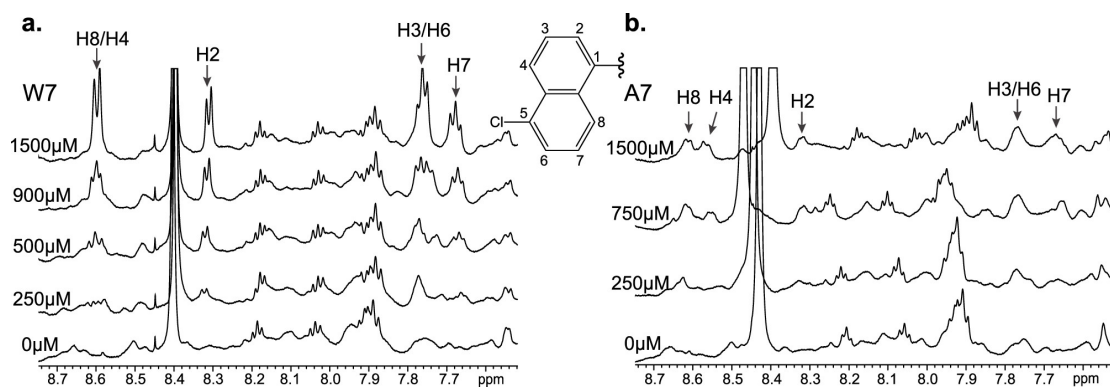


Figure 4.4. W7 and A7 binding to cChimera monitored by ^1H NMR.

Comparison of the 1D ^1H NMR spectra of a. W7 and b. A7 during titration into cChimera. [cChimera] \sim 500 μM ; [W7] \sim 0, 250, 500, 900, 1500 μM ; and [A7] \sim 0, 250, 750, 1500 μM .

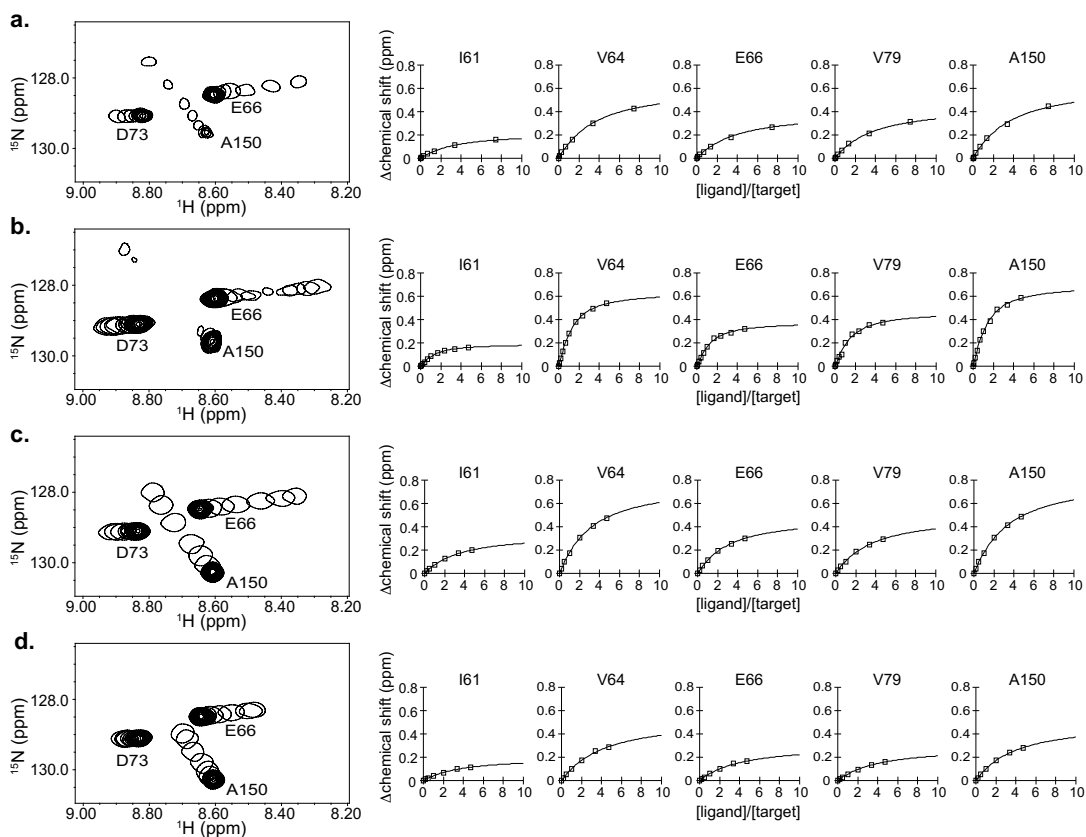


Figure 4.5. W7 and A7 binding to cChimera and gChimera.

Regions of the ^1H , ^{15}N HSQC NMR spectra of the titration of a. W7 into cChimera, b. A7 into cChimera, c. W7 into gChimera, and d. A7 into gChimera. Global fit of protein residues that experienced large chemical shift perturbations upon addition of A7 and W7 are shown to the right of each spectrum, and are used to determine K_D .

cChimera dynamics

T_2 relaxation times for backbone amides of cChimera in the absence and in the presence of A7 were measured to evaluate the changes in dynamics. In the absence of A7, R_2 rates ($1/T_2$) for most of the residues of cChimera are around 10 s^{-1} , with a few spikes (grey in Figure 4.6a) indicating some rapid conformational change. After A7 is added to $[\text{A7}]/[\text{cChimera}] = 0.5$ and 1.5 (light and dark green in Figure 4.6a, respectively), the overall R_2 profiles of cChimera were very similar to that in the absence of A7, with a slight increase after each addition of A7. A possible reason is

that cChimera has a slight tendency to aggregate when more A7 is added. The R_2 value of V64 and A150 dropped as $[A7]/[cChimera]$ was increased from 0.5 to 1.5, indicating the decrease of the exchange rate with the addition of A7. This is also observed during the R_2 evaluation when W7 was titrated into cChimera¹⁵. There are no significant differences in the overall R_2 profile of cChimera in the presence of A7 and W7.

2D NMR lineshape (TITAN) analyses²² were used to extract the dissociation rates k_{off} , and the dissociation constant K_D of A7 binding for cChimera (Figure 4.6b). The K_D calculated from TITAN is $120 \mu\text{M} \pm 10 \mu\text{M}$, which is consistent with the chemical shift perturbation based fitting results using xcrvfit. The k_{off} of A7 to cChimera is about 3000 s^{-1} . These rates indicate a k_{on} of approximately $2 \times 10^7 \text{ M}^{-1} \text{ s}^{-1}$, which is near the diffusion-controlled limit with no limiting conformational exchange.

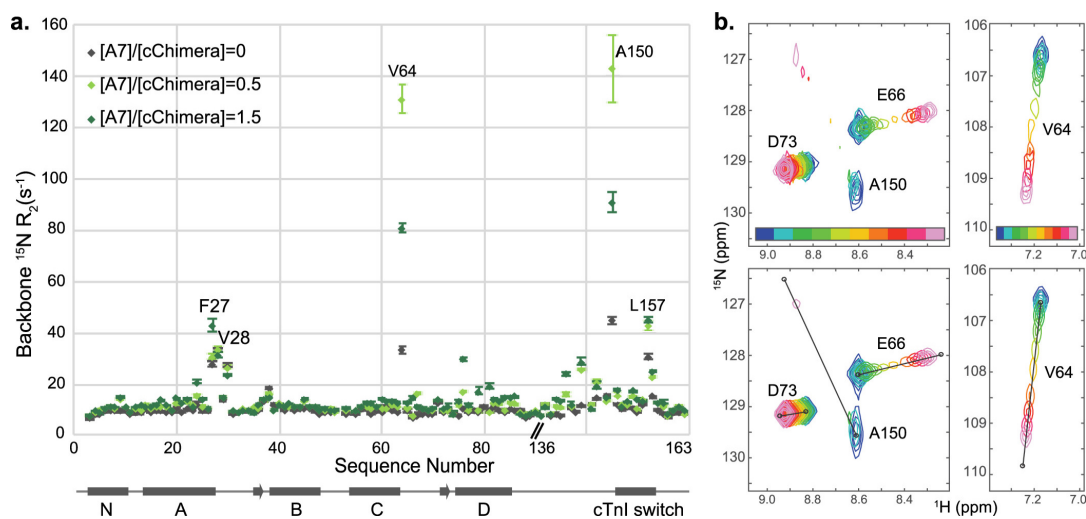


Figure 4.6. Fitting of the A7 titration of cChimera to extract kinetic information.

Fitting of the A7 titration of cChimera monitored by $^1\text{H},^{15}\text{N}$ -2D HSQC NMR spectroscopy to extract kinetic information. a. ^{15}N backbone R_2 NMR relaxation measurements during A7 titration of cChimera at A7 stoichiometry of 0 (grey) ,0.5 (light green, 250 μM) and 1.5 (dark green, 750 μM). B. Observed and fitted spectra are shown in the left and right panels for residues A150, E66, D73 and V64. The cross peaks are color-ramped from blue to pink with increasing A7 concentration.

Structural insight of cChimera-A7 complex

We determined the high-resolution solution NMR structure of cChimera-A7 complex to characterize the structure and position of A7 and cTnI switch region (Figure 4.7a). The solution structure of the cChimera-A7 complex is similar to the corresponding X-ray structure of the cTn complex with a RMSD of 1.6 Å for backbone heavy atoms (used throughout), the NMR solution structure of the cNTnC-cTnI switch peptide complex with a RMSD of 1.4 Å (Figure 4.7b), and the NMR solution structure of the liganded-free cChimera with a RMSD of 1.1 Å (excluding the linker region). The position and length of the cTnI switch region in the cChimera-A7 complex are the same as those observed in cChimera and cChimera-W7 (Figure 4.7c) with the helix from A150 to L158/ G159. The helix of the cTnI switch region sits among helices A, B, and D of cNTnC. NMR structure determination statistics are shown in Table 4.1.

A7 consists of a hydrophobic naphthalene group and a negatively charged N-(6-carboxylhexyl) tail. The chlorine-containing ring of the A7 naphthalene ring contacts I61 on helix C and V72 from the central β -sheet of cNTnC, indicating its deep binding position in the hydrophobic cleft. The naphthalene ring of A7 contacts L41 on helix B, I61 and V64 on helix C, and M153 of the cTnI switch region (Figure 4.7d). This hydrophobic binding site of A7 is comparable to that of other compounds that bind to the interface of cNTnC-cTnI switch region such as bepridil¹³, dfbp-o¹⁴, 3-mDPA¹⁷ and W7^{10,15}. We can only observe NOE contacts between cChimera and naphthalene ring of A7 because the chemical shifts of the A7 tail heavily overlap with protein methylene groups and as a result, the A7 tail in the structure is less defined. When the structures of A7 in cChimera-A7 complex is compared to the W7 in cChimera-W7 complex, the ring of A7 and W7 binds to the same hydrophobic pocket, but the positively and negatively charged tails reach out to the solvent by different routes (Figure 4.7e).

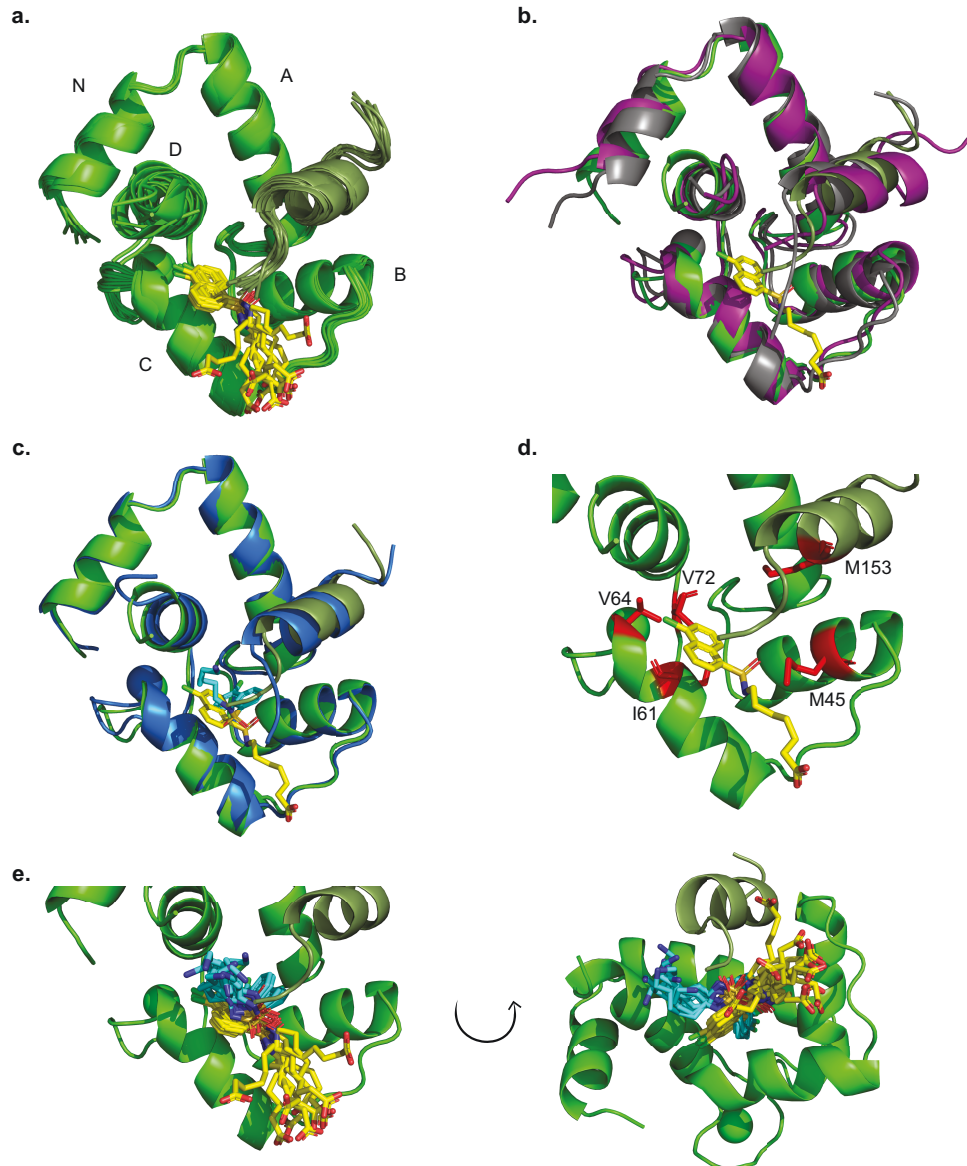


Figure 4.7. the cChimera-A7 complex solution structures.

a. The 8 lowest energy structures of the cChimera-A7 complex are colored green (the linkers have been removed for clarity): cNTnC, light green; cTnI switch peptide, dark green; A7, yellow; Ca^{2+} ions, green spheres. b. comparison of the structure of cChimera-A7 complex with the NMR structure of cNTnC-cTnI complex (1mxl.pdb, purple) and X-ray structure of cNTnC-cTnI derived from the cTn complex (1j1e.pdb, grey). c. comparison of the structure of cChimera-A7 complex with the NMR structure of cChimera-W7 complex (6mv3.pdb, blue; W7, light blue). d. A7 binding pocket, with residues contacting A7 shown in red sticks. e. superposition of the A7 and W7 chemical structures shown in sticks.

Table 4.1. Structural statistics of the chimera-A7 complex.

Intramolecular distance restraints (within cChimera)	1441
Short range ($ i \cdot j \leq 1$)	770
Medium range ($2 \leq i \cdot j \leq 4$)	284
Long range ($ i \cdot j \geq 5$)	387
Intermolecular distance restraints (between cChimera and A7)	10
Artificial restraints to Ca^{2+}	6
Backbone dihedral restraints	184

Binding of W7 and A7 to cNTnC-cTnI switch gChimera

To characterize the effect of electrostatics, we titrated W7 and A7 into a different construct of the cNTnC-cTnI switch chimera: gChimera. Both chimeras consist of cNTnC (residue 1-89) and cTnI switch region (residue 145-163, sequence RVRISADAMM QALLGARAK), but are connected by a distinct linker. The linker region for cChimera is from cTnI inhibitory region, sequence KGKFKRPTLR, which contain positively charged and neutral amino acids. In contrast, the linker region for gChimera is SGGSSGGSSGG, which are only neutral amino acids.

Figure 4.5 shows the drug-induced backbone amide resonance shifts in cChimera or gChimera as $[\text{W7}]/[\text{protein}]$ or $[\text{A7}]/[\text{protein}]$ increased from 0 to 5. Virtually all of the backbone amide signals shifted in a linear fashion, indicating a 1:1 binding stoichiometry. The residues which experienced large chemical shifts perturbations are plotted as a function of drug to protein concentration. Comparing the dissociation constant K_D of W7 to cChimera ($470 \pm 50 \mu\text{M}$)¹⁵ and the K_D of A7 to cChimera ($120 \pm 20 \mu\text{M}$), A7 is held 4X more tightly within the cChimera than W7. In contrast, the K_D of W7 and A7 to gChimera are not significantly different (410 ± 30

μM and $510 \pm 50 \mu\text{M}$, respectively), indicating that positively charged residues on the inhibitory region of cTnI play a role in stabilizing A7 binding, whereas they do not in W7 binding.

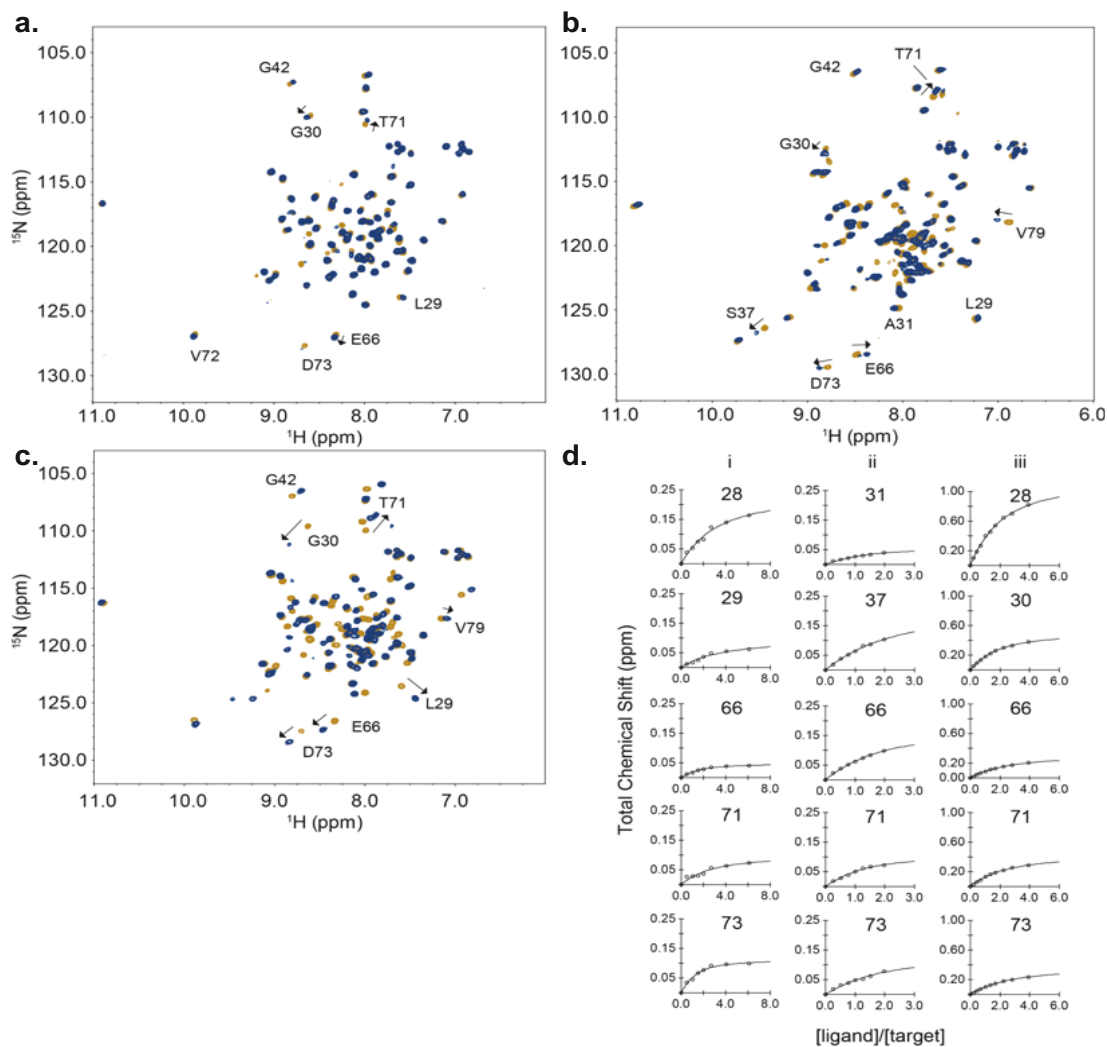


Figure 4.8. Interaction of cNTnC, cTnI and A7.

^1H , ^{15}N -HSQC NMR spectra of the titration of a. A7 into cNTnC, b. A7 into cNTnC-cTnI and c. cTnI into cNTnC-A7. d. Analysis of the titration data of i. A7 into cNTnC (a.); ii. A7 into cNTnC-cTnI (b.); and iii. cTnI into cNTnC-A7 (c.).

Interaction of cNTnC, cTnI and A7

A series of titrations were conducted to determine whether A7 and cTnI impacted one another's binding to cNTnC. A7 was titrated into cNTnC in the absence and in the presence of cTnI switch peptide. The presence of cTnI had a slight negative effect on the affinity of A7, with an increase in K_D from $260 \pm 140 \mu\text{M}$ for cNTnC to $320 \pm 140 \mu\text{M}$ for cNTnC-cTnI (see Table 4.2). The same competitive interaction was seen when cTnI was titrated into cNTnC and cNTnC-A7, with K_D to cNTnC of $150 \pm 30 \mu\text{M}$ compared to K_D to cNTnC-A7 of $230 \pm 50 \mu\text{M}$. Although the binding affinities of A7 for the cNTnC and cNTnC-cTnI switch are within experimental error, the decreased affinity ($320 \pm 140 \mu\text{M}/260 \pm 140 \mu\text{M} = 1.2 \pm 1.0$ -fold) is consistent with decreased affinity of cTnI switch peptide ($230 \pm 50 \mu\text{M}/150 \pm 30 \mu\text{M} = 1.5 \pm 0.5$ -fold) (Figure 4.8). These data are indicative of a moderate competition between A7 and cTnI switch peptide; however, the affinity of cTnI switch peptide is still approximately 9-fold tighter than the affinity of cTnI switch peptide in the presence of W7. Therefore, the charge of ligands that target the cNTnC-cTnI complex seems to be a central feature of their function.

Titrations with A8 and A6

The competition between A7 and cTnI switch peptide led us to consider whether the hydrocarbon tail competed with cTnI binding to cNTnC via a steric hindrance. We synthesized ligands with one more and one less methylene (A8 and A6, respectively). A8 was very hydrophobic and precipitated at less than $100 \mu\text{M}$, making it difficult to measure a reliable dissociation constant to protein by NMR spectroscopy. A6 is less hydrophobic than A7 and was easily monitored by NMR. The binding affinity of A6 to cNTnC and cNTnC-cTnI are very similar, $K_D = 420 \pm 350 \mu\text{M}$ and $390 \pm 50 \mu\text{M}$, respectively. The affinity of cTnI to cNTnC-A6 is $180 \pm 30 \mu\text{M}$, which is not significantly different than to cNTnC ($150 \pm 30 \mu\text{M}$). A6 showed less significant perturbation to cTnI than A7 did, so the lack of competition between A6 and cTnI implies the longer tail of the drug clashes with cTnI.

Table 4.2. Binding of W7, A7 and A6 to troponin.

a. Dissociation constants of W7, A7 and A6 to cNTnC, cNTnC-cTnI, cChimera and gChimera. b. Binding affinity of cTnI switch peptide to cNTnC in the absence and presence of W7, A7, and A6.

a.

Ligand \ Target	W7	A7	A6
cNTnC	250 ± 100 μM ³⁰	260 ± 140 μM	420 ± 350 μM
cNTnC-cTnI	500 ± 100 μM ³¹	320 ± 140 μM	390 ± 50 μM
cChimera	470 ± 60 μM	120 ± 30 μM	
gChimera	410 ± 30 μM	510 ± 50 μM	

b.

Ligand \ Target	cTnI
cNTnC	154 ± 30 μM ⁴
cNTnC-W7	2000 ± 50 μM ¹⁰
cNTnC-A7	230 ± 50 μM
cNTnC-A6	180 ± 30 μM

Effects of compounds on calcium sensitivity of force of ventricular trabeculae

To investigate the effects W7 and A7 on cardiac muscle contractility, we measured the Ca²⁺-dependent force development of demembrated rat right ventricular trabeculae in the absence or in the presence of 50 μmol/L compound (Figure 4.9). Addition of W7 significantly decreased the calcium-sensitivity force as indicated by a rightwards shift of the force-calcium relation. Data points were fitted with the Hill equation indicating that the pCa₅₀ (negative decadic logarithm of [Ca²⁺] that gives 50% activation) decreased from 5.84 ± 0.01 to 5.59 ± 0.01 (P < 0.001). A7 also caused some decrease in calcium sensitivity but not as much as W7 (pCa₅₀ of 5.77 ± 0.01 (P < 0.01)). Moreover, W7 decrease the maximal Ca²⁺-activated force from 71.79 ± 2.54 mN/mm² measured under control conditions to 45.73 ± 2.40 mN mm⁻² in the presence of W7 (P < 0.001), corresponding to a decrease by ~36%. In contrast, A7 had no significant effect on the maximal Ca²⁺-activated force (65.82 ± 2.68 mN/mm², P >

0.05). Furthermore, W7 significantly increased the rate of force redevelopment at low and intermediate levels of activation, which did not change in the presence of A7, suggesting that thin filament desensitization by W7 increased myosin cross bridge kinetics. These results are consistent with our NMR titration studies that cTnI binding affinity to cTnT-C-A7 is 4-fold tighter than cTnT-C-W7 (see Table 4.3). The effects of compound with shorter “tail” A6 was also tested in demembrated trabeculae. A6 does not have any significant effect on force development, calcium sensitivity and cross bridge kinetics of ventricular trabeculae (Figure 4.9 & Table 4.3).

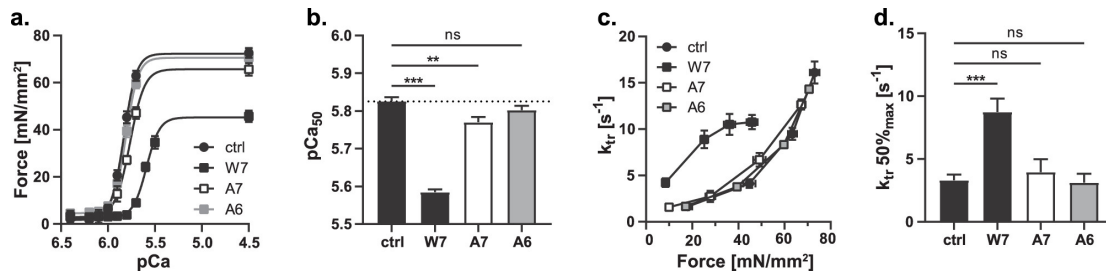


Figure 4.9. Effect of W7, A7 or A6 on trabeculae.

a. Effect of W7, A7 and A6 on the force calcium relation of ventricular trabeculae. b. Bar graph of pCa₅₀ for ventricular trabeculae. c. Force-k_{tr} relations for control trabeculae, and in the presence of W7, A7, and A6. d. Bar graph indicating the rate of force re-development at 50% maximal activation (k_{tr} 50%_{max}). Means ± SEM, n=5. Statistical significance of differences was assessed with one-way ANOVA followed by Tukey’s post-hoc test: ns-not significant, **p<0.01, ***p<0.001. control: closed circles, W7: open squares, A7: black squares, and A6: grey squares.

Table 4.3. Effect of W7, A7 or A6 on trabeculae.

Summary of the effects of 50 $\mu\text{mol/L}$ W7, A7 or A6 on rat ventricular trabeculae mechanics

	Control	W7	A7	A6
F_{min} [mN/mm²]	2.10 \pm 0.46	3.05 \pm 0.77	3.19 \pm 0.50	4.57 \pm 0.63
F_{max} [mN/mm²]	72.73 \pm 2.20	45.73 \pm 2.40 ^{***}	65.82 \pm 2.68	70.67 \pm 3.54
pCa₅₀	5.82 \pm 0.01	5.59 \pm 0.01 ^{**}	5.77 \pm 0.01 ^{**}	5.80 \pm 0.01
n_H	7.32 \pm 0.64	6.05 \pm 0.38	6.03 \pm 0.61	6.99 \pm 0.26
k_{tr 50%max} [s⁻¹]	3.30 \pm 0.48	8.74 \pm 1.01 [*]	3.96 \pm 1.03	3.12 \pm 0.71

Conclusions

The focus of this manuscript was to evaluate the importance of electrostatic interactions in the efficacy of compounds which directly modulate the calcium sensitivity of force development in cardiac muscle by binding to the sarcomere thin filament. Our hypothesis is that the interaction of cTnI with cTnC following calcium binding is a major regulatory element and that many compounds influence force by perturbing this interaction. Many compounds which are effective in modulating cardiac function have a common motif of an aromatic core which binds to the hydrophobic core of cNTnC which is exposed upon calcium binding, and a polar and often charged 'tail'. The cNTnC-cTnI interface contains many charged residues from the acidic cTnC and the basic cTnI proteins. To aid these studies we have developed cNTnC-cTnI chimera which embodies this key interaction.

In this study we have used the binding of the calcium desensitizer W7 to cNTnC, cNTnC:cTnI complexes, cNTnC-TnI chimera, and cardiac trabeculae to determine the effect of changing the charge on W7 (A7), changing the position of the charge (A6, and A8), and changing the charge of the cTnI portion of the chimera studied. The NMR solution structure of the cChimera-A7 complex revealed that the overall structure of the protein is not perturbed from that of the cChimera-W7 complex, nor was the position of the binding of the aromatic core of the small molecule changed.

However, the charge difference did result in a significant change in the route the tail took to the surface of the complex especially in respect to the switch region of cTnI. The charge changes also significantly influenced the affinities and the kinetics of the various complexes studied, and ablated the desensitization action of W7 in ventricular trabeculae.

These results indicate that electrostatic interactions are important in the negative inotropic effect of W7. The underlying mechanism could involve direct perturbation of the calcium affinity of cTnC, or different interactions with the switch peptide region of cTnI. The change of charge between W7 to A7 would be expected to decrease and not increase the intrinsic calcium sensitivity of cTnC, although electrostatics are intrinsically long range and intervening dielectric constants are difficult to evaluate. Nonetheless, the changes observed in affinity of the compound and the switch region of cTnI supporting the conclusion that the effect is on the cTnC-cTnI interface.

It is interesting that Levosimendan analog dfbp-o acts as a sensitizer whereas A7 does not given that both have a carboxyl group, and Bepridil (which has two tertiary amines and a positive charge) acts as a calcium sensitizer unlike W7. Figure 4.10 shows a comparison of the structures of A7, W7 (6mv3.pdb)¹⁵, Bepridil (11xf.pdb)¹³, dfbp-o (211r.pdb)¹⁴, and 3-methyldiphenylamine (5w88.pdb and 5wcl.pdb)¹⁷. This figure shows that the carboxyl group of dfbp-o is closer to the amino group of W7 than that of A7 and thus to potential interactions with positively charged residues in cTnI. Also, the N atoms in Bepridil are farther from the primary amino group in the tail of W7 and therefore have no repulsive interactions with positively charged residues in cTnI.

Further dissection of the role of electrostatics is complicated by two factors: first, electrostatics are intrinsically complex because they are long-range and intervening dielectric constants are difficult to evaluate, and second, the role of dynamics in the structure of the “tail” region are hard to evaluate. Dynamics affect both the electrostatic and the entropic contributions to the free energy of the interaction.

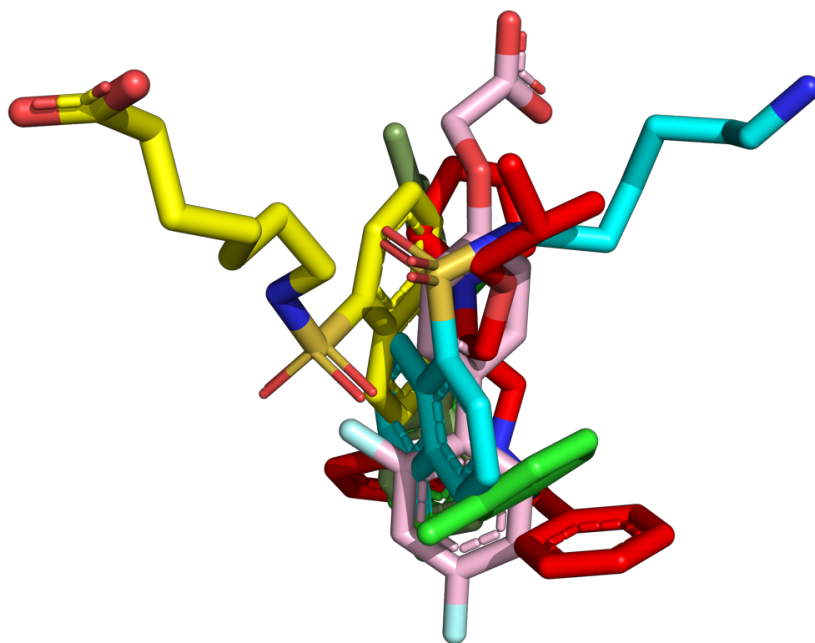


Figure 4.10. Overlay of the structures of A7, W7, bepridil, dfbp-o and 3-mDPA.

Overlay of the structures of A7 (yellow), W7 (6mv3.pdb, light blue), bepridil (1lxf.pdb, red), dfbp-o (211r.pdb, pink), and 3-methyldiphenylamine (5w88.pdb, light green; 5wcl.pdb, dark green). The lowest energy structure from the NMR assemble is used for all structures. The ‘tails’ in all structures are flexible. Nitrogen atoms are blue, oxygen atoms are light red, fluorine atoms are teal and sulfur atoms are yellow.

Acknowledgements

This study was supported by grants from the Heart and Stroke foundation of Canada (G-14-0005884 to B.D.S.), the University of Alberta Faculty of Medicine Transitional Program (B.D.S.), Queen Elizabeth II Graduate Scholarship (F.C.), 75th Anniversary Graduate Student Award (F.C.), Motyl Graduate Studentship (F.C.), Alberta Heritage Foundation for Medical Research Studentship (I.M.R.) and British Heart Foundation (Fellowship FS/16/3/31887 to T.K.). The authors would like to thank P. Hwang for the gChimera protein, P. Liu for assistance with protein purification.

References

1. EBASHI, S. Separation of Troponin into Its Three Components*. *J. Biochem.* **72**, 787–790 (1972).
2. Greaser, M. L. & Gergely, J. Purification and properties of the components from tropinin. *J. Biol. Chem.* **248**, 2125–2133 (1973).
3. Parry, D. A. D. & Squire, J. M. Structural role of tropomyosin in muscle regulation: Analysis of the X-ray diffraction patterns from relaxed and contracting muscles. *J. Mol. Biol.* **75**, 33–55 (1973).
4. Li, M. X., Spyropoulos, L. & Sykes, B. D. Binding of Cardiac Troponin-I 147-163 Induces a Structural Opening in Human Cardiac Troponin-C † , ‡. *Biochemistry* **38**, 8289–8298 (1999).
5. Li, M. X., Wang, X. & Sykes, B. D. Structural based insights into the role of troponin in cardiac muscle pathophysiology. *J. Muscle Res. Cell Motil.* **25**, 559–79 (2004).
6. Kobayashi, T., Jin, L. & de Tombe, P. P. Cardiac thin filament regulation. *Pflügers Arch. - Eur. J. Physiol.* **457**, 37–46 (2008).
7. Gordon, A. M., Homsher, E. & Regnier, M. Regulation of contraction in striated muscle. *Physiol. Rev.* **80**, 853–924 (2000).
8. Adhikari, B. B. & Wang, K. Interplay of Troponin- and Myosin-Based Pathways of Calcium Activation in Skeletal and Cardiac Muscle: The Use of W7 as an Inhibitor of Thin Filament Activation. *Biophys. J.* **86**, 359–370 (2004).
9. Thompson, B. R., Martindale, J. & Metzger, J. M. Sarcomere neutralization in inherited cardiomyopathy: small-molecule proof-of-concept to correct hyper-Ca²⁺-sensitive myofilaments. *Am. J. Physiol. Heart Circ. Physiol.* **311**, H36-43 (2016).
10. Oleszczuk, M., Robertson, I. M., Li, M. X. & Sykes, B. D. Solution structure of the regulatory domain of human cardiac troponin C in complex with the switch region of cardiac troponin I and W7: The basis of W7 as an inhibitor of cardiac muscle contraction. *J. Mol. Cell. Cardiol.* **48**, 925–933 (2010).
11. Solaro, R. J., Bousquet, P. & Johnson, J. D. Stimulation of cardiac myofilament force, ATPase activity and troponin C Ca⁺⁺ binding by bepridil. *J. Pharmacol.*

- Exp. Ther.* **238**, 502–7 (1986).
12. Li, Y., Love, M. L., Putkey, J. A. & Cohen, C. Bepridil opens the regulatory N-terminal lobe of cardiac troponin C. *Proc. Natl. Acad. Sci. U. S. A.* **97**, 5140–5 (2000).
 13. Wang, X., Li, M. X. & Sykes, B. D. Structure of the regulatory N-domain of human cardiac troponin C in complex with human cardiac troponin I147-163 and bepridil. *J. Biol. Chem.* **277**, 31124–33 (2002).
 14. Robertson, I. M., Sun, Y.-B. B., Li, M. X. & Sykes, B. D. A structural and functional perspective into the mechanism of Ca²⁺-sensitizers that target the cardiac troponin complex. *J. Mol. Cell. Cardiol.* **49**, 1031–41 (2010).
 15. Cai, F., Hwang, P. M. & Sykes, B. D. Structural Changes Induced by the Binding of the Calcium Desensitizer W7 to Cardiac Troponin. *Biochemistry* **57**, 6461–6469 (2018).
 16. Takeda, S., Yamashita, A., Maeda, K. & Maéda, Y. Structure of the core domain of human cardiac troponin in the Ca(2+)-saturated form. *Nature* **424**, 35–41 (2003).
 17. Cai, F. *et al.* Structures reveal details of small molecule binding to cardiac troponin. *J. Mol. Cell. Cardiol.* **101**, 134–144 (2016).
 18. Li, M. X. *et al.* Kinetic studies of calcium and cardiac troponin I peptide binding to human cardiac troponin C using NMR spectroscopy. *Eur. Biophys. J.* **31**, 245–56 (2002).
 19. Guo, K. & Li, L. Differential ¹²C/¹³C-isotope dansylation labeling and fast liquid chromatography/mass spectrometry for absolute and relative quantification of the metabolome. *Anal. Chem.* **81**, 3919–3932 (2009).
 20. Delaglio, F. *et al.* NMRPipe: A multidimensional spectral processing system based on UNIX pipes. *J. Biomol. NMR* **6**, 277–293 (1995).
 21. Johnson, B. A. & Blevins, R. A. NMR View: A computer program for the visualization and analysis of NMR data. *J. Biomol. NMR* **4**, 603–614 (1994).
 22. Waudby, C. A., Ramos, A., Cabrita, L. D. & Christodoulou, J. Two-Dimensional NMR Lineshape Analysis. *Sci. Rep.* **6**, 24826 (2016).
 23. Shen, Y., Delaglio, F., Cornilescu, G. & Bax, A. TALOS+: A hybrid method for

- predicting protein backbone torsion angles from NMR chemical shifts. *J. Biomol. NMR* **44**, 213–23 (2009).
24. Rieping, W. *et al.* ARIA2: Automated NOE assignment and data integration in NMR structure calculation. *Bioinformatics* **23**, 381–382 (2007).
 25. Schüttelkopf, A. W. & van Aalten, D. M. F. *PRODRG*: a tool for high-throughput crystallography of protein–ligand complexes. *Acta Crystallogr. Sect. D Biol. Crystallogr.* **60**, 1355–63 (2004).
 26. Kleywegt, G. J. Dictionaries for Heteros. *CCP4/ESF- EACBM Newsl. Protein Crystallogr.* **31**, 45–50. (1995).
 27. Schwieters, C. D., Kuszewski, J. J., Tjandra, N. & Clore, G. M. The Xplor-NIH NMR molecular structure determination package. *J. Magn. Reson.* **160**, 65–73 (2003).
 28. Kampourakis, T., Yan, Z., Gautel, M., Sun, Y.-B. & Irving, M. Myosin binding protein-C activates thin filaments and inhibits thick filaments in heart muscle cells. *Proc. Natl. Acad. Sci. U. S. A.* **111**, 18763–8 (2014).
 29. Brenner, B. & Eisenberg, E. Rate of force generation in muscle: Correlation with actomyosin ATPase activity in solution. *Proc. Natl. Acad. Sci. U. S. A.* **83**, 3542–3546 (1986).
 30. Hoffman, R. M. B., Li, M. X. & Sykes, B. D. The binding of W7, an inhibitor of striated muscle contraction, to cardiac troponin C. *Biochemistry* **44**, 15750–15759 (2005).
 31. Li, M. X., Hoffman, R. M. B. & Sykes, B. D. Interaction of Cardiac Troponin C and Troponin I with W7 in the Presence of Three Functional Regions of Cardiac Troponin I †. *Biochemistry* **45**, 9833–9840 (2006).

Chapter 5

The Mechanism of Cardiac Thin Filament Inhibition: the Precision of W7

Fangze Cai¹, Thomas Kampourakis², Brittney A. Klein¹,
Kieran T. Cockburn¹, Brian D. Sykes¹

¹Department of Biochemistry, University of Alberta, Edmonton, AB, Canada.

²Randall Centre for Cell and Molecular Biophysics, King's College London, London, United Kingdom.

This chapter is part of a manuscript in preparation. Cai, F., Kampourakis, T., Klein, B. A., Cockburn, K. T. & Sykes, B. D. The Mechanism of Cardiac Thin Filament Inhibition: the Precision of W7.

Contribution: FC and BAK performed drug titration. TK prepared the ventricular trabeculae and performed force-calcium titrations. KTC and BAK synthesized compound A4. FC acquired the NMR spectra for structure determination and wrote the manuscript. BDS guided the research.

Summary

The calmodulin antagonist W7 is a well-studied direct sarcomere inhibitor that decreases the calcium sensitivity of force development in cardiac muscle by binding to the sarcomere thin filament protein troponin. W7 binds to the interface of cTnT and the switch region of cTnI and weakens cTnI binding, possibly by electrostatic repulsion between W7 and cTnI switch region. We used a series of W7 derivatives to evaluate the precise location of the charged $-NH_3^+$ group in tuning the cTnT-cTnI interface. W6, which has one less methylene group on the tail than W7, binds tighter to cTnT-cTnI switch region chimera than W7, and does not change the calcium sensitivity on ventricular trabeculae. The shorter positively charged W4 and negatively charged A4, do not change the calcium sensitivity of trabeculae. The solution structure of cChimera-

W6 complex reveals that W6 binds to the same hydrophobic cleft as W7, with the naphthalene ring sitting in the same deep binding pocket, and the aliphatic tail taking a similar route to the surface of the complex. The only difference would be the exact location of the positively charged amino group due to the different length of the tail. These results indicate that the precise location of the charged amino group is important in the negative inotropic effect of W7.

Introduction

W7 (N-(6-aminohexyl)-5-chloro-1-naphthalenesulfonamide) is a well-studied direct sarcomere inhibitor. W7 was initially discovered to inhibit vascular smooth muscle actomyosin in a dose-dependent fashion¹. Subsequent studies showed that W7 is a calmodulin antagonist, which inhibits calmodulin regulated calcium-dependent protein kinase and ATPase². Other than calmodulin, W7 binds significantly to troponin C but not to other smooth muscle proteins such as actin, myosin, tropomyosin and serum albumin². A study investigating the interplay between thin and thick filaments during calcium activation showed that W7 reversibly inhibited ATPase and tension activation and decreased calcium sensitivity in both skeletal and cardiac muscle types³. Recent physiology studies have shown that W7 had a rapid effect in correcting contractile dysfunction in hyper-sensitive states at the myocyte and whole heart levels⁴. W7 was shown to decrease intact cardiac myocyte contractility in a calcium-independent manner, indicating the main target of W7 is the sarcomere protein cardiac troponin C (cTnC)⁴.

The cardiac troponin complex (cTn) is the key protein that turns the heart muscle contraction on and off in a calcium-dependent manner. cTn is a heterotrimeric thin filament protein formed by the calcium binding subunit troponin C (cTnC), the inhibitory subunit troponin I (cTnI) and the tropomyosin binding subunit troponin T (cTnT)^{5,6}. At resting calcium concentration, cTnI is bound to actin, maintaining tropomyosin in place that covers the myosin binding site on actin and blocks the actin-myosin interaction⁷. When the cytosolic calcium concentration increases during systole, calcium binds to the regulatory N-terminal domain of cTnC (cNTnC), causing conformational changes to induce the association of the switch region of cTnI (residues

147-163)⁸. The movement of cTnI switch region drags the adjacent inhibitory region of cTnI (residues 137-146) off the actin and tropomyosin⁹, that results in the movement of tropomyosin to expose the myosin-binding sites on actin, and triggers muscle contraction¹⁰⁻¹². The calcium-sensitive cNTnC-cTnI switch region interaction triggers the heart muscle contraction, and fine-tuning this critical interface of cNTnC and cTnI switch region by pharmaceutical compounds holds a therapeutic potential for heart diseases.

NMR studies have shown that W7 binds to both N-domain and C-domain of calcium-saturated cTnC¹³; however, in the presence of cTnI, W7 only binds to cNTnC with K_D of approximately 500 μM ¹⁴. Studies of W7 and cTnI switch peptide binding to cNTnC suggests that W7 may directly modulate the calcium sensitivity by interacting with cNTnC and cTnI switch region. The NMR solution structures of W7 bound to calcium-saturated cNTnC¹⁵ and cNTnC-cTnI switch peptide complex¹⁶ revealed that W7 binds to the hydrophobic groove of cNTnC, with similar position and orientation in both structures. In the presence of W7, the binding of cTnI switch peptide to cNTnC decreased by over 13-fold, from K_D of 150 μM to 2000 μM ¹⁶. The NMR solution structures of W7 bound to cNTnC-cTnI chimera revealed that the overall structures of cNTnC-cTnI switch region were not significantly perturbed¹⁷ in comparison to the solution structure of cNTnC-cTnI switch peptide complex⁸ or X-ray structure of the core troponin complex⁹. The competition of W7 and cTnI switch region is likely caused by electrostatic repulsion of the positively charged amino group of W7 and positively charged guanidinium group of RRVR₁₄₄₋₁₄₇ region of cTnI. A7 (N-(6-carboxylhexyl)-5-chloro-1-naphthalenesulfonamide), which has a carboxyl group in place of the amino group of W7, has been used to investigate the role of electrostatics. A7 decreased the binding affinity of cTnI to cNTnC substantially less than W7 and bound more tightly to the cNTnC-cTnI chimera. A7 also has a much weaker desensitization effect than W7 on the force-calcium relation of demembranated rat right ventricular trabeculae¹⁸. These results show the importance of the positively charged amino group in the negative inotropic effect of W7.

A6 (N-(5-carboxylhexyl)-5-chloro-1-naphthalenesulfonamide), which has one less methylene group on the hydrocarbon chain than A7, did not affect binding of cTnI

switch peptide, nor change the calcium sensitivity of ventricular trabeculae¹⁸. This suggests that the length of the tail or the location of the charged group is important. In order to evaluate the importance of both electrostatic interaction and precise location of the charged group in tuning the cNTnC-cTnI interface, we investigated a series of W7 derivatives with various tail length and different charge at the terminal end. W6 (N-(5-aminohexyl)-5-chloro-1-naphthalenesulfonamide) and W4 (N-(3-aminohexyl)-5-chloro-1-naphthalenesulfonamide) have one and three less methylene groups on the hydrocarbon chain compared to W7, while A4 (N-(3-carboxylhexyl)-5-chloro-1-naphthalenesulfonamide) has three less methylene group on the hydrocarbon chain compared to A7 (Figure 5.1). W6 binds tighter to cNTnC-cTnI switch region chimera than W7, and W4 has the lowest binding affinity, which suggests the protein does not like to bury the positive charge close to the hydrophobic pocket. We tested the effect of the compounds on the force-calcium relation of demembrated rat right ventricular trabeculae revealing that all the W7-derivatives did not have the strong negative inotropic effect on ventricular trabeculae. We determined the solution NMR structure of W6 bound to cNTnC-cTnI chimera. The structure shows that W6 binds to the same hydrophobic cleft as W7, with the naphthalene ring sitting in the same deep binding pocket, and the aliphatic tail taking a similar route to the surface of the complex. The only difference would be the exact location of the positively charged amino group because of the difference in the length of the tail. These results indicate that other than electrostatics interaction, the precise location of the charged amino group is also important in the negative inotropic effect of W7.

Material and methods

Protein expression, and purification

Recombinant cChimera were used in this study. cChimera contains cNTnC (residue 1-90), cTnI (residue 136-163), and a histidine tag. cChimera has C35 and C84 substituted with serine. The [¹⁵N, ¹³C] and [¹⁵N] cChimera proteins were expressed in *E. coli* BL21(DE3) and purified by Ni-NTA affinity chromatography followed by dialysis and lyophilization as previously described¹⁹. Protein identity and purity were confirmed by gel electrophoresis and mass spectrometry.

Chemicals

W7 (N-(6-aminoethyl)-5-chloro-1-naphthalenesulfinamide) was purchased from Sigma-Aldrich. W6 (N-(5-aminoethyl)-5-chloro-1-naphthalenesulfinamide), and W4 (N-(3-aminoethyl)-5-chloro-1-naphthalenesulfinamide) was purchased from Toronto Research Chemicals. A7 (N-(6-carboxylhexyl)-5-chloro-1-naphthalenesulfonamide), A6 (N-(5-carboxylhexyl)-5-chloro-1-naphthalenesulfonamide), and A4 (N-(3-carboxylhexyl)-5-chloro-1-naphthalenesulfonamide) were synthesized in-house. The synthesis of A6 and A7 is described in previous studies¹⁸, and the reaction scheme and procedure for A4 is similar to what was outlined previously²⁰.

Synthesis of A4: *γ-aminobutyric acid* (Sigma-Aldrich) was dissolved in 0.5 M Na₂CO₃/NaHCO₃ buffer (pH 9.4), and heated to 60 °C. 5-chloro-naphthalene-1-sulfonyl chloride (Toronto Research Chemicals) was dissolved in acetonitrile. A 10:1 molar excess of *γ-aminobutyric acid* to 5-chloro-naphthalene-1-sulfonyl chloride was used in these reactions. The 5-chloro-naphthalene-1-sulfonyl chloride solution was added dropwise to the stirring carbonate solution. The reaction was refluxed for 2 hours. The progress of the reaction was monitored using ¹H NMR spectroscopy. The solution was acidified using 6M HCl_(aq) (pH 4) and extracted with ethyl acetate and a brine solution. The organic solution was dried using NaSO₄ and the product was collected using vacuum filtration. The product was verified by Liquid Chromatography-Mass Spectrometry (LC-MS).

NMR spectroscopy

The NMR samples were prepared in 5 mm NMR tubes to a final volume of 500 μL. The protein samples were solubilized in 100 mM KCl, 10 mM imidazole, and 2-10 mM CaCl₂ in 95% H₂O/5% D₂O or 100% D₂O, using 0.25 mM 2,2-dimethyl-2-silapentane-5-sulfonate-d₆ sodium salt (DSS-d₆) as an NMR internal reference. The pH was maintained at 6.7-6.8. NMR data were collected at 30 °C on a Varian Inova 600 MHz spectrometer equipped with a triple resonance probe with pulsed field gradients. 1D NMR spectra were processed with VNMRJ v.3.2 A (Varian, Inc.), 2D and 3D NMR spectra were processed with NMRPipe²¹ and analyzed with NMRViewJ²², using scripts written in-house.

Small molecule titrations

Small molecule stocks were prepared in DMSO- d_6 (Cambridge Isotopes) and concentrations were determined by 1D 1H NMR spectroscopy. The binding of small molecules to protein was monitored by NMR spectroscopy; at each aliquot, a $^1H, ^{15}N$ -HSQC NMR spectrum was acquired. All samples contained 2 mM $CaCl_2$, and proteins were saturated with calcium. A4, A6, W4 and W6 was titrated into 0.15 mM cChimera to final concentration of 0.01, 0.03, 0.06, 0.1, 0.15, 0.25, 0.35, 0.5 and 0.7 mM. By the end of the titration, the addition of DMSO- d_6 did not exceed 5% of the sample volume. Dilution by each drug solution addition was taken into consideration when calculating the concentration of protein at each titration point. Chemical shift perturbation at each titration point were used by our in-house data fitting program, xcrvfit (www.bionmr.ualberta.ca/bds/software/xcrvfit), to calculate dissociation constants, K_D .

Structure calculations

The sample for cChimera-W6 complex structural studies contained 0.4 mM $^{15}N, ^{13}C$ - labeled cChimera with 2.5 mM W6. The chemical shift assignment of W6 in cChimera-W6 complex was achieved using 2D $^{13}C, ^{15}N$ -double-filtered TOCSY (60 ms mixing time) experiment. Intermolecular distance restraints between W6 and cChimera were derived from a 3D ^{13}C -filtered/edited NOESY-HSQC (mixing time: 75 ms) experiment.

Backbone ϕ - and ψ -dihedral angle restraints, intramolecular distance restraints within the protein were adopted from the cChimera-W7 complex structural calculation. PDB file for W6 is generated using PRODRG²³. Parameter and topology files for W6 was generated using xplo2d²⁴, and were modified manually. Intermolecular NOEs between W6 and cChimera were manually assigned, used to generate distance restraints that were added to the XPLOR-NIH structure calculations²⁵. Intermolecular NOEs between cNTnC region of the cChimera and Ca^{2+} were derived from crystallographic data of the cardiac troponin complex. The distance and dihedrals constraints were used in the simulated annealing module of Xplor-NIH, version 2.46. 150 structures were calculated, from which the lowest-energy structure was used as the

starting point for refinement. 150 structures were calculated using the water refinement protocol. The final ensemble consists of the 10 lowest-energy structures generated in the refinement step with no NOE violations $> 0.5 \text{ \AA}$ or dihedral violation $> 5^\circ$.

Preparation of ventricular trabeculae and force-calcium titrations

All animals were treated in accordance with the guidelines approved by the UK Animal Scientific procedures Act (1986) and European Union Directive 2010/63/EU. Wistar rats (male, 200-250 g) were sacrificed by cervical dislocation without the use of anesthetics (Schedule 1 procedure in accordance with UK Animal Scientific Procedure Act, 1986) and demembrated right ventricular trabeculae were prepared as described previously²⁶. Trabeculae were mounted between a force transducer (KRONEX, model A-801, resonance frequency $\sim 2 \text{ kHz}$) and length controller (Aurora Scientific, Model 312C) in relaxing solution. Each activation was preceded by a 2-min incubation in pre-activating. Solutions with varying concentrations of free $[\text{Ca}^{2+}]$ were prepared by mixing relaxing and activating solutions using MAXCHELATOR software (maxchelator.stanford.edu). The dependence of force on free calcium concentration was fitted to data from individual trabeculae as described previously¹⁸. Trabeculae which showed a decline in maximal calcium activated force of more than 15% after the pCa titrations were discarded.

Stock solutions of A4, W4 and W6 were prepared in DMSO (molecular biology grade, Sigma, D8418). Compound stocks were directly diluted in physiological buffers used for trabeculae experiments. The DMSO concentration was typically not more than 0.2% (v/v) and control experiments showed that addition of 0.2% (v/v) DMSO had no effect on calcium sensitivity or cooperativity of force. Prior to the experiments, demembrated rat ventricular trabeculae were incubated in relaxing solution containing the appropriate concentration of either A4, W4 and W6 for 15-20 min at 22°C .

Results and Discussion

W-series and A-series compounds

The sarcomere inhibitor W7 consists of a hydrophobic naphthalene group and an aliphatic tail with a positively charged terminal amino group. The negative inotropic effect of W7 is likely result of electrostatics repulsion of the positively charged amino group of W7 and the positively charged guanidinium group of RRVR_{144–147} region of cTnI. In contrast, A7 (N-(6-carboxylhexyl)-5-chloro-1-naphthalenesulfonamide), where the positively charged amino group of W7 was replaced with a negatively charged carboxyl group, has been shown to lose the strong inhibition effect on sarcomere comparing to W7. A7 slightly reduced the affinity of cTnI switch peptide to cNTnC (approximately by 1.2 fold)¹⁸, while W7 significantly reduces the affinity of cTnI switch peptide to cNTnC by 13 fold¹⁶. Moreover, A6 (N-(5-carboxylhexyl)-5-chloro-1-naphthalenesulfonamide), which is one methylene shorter than A7, did not affect binding of cTnI switch peptide at all, suggesting the importance of the tail length and precise location of the charged group. In order to test our hypothesis that both electrostatics and the location of the charged group are important in tuning the cNTnC-cTnI association, we synthesized a new compound, N-(3-carboxylhexyl)-5-chloro-1-naphthalenesulfonamide (A4), which has three less methylene groups on the aliphatic linker compared to A7, and purchased W6 (N-(5-aminoethyl)-5-chloro-1-naphthalenesulfonamide), and W4 (N-(3-aminoethyl)-5-chloro-1-naphthalenesulfonamide), which have one and three less methylene groups on the aliphatic linker compared to W7. The chemical structures are shown in Figure 5.1.

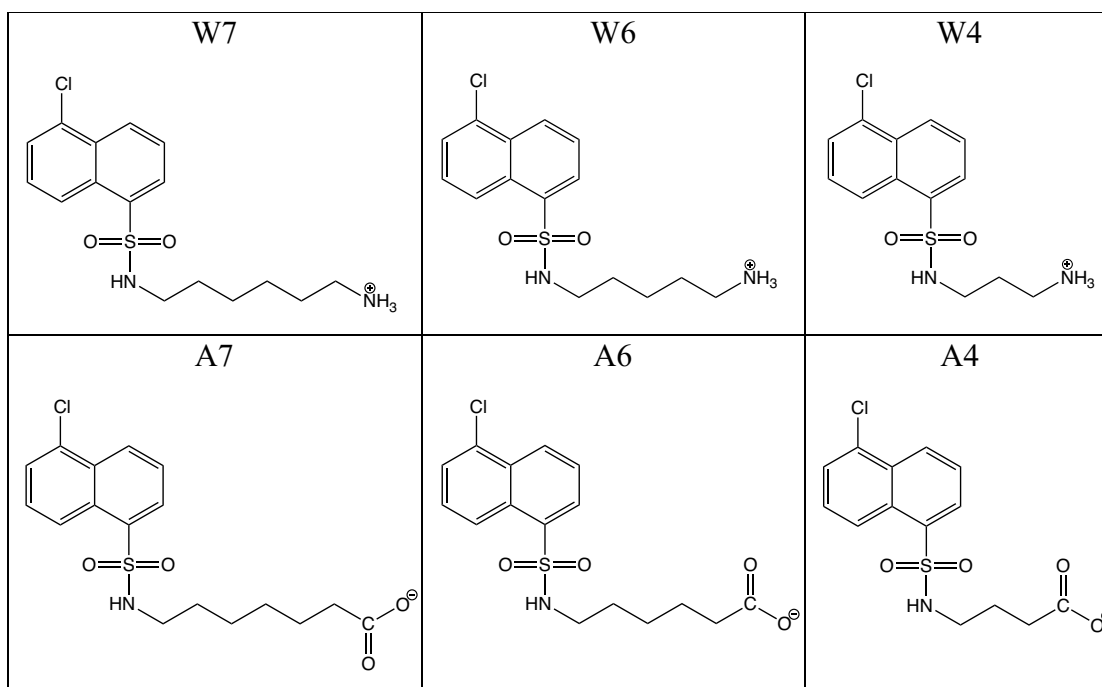


Figure 5.1. Chemical structures of W7, W6, W4, A7, A6 and A4.

Binding of W-series compounds to cTnC-cTnI chimera

W-series (W6 and W4) and A-series (A6 and A4) compounds were titrated into calcium-saturated ^{15}N -labeled cTnC-cTnI switch region chimera (cChimera), monitored by 2D ^1H , ^{15}N -HSQC NMR spectra. cChimera has been shown to faithfully represent the cTnC-cTnI complex, and the 2D ^1H - ^{15}N HSQC NMR spectrum of cChimera has been assigned previously¹⁹. The dissociation constant K_D of $470 \pm 50 \mu\text{M}$ was determined for W7 binding to cChimera¹⁷, which is consistent with the W7 binding constant for the cTnC-cTnI switch peptide binary complex ($K_D = 500 \pm 100 \mu\text{M}$)¹⁴, validating the use of cChimera for binding and structural studies.

Backbone amide resonance shift in cChimera induced by W-series compounds titration is shown in Figure 5.2a. All of the backbone amide signals shifted in a linear fashion, indicating a 1:1 stoichiometric binding of the W-series compounds to cTnC-cTnI chimera. The residues that experienced the largest chemical shifts perturbation are plotted as a function of small molecules to cChimera concentration and the global dissociation constant K_D is $390 \pm 50 \mu\text{M}$ for W6, and $950 \pm 100 \mu\text{M}$ for W4 (Table

5.1). The binding of W6 to cChimera is slightly tighter than W7 to cChimera by approximately 1.2 times, while W4 binds 2 times weaker to cChimera comparing to W7. Almost all of the peaks experience fast exchange in the W7, W6 and W4 titrations to cChimera.

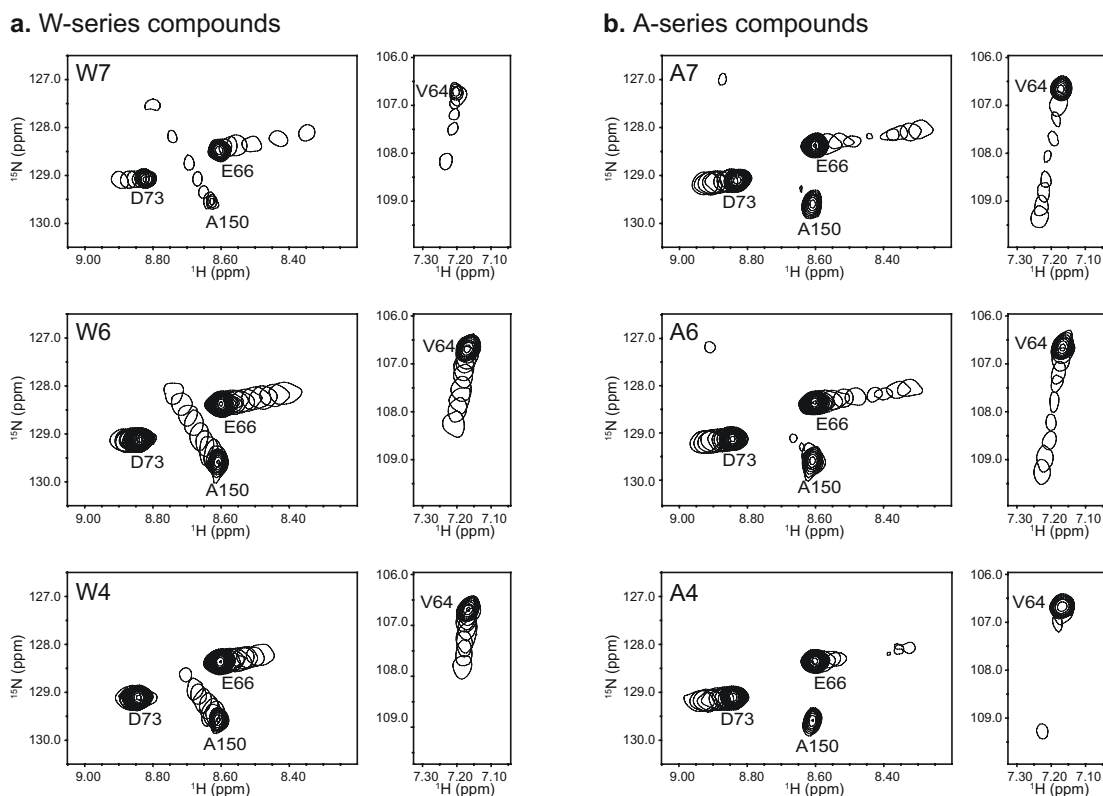


Figure 5.2. Small molecule titrations into the cNTnC-cTnI chimera.

Comparison of regions of the ^1H , ^{15}N HSQC NMR spectra of cChimera during titration with a. W-series compounds (W7, W6 and W4) and b. A-series compounds (A7, A6 and A4). [cChimera] $\sim 100 \mu\text{M}$; [W7] $\sim 15, 45, 95, 195,$ and $495 \mu\text{M}$; and [A7], [A6], [A4], [W6], [W4] $\sim 10, 30, 60, 100, 150, 250, 350, 500,$ and $700 \mu\text{M}$. The first point of each titration is shown with multiple contours, and subsequent titration points in the titrations shown with single contours.

The slightly increased binding constant of W6 to cChimera comparing to W7 may possibly be the results of less steric clashing and electrostatic repulsion between W6 and cTnI switch region. As the “tail” gets shorter in the case of W4, the positively charged terminal amino group moves closer to the hydrophobic pocket of cNTnC. The protein might not like to bury the positive charge close to the hydrophobic pocket, resulting in a weaker binding of W4 to cChimera.

Binding of A-series compounds to cNTnC-cTnI cChimera

The backbone amide chemical shift in calcium-saturated cNTnC-cTnI chimera induced by A-series compounds titration is shown in Figure 5.2b. In the titrations of A-series compounds to cChimera, the backbone chemical shifts migrate in a linear fashion indicating a 1:1 stoichiometry, same as the W-series compounds. The residues that experienced the largest chemical shift perturbation are used to calculate the dissociation constant for A6 and A4 bound to cChimera; the global dissociation constant K_D of A6 to cChimera is of $240 \pm 30 \mu\text{M}$ and of A4 to cChimera is $140 \pm 50 \mu\text{M}$ (Table 5.1). The dissociation constant K_D of $120 \pm 30 \mu\text{M}$ was previously determined for A7 bound to cChimera¹⁸. Although A4 and A7 have a similar binding affinity, some peaks of cChimera have experienced more exchange broadening during the A4 titration. On the other hand, A6 binds about 2 times weaker to cChimera compared to A7 and A4.

Many of the peaks experiencing fast exchange in the W-series compounds titration undergoes intermediate exchange in the A-series titration. Despite the length of the tail, all A-series compounds were found to bind tighter to cNTnC-cTnI chimera than the W-series compounds. Moreover, almost all of the peaks of cChimera move in the same directions among W-series and A-series compounds titrations, suggesting that the binding pockets for all of the compounds are similar.

Table 5.1. Binding of W7-derivatives to cChimera.

Dissociation constants of W7, W6, W4, A7, A6 and A4 to cNTnC-cTnI chimera.

	cNTnC-cTnI chimera
W7	470 ± 50 μM
W6	390 ± 50 μM
W4	950 ± 100 μM
A7	120 ± 30 μM
A6	240 ± 30 μM
A4	140 ± 50 μM

Effects of compounds on ventricular trabeculae

To investigate the effect electrostatics and position of the charged group of the small molecules on cardiac muscle contractility, we measured the calcium dependent force development of demembranated rat right ventricular trabeculae in the absence or in the presence of 50 μmol/L W-series and A-series of compounds (Figure 5.3). We reported that W7 significantly decreases the calcium-sensitivity force, while A7 causes much less decrease in calcium sensitivity¹⁸. Furthermore, A6 does not have any significant effect on calcium sensitivity¹⁸, suggesting the slight desensitizing effect of A7 is caused by sterically clashing with cTnI switch peptide. The effects of A4 with an even shorter tail was tested in demembranated trabeculae. Interestingly, A4 does not show any significant effect on the calcium sensitivity of ventricular trabeculae at concentration of 50 μM, and not even in a concentration range of up to 500 μM (Figure 5.3a).

The effects of W-series of compounds was also tested in demembranated trabeculae. Surprisingly, although W6 is only one methylene-group shorter than W7, it had no effect on the calcium sensitivity of cardiac trabeculae (Figure 5.3). The shorter tailed W4 also has no strong inhibition effect on calcium sensitivity. However, W4 slightly increases force production at lower levels of activation (around pCa 6), but

decreases force at maximal activation. These results suggest that the precise position of the positive charge of W7 in the protein-drug complex is very important.

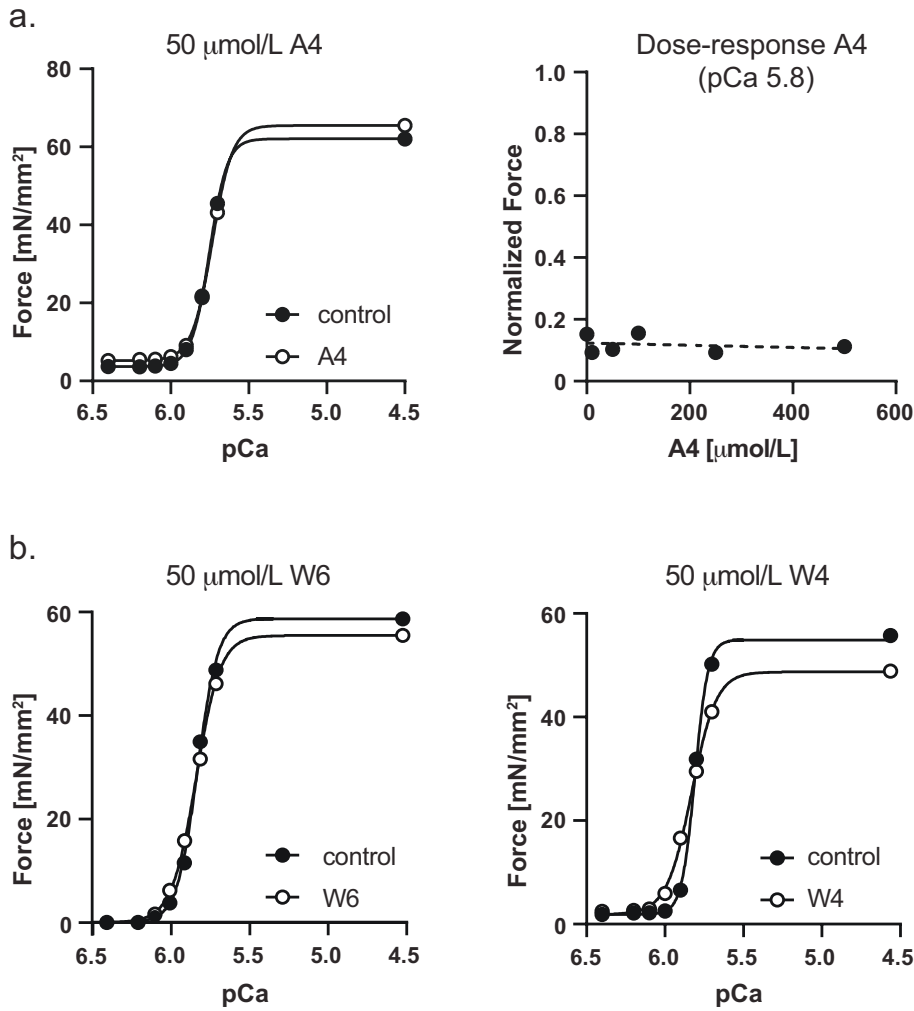


Figure 5.3. Effect of A4, W6 and W4 on ventricular trabeculae force.

a. Force-calcium relation of ventricular trabeculae in the absence (closed circles) and in the presence (open circles) of 50 μM A4, and dose-response of A4 on force at pCa 5.8. b. Force-calcium relation of ventricular trabeculae in the absence (closed circles) and in the presence (open circles) of 50 μM W6 and W4.

Structural insight of cChimera-W6 complex

Several NMR solution structures of small molecules bound to calcium-saturated cNTnC-cTnI switch region chimera complex has been determined, including 3-mDPA¹⁹, W7¹⁷ and A7¹⁸. The overall protein structures in these complexes are very similar to each other, and is consistent with the solution structure of liganded-free cChimera¹⁹, the solution structure of cNTnC-cTnI switch peptide complex²⁷, as well as the corresponding region in the X-ray structure of the cTn complex⁹. The small molecules bind to the hydrophobic pocket formed by the cNTnC and cTnI switch region and cause little perturbation to the overall protein structure, including the helical length and the position of the cTnI switch region. Therefore, we simplified the structure determination process for cChimera-W6 complex by adopting the cChimera intramolecular distance restraints from the structure of cChimera-W7 complex. We acquired the 2D ¹³C,¹⁵N-double-filtered TOCSY experiment for the chemical shift assignment of W6 in cChimera-W6 complex, and 3D ¹³C-filtered/edited NOESY-HSQC experiment for intermolecular distance restraints between W6 and cChimera. There were 37 intermolecular contacts between cChimera and W6, including 26 between cNTnC and W6, and 11 between cTnI switch region and W6.

Intermolecular NOEs between cChimera and W6 are very similar to those between cChimera and W7. Figure 5.4 shows a section of 2D projection view of 3D ¹³C-filtered/edited NOESY-HSQC experiments of cChimera-W7 complex and cChimera-W6 complex. Proton nomenclature of W6 is shown in Figure 5.5C, and the nomenclature of W6 and W7 naphthalene ring are the same. Most of the contacts for both compounds to the cChimera protein are very similar, indicating a very similar binding pocket between W7 and W6 to cChimera.

We determined the NMR solution structure of cChimera-W6 complex to characterize the W6 binding pocket (Figure 5.5A). The chlorine-containing ring of the W6 naphthalene ring contacts I61 on helix C from the central β -sheet of cNTnC, indicating the deep binding site in the hydrophobic cleft. The naphthalene ring of W6 contacts V44 and M45 on helix B, M60, I61 and V64 on helix C, M80 on helix D and I148, A150 and M153 of the cTnI switch region. This hydrophobic binding pocket of W6 in cChimera-W6 complex structure is comparable to that of other small molecules

that bind to the interface of cNTnC-cTnI switch region such as bepridil²⁸, dfbp-o²⁹, 3-mDPA¹⁹, W7^{16,17}, and A7¹⁸. Several hydrophobic residues contact both the naphthalene rings and the aliphatic part of the tail. M45 and I148 contact H11; M80 and A150 contact H11 and H13; V64 H11, H12/14, and H13 (H12 and H14 have similar chemical shifts). H16, the methylene group on the tail adjacent to the positively charged amine, is not observed making contact to cChimera. All residues of cChimera contacting W6 are colored in pink shown in Figure 5.5B, and residues contacting both ring and tail of W6 is underlined. W6, including both the rings and the tail parts, is well defined in the cChimera-W6 solution structure (Figure 5.5C).

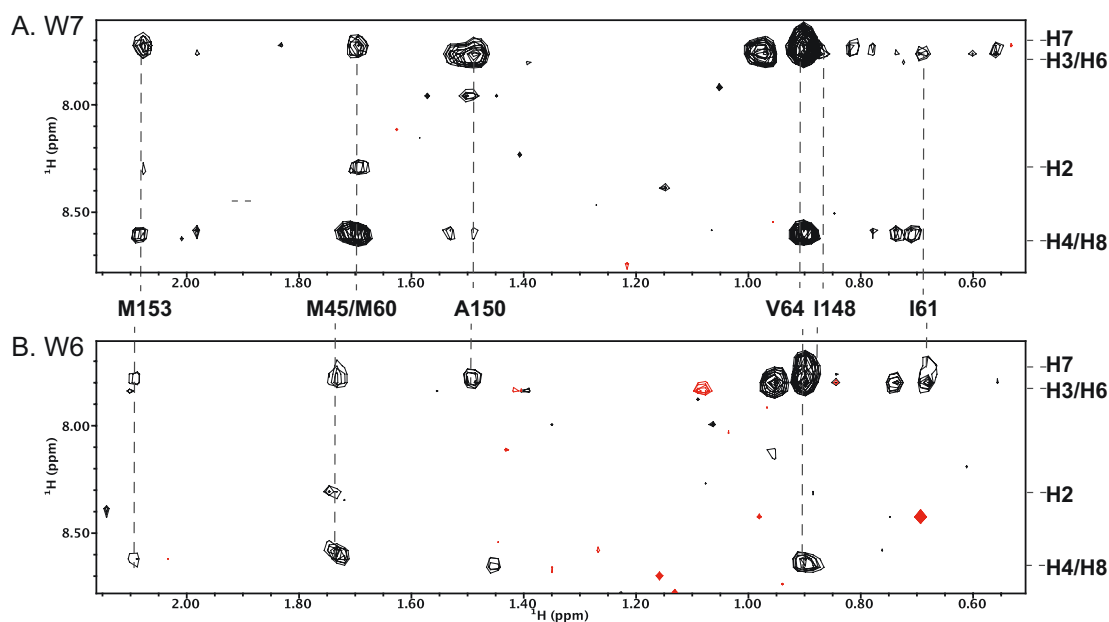


Figure 5.4. Intramolecular NOEs between cChimera and W7 or W6.

Sections of 2D projection view of 3D ¹³C-filtered/edited NOESY-HSQC experiments of A. cChimera-W7 and B. cChimera-W6. The x-axis corresponds to protein ¹H chemical shift, with the assignments shown between the two spectra. The y-axis corresponds to the W6 or W7 ¹H chemical shifts, with the assignments shown to the right of the spectra.

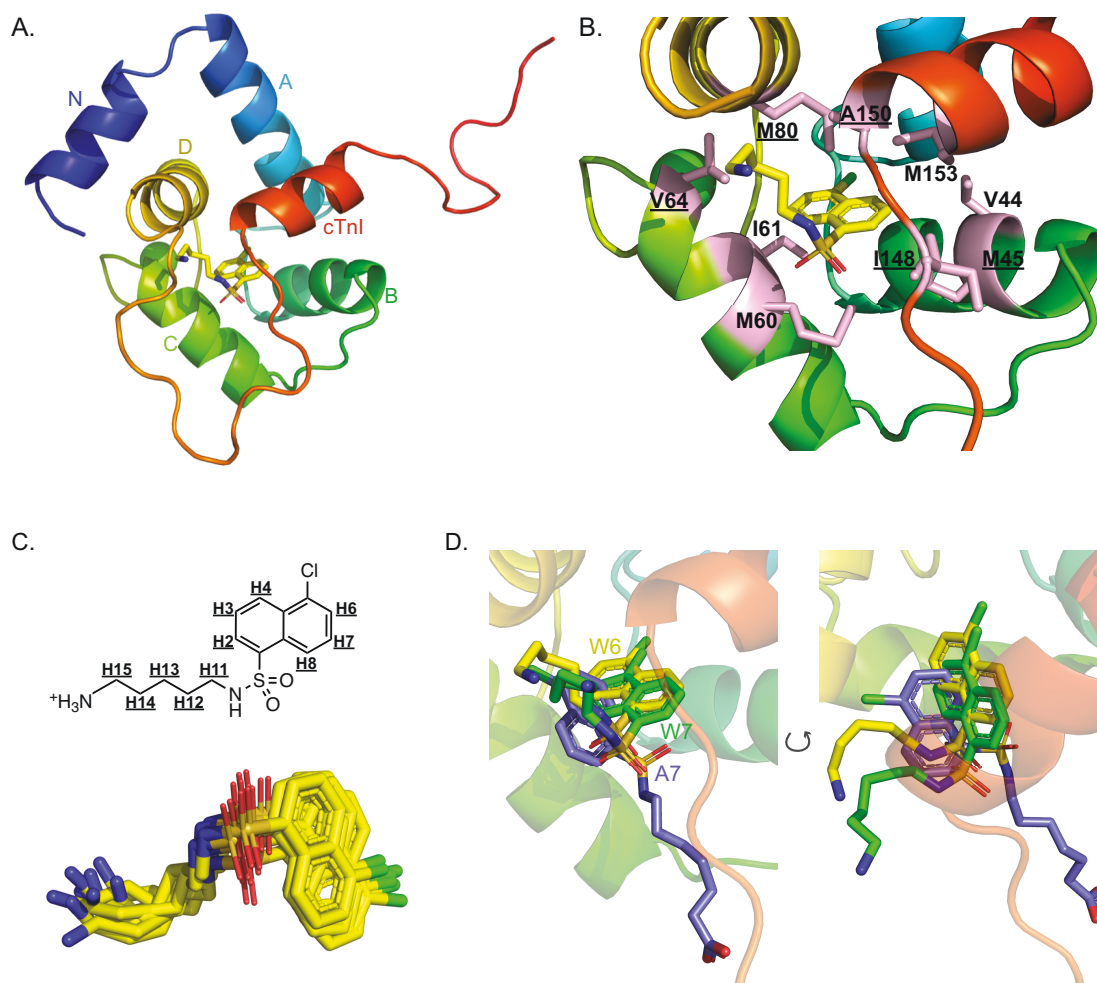


Figure 5.5 The solution structure of the cChimea-W6 complex.

A. The solution structure of the cChimera-W6 complex. cNTnC region: blue (N-helix), cyan (A-helix), green (B-helix), light green (C-helix) and yellow (D-helix), cTnI inhibitory region linker: orange, cTnI switch region: red. Ca^{2+} ions: green spheres. W6: light yellow. B. W6 binding pocket in cChimera-W6 complex structure, with residues contacting W6 shown in pink sticks, and residues contacting both ring and tail parts of W6 is underlined. The linker has been removed for clarity. C. W6 chemical structure and superposition of 10 structures of W6 shown in sticks. D. Superposition of the cChimera-W6, cChimera-W7 and cChimera-A7 solution structures; W6 (yellow), W7 (green) and A7 (blue) are shown in sticks.

When the structures of W6 in cChimera-W6 complex is compared to the W7 in cChimera-W7 complex and A7 in cChimera-A7 complex (Figure 5.5D), the naphthalene ring of all three small molecule structures are in the same hydrophobic binding pocket, surrounded by hydrophobic residues such as I61, V64, and M153. The tail part of W7 and W6 go to the same route while A7 takes a different route to the surface of the complex. However, it is important to note that the NOEs between A7 and the cChimera was not observed, so the A7 tail position is predicted as the lowest energy position and possibly more flexible than W6 and W7.

Conclusions

The sarcomere inhibitor W7 directly modulates the calcium sensitivity of force development in cardiac muscle by binding to the sarcomere thin filament protein troponin. Studies have shown that the negative inotropic effect of W7 results from electrostatics repulsion with cTnI switch region¹⁸. In this study, we have used a series of W7 derivatives to evaluate the importance of both electrostatics and the precise location of the charged group. None of the W7-derivatives had the strong negative inotropic effect on ventricular trabeculae. The solution structure of cChimera-W6 reveals that W6 binds to the same hydrophobic cleft as W7; the naphthalene rings sit in the same deep binding pocket and the aliphatic tails extended into the solvent in a similar route. The only difference would be the exact location of the positively charged amino group of W7 and W6 due to the different in tail length. These results indicate that aside from electrostatics repulsion, the precise location of the charged amino group is also important in the negative inotropic effect of W7.

Acknowledgements

This study was supported by grants from the Heart and Stroke foundation of Canada (G-14-0005884 to B.D.S.), the University of Alberta Faculty of Medicine Transitional Program (B.D.S.), Motyl Graduate Studentship (F.C.) and British Heart Foundation (Fellowship FS/16/3/31887 to T.K.).

References

1. Hidaka, H. *et al.* A Novel Vascular Relaxing Agent, N-(6-Aminohexyl)-5-Chloro-1-Naphthalenesulfonamide Which Affects Vascular Smooth Muscle Actomyosin. *J. Pharmacol. Exp. Ther.* **207**, 8–15 (1978).
2. Hidaka, H. *et al.* Calcium-regulated modulator protein interacting agents inhibit smooth muscle calcium-stimulated protein kinase and ATPase. *Mol. Pharmacol.* **17**, 66–72 (1980).
3. Adhikari, B. B. & Wang, K. Interplay of Troponin- and Myosin-Based Pathways of Calcium Activation in Skeletal and Cardiac Muscle: The Use of W7 as an Inhibitor of Thin Filament Activation. *Biophys. J.* **86**, 359–370 (2004).
4. Thompson, B. R., Martindale, J. & Metzger, J. M. Sarcomere neutralization in inherited cardiomyopathy: small-molecule proof-of-concept to correct hyper-Ca²⁺-sensitive myofilaments. *Am. J. Physiol. Heart Circ. Physiol.* **311**, H36-43 (2016).
5. EBASHI, S. Separation of Troponin into Its Three Components*. *J. Biochem.* **72**, 787–790 (1972).
6. Greaser, M. L. & Gergely, J. Purification and properties of the components from tropinin. *J. Biol. Chem.* **248**, 2125–2133 (1973).
7. Parry, D. A. D. & Squire, J. M. Structural role of tropomyosin in muscle regulation: Analysis of the X-ray diffraction patterns from relaxed and contracting muscles. *J. Mol. Biol.* **75**, 33–55 (1973).
8. Li, M. X., Spyropoulos, L. & Sykes, B. D. Binding of Cardiac Troponin-I 147-163 Induces a Structural Opening in Human Cardiac Troponin-C † , ‡. *Biochemistry* **38**, 8289–8298 (1999).
9. Takeda, S., Yamashita, A., Maeda, K. & Maéda, Y. Structure of the core domain of human cardiac troponin in the Ca(2+)-saturated form. *Nature* **424**, 35–41 (2003).
10. Li, M. X., Wang, X. & Sykes, B. D. Structural based insights into the role of troponin in cardiac muscle pathophysiology. *J. Muscle Res. Cell Motil.* **25**, 559–79 (2004).
11. Gordon, A. M., Homsher, E. & Regnier, M. Regulation of contraction in striated

- muscle. *Physiol. Rev.* **80**, 853–924 (2000).
12. Narita, A., Yasunaga, T., Ishikawa, T., Mayanagi, K. & Wakabayashi, T. Ca²⁺-induced switching of troponin and tropomyosin on actin filaments as revealed by electron cryo-microscopy¹ Edited by A. Klug. *J. Mol. Biol.* **308**, 241–261 (2001).
 13. Hoffman, R. M. B., Li, M. X. & Sykes, B. D. The binding of W7, an inhibitor of striated muscle contraction, to cardiac troponin C. *Biochemistry* **44**, 15750–15759 (2005).
 14. Li, M. X., Hoffman, R. M. B. & Sykes, B. D. Interaction of Cardiac Troponin C and Troponin I with W7 in the Presence of Three Functional Regions of Cardiac Troponin I †. *Biochemistry* **45**, 9833–9840 (2006).
 15. Hoffman, R. M. B. & Sykes, B. D. Structure of the Inhibitor W7 Bound to the Regulatory Domain of Cardiac Troponin C. *Biochemistry* **48**, 5541–5552 (2009).
 16. Oleszczuk, M., Robertson, I. M., Li, M. X. & Sykes, B. D. Solution structure of the regulatory domain of human cardiac troponin C in complex with the switch region of cardiac troponin I and W7: The basis of W7 as an inhibitor of cardiac muscle contraction. *J. Mol. Cell. Cardiol.* **48**, 925–933 (2010).
 17. Cai, F., Hwang, P. M. & Sykes, B. D. Structural Changes Induced by the Binding of the Calcium Desensitizer W7 to Cardiac Troponin. *Biochemistry* **57**, 6461–6469 (2018).
 18. Cai, F., Robertson, I. M., Kampourakis, T., Klein, B. A. & Sykes, B. D. The Role of Electrostatics in the Mechanism of Cardiac Thin Filament Based Sensitizers. *ACS Chem. Biol.* **15**, 2289–2298 (2020).
 19. Cai, F. *et al.* Structures reveal details of small molecule binding to cardiac troponin. *J. Mol. Cell. Cardiol.* **101**, 134–144 (2016).
 20. Guo, K. & Li, L. Differential ¹²C/¹³C-isotope dansylation labeling and fast liquid chromatography/mass spectrometry for absolute and relative quantification of the metabolome. *Anal. Chem.* **81**, 3919–3932 (2009).
 21. Delaglio, F. *et al.* NMRPipe: A multidimensional spectral processing system based on UNIX pipes. *J. Biomol. NMR* **6**, 277–293 (1995).

22. Johnson, B. A. & Blevins, R. A. NMR View: A computer program for the visualization and analysis of NMR data. *J. Biomol. NMR* **4**, 603–614 (1994).
23. Schüttelkopf, A. W. & van Aalten, D. M. F. *PRODRG*: a tool for high-throughput crystallography of protein–ligand complexes. *Acta Crystallogr. Sect. D Biol. Crystallogr.* **60**, 1355–63 (2004).
24. Kleywegt, G. J. Dictionaries for Heteros. *CCP4/ESF- EACBM Newsl. Protein Crystallogr.* **31**, 45–50. (1995).
25. Schwieters, C. D., Kuszewski, J. J., Tjandra, N. & Clore, G. M. The Xplor-NIH NMR molecular structure determination package. *J. Magn. Reson.* **160**, 65–73 (2003).
26. Kampourakis, T., Yan, Z., Gautel, M., Sun, Y.-B. & Irving, M. Myosin binding protein-C activates thin filaments and inhibits thick filaments in heart muscle cells. *Proc. Natl. Acad. Sci. U. S. A.* **111**, 18763–8 (2014).
27. Li, M. X., Spyrapoulos, L. & Sykes, B. D. Binding of cardiac troponin-I147-163 induces a structural opening in human cardiac troponin-C. *Biochemistry* **38**, 8289–98 (1999).
28. Wang, X., Li, M. X. & Sykes, B. D. Structure of the regulatory N-domain of human cardiac troponin C in complex with human cardiac troponin I147-163 and bepridil. *J. Biol. Chem.* **277**, 31124–33 (2002).
29. Robertson, I. M., Sun, Y.-B. B., Li, M. X. & Sykes, B. D. A structural and functional perspective into the mechanism of Ca²⁺-sensitizers that target the cardiac troponin complex. *J. Mol. Cell. Cardiol.* **49**, 1031–41 (2010).

Chapter 6

A Fluorescent Reversible-Covalent Cardiac Muscle Inhibitor

Fangze Cai¹, Thomas Kampourakis², Brittney A. Klein¹, and Brian D. Sykes¹

¹Department of Biochemistry, University of Alberta, Edmonton, AB, Canada.

² Randall Centre for Cell and Molecular Biophysics, King's College London, London, United Kingdom

This chapter is part of a manuscript in preparation. Cai, F., Kampourakis, T. Klein, B. A., & Sykes, B. D. A Fluorescent Reversible-covalent Cardiac Muscle Inhibitor.

Contribution: TK prepared the cardiac myofibril and performed the ATPase measurement. BAK performed the fluorescence experiments. FC performed the NMR titration, analyzed the data and wrote the manuscript. All authors helped review and edit the manuscript. BDS directed the reaserch.

Summary

Compounds that directly and specifically alter the response of the cardiac sarcomere without altering cytosolic calcium homeostasis have therapeutic potential for the treatment of cardiac dysfunction. We report a very strong cardiac sarcomere inhibitor, DN-F01, targeting the thin filament protein troponin complex. This study substantiates the effective role of reversible covalent modification to cNTnC C84 by nitriles for the modulation of calcium sensitivity in cardiac muscle. The ATPase activity studies show that DN-F01 has a strong inhibiting effect on cardiomyofibrils. The fluorescence intensity changes when DN-F01 binds to protein, which could be a great tool for future screening new compounds. The NMR titrations of DN-F01 to C35S and A-cys cNTnC-cTnI chimera shows that the binding position of DN-F01 bound covalently or non-covalently to the cNTnC-cTnI chimera might be different.

The bulky DN-F01 might clash with the cTnI switch peptide when covalently bond to C84, which could be the mechanism underlying its strong sarcomere inhibitory effect.

Introduction

Both systolic and diastolic dysfunction can lead to heart failure, which occurs when the heart cannot pump enough blood to satisfy the body's needs. Systolic dysfunction occurs when the heart muscle is weak and dilated, losing its ability to contract; while diastolic dysfunction is caused by thick and stiff heart muscle, impairing the relaxation process. Common therapeutics that are available increase or decrease the cardiac muscle contractility by regulating the calcium-based signaling pathway and alter the calcium transients, but this can also affect other signaling systems¹. Compounds that directly and specifically alter the response of the cardiac sarcomere without altering cytosolic calcium homeostasis have therapeutic potential for the treatment of cardiac dysfunction.

Heart muscle contraction is regulated by the binding of calcium to the thin filament cardiac troponin protein complex (cTn). cTn has three subunits: the calcium binding subunit troponin C (cTnC), the inhibitory subunit troponin I (cTnI), and the tropomyosin binding subunit (cTnT)². When calcium binds to the regulatory N-terminal domain of cTnC (cNTnC), it undergoes a conformational change that promotes the binding of the switch region of cTnI³. The binding of cTnI switch region pulls the inhibitory region of cTnI off actin, shifting tropomyosin to expose the myosin binding sites on actin, triggering muscle contraction through the formation of actin-myosin cross-bridges⁴. The troponin protein complex is therefore a logical target for direct cardiac sarcomere modulating compounds.

Several small molecules are known to bind to the interface of cNTnC and cTnI switch region and change the calcium sensitivity of the sarcomere. One of the most widely studied activator bound to this interface is levosimendan (marketed as SimDaX)^{5,6}. SimDax has marketing authorization in over 60 countries worldwide to treat acute heart failure. Recent studies show that levosimendan forms a reversible-covalent thioimidate bond with C84 of cNTnC both *in vitro*⁷ and *in situ*⁸. A levosimendan analogue, DLEV, was reported to form a reversible covalent bond with

C84 and increase ATPase activity of bovine cardiac muscle myofibrils⁹. Targeting this unique cTnC C84 reactivity could be a promising way to discover calcium modulating drugs for cardiac dysfunction. Whilst equally important as activators, very few inhibitors have been identified. Epigallocatechin gallate (EGCg) and *N*-(6-aminohexyl)-5-chloro-1-naphthalenesulfonamide (W7) have been studied as small-molecule sarcomere inhibitors. EGCg has been suggested to bind to cTnC and decrease calcium sensitivity¹⁰, while W7 was shown to bind to the interface of cTnC and cTnI switch region and decrease the cTnI switch region binding¹¹.

In this note, we report a very strong cardiac sarcomere inhibitor, DN-F01 (4-(diphenylamino)phenylcyanoacrylic acid), targeting the thin filament protein troponin complex. DN-F01 shares structural similarities to levosimendan, and was previously determined to form a reversible covalent thioimide bond with cTnC Cys 84⁹. The ATPase activity studies show that DN-F01 has a strong inhibiting effect on cardiomyofibrils. The fluorescence intensity increases when DN-F01 binds to protein, which could be a great tool for future screening new compounds. NMR titration of DN-F01 to C35S cTnC-cTnI switch region chimera (C84) is undergoing slow exchange, while the titration of DN-F01 to A-cys cTnC-cTnI switch region chimera (C35S, C84S) is undergoing fast exchange. This suggests that the DN-F01 covalently binds to the cTnC Cys 84, and the binding position of DN-F01 bound covalently or non-covalently to the cTnC-cTnI chimera might be different. The bulky DN-F01 might clash with the cTnI switch peptide when covalently bond to C84, which could be the mechanism underlying its strong sarcomere inhibitory effect.

Material and methods

Material

4-(diphenylamino)phenylcyanoacrylic acid (DN-F01) was purchased from Dyenamo AB.

Fluorescence spectroscopy

All steady-state fluorescence measurements were performed at 24 °C. DN-F01 fluorescence was excited at 400 nm and monitored from 450 nm to 600 nm for emission

scan, and 530 nm for DN-F01 titration. Each 2ml of fluorescence sample was prepared in 50 mM MOPS, 100 mM KCl, 2 mM EGTA, 3 mM MgCl₂, and 2mM CaCl₂, pH 7.0 aqueous buffer. Stock solution of 10 mM DN-F01 were prepared in DMSO. For the DN-F01 titration, 0-15 μ M of DN-F01 is added to the sample containing 2 μ M of Thm_chimera protein. A solubility curve was obtained by titrating DN-F01 into buffer solution.

The protein used for fluorescence experiments is the recombinant Thm_chimera, which contains an N-terminal histidine tag, the TEV protease recognition site ENLYFQG, cTnI C35S (residues 1 to 89), the thrombin protease recognition site LVPRGS, and cTnI switch region (residues 144 to 173). The Thm_chimera used in this study contains both Cys 35 and Cys 84. Thm_chimera proteins were expressed in E. coli BL21(DE3) and purified by Ni-NTA affinity chromatography followed by size exclusion chromatography and lyophilization as previously described¹².

NMR spectroscopy

NMR experiments were performed at 30 °C on a Varian Inova 600 MHz spectrometer equipped with a triple resonance probe with pulsed field gradients. Samples were prepared in 5 mm NMR tubes with a starting sample volume of 500 μ L. The protein samples were in 100 mM KCl, 10 mM imidazole, and 2 mM CaCl₂ in 95% H₂O/5% D₂O, pH 6.7-6.8, using 5% (v/v) 2,2- dimethyl-2-silapentane-5-sulfonate-d₆ sodium salt (DSS-d₆) as an NMR internal reference. Stock solution of 10 mM DN-F01 were prepared in DMSO-d₆ (Cambridge Isotopes). DMSO-d₆ concentration was kept below 5% (v/v) to reduce solvent effect. Recombinant C35S cTnI_chimera and A-cys cTnI_chimera were used in the NMR studies. cTnI_chimera contains cNTnI (residues 1–90), cTnI (residues 136–163), and a histidine tag. C35S cTnI_chimera has C84, and A-cys cTnI_chimera have both Cys 35 and Cys 84 substituted with serine. [¹⁵N]-C35S and [¹⁵N]-A-cys cTnI_chimera proteins were expressed in E. coli BL21(DE3) and purified by Ni-NTA affinity chromatography followed by dialysis and lyophilization as previously described¹³.

The binding of DN-F01 to protein was monitored at each aliquot by 1D ¹H and 2D ¹⁵N,¹H HSQC NMR experiments. DN-F01 was titrated into 30 μ M of A-cys

cTnI_chimera to a final concentration of 5, 15, 30, 50, 75, 100 μM . DN-F01 was titrated into 40 μM C35S cTnI_chimera (attached to BME) or 40 μM C35S cTnI_chimera + 10mM DTT to a final concentration of 5, 15, 25, 40, 60, 100 μM . A solubility curve was obtained by titrating DN-F01 into NMR buffer solution monitored by 1D ^1H NMR experiments. 1D ^1H NMR experiments were collected to monitor the state of 50 μM DN-F01 in the absence or presence of 2 mM DTT. 1D NMR spectra were processed with VNMRJ v.3.2 A (Varian, Inc.); 2D NMR spectra were processed with NMRPipe¹⁴ and analyzed with NMRViewJ¹⁵.

ATPase activity measurements

Cardiac myofibril preparation and ATPase measurements were performed as described previously. Cardiomyofibrils (CMFs) were prepared by homogenising freshly frozen bovine ventricular tissue samples in myofibril buffer (composition in mM: 20 Imidazole pH 7.4, 75 KCl, 2 MgCl₂, 2 EDTA, 1 DTT, 1% (v/v) Triton X-100, protease inhibitor cocktail (ROCHE), PhosStop cocktail (ROCHE)) followed by centrifugation at 5,000 g for 5 min at 4°C. CMFs were washed and homogenised three more times in the same buffer without Triton X-100.

CMFs were washed three times in ATPase assay buffer (composition in mmol/L: 20 MOPS pH 7.0, 35 NaCl, 5 MgCl₂, 1 EGTA) with varying concentrations of CaCl₂ (pCa 9 to pCa 4.5) and the CMF concentration adjusted to 1 mg/ml. For ATPase measurements in the presence of drug, CMFs were incubated with varying concentrations of DN-F01 at room temperature for 30 min. DN-F01 was prepared as a stock solution in DMSO and the final DMSO concentration during ATPase measurements was held constant at 0.1% (v/v).

Reactions were started by the addition of 2.5 mmol/L ATP and quenched with 0.5 volumes ice cold 25% (w/v) TCA solution. Samples were kept on ice at all times, diluted with double-deionized water, precipitation removed by centrifugation at 5000g for 10 min and inorganic phosphate content measured using the malachite green assay according to manufacturer's instructions (Sigma, MAK307).

Results and discussion

DN-F01 chemical structure

DN-F01 (4-(diphenylamino) phenylcyanoacrylic acid) was initially used as a fluorescent dye, with the triphenylamine donor and the cyanoacetic acid acceptor¹⁶. DN-F01 shares structural similarities to the principal compounds we have studied for their sarcomere activating potential: diphenylamine (DPA)-containing compounds and the notable activator levosimendan (Figure 6.1). Compounds based on diphenylamine (DPA) show moderate binding affinity to a cNTnC-cTnI switch region chimera ($K_D \sim 10\text{-}120 \mu\text{M}$)¹³. NMR solution structures indicate that 3-methyldiphenylamine (3-mDPA) binds deeply in the hydrophobic pocket between cNTnC and cTnI switch region, and does not perturb the binding of cTnI switch region to cNTnC. 3-chlorodiphenylamine (3-CIDPA) was found to increase the calcium sensitivity of force development in skinned cardiac muscle¹⁷. DN-F01 also contains a nitrile group like levosimendan. It was reported that the cyanoacrylic acid of DN-F01 reversibly covalently binds to cNTnC through a thioimidate bond with cNTnC C84, in the same manner as the malononitrile functionality of Levosimendan⁹.

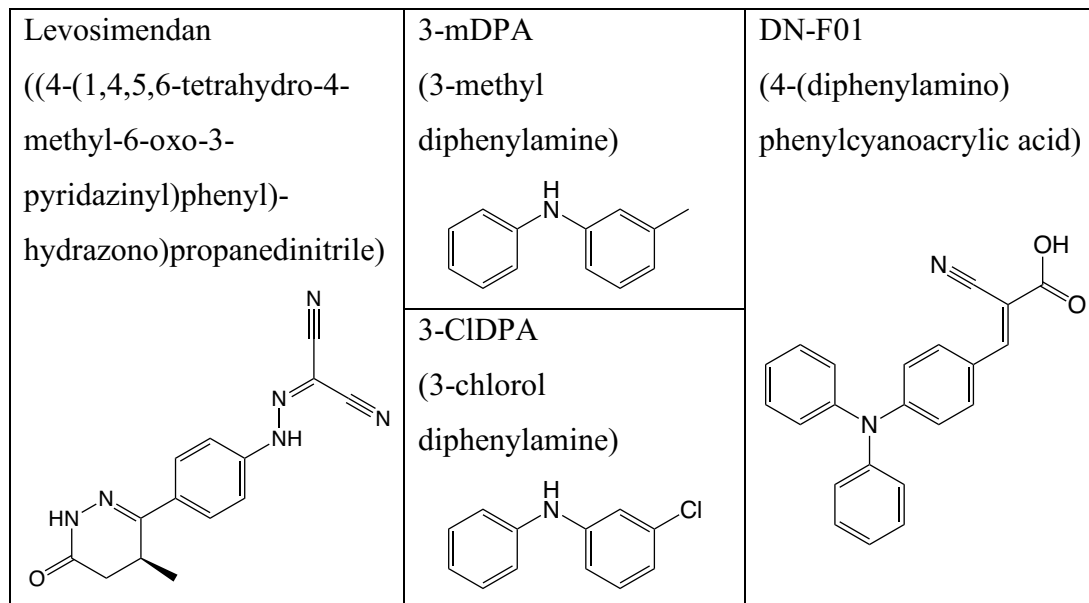


Figure 6.1. Structures of Levosimendan, 3-mDPA, 3-CIDPA, and DN-F01.

Effect of DN-F01 on ATPase activity

To assess the function of DN-F01 as a troponin modulator, actomyosin ATPase activity measurements were conducted with bovine cardiomyofibrils (CMFs). Although DN-F01 is a fluorescence dye, it does not interfere with Malachite green assay for determining phosphate concentrations (Figure 6.2). Addition of DN-F01 to CMFs caused a drastic decrease in ATPase activity indicating that DN-F01 has a strong inhibitory effect (Figure 6.3A). All of the other compounds studied previously, including the reversible covalent compounds Levosimendan and DLEV, showed no or little effect on CMF ATPase⁹.

DN-F01 has different effect on the CMF ATPase activity at low (pCa 9), intermediate (pCa 6) and high calcium concentrations (pCa 4.5). DN-F01 only affects the calcium-dependent CMF ATPase activity (pCa 6 and 4.5), but not the resting CMF ATPase activity (pCa 9). This suggests that DN-F01 specifically inhibits the calcium-dependent activation of the myofilaments (Figure 6.3B).

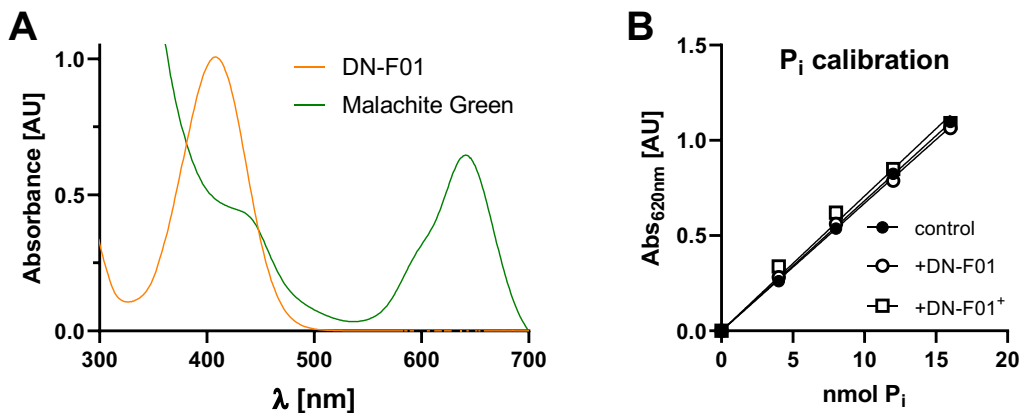


Figure 6.2. Malachite green assay is not affected by DN-F01 fluorescence.

a. Absorbance spectrum of DN-F01 (orange) and Malachite Green (green) in the presence of ortho-phosphate. B Phosphate calibration of Malachite Green reagent in the absence (control) and in the presence of 50 mmol/L deprotonated (DN-F01) and protonated DN-F01 (DN-F01+).

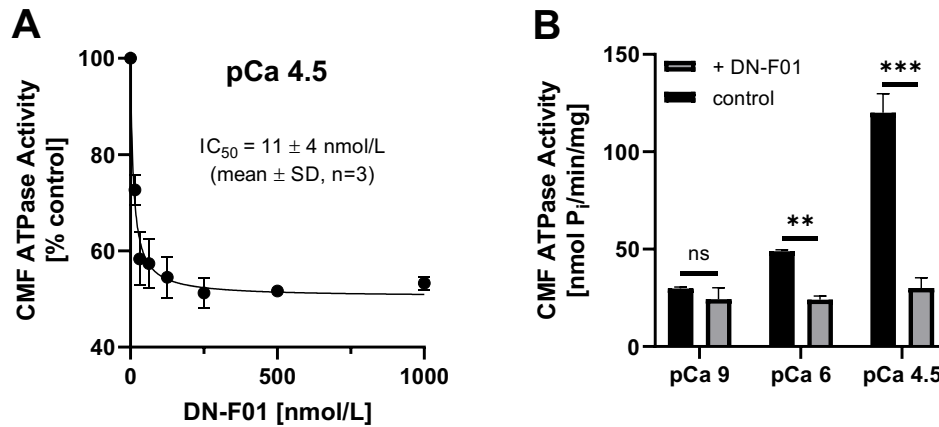


Figure 6.3. Effect of DN-F01 on ATPase Activity.

A. Dose-response curve for the effect of DN-F01 on cardiac myofibrillar ATPase activity at full calcium activation (pCa 4.5). B. Effect of DN-F01 on the CMF ATPase activity at low (pCa 9), intermediate (pCa 6) and high calcium concentrations (pCa 4.5).

The use of cNTnC-cTnI chimera

We used the cNTnC-cTnI chimera to investigate the binding properties of DN-F01 in this study. Chimeric proteins have been widely used to simplify the complex protein-protein interaction, including both skeletal and cardiac troponin^{12,18}. We have constructed the cNTnC-cTnI switch region chimera for structure, dynamics, and drug binding studies. The chimeras have been constructed with different linkers between cNTnC and cTnI and have included different amino acid mutations for various experiments. The NMR solution structure shows that cNTnC-cTnI chimera reproduces the native interface between cNTnC and cTnI switch region, with the cNTnC in an open conformation¹³. Solution structures of cNTnC-cTnI switch chimera bound to several small molecules, including levosimendan analogue i⁹, bepridil derivative 3-mDPA¹³ and troponin inhibitor W7²⁰ have been determined using NMR spectroscopy. Previous studies indicated that DN-F01 is covalently bound to cNTnC C84 by mass spectrometry⁹. Wild type cNTnC has two cysteines C35 and C84. In this study, the A-cys chimera represents C35S and C84S protein, whereas the C35S chimera has Cys 84.

Fluorescence study of DN-F01

Fluorescence spectroscopy is used to study the binding property of DN-F01 to cNTnC-cTnI chimera. All steady-state fluorescence measurements were performed at 24°C. DN-F01 fluorescence was excited at 400 nm and monitored at 530 nm during the titration. A cNTnC-cTnI switch region Thm_chimera containing both C35 and C84 was used for this experiment. The emission scan of chimera showed no fluorescence, except a small fluorescence peak around 460 nm coming from the buffer. The emission scan of DN-F01 without protein showed a broad peak about 500-580 nm. The fluorescence intensity of DN-F01 drastically increased in the presence of cNTnC-cTnI chimera (Figure 6.4a). To determine the binding affinity of DN-F01 to this chimera, we titrated DN-F01 into a calcium saturated protein sample and monitored the change in fluorescence intensity as a function of DN-F01 concentration. It has been reported that DN-F01 only reacts with C84 even though both cysteines are present in cNTnC⁹. The dissociation constant, K_D , of DN-F01 to cNTnC-cTnI chimera is approximately 3 μM (Figure 6.4b).

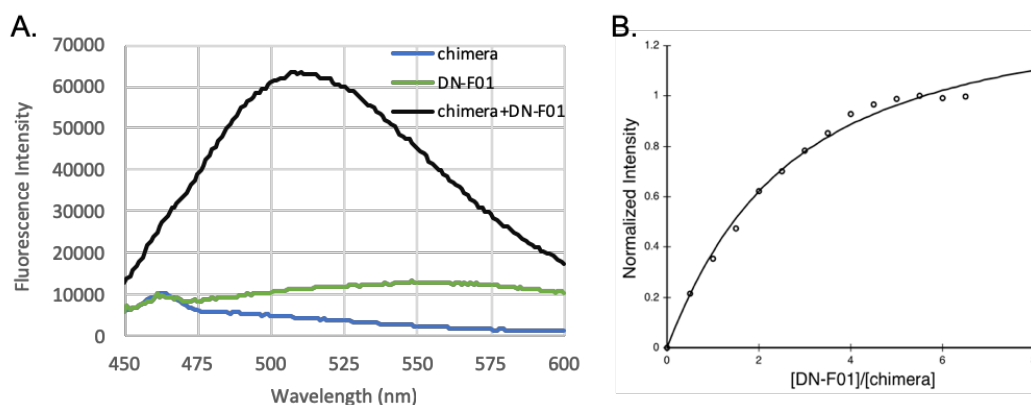


Figure 6.4. DN-F01 fluorescence scan and titration.

(a) Emission scans of 10 μM DN-F01 (green), 2 μM cNTnC-cTnI chimera (blue), and 10 μM DN-F01 + 2 μM DN-F01 (black) in MOPs buffer. (b) DN-F01 titrations into calcium-saturated cNTnC-cTnI chimera.

NMR study of DN-F01 to cNTnC-cTnI chimera

NMR spectroscopy was used to further investigate the binding of DN-F01 to cNTnC-cTnI switch region complex. All of the spectroscopic experiments were conducted using recombinant human ^{15}N labeled A-cys cTnI_chimera or C35S cTnI_chimera. 10 mM DTT was used in the C35S chimera sample to ensure C84 was reduced. We measured the solubility of DN-F01 in aqueous solution using fluorescence and 1D ^1H NMR spectroscopies (Figure 6.5). The solubility of DN-F01 is only about 50-60 μM , which is low for NMR, and the protein concentration for DN-F01 titrations needs to be lower to report a valid and accurate binding affinity. For each DN-F01 titration, a protein concentration of 25 μM was used for A-cys chimera and 40 μM for C35S chimera. Each titration point is acquired for 24 hours (256 scans).

We titrated DN-F01 into A-cys and C35S ^{15}N cNTnC-cTnI switch region chimera monitored by 1D ^1H and 2D $^{15}\text{N}, ^1\text{H}$ HSQC NMR experiments. For the A-cys chimera, the exchange of the DN-F01 between the free and bound forms is in the NMR fast exchange limit and the line shape of the unliganded and liganded protein resonances is the weighted average of the two. DN-F01 binds tightly to the cNTnC-cTnI switch region complex in the absence of C84 (Figure 6.6B), and the dissociation constant K_D is determined to be around 10 μM . On the other hand, separated unliganded and liganded protein resonances are observed when DN-F01 is titrated into C35S chimera (Figure 6.6A). Slow exchange happens when the lifetime of protein-ligand complex is much longer than the chemical shift difference between free and bound forms, so the signals from both free and bound states are observed. The binding constant cannot be accurately calculated for slow exchange regime, but it is much tighter binding comparing to DN-F01:A-cys chimera. The estimated dissociation constant for DN-F01 to cNTnC-cTnI chimera would be in the sub-micromolar range (typically $K_D < 0.5 \mu\text{M}$ for slow exchange). The mass spectra of sample containing C35S chimera and DN-F01 solution shows two protein species: chimera and chimera-DN-F01 complex (Figure 6.7), further confirming the covalent binding of DN-F01 and C35S chimera.

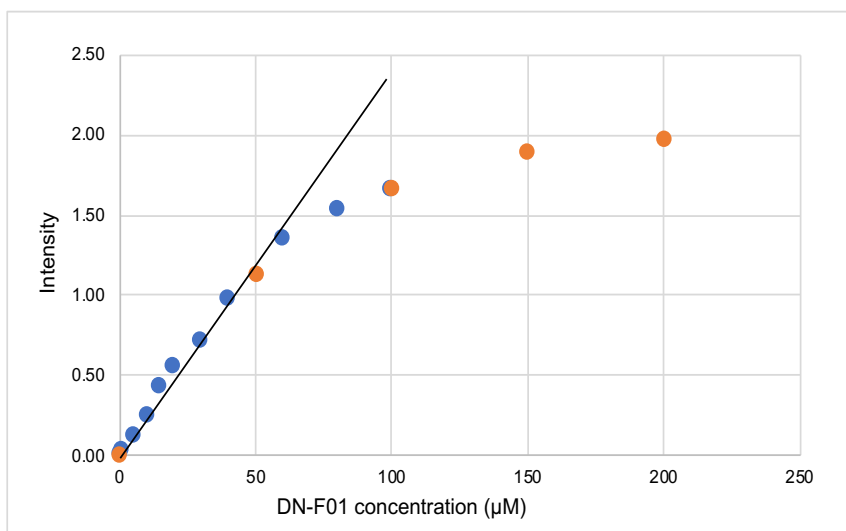


Figure 6.5. DN-F01 solubility test.

DN-F01 solubility measured using fluorescence (blue) and 1D ¹H NMR (orange) spectroscopies.

During the titration of DN-F01 into C35S chimera, peaks corresponding to the drug bound form increase in intensity, while peaks corresponding to the drug free form decrease in intensity. This trend continues with the addition of DN-F01 until the concentration reaches 40 µM, corresponding to a 1:1 ratio of C35S chimera concentration. As the concentration of DN-F01 is increased extra peaks start to appear. These peaks share a similar chemical shift with the corresponding peaks from the titration of DN-F01 to A-cys chimera (Figure 6.8A and B). Those peaks are likely from non-covalently binding of DN-F01 to cNTnC-cTnI chimera.

DN-F01 was also titrated into C35S chimera in the absence of DTT. The mass spectrum shows that without adding DTT, the chimera is covalently attached to beta-mercaptoethanol (BME), a reducing agent used during protein purification. Fast exchange is observed for DN-F01 titration into C35S chimera-BME, which is similar to the DN-F01 titration into A-cys chimera (Figure 6.8C). In this sample the C84 is covalently attached to BME, preventing DN-F01 to form a covalent bond with C84.

This shows that C84 is crucial for tight DN-F01 binding and the slow exchange comes from the covalent bond between DN-F01 and C84.

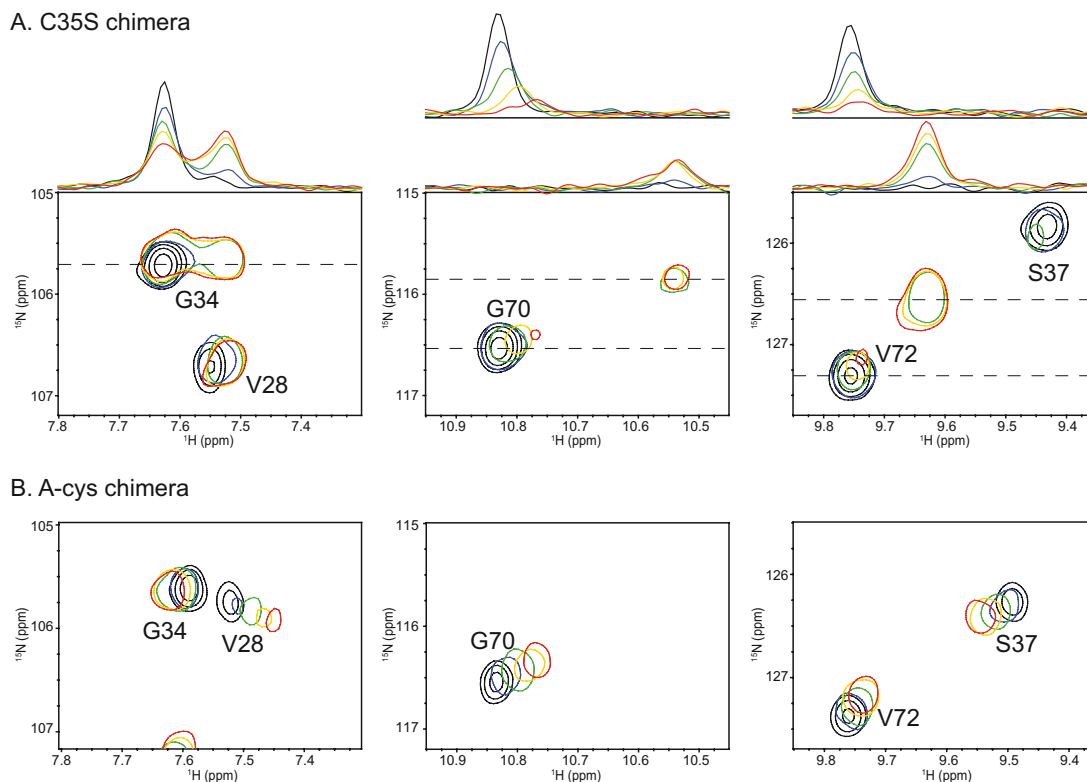


Figure 6.6. DN-F01 titration to C35S and A-cys chimera.

Comparison of regions of the 2D ^1H , ^{15}N HSQC NMR spectra of A. C35S and B. A-cys cNTnC-cTnI chimera during DN-F01 titrations. The first point of each titration represented with multiple contours and subsequent titration points represented by a single contour. For A. [C35S chimera] $\sim 40 \mu\text{M}$, [DN-F01] ~ 0 (black), 5 (blue), 15 (green), 25 (yellow) and 40 (red); 1D slice for slow exchange peaks are indicated by dashed lines. For B. [A-cys chimera] $\sim 25 \mu\text{M}$, [DN-F01] ~ 0 (black), 5 (blue), 15 (green), 30 (yellow) and 50 (red) μM .

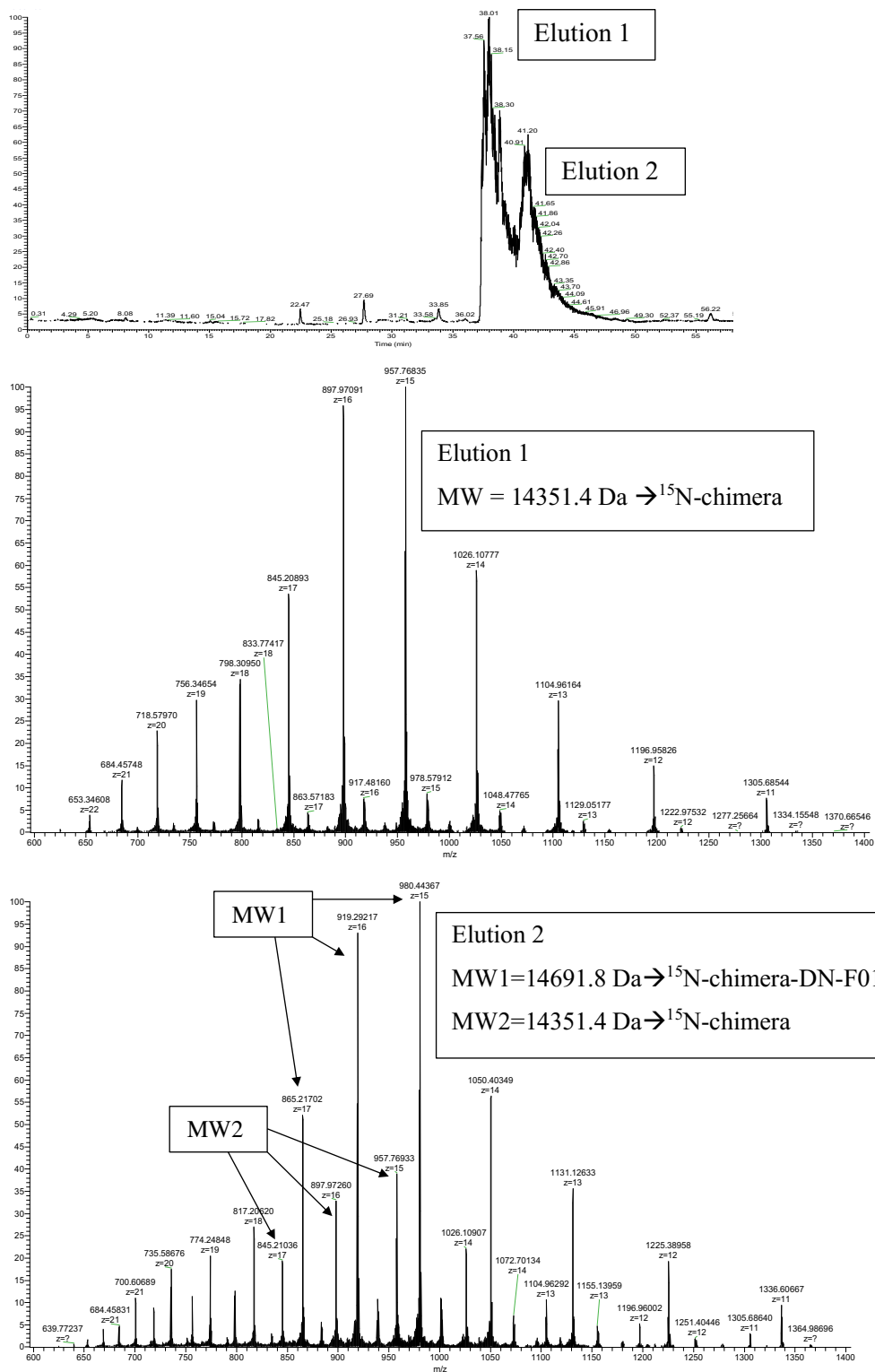


Figure 6.7. Mass spectra of C35S chimera and DN-F01.

Sample containing 40 μM ^{15}N labelled C35S chimera and 40 μM freshly prepared DN-F01 solution, pH 8.8.

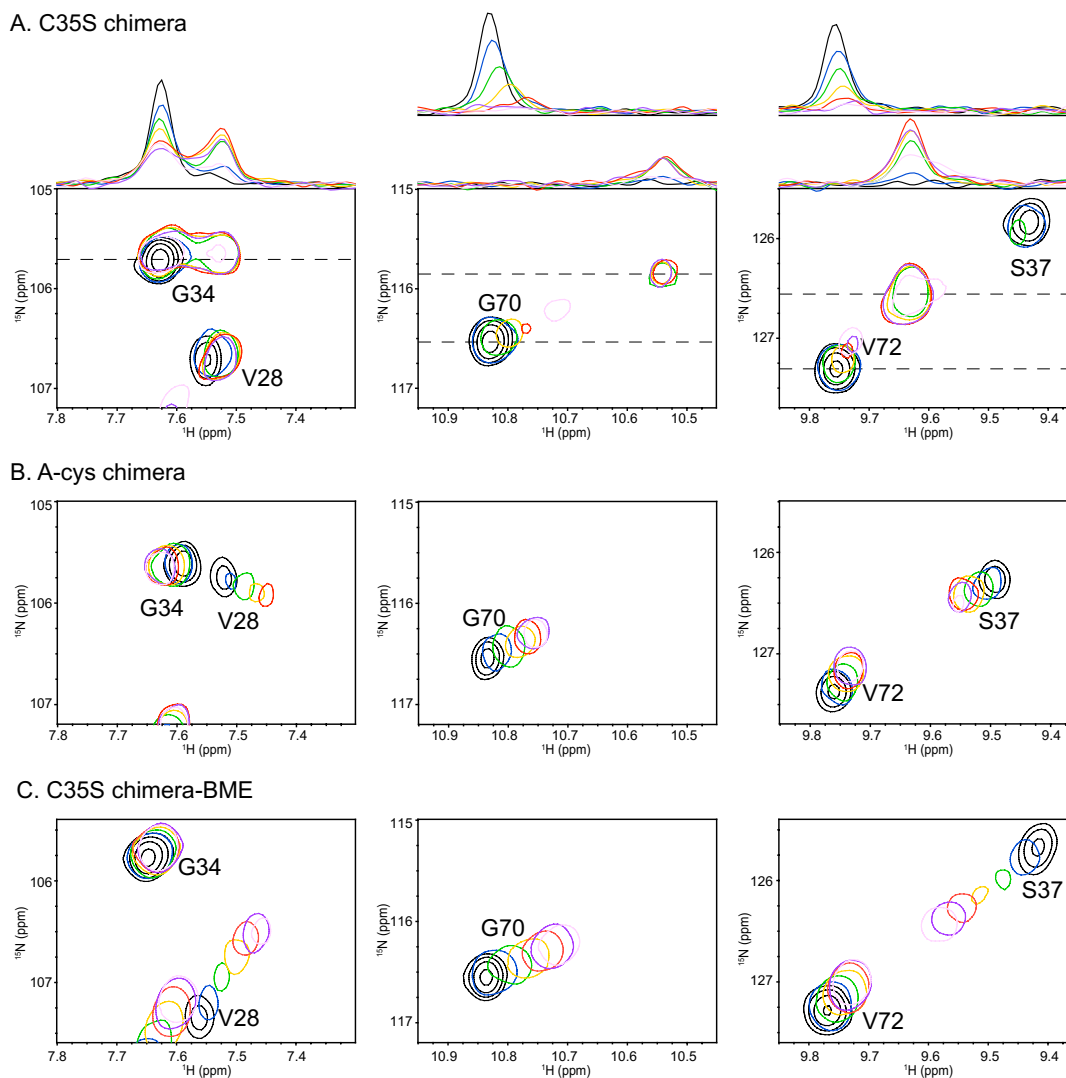


Figure 6.8. DN-F01 titration to C35S, A-cys and C35S C84-BME chimera.

Comparison of regions of the 2D ^1H , ^{15}N HSQC NMR spectra of (a) C35S chimera, (b) A-cys chimera and (c) C35S chimera-BME during titration with DN-F01. The first point of each titration represented with multiple contours and subsequent titration points represented by a single contour. For (a) and (c), [C35S chimera] and [C35S chimera-BME] $\sim 40 \mu\text{M}$, [DN-F01] ~ 0 (black), 5 (blue), 15 (green), 25 (yellow), 40 (red), 60 (purple) and 100 (pink) μM . For (b). [A-cys chimera] $\sim 25 \mu\text{M}$, [DN-F01] ~ 0 (black), 5 (blue), 15 (green), 30 (yellow), 50 (red), 75 (purple) and 100 (pink) μM . 1D slice for slow exchange peaks indicated by dashed lines are shown for (a) C35S chimera.

Stability of DN-F01

One concern for the use of reducing agent DTT to reduce the Cys 84 in protein would be that DTT could interact with DN-F01. It has been shown that DTT interacts with levosimendan, possibly by reacting with the cyano group of levosimendan. As DN-F01 containing the cyano group as well, it most likely will also be affected by DTT. The stability of DN-F01 was monitored by 1D ^1H NMR spectra in the absence and presence of reducing agent DTT, showing the aromatic region of DN-F01 in Figure 6.9. A freshly prepared DN-F01 is stable after 40 hours at 30 °C in the absence of DTT. The spectrum changed immediately after adding excess DTT (2mM), with a reduction in the intensity combined with the appearance of new resonances indicative of a formation of a new compound. However, the peak corresponding to the new compound did not increase intensity for the next 24 hours. We suspect that the cyano group of DN-F01 reacted with DTT reversible covalently at an equilibrium of approximately 30-40% of DN-F01 forming DTT adduct. In fact, after 24 hours of adding DTT, only 20% of DN-F01 DTT adduct were present, although there were still excess reduced DTT in the sample.

At least 60% of the DN-F01 we added into the NMR sample during DN-F01 titration to C35S chimera are available to react with Cys 84 of cNTnC. The mass spectra also show the species of covalent reacted C35S chimera-DN-F01. We would expect an even tighter binding of DN-F01 to reduced C35S chimera without adding DTT. The C35S chimera protein will be reduced and purified, and the NMR titration of DN-F01 to C35S chimera will be repeat without the presence of DTT.

We also observed that DN-F01 changed chemical structure over time. DN-F01 is a fluorophore, which may break down or degrade with exposure to light or changes in temperature, leading to irreversible photobleaching. The mass spectra of sample containing C35S chimera and freshly made DN-F01 stock shows two protein species: chimera and chimera-DN-F01 (Figure 6.7). In contrast, a sample containing C35S chimera and 8-month-old DN-F01 stock showed more than 2 species. The most abundant new species are chimera-DN-F01+202Da and chimera-DN-F01+404Da (Figure 6.10). We have shown that DN-F01 does not change structure in a short period of time by the NMR experiments (Figure 6.9), but DN-F01 must be broken down and

interact with each other over long period of time, with exposure to light, and temperature changes.

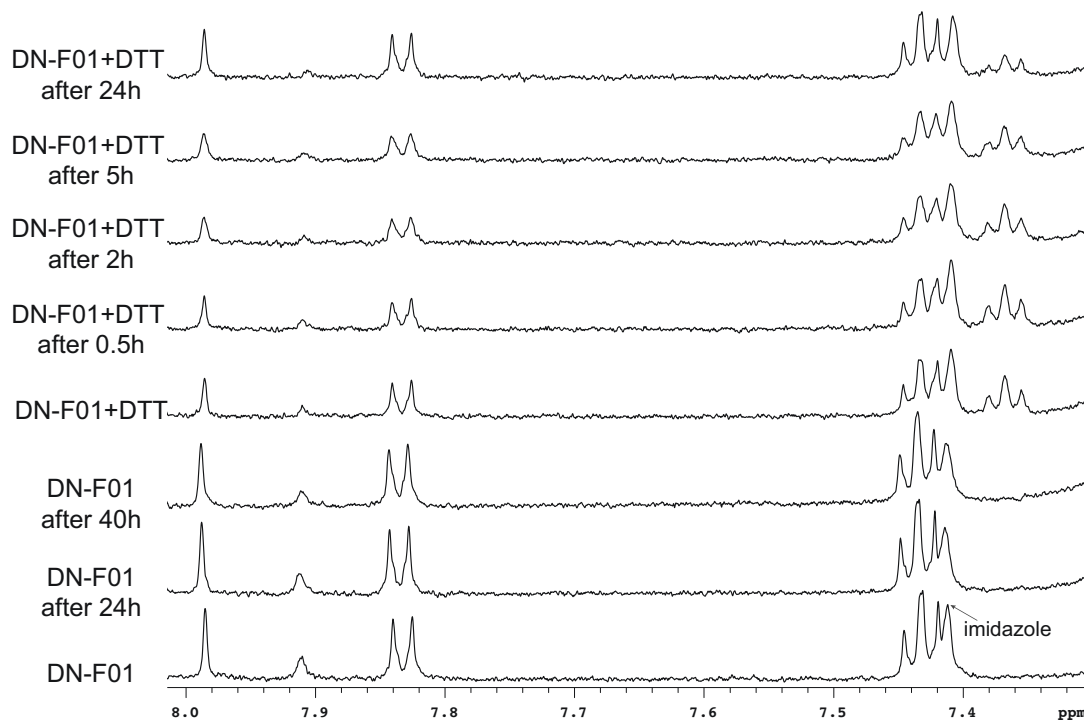


Figure 6.9. Stability of DN-F01 in the absence and presence of DTT.

A freshly prepared 50 μ M DN-F01 sample in NMR buffer after 24 h and 40 h at 30 $^{\circ}$ C shows the aromatic region of DN-F01. Stability of the drug in presence of 2mM DTT over a time course of 24 h. Note the peak at 7.41 ppm is from imidazole.

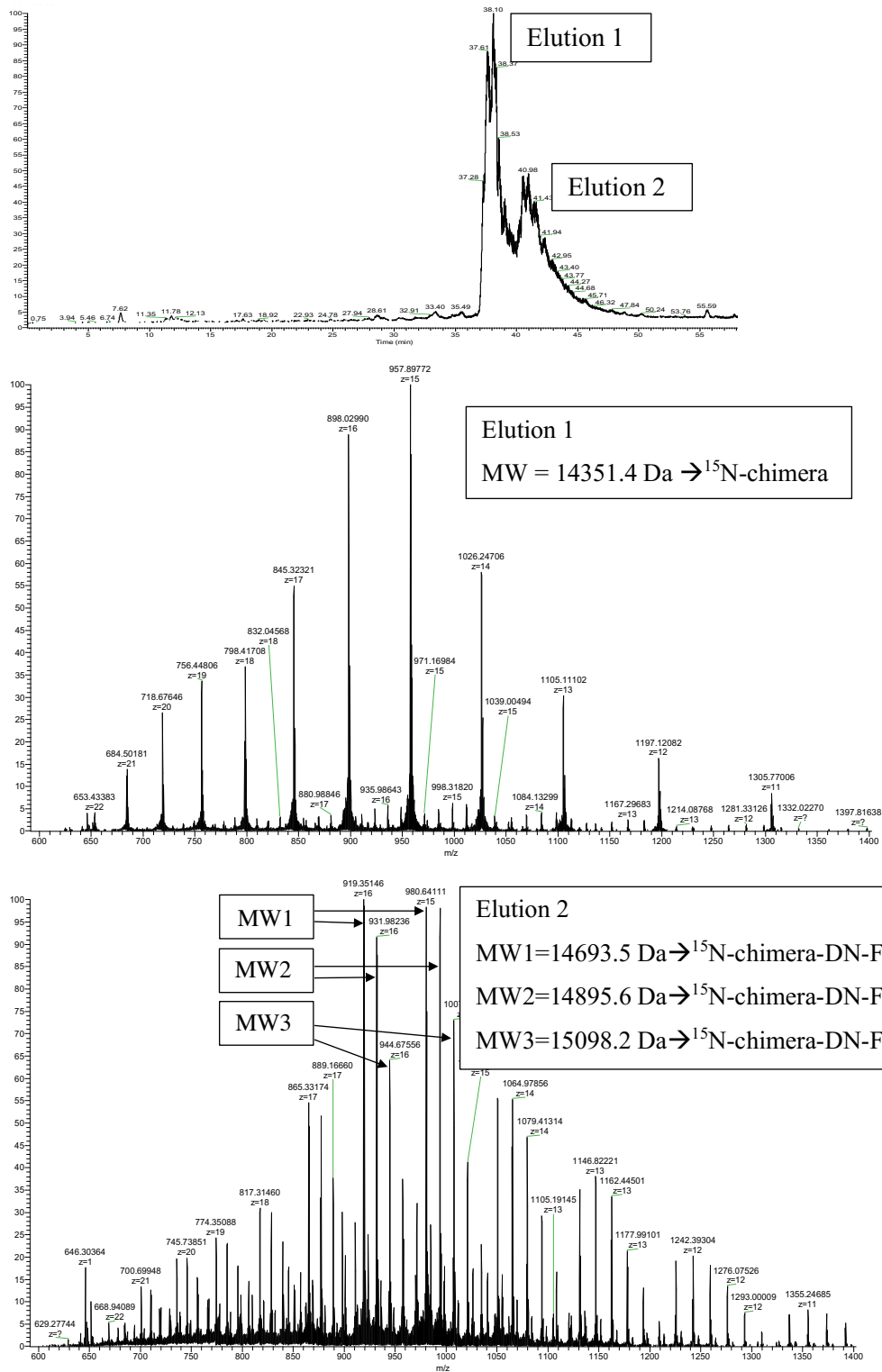


Figure 6.10. Mass spectra of C35S chimera and degraded DN-F01.

Sample containing 40 μM ^{15}N labelled C35S chimera and 40 μM 8-month-old DN-F01 solution, pH 6.8.

Conclusions

In this note, we report a very strong cardiac sarcomere inhibitor, DN-F01, targeting the thin filament protein troponin complex. This study substantiates the effective role of reversible covalent modification to cNTnC C84 by nitriles for the modulation of calcium sensitivity in cardiac muscle. The binding position of DN-F01 bound covalently or non-covalently to the cNTnC-cTnI chimera might be different. The bulky DN-F01 might clash with the cTnI switch peptide when covalently bond to C84, which could be the mechanism underlying its strong sarcomere inhibitory effect. In order to get the detailed binding position of DN-F01 to cNTnC and cTnI switch region complex, we need to determine the high-resolution NMR solution structure of DN-F01 bond form of the chimera. However, this has been hindered by the low solubility of DN-F01.

Acknowledgements

This study was supported by grants from the Heart and Stroke foundation of Canada (G-14-0005884 to B.D.S.), the University of Alberta Faculty of Medicine Transitional Program (B.D.S.), Motyl Graduate Studentship (F.C.), and British Heart Foundation (Fellowship FS/16/3/31887 to T.K.).

References

1. Endoh, M. Cardiac Ca²⁺ Signaling and Ca²⁺ Sensitizers. *Circ. J.* **72**, 1915–1925 (2008).
2. Takeda, S., Yamashita, A., Maeda, K. & Maéda, Y. Structure of the core domain of human cardiac troponin in the Ca(2+)-saturated form. *Nature* **424**, 35–41 (2003).
3. Li, M. X., Spyropoulos, L. & Sykes, B. D. Binding of cardiac troponin-I147-163 induces a structural opening in human cardiac troponin-C. *Biochemistry* **38**, 8289–98 (1999).
4. Li, M. X., Wang, X. & Sykes, B. D. Structural based insights into the role of troponin in cardiac muscle pathophysiology. *J. Muscle Res. Cell Motil.* **25**, 559–79 (2004).
5. Haikala, H. *et al.* Cardiac troponin C as a target protein for a novel calcium sensitizing drug, levosimendan. *J. Mol. Cell. Cardiol.* **27**, 1859–1866 (1995).
6. Papp, Z. *et al.* Pharmacological Therapy Levosimendan Efficacy and Safety : 20 years of SIMDAX in Clinical Use Pharmacological Therapy. (2020).
7. Robertson, I. M. *et al.* Reversible Covalent Binding to Cardiac Troponin C by the Ca²⁺ -Sensitizer Levosimendan. *Biochemistry* **55**, 6032–6045 (2016).
8. Klein, B. A. *et al.* Reversible Covalent Reaction of Levosimendan with Cardiac Troponin C in Vitro and in Situ. *Biochemistry* **57**, 2256–2265 (2018).
9. Klein, B. A. *et al.* Thioimidate Bond Formation between Cardiac Troponin C and Nitrile-containing Compounds. *ACS Med. Chem. Lett.* **10**, 1007–1012 (2019).
10. Robertson, I. M., Li, M. X. & Sykes, B. D. Solution structure of human cardiac troponin C in complex with the green tea polyphenol, (-)-epigallocatechin 3-gallate. *J. Biol. Chem.* **284**, 23012–23023 (2009).
11. Oleszczuk, M., Robertson, I. M., Li, M. X. & Sykes, B. D. Solution structure of the regulatory domain of human cardiac troponin C in complex with the switch region of cardiac troponin I and W7: The basis of W7 as an inhibitor of cardiac muscle contraction. *J. Mol. Cell. Cardiol.* **48**, 925–933 (2010).
12. Pineda-Sanabria, S. E., Julien, O. & Sykes, B. D. Versatile Cardiac Troponin

- Chimera for Muscle Protein Structural Biology and Drug Discovery. *ACS Chem. Biol.* **9**, 2121–2130 (2014).
13. Cai, F. *et al.* Structures reveal details of small molecule binding to cardiac troponin. *J. Mol. Cell. Cardiol.* **101**, 134–144 (2016).
 14. Delaglio, F. *et al.* NMRPipe: A multidimensional spectral processing system based on UNIX pipes. *J. Biomol. NMR* **6**, 277–293 (1995).
 15. Johnson, B. A. & Blevins, R. A. NMR View: A computer program for the visualization and analysis of NMR data. *J. Biomol. NMR* **4**, 603–614 (1994).
 16. Hagberg, D. P. *et al.* Tuning the HOMO and LUMO energy levels of organic chromophores for dye sensitized solar cells. *J. Org. Chem.* **72**, 9550–9556 (2007).
 17. Houdusse, A., Love, M. L., Dominguez, R., Grabarek, Z. & Cohen, C. Structures of four Ca²⁺-bound troponin C at 2.0 Å resolution: further insights into the Ca²⁺-switch in the calmodulin superfamily. *Structure* **5**, 1695–1711 (1997).
 18. Julien, O. *et al.* Is there nascent structure in the intrinsically disordered region of troponin I? *Proteins* **79**, 1240–1250 (2011).
 19. Pineda-Sanabria, S. E., Robertson, I. M., Sun, Y.-B. B., Irving, M. & Sykes, B. D. Probing the mechanism of cardiovascular drugs using a covalent levosimendan analog. *J. Mol. Cell. Cardiol.* **92**, 174–184 (2016).
 20. Cai, F., Hwang, P. M. & Sykes, B. D. Structural Changes Induced by the Binding of the Calcium Desensitizer W7 to Cardiac Troponin. *Biochemistry* **57**, 6461–6469 (2018).

Chapter 7

The cardiac-specific N-terminal region of cardiac troponin I electrostatically positions the regulatory domain of troponin C despite remaining in an intrinsically disordered state

Peter M. Hwang^{1,2}, Fangze Cai², Sandra E. Pineda-Sanebria², David C. Corson², and Brian D. Sykes²

¹Department of Medicine, University of Alberta, Edmonton, AB, Canada.

²Department of Biochemistry, University of Alberta, Edmonton, AB, Canada.

A version of this chapter has been previously published: Hwang, P. M., Cai, F., Pineda-Sanabria, S. E., Corson, D. C. & Sykes, B. D. The cardiac-specific N-terminal region of troponin I positions the regulatory domain of troponin C. *Proc. Natl. Acad. Sci. U. S. A.* **111**, 14412–7 (2014).

Contribution: FC performed the fluorescence experiments with help of SEPS. PMH acquired the NMR experiments, analyzed the results and wrote the manuscript. DCC purified the protein. PMH and BDS directed the research.

Summary

The cardiac isoform of troponin I (cTnI) has a unique 31-residue N-terminal region that binds cardiac troponin C (cTnC) to increase the calcium sensitivity of the sarcomere. The interaction can be abolished by cTnI phosphorylation at Ser22 and Ser23, an important mechanism for regulating cardiac contractility. cTnC contains two EF-hand domains (the N and C domain of cTnC, cNTnC and cCTnC) connected by a flexible linker. Calcium binding to either domain favors an “open” conformation, exposing a large hydrophobic surface that is stabilized by target binding, cTnI[148–158] for cNTnC and cTnI[39–60] for cCTnC. We used multinuclear multidimensional solution NMR spectroscopy to study cTnI[1–73] in complex with cTnC. cTnI[39–60]

binds to the hydrophobic face of cTnC, stabilizing an alpha helix in cTnI[41–67] and a type VIII turn in cTnI[38–41]. In contrast, cTnI[1–37] remains disordered, although cTnI[19–37] is electrostatically tethered to the negatively charged surface of cTnC (opposite its hydrophobic surface). The interaction does not directly affect the calcium binding affinity of cTnC. However, it does fix the positioning of cTnC relative to the rest of the troponin complex, similar to what was previously observed in an X-ray structure [Takeda S, et al. (2003) *Nature* 424(6944):35–41]. Domain positioning impacts the effective concentration of cTnI[148–158] presented to cTnC, and this is how cTnI[19–37] indirectly modulates the calcium affinity of cTnC within the context of the cardiac thin filament. Phosphorylation of cTnI at Ser22/23 disrupts domain positioning, explaining how it impacts many other cardiac regulatory mechanisms, like the Frank–Starling law of the heart.

Introduction

The balance between contraction and relaxation must be carefully regulated in the heart. Impaired relaxation can lead to diastolic heart failure, whereas systolic failure is characterized by insufficient contractility. Despite having different etiologies, both forms of heart failure are similar in terms of prevalence, symptoms, and mortality¹. Of all of the signaling pathways that regulate contractile function, the best studied is sympathetic β 1-adrenergic stimulation², which leads to cardiomyocyte cAMP production and activation of protein kinase A (PKA). Downstream phosphorylation of L-type calcium channels and phospholamban increases calcium fluxes, whereas phosphorylation of sarcomeric proteins, cardiac troponin I (cTnI), cardiac myosin binding protein-C, and titin³ regulates the calcium-induced mechanical response.

In human cTnI, Ser22 and Ser23 are the residues most consistently phosphorylated^{4,5}. (There are some numbering inconsistencies in the literature, and we will refer to Ser22/23 instead of Ser23/24 to account for physiologic removal of the N-terminal methionine residue.) Originally identified as PKA targets, Ser22/23 are now known to be phosphorylated by other kinases, including PKG, PKC β , PKC δ , and PKD1⁶, showing it to be an important locus at which multiple signaling pathways converge. Phosphorylation at cTnI Ser22/23 decreases the calcium sensitivity of the

cardiac sarcomere⁷. High levels of phosphorylation are seen in healthy individuals, but decreased phosphorylation levels occur in a number of pathologic states, including heart failure with reduced ejection fraction, heart failure with preserved ejection fraction, dilated cardiomyopathy, and hypertrophic cardiomyopathy^{5,8}. Although dephosphorylation is likely a compensatory mechanism in many cases, it may be a disease-driving dysregulation in others.

Other regulatory mechanisms are strongly influenced by the phosphorylation state of Ser22/23. The Frank–Starling law of the heart, also known as length-dependent activation or stretch activation, is more pronounced when Ser22/23 are phosphorylated^{9,10}. In contrast, Ser5¹¹ or Ser41/43^{12,13} phosphorylation has more of an impact when Ser22/23 are unphosphorylated. Finally, some mutations that cause familial dilated cardiomyopathy have been shown to mitigate the effect of Ser22/23 phosphorylation¹⁴. Despite the physiologic importance of Ser22/23 phosphorylation in regulating cardiac calcium sensitivity, the extent of its modulatory capacity has remained elusive.

Ser22/23 lie within the cardiac-specific N-terminal region, cTnI[1–31], not present in the skeletal muscle isoforms. cTnI [1–209] forms long stretches of helical structure along a winding course that binds to troponin C, troponin T, and actin–tropomyosin. The X-ray structure of the cardiac troponin complex¹⁵ did not include cTnI[1–34], so the structure of this region has not been determined, although there have been some preliminary investigations^{16,17}. It is known that cTnI[1–31] interacts with cTnC in its unphosphorylated state¹⁸, but phosphorylation abolishes this interaction, having an effect similar to truncation or removal of cTnI[1–31]¹⁹. Our present study provides a detailed analysis of the structure and dynamics of cTnI[1–73] in complex with cTnC using solution NMR spectroscopy, highlighting its unique mechanism of action and physiologic implications.

Materials and Methods

Protein production and purification

Wild type– or C35S,C84S–cTnC was expressed in *Escherichia coli* using a pET3a-derived expression vector⁴⁵ and purified according to previously published

protocols⁴⁶. In brief, purification involved three chromatographic steps: anion exchange, hydrophobic, and gel filtration chromatography. cTnI[1–73] with a C-terminal His-tag was expressed in a modified pET31b vector altered to fuse cTnI[1–73] to the C terminus of the β -barrel membrane protein, PagP, as previously described⁴⁷. cTnI[1–73] was separated from PagP via cyanogen bromide cleavage in 0.1 M HCl and 6 M Gdn·HCl and purified using nickel affinity chromatography under denaturing conditions. cTnI[144–163] and cTnI[34–71] peptides were synthesized and purified by GL Biochem. The cTnI[1–73] protein purified from the PagP fusion construct was stable over the course of NMR experiments. However, after addition of cTnC, it was not uncommon for cTnI[1–73] to be slowly degraded, with proteolytic cleavage occurring N-terminal to Tyr25 or Tyr28, similar to what was observed from cTnI from human heart tissue⁵. The change could be monitored by following the disappearance of NMR peaks corresponding to Tyr25–Ala29. Alternatively, it could be detected in cTnC by measuring ¹⁵N R₂ relaxation rates, which would show that the two domains of cTnC were no longer tethered together by cTnI[1–73].

NMR spectroscopy sample preparation

For spectral simplicity, only one component of the protein complexes was isotopically labeled at a time. Enough labeled (¹⁵N-or ²H,¹⁵N-or ¹³C,¹⁵N-enriched) lyophilized protein to make a 0.5–1.0 mM sample was dissolved in 450 μ L of buffer, consisting of 100 mM KCl, 10 mM imidazole, 10 mM CaCl₂, 0.5 mM DSS, CalBiochem Protease Inhibitor Mixture Set I, and 5% (vol/vol) D₂O. When wild type–cTnC was used, the buffer was further supplemented with 20 mM DTT. The pH was corrected to about 6.2 and monitored using 1D-¹H NMR by measuring the pH-sensitive downfield imidazole H₂ peak⁴⁸. A ¹H,¹⁵N-heteronuclear single quantum coherence (HSQC) spectrum of the initial sample was obtained at 40 °C, and a 5-mM solution of the unlabeled binding partner was titrated in 10–15- μ L aliquots. The titration was followed by serial ¹H,¹⁵N- HSQC spectra. The binding equilibrium was in the slow exchange regime, so the titration was continued until the peaks corresponding to the unbound form disappeared completely. A ternary complex was also made by adding an excess (2 mg) of unlabeled cTnI[144–163] switch peptide.

NMR spectroscopy and data analysis

The 3D backbone assignment spectra were recorded on a Varian Inova 600 spectrometer. All experiments were from Agilent BioPack (VnmrJ 3.2D) unless otherwise specified. The experiments used for backbone assignment were HNCA, HN(CO)CA, HN(CA)CO, and HNCO. The molecular weight of the cTnC–cTnI[1–73] complex was 28 kDa, and sensitivity was further limited by exchange broadening. Additional experiments were used to assign the flexible regions of cTnI[1–73]: HNCACB, H(CCO)NH-TOCSY, and (H)C(CO)NH-TOCSY. To obtain the complete assignments of cTnC, HN(CA)HA and HA(CACO)NH⁴⁹ experiments were recorded, in-house modified from the BioPack HNCACB and CBCA(CO)NH experiments, respectively. ¹⁵N-edited nuclear Overhauser enhancement spectroscopy (NOESY)–HSQC spectra were also used for backbone assignment. Enhanced sensitivity and gradient selection was used in the backbone assignment triple resonance experiments, but TROSY was not used for the ¹⁵N and ¹H dimensions.

The 3D NOESY spectra were acquired on a Varian Inova 800 spectrometer equipped with cryoprobe. ¹³C-edited HMQC–NOESY spectra were run on ¹³C,¹⁵N-labeled samples in H₂O, although the majority of intramolecular NOE data were obtained from ¹³C-edited NOESY–HSQC spectra acquired in D₂O, and intermolecular NOEs were obtained from ¹²C-filtered, ¹³C-edited NOESY–HSQC spectra in D₂O. NMR data were processed using NMRPipe⁵⁰ software and visualized and analyzed with NMRViewJ⁵¹.

¹⁵N T₁, T₂, and ¹H-¹⁵N NOE experiments were conducted using ²H, ¹⁵N-labeled cTnI[1,73] with unlabeled aCys–cTnC. TROSY was used in the ¹H and ¹⁵N dimensions. A 6-s saturation time or recycle delay was used in the NOE experiments. For T₁ and T₂, curves were fit using a mono exponential decay function using the simplex minimization algorithm in MATLAB. The variance for each time point was estimated from the sum of the squares of the residuals divided by (N – 2), where N is the number of data points for each curve and 2 is the number of fitting parameters. A Monte Carlo method was then applied to obtain error estimates for R₁ and R₂. For ¹H-¹⁵N NOE, the error estimate was based on the ratio of spectral noise to signal intensity in the reference spectrum, multiplied by a factor of $\sqrt{2}$ to reflect the fact that the ¹H-

^{15}N NOE is a ratio. ^{15}N R_1 , R_2 , and ^1H - ^{15}N NOE data were further analyzed using a model-free analysis of internal motions⁵².

Fluorescence spectroscopy

IAANS reacted with C35S cTnC Cys84 in labeling buffer (in 50 mM Tris, 150 mM KCl, 1 mM EGTA, and 6 M urea, pH 7.0) for 4 h at 4 °C³². The labeling reaction was stopped by addition of 2 mM DTT, and the labeled protein was exhaustively dialyzed against refolding buffer (600 mM Mops, 150 mM KCl, and 2 mM EGTA, pH 7.0) to remove unreacted label. All steady-state fluorescence measurements were performed at 22 °C.

IAANS fluorescence was excited at 325 nm and monitored at 450 nm. Microliter amounts of CaCl_2 were titrated into a 2-mL solution containing cTnC–cTnI[1–73] or cTnC–cTnI[34–71] (0.2 μM), 200 mM Mops, pH 7.0, 150 mM KCl, 2 mM EGTA, 1 mM DTT, and 3mM MgCl_2 . An excess of cTnI peptide was used for the complexes ($[\text{cTnI}] / [\text{cTnC}] = 1.3$), with protein concentrations quantitated by amino acid analysis following acid hydrolysis. Free $[\text{Ca}^{2+}]$ was calculated with the program Maxchelator developed by Chris Patton and available at <http://maxchelator.stanford.edu/CaMgATPEGTA-NIST.htm>. Fluorescence experiments were performed in triplicate to determine error ranges for individual measurements as well as pCa.

Results

Chemical shift assignment and secondary structure of cTnI[1–73] free and in complex with cTnC.

NMR chemical shift assignment of protein backbone atoms $^1\text{H}\alpha$, $^{13}\text{C}\alpha$, $^{13}\text{C}\beta$, ^{13}CO , ^1HN , and ^{15}N provides information about secondary structure on a per-residue basis. For example, α -helical residues have downfield $^{13}\text{C}\alpha$ chemical shifts compared with random coil values, whereas residues with extended structure appear upfield. In free cTnI[1–73], residues 42–67 possess downfield $^{13}\text{C}\alpha$ shifts indicative of a nascent helical structure (Figure 7.1). The chemical shift analysis program $\delta 2\text{D}^{20}$ indicates overall <25% helical content for this region and random coil for the rest of the protein

(Figure 7.2A). There is no suggestion of a stable helix from residues 19–31, as had been suggested by a previous NMR analysis¹⁶ that did not have the benefit of ¹³C chemical shift data. Large deviations from random coil chemical shifts are observed in residues preceding proline (Fig. A.1), which are almost always in an extended conformation. (Prolines themselves can adopt either turn-like or extended conformations.) The chemical shift analysis program DANGLE analyzes glycine, proline, and preproline residues separately from other amino acid residues because of their unique conformational preferences²¹. DANGLE predicted an extended conformation for the proline-rich region spanning residues 10–18 (containing P11, P13, P15, and P17), although it does not specify a percentage, like $\delta 2D$, which predicted a random coil conformation with a small degree of extended conformation (Figure 7.2). NOE assignments showed that all prolines in cTnI[1–73] preferred the trans conformation, although there is evidence of some minor peaks corresponding to cis forms.

Addition of wild type– or C35S,C84S–cTnC to cTnI[1–73] causes pronounced chemical shift changes in cTnI residues 42–68, suggestive of increased helical content (Figure 7.1 and Figure 7.2B), with Ser41 acting as the N-terminal helix cap residue²². Helical structure is induced by binding of cTnI[39–60] to the large hydrophobic patch of the cTnC C-domain (cCTnC), forming a very tight complex with a nanomolar range dissociation constant¹⁸ that effectively anchors cCTnC to the rest of troponin at all physiologic calcium concentrations.

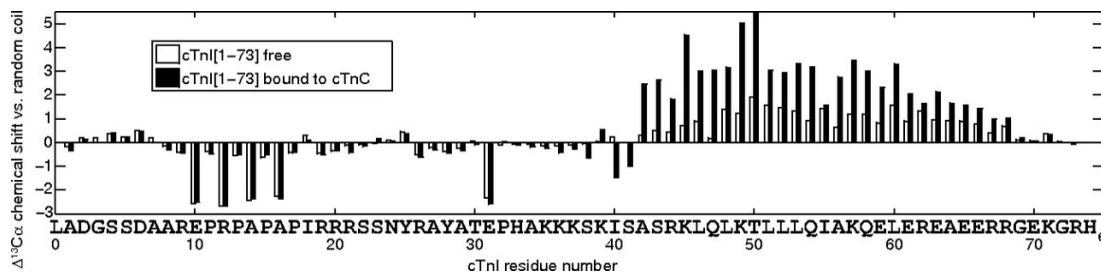


Figure 7.1. Chemical shift analysis of cTnI[1-73].

Deviation from random coil values for backbone ¹³C_α chemical shifts in free cTnI[1–73] (openbars) and cTnI[1–73] in complex with cTnC (filled bars).

Negligible chemical shift changes occur in cTnI residues 1–34 upon addition of cTnC (Figure 7.1), despite a wealth of biochemical data documenting an interaction between this region and the N domain of cTnC (cNTnC) (for example, see references^{23,24}). Using chemical shift data alone, there is no evidence of helix formation or other induced conformational preference anywhere along cTnI[1–34] as a result of the interaction (Figure 7.2). There are examples in the literature of “fuzzy complexes”²⁵, some of which involve intrinsically disordered regions (IDRs) that show minimal chemical shift changes upon binding, like the phosphorylated Sic1–Cdc4 protein complex²⁶ and cystic fibrosis transmembrane conductance regulator (CFTR) R domain complexes²⁷. Evidence of an interaction can still be found through ¹H-¹H NOEs, signal broadening, or relaxation measurements, as turns out to be the case for cTnI[19–37]–cNTnC.

Reciprocal chemical shift changes in cTnC are also observed when cTnI[1–73] is added. The hydrophobic binding of cTnI [39–60] induces large chemical shift changes in cTnC, but the interaction with cNTnC produced only minimal chemical shift changes (Figure 7.3). It has previously been suggested that the interaction between cTnI[1–31] and cNTnC shifts the equilibrium of cNTnC toward the “open” state²⁸. The dominant conformation of calcium-bound cNTnC is in fact closed²⁹, with the open conformation sampled less than 20% of the time³⁰. The equilibrium is shifted to the open conformation when cNTnC binds hydrophobically to the helical switch region cTnI[148–158]³¹, the critical step that releases the flanking inhibitory segments of cTnI and triggers muscle contraction. The shift to the open conformation manifests in large NMR chemical shift changes, particularly in loops I and II (Figure 7.3). Stabilization of the calcium-bound open conformation also markedly increases the calcium affinity of cNTnC³². However, because minimal chemical shift changes are observed when cNTnC interacts with cTnI[1–73], the cardiac-specific cTnI[1–31] must exert its calcium sensitizing effect through a different mechanism than stabilization of the open conformation.

In summary, the interaction between cTnI[1–31] and cNTnC has no observable effect on the secondary structure of cTnI [1–31] or the closed–open equilibrium of cNTnC.

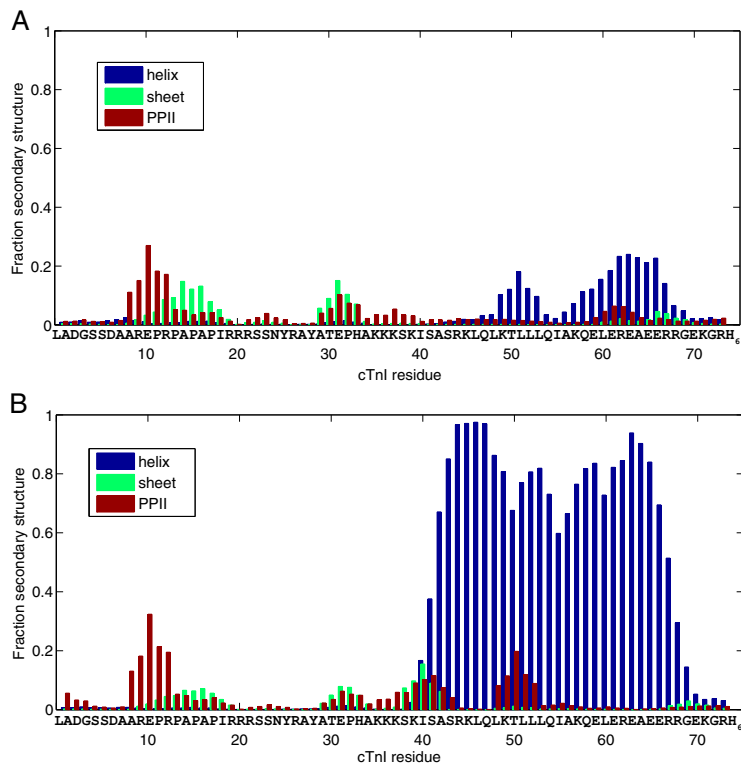


Figure 7.2. Predicted secondary structure for cTnI[1-73].

Predicted fraction secondary structure calculated from backbone chemical shift data using the program $\delta 2D$ (see main text for details). (A) Free cTnI[1-73]. (B) cTnI[1-73] in complex with cTnC. Note that the fractions of helix, sheet, polyproline type II helix, and random coil add up to 1 (the remainder is all random coil).

¹H-¹H NOE analysis of the cTnC-cTnI[1-73] complex

Homonuclear ¹H-¹H NOEs can be observed between any two ¹H atoms within ~6 Å, critical for any NMR-based structure determination. The vast majority of intermolecular ¹H-¹H NOEs occur between cTnI[39-60] and cTnC, consistent with extensive hydrophobic binding. There are few intermolecular NOEs observed between cTnC and cTnI[1-73], but the most critical NOEs are between cTnC Ala7 and cTnI Ala42/Ser43. The importance of this contact is underscored by the fact that a double Ser41/43 mutation to aspartate (mimicking phosphorylation) markedly decreases troponin calcium affinity³³. Because cTnI Ala42/ Ser43 are part of a rigid alpha helix bound to cTnC and Ala7 is part of cTnC helix N, the interaction fixes the position

of cNTnC relative to cCTnC. This contact is actually present in the X-ray crystal structure (Figure 7.4A and B), suggesting that the true interdomain orientation in solution is in fact very similar. This single contact point is alone insufficient to stably fix the domains in solution, but it is stabilized by crystal packing contacts in the X-ray structure. In solution, the orientation is bolstered by additional electrostatic interactions from the disordered N-terminal tail of cTnI.

cTnI Ser41 is the N-terminal helix cap residue, but it is also part of a type VIII turn based on Ser38–Lys39–Ile40–Ser41 backbone chemical shifts, according to the Motif Identification from Chemical Shifts (MICS) program²². Lys39 shows NOE contacts with Asp131 and Glu135 of helix G in cCTnC, whereas Ser38 has intermolecular NOEs to a lysine residue consistent with cNTnC Lys6 in the crystal structure (Figure 7.4C). This brings Lys35–Lys36–Lys37 into contact with a prominent negatively charged surface that includes EF-hand loop II, the all-important calcium-binding loop (Figure 7.4C). cTnI Lys35–37 display NOEs to residues with Asp- and Glu-like chemical shifts, but these could not be unambiguously separated from each other. In the crystal structure, there are two troponin complexes per asymmetric unit. In one complex, Lys35–37 are invisible, but in the other, they are modeled hovering over EF-hand loop II, with Lys37 closest to Asp75 of cNTnC. Finally, cTnI Arg21 and Arg26 also make weak NOEs to cTnC residues with Glu-like chemical shifts (Figure 7.5), but these could not be unambiguously assigned either.

cTnI Ser41 is the N-terminal helix cap residue, but it is also part of a type VIII turn based on Ser38–Lys39–Ile40–Ser41 backbone chemical shifts, according to the Motif Identification from Chemical Shifts (MICS) program²². Lys39 shows NOE contacts with Asp131 and Glu135 of helix G in cCTnC, whereas Ser38 has intermolecular NOEs to a lysine residue consistent with cNTnC Lys6 in the crystal structure (Figure 7.4C). This brings Lys35–Lys36–Lys37 into contact with a prominent negatively charged surface that includes EF-hand loop II, the all-important calcium-binding loop (Figure 7.4C). cTnI Lys35–37 display NOEs to residues with Asp- and Glu-like chemical shifts, but these could not be unambiguously separated from each other. In the crystal structure, there are two troponin complexes per asymmetric unit. In one complex, Lys35–37 are invisible, but in the other, they are modeled hovering

over EF-hand loop II, with Lys37 closest to Asp75 of cNTnC. Finally, cTnI Arg21 and Arg26 also make weak NOEs to cTnC residues with Glu-like chemical shifts (Figure 7.5), but these could not be unambiguously assigned either.

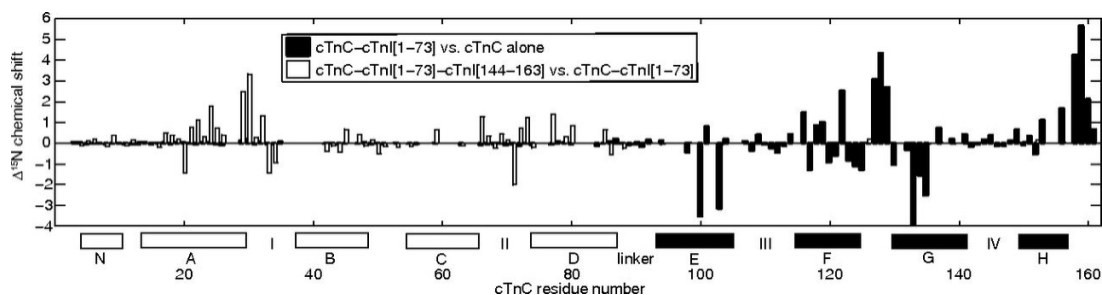


Figure 7.3. Structural changes in C35S,C84S-cTnC induced by binding of cTnI.

Binding-induced structural changes in C35S,C84S-cTnC are highlighted by backbone amide ^{15}N chemical shift changes. The filled bars denote changes that occur when cTnC binds to cTnI[1–73]. The largest changes occur in cCTnC (see helices E–H along the x axis), whereas negligible changes are observed in cNTnC (helices N, A–D). This is because of the extensive hydrophobic interface between cTnI[39–60] and cCTnC, as opposed to the more superficial electrostatic interactions between cTnI[19–37] and cNTnC. In contrast, the open bars highlight the structural changes that occur when cTnI[144–163] binds cNTnC hydrophobically, driving a closed-to-open conformational transition in cNTnC. In this case, the predominant structural changes occur in cNTnC and not cCTnC. Stretches of missing assignments due to conformational exchange include residues 36–41, 60–62, 81–83, and 95–97.

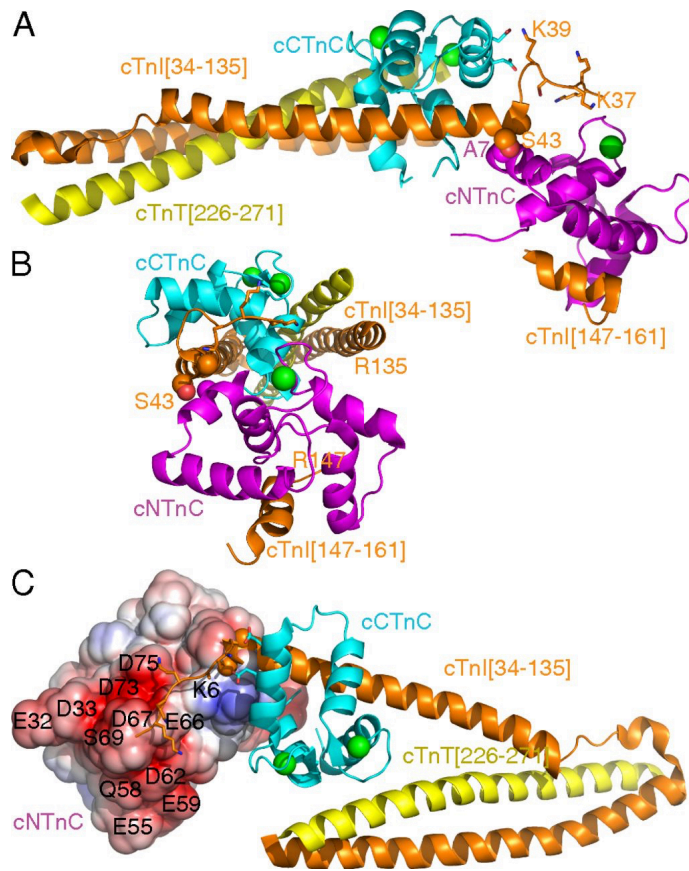


Figure 7.4. Localization of NOEs between cTnC and cTnI[1-73].

Ribbon diagrams of the troponin complex drawn by PyMol and derived from reference¹⁵. cNTnC is shown in magenta, and cCTnC is shown in cyan. Calcium ions are shown as green spheres. Troponin T, residues 226–271, is shown in yellow. cTnI, residues 34–135 and 147–161, is shown in orange. (A and B) The key contact that fixes the position of cNTnC relative to cCTnC is between A7 of cNTnC and A42/S43 of cTnI, shown as space-filling spheres. The side chains of cTnI[35–39] are also shown in stick figures, with K39 of cTnI contacting D131 and E135 of cCTnC (shown in sticks) and K35-S38 hovering over cNTnC. (C) Electrostatic surface representation of cNTnC showing the negatively charged surface that interacts with cTnI[19–37].

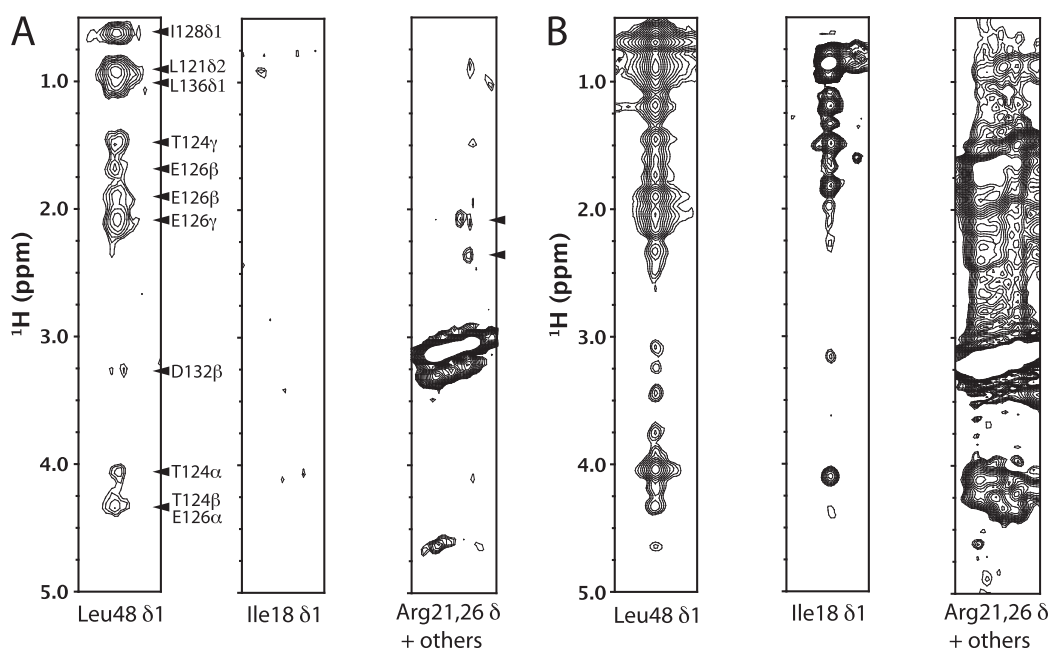


Figure 7.5. Intermolecular ^1H - ^1H NOEs from cTnC to cTnI[1-73].

(A) Strip plots taken from the ^{12}C -filtered, ^{13}C -edited NOESY–HSQC spectrum, designed to select for intermolecular ^1H - ^1H NOEs from unlabeled cTnC to ^{13}C -labeled cTnI[1–73]. From Left to Right, a cTnI Leu48 δ 1-methyl group shows multiple intermolecular NOEs to cTnC, consistent with tight hydrophobic binding between cTnI[39–60] and cTnC. In contrast, the cTnI Ile18 δ -methyl group shows no intermolecular NOEs, as with all other hydrophobic residues in cTnI[1–37]. Weak intermolecular NOEs can be observed between Arg26 H δ (3.13 ppm) and a Glu-like residue in cTnC with chemical shifts at 2.11 and 2.35 ppm (unlabeled arrows). An NOE can also be observed between Arg21 H δ (3.15 ppm) and an unassigned signal at 2.09 ppm. These NOEs are suggestive of weak electrostatic interactions between cTnI[19–37] and cTnC. (Note that the strong peaks around 3.2 ppm are diagonal artifacts due to incomplete filtering.) (B) Corresponding strip plots for Leu48, Ile18, and arginine residues from the unfiltered ^{13}C -edited NOESY–HSQC spectrum, which contains both inter- and in- tramolecular NOEs (dominated by short-range intraresidue NOEs). Note that the signal from Ile18 is much more intense than that from Leu48, because it is part of an IDR with slower signal decay due to R_2 relaxation.

The considerable chemical shift overlap for charged Lys, Arg, Asp, and Glu side chains makes unambiguous intermolecular NOE assignment near impossible. Nevertheless, these NOEs demonstrate specific and stable electrostatic interactions involving cTnI Arg21, Arg26, and part of Lys35–37. This is in marked contrast to the lack of NOEs involving hydrophobic residues, which are usually critical for defining intermolecular contacts. cTnI Pro17, Ile18, Tyr25, Ala27, Tyr28, and Ala29 showed no intermolecular NOEs (see Figure 5A for an example). Classically, protein–protein interactions are dominated by hydrophobic interactions, which require close packing, exclusion of water, and a rigid structuring of the backbone, as exemplified by the interaction between cTnI[39–60] and cTnC. In contrast, the electrostatic interactions involving cTnI[19–37] occur in a solvated environment that does not require as much rigidification of the backbone. It does require many positive charges, with as many as eight potentially involved (if His33 is included). Notably, Lys35 has been strongly implicated in autosomal dominant dilated cardiomyopathy (K36Q by the alternate numbering scheme), decreasing the calcium sensitivity of reconstituted thin filaments by 0.3–0.6 pCa units^{14,34}.

¹⁵N relaxation of cTnI[1–73] free and in complex with cTnC

¹⁵N relaxation rates provide a window into nanosecond to picosecond (10^{-9} to 10^{-12} s) timescale conformational fluctuations in a protein. Structured proteins tumble with a global rotational correlation time, τ_C , on the order of several nanoseconds for a small domain, with τ_C scaling roughly proportionally to molecular weight. In rigidly structured regions, the overall motion is approximated by the global correlation time. As structural flexibility increases, for example, toward the N or C terminus, faster internal motions begin to dominate NMR relaxation behavior. Binding causes a decrease in internal motions that can be detected via changes in relaxation.

¹⁵N backbone relaxation studies were obtained for cTnI[1–73] both free and bound to C35S,C84S–cTnC (Figure 7.6). The transverse relaxation rate, R_2 , is roughly proportional to the weighted average correlation time (including global tumbling and internal motions) at each backbone amide site. R_1 relaxation is most effectively induced by motions with a timescale near 2–3ns (¹⁵N nucleus on a 600-MHz spectrometer). A

negative ^1H - ^{15}N heteronuclear NOE is most effectively induced by motions with a timescale near 0.2–0.3 ns.

Looking at the plots of R_1 , R_2 , and heteronuclear NOEs in free cTnI[1–73], it becomes evident that residues 45–67 are the most rigid in all of cTnI[1–73], with the highest R_1 , R_2 , and least negative heteronuclear NOE values, consistent with nascent helix formation. When this region binds to cTnC, it appears more massive and tumbles with a correlation time of about 15 ns (calculated using a model-free analysis: R_2 , $\sim 29\text{ s}^{-1}$; R_1 , $\sim 0.9\text{ s}^{-1}$; NOE, ~ 0.8). The 15-ns correlation time is consistent with a 28-kDa protein. This suggests that not only is cTnI[1–73] tightly bound to cTnC, but cTnC is immobilized as well, with the whole complex tumbling as a single 28-kDa unit.

R_2 values for cTnI[1–73] are consistent with those measured by Rosevear and coworkers for cTnC bound to cTnI[1–80]³⁵. In the absence of cTnI[1–80], the two domains of cTnC tumbled independently (like two smaller proteins) (mean R_2 , 13 s^{-1}). Upon addition of cTnI[1–80], the two domains became rigidly fixed and tumbled as a single unit (mean R_2 , 31 s^{-1}). Pseudo-phosphorylation of cTnI Ser22/Ser23 by mutation to aspartate caused the two domains of cTnC to tumble as two separate proteins (mean R_2 , 15 s^{-1}). This work, along with the present study, shows that interaction with the cardiac-specific N-terminal extension of cTnI fixes the position of the cTnC regulatory domain relative to the rest of the troponin complex, whereas phosphorylation of cTnI Ser22/Ser23 abolishes this.

The relaxation data for cTnI[19–37] are quite informative. Upon addition of cTnC, the most striking change is the plateau of increased R_2 values in this region (Figure 7.6). This indicates that although cTnI[19–37] is intrinsically disordered with no secondary structure preference, there is a substantial restriction of mobility. This would be expected if Arg19–21, Arg26, and Lys35–37 are electrostatically tethered, but there is likely transient structuring occurring in the intervening segments as well. Faint intermediate-range (i , $i+3$ and i , $i+4$) intramolecular ^1H - ^1H NOEs are scattered throughout residues 18–32, indicating a transient helix- or turn-like structure, although chemical shift analysis indicates no net helical preference. Interestingly, the MICS Protein Structural Motif Prediction program indicates some potential turn structure at residues 22–25 and 31–34. The increased R_2 values in cTnI[19–37] could result from

fast conformational exchange (microsecond to millisecond timescale) and/or conformational restriction on the nanosecond timescale. Support for the latter comes from accompanying changes in R_1 and heteronuclear NOE values. Note that the R_1 values for cTnI[19–37] are the highest in all of cTnI, and these could not arise from an equilibrium between a strongly bound structured state (which would have a correlation time of 15 ns and $R_1 < 1 \text{ s}^{-1}$) and a free state (with $R_1 < 1.5 \text{ s}^{-1}$ from Figure 7.6). If this were the case, the R_1 values would be an average of these two states and significantly lower (so long as the exchange time constants were significantly longer than the nanosecond timescale correlation times). Instead, the high R_1 values (up to 2 s^{-1}) suggest a single partially structured state (or ensemble of very rapidly interconverting partially structured states).

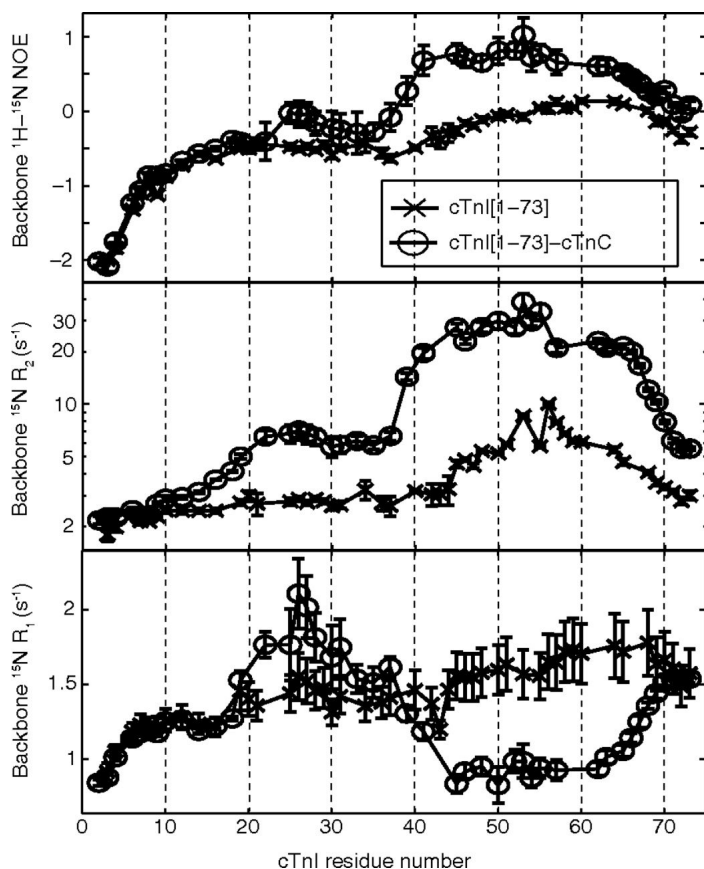


Figure 7.6. ^{15}N backbone relaxation data for cTnI[1–73].

“x” denotes free, and “o” denotes bound to C35S,C84S–cTnC.

Residues 2–18 of cTnI appear to be very mobile with considerable subnanosecond timescale motions and increasing mobility toward the N terminus. Upon addition of cTnC, there is no change in the rapid motions (followed by R_1 and NOEs) in this region, suggesting that it is not tethered in the same way as cTnI[19–37].

Calcium titration of cTnI[1–73]–cTnC.

The calcium binding affinity of the 2-(4'-(iodoacetamido)anilino)naphthalene-6-sulfonic acid (IAANS) – Cys84 conjugate of C35S – cTnC was studied using fluorescence, in complex with either cTnI[1–73] or cTnI[34–71] (Figure 7.7). cTnI[1–73]–cTnC had a calcium pCa_{50} of 6.04 ± 0.03 , and cTnI[34–71]–cTnC, 6.04 ± 0.04 . Thus, there was no measurable difference between the calcium affinities of the complexes. Thus, the electrostatic interaction between cTnI[19–37] and cTnC does not exert a direct effect on the calcium binding affinity of cTnC.

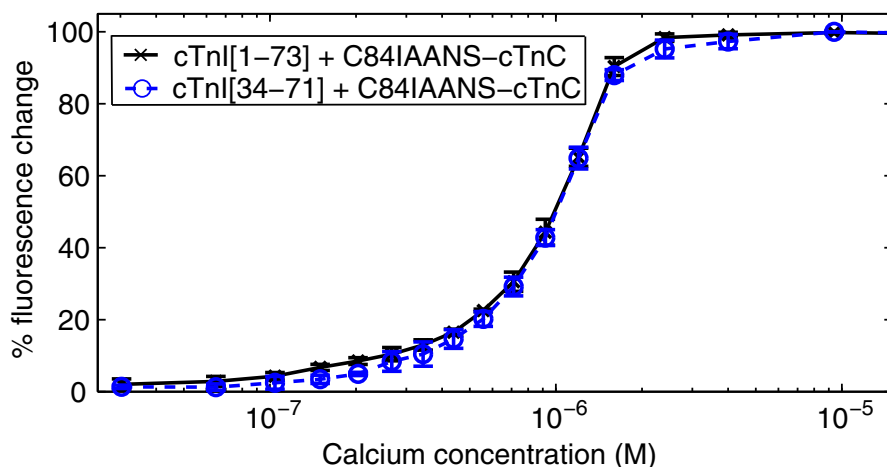


Figure 7.7. Calcium binding to C35S-cTnC bound to cTnI[1-73] or cTnI[34-71]. Calcium titrations of IAANS-labeled C35S-cTnC bound to either cTnI[1–73] or cTnI[34–71] ($n = 3$, error bars show SD). The total percentage fluorescence change is plotted against calcium concentration.

Discussion

The unphosphorylated cardiac-specific N-terminal extension of cTnI interacts with cTnTnC while remaining in a mobile, disordered state. IDRs are believed to make up a large proportion of protein sequences in eukaryotic proteomes. Due to their high solvent accessibility, they are readily available for posttranslational modifications like proteolysis and phosphorylation³⁶. IDRs can be regulated by multiple weak electrostatic interactions, and multiple phosphorylations are an effective means to add to or overcome these. A good example of the former is the increasing binding affinity between Sic-1 and Cdc4 as Sic-1 is increasingly phosphorylated^{26,37}. In contrast, phosphorylation of both Ser22 and Ser23 in cTnI has been shown to abolish the interaction with cTnTnC^{23,35,38}, with the two phosphate groups neutralizing the +4 positive charge locally contributed by Arg19, Arg20, Arg21, and Arg26. The physiologic effect of arginine mutation or PKA phosphorylation is to reduce the calcium sensitivity of troponin^{24,38}. On the other hand, the R21C (R20C by our numbering) mutation disrupts the PKA consensus phosphorylation sequence, RRXS, causing increased calcium sensitivity and hypertrophic cardiomyopathy in humans³⁹ and animal models^{40,41}.

The direct consequence of the interaction between cTnTnC and unphosphorylated cTnI[1–37] is that the orientation of cTnTnC becomes fixed relative to the rest of the troponin complex. Any posttranslational modification or mutation within the troponin complex that disrupts the delicate positioning of the cTnTnC domain would then be expected to have an effect similar to cTnI Ser22/23 phosphorylation, releasing cTnTnC and allowing it to gyrate independently of the troponin complex. This may explain why many of these modifications abolish the effect of Ser22/23 phosphorylation or have a greater influence on the unphosphorylated state (see Introduction).

The positioning of cTnTnC is critically important because it binds to the switch region, cTnI[148–158], to initiate cardiac contraction. The switch region is flanked by the inhibitory and regulatory regions, cTnI[136–147] and cTnI[161–209], that are anchored to actin during diastole⁴². During calcium-activated systole, hydrophobic binding of “opened” cTnTnC induces helix formation in cTnI[148–158] and sequesters the inhibitory and regulatory segments from their respective binding sites on actin. The

positioning of cTnI[148–158] in the context of the thin filament is currently unknown, but it is quite possible that when cTnI is unphosphorylated, cNTnC is well positioned to bind cTnI[148–158] as soon as calcium becomes available during systole. This would increase the effective concentration of the cTnI[148–158] switch peptide, driving the cNTnC equilibrium toward the calcium-stabilized open state and thereby enhancing the calcium sensitivity of the cardiac thin filament.

Optimal positioning of the cNTnC domain may also explain the steeper length dependence curve of the Frank–Starling law of the heart when cTnI is phosphorylated^{9,10}. The Frank–Starling law is caused by an unknown structural change that brings myosin heads into closer proximity of actin^{43,44}, increasing duty ratio, the proportion of myosin heads strongly bound to actin. This change displaces tropomyosin and the inhibitory segments of cTnI from their diastolic actin binding sites, making the switch region, cTnI[148–158], more readily available for cNTnC binding. The effective concentration of free cTnI [148–158] may be a more important factor when cNTnC is unrestrained and must randomly “search” for its binding partner. Alternatively, downstream structural changes resulting from the actin–myosin interaction may lead to a positioning of cNTnC (through an as-of-yet uncharacterized interaction) that is redundant to that set up by unphosphorylated cTnI[1–37].

One limitation of the current study is that not all of the troponin complex components are present. It is quite possible that the large volume of space accessible to the mobile cTnI[1–37] segment intersects with that of cTnI[136–147], cTnI[161–209], and cTnT[272–288], highly charged IDRs invisible in the crystal structure but known to interact with actin. Indeed, a major consequence of fixing the orientation of cNTnC via the cTnI [1–37] IDR could be that potentially nonproductive interactions with other IDRs are prevented. The extent to which all of these IDRs interact with each other and with charged surfaces on troponin, tropomyosin, or actin remains to be clarified by future NMR studies.

In conclusion, our findings contradict an earlier model that proposed a rigid structure for cTnI[1–37] that stabilizes the open state of cNTnC to directly increase its calcium affinity¹⁶. We did not observe evidence for a rigid structure in any way or a direct increase in calcium affinity. In our proposed model, the cardiac-specific N-

terminal extension of cTnI remains largely disordered while it interacts electrostatically with cNTnC. This interaction does not affect the closed–open equilibrium of cNTnC but indirectly increases calcium affinity by optimally positioning cNTnC to bind the cTnI switch peptide. Phosphorylation at cTnI Ser22/23 disrupts this delicate arrangement, which we predict will be impacted by other regulatory mechanisms as well.

Acknowledgements

The authors gratefully acknowledge the work of Eric Tai Kong Chan and Cathy Qin in developing the fluorescence assay. The work was supported by Canadian Institutes of Health Research (CIHR) Grant 37769. P.M.H. is supported by a CIHR Phase I Clinician Scientist Award and an Alberta Innovates–Health Solutions (AIHS) Incentive Award. S.E.P.S. is supported by an AIHS graduate student award.

References

1. Sharma, K. & Kass, D. A. Heart failure with preserved ejection fraction: mechanisms, clinical features, and therapies. *Circ. Res.* **115**, 79–96 (2014).
2. Solaro, R. J., Moir, A. J. G. & Perry, S. V. Phosphorylation of troponin I and the inotropic effect of adrenaline in the perfused rabbit heart. *Nature* **262**, 615–617 (1976).
3. van der Velden, J. Diastolic myofilament dysfunction in the failing human heart. *Pflugers Arch.* **462**, 155–63 (2011).
4. Solaro, R. J. & van der Velden, J. Why does troponin I have so many phosphorylation sites? Fact and fancy. *J. Mol. Cell. Cardiol.* **48**, 810–6 (2010).
5. Zhang, J. *et al.* Top-down quantitative proteomics identified phosphorylation of cardiac troponin I as a candidate biomarker for chronic heart failure. *J. Proteome Res.* **10**, 4054–65 (2011).
6. Solaro, R. J., Henze, M. & Kobayashi, T. Integration of troponin I phosphorylation with cardiac regulatory networks. *Circ. Res.* **112**, 355–66 (2013).
7. Wattanapermpool, J., Guo, X. & Solaro, R. J. The unique amino-terminal peptide of cardiac troponin I regulates myofibrillar activity only when it is phosphorylated. *J. Mol. Cell. Cardiol.* **27**, 1383–91 (1995).
8. Hamdani, N. *et al.* Distinct myocardial effects of beta-blocker therapy in heart failure with normal and reduced left ventricular ejection fraction. *Eur. Heart J.* **30**, 1863–72 (2009).
9. Hanft, L. M., Biesiadecki, B. J. & McDonald, K. S. Length dependence of striated muscle force generation is controlled by phosphorylation of cTnI at serines 23/24. *J. Physiol.* **591**, 4535–47 (2013).
10. Wijnker, P. J. M. *et al.* Length-dependent activation is modulated by cardiac troponin I bisphosphorylation at Ser23 and Ser24 but not by Thr143 phosphorylation. *Am. J. Physiol. Heart Circ. Physiol.* **306**, H1171–81 (2014).
11. Henze, M. *et al.* New insights into the functional significance of the acidic region of the unique N-terminal extension of cardiac troponin I. *Biochim. Biophys. Acta - Mol. Cell Res.* **1833**, 823–832 (2013).

12. Hinken, A. C. *et al.* Protein kinase C depresses cardiac myocyte power output and attenuates myofilament responses induced by protein kinase A. *J. Muscle Res. Cell Motil.* **33**, 439–48 (2012).
13. van der Velden, J. *et al.* Functional effects of protein kinase C-mediated myofilament phosphorylation in human myocardium. *Cardiovasc. Res.* **69**, 876–87 (2006).
14. Memo, M. *et al.* Familial dilated cardiomyopathy mutations uncouple troponin I phosphorylation from changes in myofibrillar Ca²⁺ sensitivity. *Cardiovasc. Res.* **99**, 65–73 (2013).
15. Takeda, S., Yamashita, A., Maeda, K. & Maéda, Y. Structure of the core domain of human cardiac troponin in the Ca(2+)-saturated form. *Nature* **424**, 35–41 (2003).
16. Howarth, J. W., Meller, J., Solaro, R. J., Trewhella, J. & Rosevear, P. R. Phosphorylation-dependent conformational transition of the cardiac specific N-extension of troponin I in cardiac troponin. *J. Mol. Biol.* **373**, 706–22 (2007).
17. Ward, D. G. *et al.* Characterization of the interaction between the N-terminal extension of human cardiac troponin I and troponin C. *Biochemistry* **43**, 4020–7 (2004).
18. Ferrières, G. *et al.* Systematic mapping of regions of human cardiac troponin I involved in binding to cardiac troponin C: N- and C-terminal low affinity contributing regions. *FEBS Lett.* **479**, 99–105 (2000).
19. Biesiadecki, B. J. *et al.* Removal of the cardiac troponin I N-terminal extension improves cardiac function in aged mice. *J. Biol. Chem.* **285**, 19688–98 (2010).
20. Camilloni, C., De Simone, A., Vranken, W. F. & Vendruscolo, M. Determination of secondary structure populations in disordered states of proteins using nuclear magnetic resonance chemical shifts. *Biochemistry* **51**, 2224–31 (2012).
21. Cheung, M.-S., Maguire, M. L., Stevens, T. J. & Broadhurst, R. W. DANGLE: A Bayesian inferential method for predicting protein backbone dihedral angles and secondary structure. *J. Magn. Reson.* **202**, 223–33 (2010).
22. Shen, Y. & Bax, A. Identification of helix capping and b-turn motifs from NMR

- chemical shifts. *J. Biomol. NMR* **52**, 211–32 (2012).
23. Baryshnikova, O. K., Li, M. X. & Sykes, B. D. Modulation of cardiac troponin C function by the cardiac-specific N-terminus of troponin I: influence of PKA phosphorylation and involvement in cardiomyopathies. *J. Mol. Biol.* **375**, 735–51 (2008).
 24. Ward, D. G., Cornes, M. P. & Trayer, I. P. Structural consequences of cardiac troponin I phosphorylation. *J. Biol. Chem.* **277**, 41795–801 (2002).
 25. Fuxreiter, M. Fuzziness: linking regulation to protein dynamics. *Mol. Biosyst.* **8**, 168–77 (2012).
 26. Mittag, T. *et al.* Dynamic equilibrium engagement of a polyvalent ligand with a single-site receptor. *Proc. Natl. Acad. Sci. U. S. A.* **105**, 17772–7 (2008).
 27. Bozoky, Z. *et al.* Regulatory R region of the CFTR chloride channel is a dynamic integrator of phospho-dependent intra- and intermolecular interactions. *Proc. Natl. Acad. Sci. U. S. A.* **110**, E4427-36 (2013).
 28. Finley, N. *et al.* NMR analysis of cardiac troponin C-troponin I complexes: effects of phosphorylation. *FEBS Lett.* **453**, 107–12 (1999).
 29. Sia, S. K. *et al.* Structure of cardiac muscle troponin C unexpectedly reveals a closed regulatory domain. *J. Biol. Chem.* **272**, 18216–21 (1997).
 30. Eichmüller, C. & Skrynnikov, N. R. A new amide proton R1rho experiment permits accurate characterization of microsecond time-scale conformational exchange. *J. Biomol. NMR* **32**, 281–93 (2005).
 31. Li, M. X., Spyropoulos, L. & Sykes, B. D. Binding of cardiac troponin-I147-163 induces a structural opening in human cardiac troponin-C. *Biochemistry* **38**, 8289–98 (1999).
 32. Davis, J. P. *et al.* Effects of thin and thick filament proteins on calcium binding and exchange with cardiac troponin C. *Biophys. J.* **92**, 3195–206 (2007).
 33. Wijnker, P. J. M. *et al.* Phosphorylation of protein kinase C sites Ser42/44 decreases Ca²⁺-sensitivity and blunts enhanced length-dependent activation in response to protein kinase A in human cardiomyocytes. *Arch. Biochem. Biophys.* **554**, 11–21 (2014).
 34. Carballo, S. *et al.* Identification and functional characterization of cardiac

- troponin I as a novel disease gene in autosomal dominant dilated cardiomyopathy. *Circ. Res.* **105**, 375–82 (2009).
35. Gaponenko, V. *et al.* Effects of Troponin I Phosphorylation on Conformational Exchange in the Regulatory Domain of Cardiac Troponin C. *J. Biol. Chem.* **274**, 16681–16684 (1999).
 36. Iakoucheva, L. M. The importance of intrinsic disorder for protein phosphorylation. *Nucleic Acids Res.* **32**, 1037–1049 (2004).
 37. Tang, X. *et al.* Composite low affinity interactions dictate recognition of the cyclin-dependent kinase inhibitor Sic1 by the SCFCdc4 ubiquitin ligase. *Proc. Natl. Acad. Sci. U. S. A.* **109**, 3287–92 (2012).
 38. Ward, D. G. *et al.* NMR and mutagenesis studies on the phosphorylation region of human cardiac troponin I. *Biochemistry* **43**, 5772–81 (2004).
 39. Arad, M. *et al.* Gene mutations in apical hypertrophic cardiomyopathy. *Circulation* **112**, 2805–11 (2005).
 40. Gomes, A. V, Harada, K. & Potter, J. D. A mutation in the N-terminus of troponin I that is associated with hypertrophic cardiomyopathy affects the Ca(2+)-sensitivity, phosphorylation kinetics and proteolytic susceptibility of troponin. *J. Mol. Cell. Cardiol.* **39**, 754–65 (2005).
 41. Wang, Y. *et al.* Generation and functional characterization of knock-in mice harboring the cardiac troponin I-R21C mutation associated with hypertrophic cardiomyopathy. *J. Biol. Chem.* **287**, 2156–67 (2012).
 42. Tripet, B., Van Eyk, J. E. & Hodges, R. S. Mapping of a second actin-tropomyosin and a second troponin C binding site within the C terminus of troponin I, and their importance in the Ca²⁺-dependent regulation of muscle contraction. *J. Mol. Biol.* **271**, 728–50 (1997).
 43. Farman, G. P. *et al.* Myosin head orientation: a structural determinant for the Frank-Starling relationship. *Am. J. Physiol. Heart Circ. Physiol.* **300**, H2155–60 (2011).
 44. Mateja, R. D. & de Tombe, P. P. Myofilament length-dependent activation develops within 5 ms in guinea-pig myocardium. *Biophys. J.* **103**, L13–5 (2012).
 45. Li, M. X. *et al.* Kinetic studies of calcium and cardiac troponin I peptide binding

- to human cardiac troponin C using NMR spectroscopy. *Eur. Biophys. J.* **31**, 245–56 (2002).
46. Wang, X., Mercier, P., Letourneau, P.-J. & Sykes, B. D. Effects of Phe-to-Trp mutation and fluorotryptophan incorporation on the solution structure of cardiac troponin C, and analysis of its suitability as a potential probe for in situ NMR studies. *Protein Sci.* **14**, 2447–60 (2005).
 47. Hwang, P. M., Pan, J. S. & Sykes, B. D. A PagP fusion protein system for the expression of intrinsically disordered proteins in *Escherichia coli*. *Protein Expr. Purif.* **85**, 148–51 (2012).
 48. Baryshnikova, O. K., Williams, T. C. & Sykes, B. D. Internal pH indicators for biomolecular NMR. *J. Biomol. NMR* **41**, 5–7 (2008).
 49. Boucher, W., Laue, E. D., Campbell-Burk, S. & Domaille, P. J. Four-dimensional heteronuclear triple resonance NMR methods for the assignment of backbone nuclei in proteins. *J. Am. Chem. Soc.* **114**, 2262–2264 (1992).
 50. Delaglio, F. *et al.* NMRPipe: A multidimensional spectral processing system based on UNIX pipes. *J. Biomol. NMR* **6**, 277–293 (1995).
 51. Johnson, B. A. & Blevins, R. A. NMR View: A computer program for the visualization and analysis of NMR data. *J. Biomol. NMR* **4**, 603–614 (1994).
 52. Lipari, G. & Szabo, A. Model-free approach to the interpretation of nuclear magnetic resonance relaxation in macromolecules. 1. Theory and range of validity. *J. Am. Chem. Soc.* **104**, 4546–4559 (1982).

Chapter 8

Conclusions

The main focus of this thesis is to provide a more thorough understanding on the underlying mechanisms of direct cardiac sarcomere modulators that target the cNTnC-cTnI interface. Since each chapter already contains its own conclusion, for this chapter I will highlight how I got through my six years of PhD studies.

My first project was to develop new calcium sensitizing drugs targeting the interface of cNTnC and cTnI switch region within the thin filament. The cNTnC-cTnI switch region chimera (cChimera) is developed to represent the key aspects of the cNTnC-cTnI interface in the saturated state¹. The cChimeras have been constructed with different linkers between cNTnC and cTnI and have included different amino acid mutations for various experiments. We determined the NMR solution structure of calcium-saturated cChimera, showing that cChimera faithfully reproduces the native interface between cNTnC and the switch region of cTnI². cChimera was extensively used throughout the work in this thesis for structure, dynamics, and drug binding studies.

The early stage of this project was to screen for compounds that bind tightly to cNTnC-cTnI chimera. Our small molecule library was initially built upon the calcium sensitizer bepridil, which has the highest binding affinity to cNTnC (with a K_D of 20 μ M) and cNTnC-cTnI complex (with a K_D of 80 μ M) back when we started the project. In chapter 2, we discovered that diphenylamine (DPA) and its derivatives can bind tightly to cNTnC-cTnI chimera with a K_D as low as 10 μ M. Solution NMR structures show that minimal structural perturbations in cChimera are needed to accommodate 3-methyl diphenylamine (3-mDPA), suggesting preservation of the native interaction between cNTnC and cTnI might be the key to the development of high affinity cardiac troponin modulators². A subsequent study has found that our tightest binding compounds, 3-chlorodiphenylamine (3-CIDPA), increases the calcium sensitivity of force development in skinned cardiac muscle³.

We used NMR spectroscopy to screen hundreds of small molecules based on DPA for cChimera in order to find a base structure for drug development. The benefit

of using NMR for screening is that no modification of protein is needed and an accurate dissociation constant can be calculated in the micromolar to millimolar range. However, screening with NMR is time consuming, and requires a large amount of isotope labeled protein. We also tried to develop the fluorescence-based screening by measuring the fluorescence changes induced by ligand displacing the IAANS fluorophore attached on Cys 84 of cTnT. This method was used to determine the dissociation constant of different cTnI peptides to cTnT in chapter 7⁴. However, many complications arose when measuring the small molecule binding using fluorescence, including fluorescence from small molecule and fluorophore non-specifically interacting with small molecule or organic solvent. Discovering and developing new drugs is a very challenging endeavor even for large and well-known organizations within the pharmaceutical industries that have established methods with high-throughput screening technologies. Instead of attempting to screen for the hit, our goal in a research lab is to understand the underlying mechanisms of the cardiac sarcomere modulators that target the cTnT-cTnI interface.

Several small molecules are known to bind to the interface of cTnT and cTnI switch region and change the calcium sensitivity of the sarcomere. Most of them are calcium sensitizers and few are calcium desensitizers. We used to use the term ‘calcium sensitizer’, such as bepridil and levosimendan, and ‘calcium desensitizer’, such as W7, to describe the compounds directly alter the muscle contractility by targeting the sarcomere without altering the calcium homeostasis in the heart. However, cTnT acts in part as a calcium buffer in the cell, and changing the calcium sensitivity of cTnT directly would change the calcium concentration in the cardiomyocyte⁵. The ideal compound would alter the contractile response to the calcium but not impact the calcium pumps or channels that transport calcium across cellular membranes. Therefore, instead of naming the compounds ‘calcium sensitizer’ or ‘calcium desensitizer’, we use the term ‘sarcomere modulator’ (‘activator’ or ‘inhibitor’).

The most well-studied direct sarcomere inhibitor is the calmodulin antagonist W7, which decreases the calcium sensitivity of force development in cardiac muscle^{6,7}. W7 binds to the interface of cTnT and cTnI switch region and significantly weakens cTnI binding⁸. The NMR structure of cTnT-cTnI switch peptide-W7 complex

showed that W7 pushed cTnI switch region away from its preferred binding site and diminished some of its helical structure. However, the cTnI structure is not well-resolved due to the weak binding affinity to cNTnC and the use of unlabeled cTnI peptide⁸. The cChimera have the advantage of labeling the cTnI switch region with cNTnC, which allows the use of heteronuclear NMR experiments to fully assign the cTnI switch peptide. We determined the NMR solution structure of W7 bound to cNTnC-cTnI cChimera in chapter 3⁹. The structure shows that W7 does not perturb the overall structure of the interface of cNTnC and cTnI, with the helical structure and position of the cTnI switch region remaining intact upon W7 binding. The naphthalene ring of W7 sits in the hydrophobic pocket created by the cNTnC and cTnI switch peptide, while the positively charged amine tail extends into the solvent. The positively charged tail of the W7 is in close proximity of Arg 147 of cTnI switch region, supporting the theory that electrostatic repulsion is an aspect underlying the mechanism of negative inotropic effect of W7.

Many of the small molecule targeting the cNTnC-cTnI interface have an aromatic core and a polar or charged tail. The sarcomere inhibitor W7 decreases the binding of cTnI switch region to cNTnC, possibly through the electrostatic repulsion between the positively charged terminal amino group of W7 and the negatively charged guanidinium group of Arg 147 of cTnI⁸. On the other hand, the sarcomere activator dfbp-o enhances the binding of the cTnI, possibly by electrostatic attraction between the positively charged carboxyl group of dfbp-o and the negatively charged Arg 147¹⁰. To evaluate the role of electrostatics in tuning the cNTnC-cTnI interface, Dr. Ian Robertson synthesized A7, where the amino group of W7 was replaced with a carboxyl group. In chapter 4, we found that A7 decreased the binding affinity of cTnI to cNTnC substantially less than W7 and has a much weaker negative inotropic effect than W7 on ventricular trabeculae. The NMR solution structure of the cChimera-A7 complex revealed that A7 does not change the overall conformation of the cNTnC-cTnI interface, and the naphthalene ring of A7 sits in the same hydrophobic pocket as that of W7, but the tail takes a different route to the surface of the complex¹¹.

A6, which has one less methylene group than A7, does not affect binding of cTnI switch peptide nor change the calcium sensitivity of ventricular trabeculae,

suggesting that the location of the charged group might also be important. In chapter 5, we found that W6, which has one less methylene group than W7, binds tighter to cChimera than W7, and does not change the calcium sensitivity on ventricular trabeculae. The solution structure of cChimera-W6 complex reveals that W6 binds to the same hydrophobic cleft as W7, with the naphthalene ring sitting in the same deep binding pocket, and the aliphatic tail taking a similar route to the surface of the complex. The only difference would be the exact location of the positively charged amino group due to the different length of the tail. These results from chapter 4 and 5 indicate that both electrostatic repulsion and the precise location of the charged amino group is important with regard to the negative inotropic effect of W7.

The results from this thesis strengthen our hypothesis that the interface of cNTnC and cTnI switch region within the thin filament is a potential site for the development of drugs that modulate the performance of the heart. It is important to note that a drug targeting the heart would only attempt to make minor changes to correct the diseased heart back to physiological zone, instead of stopping the heart completely¹². Using small molecules to modulate the cNTnC-cTnI interface can be effective in regulating the fine balance between contraction and relaxation in the heart.

More generally, this thesis has demonstrated that the cTnC-cTnI chimera is an excellent tool to study thin filament modulators; that one needs structure, affinity, dynamics, and physiology to get complete picture; that very small changes in 'structure' can have a significant effect; and that electrostatics are important in the negative inotropic effect of W7.

Some future directions are discussed below: can we study the dynamics in these complexes; can we convert another activator to an inhibitor and duplicate the results; and can we model the electrostatic force in protein-ligand complexes to understand structure, dynamics, affinity and physiology.

The charge difference between W7 and A7 results in a change of dynamics in the structure of the small molecule tail region, with the tail of W7 appearing to be more rigid and the tail of A7 to be more flexible, judging by the number of NOE contacts. Dynamics affect the entropic contributions to the free energy of the interaction and it is possible that the dynamics of the tail is important for the inhibition effect of W7. To

evaluate the flexibility of the tail region, we have synthesized A4, which has three less methylene group than A7, labeling with ^{13}C on the tail region (A4- $^{13}\text{C}4$) (Figure 8.1). The ^{13}C labeled A4 allowing us to measuring the relaxation on each ^{13}C and study the dynamics of the tail region in the cChimera-A4 complex. Other isotopically labelled molecules are underway.

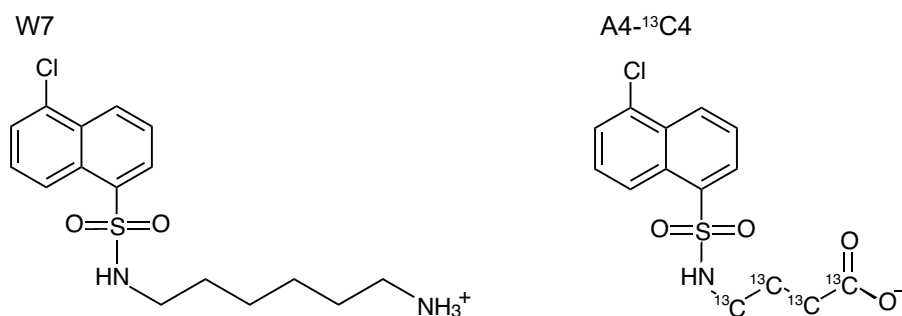


Figure 8.1. ^{13}C labelled compounds for future studies.

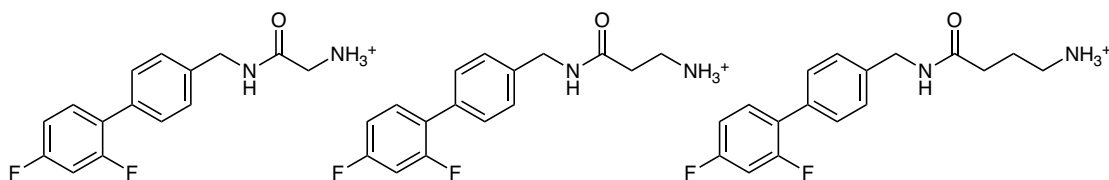


Figure 8.2. Dfbp-o amine series compounds.

Since changing the positively charged amino group of W7 to negatively charged carboxyl group significantly decreased the inhibition effect of W7, we could attempt to duplicate the results by altering another activator such as dfbp-o. We changed the negatively charged carboxyl group of dfbp-o to positively charge amino group with various tail length (Figure 8.2). If the electrostatic interaction between small molecule and cTnI is a key to modulate the cNTnC-cTnI interface, we would be expecting the new compounds to be inhibitors.

NMR is a great tool for binding and structural studies, but we would not be able to explore the underlying mechanism of W7 this far without the physiological studies performed by our collaborator Dr. Thomas Kampourakis. The NMR structural studies and physiological studies complimented each other and helped direct the research. At this point, we are trying to explain how W7 and W6 would have such a huge difference in the inhibition effect on trabeculae, when they bind to the same pocket and the positively charged amino group is only less than 2 Å apart. Computational simulation studies to model the electrostatic force in protein-ligand complexes would be helpful to understand the structure, dynamics, affinity and physiological studies.

The last piece of work in this thesis is to report a strong cardiac sarcomere inhibitor, DN-F01, targeting the cNTnC-cTnI interface. DN-F01 shares structural similarities to levosimendan, which is one of the most widely studied troponin activator and has been used to treat acute heart failure in over 60 countries worldwide^{13,14}. Recent studies show that the nitrile group of levosimendan forms a reversible-covalent thioimide bond with C84 of cNTnC both *in vitro*¹⁵ and *in situ*¹². The nitrile group containing DN-F01 was previously determined to form a reversible covalent thioimide bond with cNTnC Cys 84¹⁶. In chapter 6, the ATPase activity studies show that DN-F01 has a strong inhibiting effect on cardiomyofibrils. The NMR titrations reveals that the binding position of DN-F01 bound covalently or non-covalently to the cNTnC-cTnI chimera might be different. The bulky DN-F01 might clash with the cTnI switch peptide when covalently bond to C84, which could be the mechanism underlying its strong sarcomere inhibitory effect. One concern regarding to the low IC₅₀ in the effect of DN-F01 on ATPase activity study and the relatively weaker binding affinity in NMR and fluorescence studies is that DN-F01 could potentially inhibit the cardiomyofibrils by interacting with other targets other than cNTnC Cys 84. We propose labelling the cTnC with DN-F01 and then exchanging the native cTnC for cTnC-DN-F01 to eliminate nonspecific binding.

References

1. Pineda-Sanabria, S. E., Julien, O. & Sykes, B. D. Versatile Cardiac Troponin Chimera for Muscle Protein Structural Biology and Drug Discovery. *ACS Chem. Biol.* **9**, 2121–2130 (2014).
2. Cai, F. *et al.* Structures reveal details of small molecule binding to cardiac troponin. *J. Mol. Cell. Cardiol.* **101**, 134–144 (2016).
3. Tikunova, S. B. *et al.* 3-Chlorodiphenylamine activates cardiac troponin by a mechanism distinct from bepridil or TFP. *J. Gen. Physiol.* **151**, 9–17 (2019).
4. Hwang, P. M., Cai, F., Pineda-Sanabria, S. E., Corson, D. C. & Sykes, B. D. The cardiac-specific N-terminal region of troponin I positions the regulatory domain of troponin C. *Proc. Natl. Acad. Sci. U. S. A.* **111**, 14412–7 (2014).
5. Berlin, J. R., Bassani, J. W. & Bers, D. M. Intrinsic cytosolic calcium buffering properties of single rat cardiac myocytes. *Biophys. J.* **67**, 1775–1787 (1994).
6. Adhikari, B. B. & Wang, K. Interplay of Troponin- and Myosin-Based Pathways of Calcium Activation in Skeletal and Cardiac Muscle: The Use of W7 as an Inhibitor of Thin Filament Activation. *Biophys. J.* **86**, 359–370 (2004).
7. Thompson, B. R., Martindale, J. & Metzger, J. M. Sarcomere neutralization in inherited cardiomyopathy: small-molecule proof-of-concept to correct hyper-Ca²⁺-sensitive myofilaments. *Am. J. Physiol. Heart Circ. Physiol.* **311**, H36-43 (2016).
8. Oleszczuk, M., Robertson, I. M., Li, M. X. & Sykes, B. D. Solution structure of the regulatory domain of human cardiac troponin C in complex with the switch region of cardiac troponin I and W7: The basis of W7 as an inhibitor of cardiac muscle contraction. *J. Mol. Cell. Cardiol.* **48**, 925–933 (2010).
9. Cai, F., Hwang, P. M. & Sykes, B. D. Structural Changes Induced by the Binding of the Calcium Desensitizer W7 to Cardiac Troponin. *Biochemistry* **57**, 6461–6469 (2018).
10. Robertson, I. M., Sun, Y.-B. B., Li, M. X. & Sykes, B. D. A structural and functional perspective into the mechanism of Ca²⁺-sensitizers that target the cardiac troponin complex. *J. Mol. Cell. Cardiol.* **49**, 1031–1041 (2010).
11. Cai, F., Robertson, I. M., Kampourakis, T., Klein, B. A. & Sykes, B. D. The

- Role of Electrostatics in the Mechanism of Cardiac Thin Filament Based Sensitizers. *ACS Chem. Biol.* **15**, 2289–2298 (2020).
12. Klein, B. A. *et al.* Reversible Covalent Reaction of Levosimendan with Cardiac Troponin C in Vitro and in Situ. *Biochemistry* **57**, 2256–2265 (2018).
 13. Haikala, H. *et al.* Cardiac troponin C as a target protein for a novel calcium sensitizing drug, levosimendan. *J. Mol. Cell. Cardiol.* **27**, 1859–1866 (1995).
 14. Papp, Z. *et al.* Pharmacological Therapy Levosimendan Efficacy and Safety : 20 years of SIMDAX in Clinical Use Pharmacological Therapy. (2020).
 15. Robertson, I. M. *et al.* Reversible Covalent Binding to Cardiac Troponin C by the Ca²⁺-Sensitizer Levosimendan. *Biochemistry* **55**, 6032–6045 (2016).
 16. Klein, B. A. *et al.* Thioimidate Bond Formation between Cardiac Troponin C and Nitrile-containing Compounds. *ACS Med. Chem. Lett.* **10**, 1007–1012 (2019).

Bibliography

- Abusamhadneh, E., Abbott, M. B., Dvoretzky, A., Finley, N., Sasi, S., & Rosevear, P. R. (2001). Interaction of bepridil with the cardiac troponin C/troponin I complex. *FEBS Letters*, *506*(1), 51–54. [https://doi.org/10.1016/S0014-5793\(01\)02790-9](https://doi.org/10.1016/S0014-5793(01)02790-9)
- Adhikari, B. B., & Wang, K. (2004). Interplay of Troponin- and Myosin-Based Pathways of Calcium Activation in Skeletal and Cardiac Muscle: The Use of W7 as an Inhibitor of Thin Filament Activation. *Biophysical Journal*, *86*(1), 359–370. [https://doi.org/10.1016/S0006-3495\(04\)74112-0](https://doi.org/10.1016/S0006-3495(04)74112-0)
- Agarkova, I., & Perriard, J. C. (2005). The M-band: An elastic web that crosslinks thick filaments in the center of the sarcomere. *Trends in Cell Biology*, *15*(9), 477–485. <https://doi.org/10.1016/j.tcb.2005.07.001>
- Ahmed, A., Rich, M. W., Fleg, J. L., Zile, M. R., Young, J. B., Kitzman, D. W., ... Gheorghiade, M. (2006). Effects of Digoxin on Morbidity and Mortality in Diastolic Heart Failure. *Circulation*, *114*(5), 397–403. <https://doi.org/10.1161/CIRCULATIONAHA.106.628347>
- An Account of the Fox Glove, and Some of Its Medical Uses; with Practical Remarks on Dropsy, and Other Diseases. (1785). *Lond Med J*.
- Aprahamian, M. L., Tikunova, S. B., Price, M. V., Cuesta, A. F., Davis, J. P., & Lindert, S. (2017). Successful Identification of Cardiac Troponin Calcium Sensitizers Using a Combination of Virtual Screening and ROC Analysis of Known Troponin C Binders. *Journal of Chemical Information and Modeling*, *57*(12), 3056–3069. <https://doi.org/10.1021/acs.jcim.7b00536>
- Arad, M., Penas-Lado, M., Monserrat, L., Maron, B. J., Sherrid, M., Ho, C. Y., ... Seidman, C. E. (2005). Gene mutations in apical hypertrophic cardiomyopathy. *Circulation*, *112*(18), 2805–2811. <https://doi.org/10.1161/CIRCULATIONAHA.105.547448>
- Baldo, J. H., Halford, S. E., Patt, S. L., & Sykes, B. D. (1975). The Stepwise Binding of Small Molecules to Proteins. Nuclear Magnetic Resonance and Temperature Jump Studies of the Binding of 4-(N-Acetylaminoglucosyl)-N-acetylglucosamine to Lysozyme. *Biochemistry*, *14*(9), 1893–1899.

<https://doi.org/10.1021/bi00680a014>

- Baryshnikova, O. K., Li, M. X., & Sykes, B. D. (2008). Modulation of cardiac troponin C function by the cardiac-specific N-terminus of troponin I: influence of PKA phosphorylation and involvement in cardiomyopathies. *Journal of Molecular Biology*, 375(3), 735–751. <https://doi.org/10.1016/j.jmb.2007.10.062>
- Baryshnikova, O. K., Williams, T. C., & Sykes, B. D. (2008). Internal pH indicators for biomolecular NMR. *Journal of Biomolecular NMR*, 41(1), 5–7. <https://doi.org/10.1007/s10858-008-9234-6>
- Becker, W., Bhattacharjee, K. C., Gubensäk, N., & Zangger, K. (2018). Investigating Protein–Ligand Interactions by Solution Nuclear Magnetic Resonance Spectroscopy. *ChemPhysChem*, 19(8), 895–906. <https://doi.org/10.1002/cphc.201701253>
- Berjanskii, M. V., & Wishart, D. S. (2005). A Simple Method To Predict Protein Flexibility Using Secondary Chemical Shifts. *Journal of the American Chemical Society*, 127(43), 14970–14971. <https://doi.org/10.1021/ja054842f>
- Berlin, J. R., Bassani, J. W., & Bers, D. M. (1994). Intrinsic cytosolic calcium buffering properties of single rat cardiac myocytes. *Biophysical Journal*, 67(4), 1775–1787. [https://doi.org/10.1016/S0006-3495\(94\)80652-6](https://doi.org/10.1016/S0006-3495(94)80652-6)
- Biesiadecki, B. J., Tachampa, K., Yuan, C., Jin, J.-P., de Tombe, P. P., & Solaro, R. J. (2010). Removal of the cardiac troponin I N-terminal extension improves cardiac function in aged mice. *The Journal of Biological Chemistry*, 285(25), 19688–19698. <https://doi.org/10.1074/jbc.M109.086892>
- Boswell-Smith, V., Spina, D., & Page, C. P. (2006). Phosphodiesterase inhibitors. *British Journal of Pharmacology*, 147(S1), S252–S257. <https://doi.org/10.1038/sj.bjp.0706495>
- Boucher, W., Laue, E. D., Campbell-Burk, S., & Domaille, P. J. (1992). Four-dimensional heteronuclear triple resonance NMR methods for the assignment of backbone nuclei in proteins. *Journal of the American Chemical Society*, 114(6), 2262–2264. <https://doi.org/10.1021/ja00032a053>
- Boyle, K. L., & Leech, E. (2012). A review of the pharmacology and clinical uses of pimobendan. *Journal of Veterinary Emergency and Critical Care*, 22(4), 398–

408. <https://doi.org/10.1111/j.1476-4431.2012.00768.x>
- Bozoky, Z., Krzeminski, M., Muhandiram, R., Birtley, J. R., Al-Zahrani, A., Thomas, P. J., ... Forman-Kay, J. D. (2013). Regulatory R region of the CFTR chloride channel is a dynamic integrator of phospho-dependent intra- and intermolecular interactions. *Proceedings of the National Academy of Sciences of the United States of America*, *110*(47), E4427-36. <https://doi.org/10.1073/pnas.1315104110>
- Brenner, B., & Eisenberg, E. (1986). Rate of force generation in muscle: Correlation with actomyosin ATPase activity in solution. *Proceedings of the National Academy of Sciences of the United States of America*, *83*(10), 3542–3546. <https://doi.org/10.1073/pnas.83.10.3542>
- Brunger, A. T. (2007). Version 1.2 of the Crystallography and NMR system. *Nature Protocols*, *2*(11), 2728–2733. <https://doi.org/10.1038/nprot.2007.406>
- Cai, F., Hwang, P. M., & Sykes, B. D. (2018). Structural Changes Induced by the Binding of the Calcium Desensitizer W7 to Cardiac Troponin. *Biochemistry*, *57*(46), 6461–6469. <https://doi.org/10.1021/acs.biochem.8b00882> research-article.
- Cai, F., Li, M. X., Pineda-Sanabria, S. E., Gelozia, S., Lindert, S., West, F., ... Hwang, P. M. (2016). Structures reveal details of small molecule binding to cardiac troponin. *Journal of Molecular and Cellular Cardiology*, *101*, 134–144. <https://doi.org/10.1016/j.yjmcc.2016.10.016>
- Cai, F., Robertson, I. M., Kampourakis, T., Klein, B. A., & Sykes, B. D. (2020). The Role of Electrostatics in the Mechanism of Cardiac Thin Filament Based Sensitizers. *ACS Chemical Biology*, *15*(8), 2289–2298. <https://doi.org/10.1021/acscchembio.0c00519>
- Camilloni, C., De Simone, A., Vranken, W. F., & Vendruscolo, M. (2012). Determination of secondary structure populations in disordered states of proteins using nuclear magnetic resonance chemical shifts. *Biochemistry*, *51*(11), 2224–2231. <https://doi.org/10.1021/bi3001825>
- Carballo, S., Robinson, P., Otway, R., Fatkin, D., Jongbloed, J. D. H., de Jonge, N., ... Watkins, H. (2009). Identification and functional characterization of cardiac troponin I as a novel disease gene in autosomal dominant dilated cardiomyopathy.

Circulation Research, 105(4), 375–382.
<https://doi.org/10.1161/CIRCRESAHA.109.196055>

- Cheung, M.-S., Maguire, M. L., Stevens, T. J., & Broadhurst, R. W. (2010). DANGLE: A Bayesian inferential method for predicting protein backbone dihedral angles and secondary structure. *Journal of Magnetic Resonance (San Diego, Calif. : 1997)*, 202(2), 223–233. <https://doi.org/10.1016/j.jmr.2009.11.008>
- Cleland, J. G. F., Freemantle, N., Coletta, A. P., & Clark, A. L. (2006). Clinical trials update from the American Heart Association: REPAIR-AMI, ASTAMI, JELIS, MEGA, REVIVE-II, SURVIVE, and PROACTIVE. *European Journal of Heart Failure*, 8(1), 105–110. <https://doi.org/10.1016/j.ejheart.2005.12.003>
- Cleland, J. G. F., Teerlink, J. R., Senior, R., Nifontov, E. M., McMurray, J. J. V., Lang, C. C., ... Malik, F. I. (2011). The effects of the cardiac myosin activator, omecamtiv mecarbil, on cardiac function in systolic heart failure: A double-blind, placebo-controlled, crossover, dose-ranging phase 2 trial. *The Lancet*, 378(9792), 676–683. [https://doi.org/10.1016/S0140-6736\(11\)61126-4](https://doi.org/10.1016/S0140-6736(11)61126-4)
- Craig, R., & Woodhead, J. L. (2006). Structure and function of myosin filaments. *Current Opinion in Structural Biology*, 16(2), 204–212. <https://doi.org/10.1016/j.sbi.2006.03.006>
- Davis, J. P., Norman, C., Kobayashi, T., Solaro, R. J., Swartz, D. R., & Tikunova, S. B. (2007). Effects of thin and thick filament proteins on calcium binding and exchange with cardiac troponin C. *Biophysical Journal*, 92(9), 3195–3206. <https://doi.org/10.1529/biophysj.106.095406>
- Davis, J., Wen, H., Edwards, T., & Metzger, J. M. (2008). Allele and species dependent contractile defects by restrictive and hypertrophic cardiomyopathy-linked troponin I mutants. *Journal of Molecular and Cellular Cardiology*, 44(5), 891–904. <https://doi.org/10.1016/j.yjmcc.2008.02.274>
- Delaglio, F., Grzesiek, S., Vuister, G. W., Zhu, G., Pfeifer, J., & Bax, A. (1995). NMRPipe: A multidimensional spectral processing system based on UNIX pipes. *Journal of Biomolecular NMR*, 6(3), 277–293. <https://doi.org/10.1007/BF00197809>
- Doerr, A. (2008). Solution for solution structures. *Nature Physics*, 4(S1), S15–S15.

- <https://doi.org/10.1038/nphys871>
- EBASHI, S. (1972). Separation of Troponin into Its Three Components*. *The Journal of Biochemistry*, 72(3), 787–790. <https://doi.org/10.1093/oxfordjournals.jbchem.a129961>
- Eichmüller, C., & Skrynnikov, N. R. (2005). A new amide proton R1rho experiment permits accurate characterization of microsecond time-scale conformational exchange. *Journal of Biomolecular NMR*, 32(4), 281–293. <https://doi.org/10.1007/s10858-005-0658-y>
- Endoh, M. (2008). Cardiac Ca²⁺ Signaling and Ca²⁺ Sensitizers. *Circulation Journal*, 72(12), 1915–1925. <https://doi.org/10.1253/circj.CJ-08-0838>
- Farmakis, D., Alvarez, J., Gal, T. Ben, Brito, D., Fedele, F., Fonseca, C., ... Parissis, J. (2016, November 1). Levosimendan beyond inotropy and acute heart failure: Evidence of pleiotropic effects on the heart and other organs: An expert panel position paper. *International Journal of Cardiology*. <https://doi.org/10.1016/j.ijcard.2016.07.202>
- Farman, G. P., Gore, D., Allen, E., Schoenfelt, K., Irving, T. C., & de Tombe, P. P. (2011). Myosin head orientation: a structural determinant for the Frank-Starling relationship. *American Journal of Physiology. Heart and Circulatory Physiology*, 300(6), H2155-60. <https://doi.org/10.1152/ajpheart.01221.2010>
- Ferrières, G., Pugnère, M., Mani, J. C., Villard, S., Laprade, M., Doutre, P., ... Granier, C. (2000). Systematic mapping of regions of human cardiac troponin I involved in binding to cardiac troponin C: N- and C-terminal low affinity contributing regions. *FEBS Letters*, 479(3), 99–105. [https://doi.org/10.1016/s0014-5793\(00\)01881-0](https://doi.org/10.1016/s0014-5793(00)01881-0)
- Finley, N., Abbott, M. B., Abusamhadneh, E., Gaponenko, V., Dong, W., Gasmi-Seabrook, G., ... Rosevear, P. R. (1999). NMR analysis of cardiac troponin C-troponin I complexes: effects of phosphorylation. *FEBS Letters*, 453(1–2), 107–112. [https://doi.org/10.1016/s0014-5793\(99\)00693-6](https://doi.org/10.1016/s0014-5793(99)00693-6)
- Finley, N. L., Howarth, J. W., & Rosevear, P. R. (2004). Structure of the Mg²⁺-Loaded C-Lobe of Cardiac Troponin C Bound to the N-Domain of Cardiac Troponin I: Comparison with the Ca²⁺-Loaded Structure^{†,‡}. *Biochemistry*, 43(36),

- 11371–11379. <https://doi.org/10.1021/bi049672i>
- Flashman, E., Redwood, C., Moolman-Smook, J., & Watkins, H. (2004). Cardiac myosin binding protein C: Its role in physiology and disease. *Circulation Research*, 94(10), 1279–1289. <https://doi.org/10.1161/01.RES.0000127175.21818.C2>
- Friesner, R. A., Murphy, R. B., Repasky, M. P., Frye, L. L., Greenwood, J. R., Halgren, T. A., ... Mainz, D. T. (2006). Extra precision glide: Docking and scoring incorporating a model of hydrophobic enclosure for protein-ligand complexes. *Journal of Medicinal Chemistry*, 49(21), 6177–6196. <https://doi.org/10.1021/jm051256o>
- Fuxreiter, M. (2012). Fuzziness: linking regulation to protein dynamics. *Molecular BioSystems*, 8(1), 168–177. <https://doi.org/10.1039/c1mb05234a>
- Gagné, S M, Tsuda, S., Li, M. X., Chandra, M., Smillie, L. B., & Sykes, B. D. (1994). Quantification of the calcium-induced secondary structural changes in the regulatory domain of troponin-C. *Protein Science : A Publication of the Protein Society*, 3(11), 1961–1974. <https://doi.org/10.1002/pro.5560031108>
- Gagné, Stéphane M., Tsuda, S., Li, M. X., Smillie, L. B., & Sykes, B. D. (1995). Structures of the troponin C regulatory domains in the apo and calcium-saturated states. *Nature Structural & Molecular Biology*, 2(9), 784–789. <https://doi.org/10.1038/nsb0995-784>
- Gaponenko, V., Abusamhadneh, E., Abbott, M. B., Finley, N., Gasmi-Seabrook, G., Solaro, R. J., ... Rosevear, P. R. (1999). Effects of Troponin I Phosphorylation on Conformational Exchange in the Regulatory Domain of Cardiac Troponin C. *Journal of Biological Chemistry*, 274(24), 16681–16684. <https://doi.org/10.1074/jbc.274.24.16681>
- Gasmi-Seabrook, G. M. C., Howarth, J. W., Finley, N., Abusamhadneh, E., Gaponenko, V., Brito, R. M. M., ... Rosevear, P. R. (1999). Solution Structures of the C-Terminal Domain of Cardiac Troponin C Free and Bound to the N-Terminal Domain of Cardiac Troponin I[†]·[‡]. *Biochemistry*, 38(26), 8313–8322. <https://doi.org/10.1021/bi9902642>
- Geeves, M. A., & Holmes, K. C. (2005). The molecular mechanism of muscle

- contraction. *Advances in Protein Chemistry*, 71(04), 161–193.
[https://doi.org/10.1016/S0065-3233\(04\)71005-0](https://doi.org/10.1016/S0065-3233(04)71005-0)
- Gifford, J. L., Walsh, M. P., & Vogel, H. J. H. J. Structures and metal-ion-binding properties of the Ca²⁺-binding helix-loop-helix EF-hand motifs., 405 *The Biochemical journal* § (2007). Portland Press Limited.
<https://doi.org/10.1042/BJ20070255>
- Gillis, T. E., Blumenschein, A., T. M., Sykes, B. D., & Tibbits, G. F. (2003). Effect of Temperature and the F27W Mutation on the Ca²⁺ Activated Structural Transition of Trout Cardiac Troponin C†. *Biochemistry*, 42, 6418–6426.
<https://doi.org/10.1021/BI0340494>
- Gomes, A. V, Harada, K., & Potter, J. D. (2005). A mutation in the N-terminus of troponin I that is associated with hypertrophic cardiomyopathy affects the Ca(2+)-sensitivity, phosphorylation kinetics and proteolytic susceptibility of troponin. *Journal of Molecular and Cellular Cardiology*, 39(5), 754–765.
<https://doi.org/10.1016/j.yjmcc.2005.05.013>
- Gordon, A. M., Homsher, E., & Regnier, M. (2000). Regulation of contraction in striated muscle. *Physiological Reviews*, 80(2), 853–924.
<https://doi.org/10.1152/physrev.2000.80.2.853>
- Greaser, M. L., & Gergely, J. (1973). Purification and properties of the components from tropinin. *Journal of Biological Chemistry*, 248(6), 2125–2133.
- Grossini, E., Molinari, C., Caimmi, P. P., Uberti, F., & Vacca, G. (2009). Levosimendan induces NO production through p38 MAPK, ERK and Akt in porcine coronary endothelial cells: role for mitochondrial K(ATP) channel. *British Journal of Pharmacology*, 156(2), 250–261.
<https://doi.org/10.1111/j.1476-5381.2008.00024.x>
- Guo, K., & Li, L. (2009). Differential 12C-/13C-isotope dansylation labeling and fast liquid chromatography/mass spectrometry for absolute and relative quantification of the metabolome. *Analytical Chemistry*, 81(10), 3919–3932.
<https://doi.org/10.1021/ac900166a>
- Hafsa, N. E., Arndt, D., & Wishart, D. S. (2015). CSI 3.0: A web server for identifying secondary and super-secondary structure in proteins using NMR chemical shifts.

- Nucleic Acids Research*, 43(W1), W370–W377.
<https://doi.org/10.1093/nar/gkv494>
- Hagberg, D. P., Marinado, T., Karlsson, K. M., Nonomura, K., Qin, P., Boschloo, G., ... Sun, L. (2007). Tuning the HOMO and LUMO energy levels of organic chromophores for dye sensitized solar cells. *Journal of Organic Chemistry*, 72(25), 9550–9556. <https://doi.org/10.1021/jo701592x>
- Haikala, H., Kaivola, J., Nissinen, E., Wall, Pz., Levijoki, J., & Lindin, I.-B. (1995). Cardiac troponin C as a target protein for a novel calcium sensitizing drug, levosimendan. *Journal of Molecular and Cellular Cardiology*, 27(9), 1859–1866. [https://doi.org/10.1016/0022-2828\(95\)90009-8](https://doi.org/10.1016/0022-2828(95)90009-8)
- Hamdani, N., Paulus, W. J., van Heerebeek, L., Borbély, A., Boontje, N. M., Zuidwijk, M. J., ... van der Velden, J. (2009). Distinct myocardial effects of beta-blocker therapy in heart failure with normal and reduced left ventricular ejection fraction. *European Heart Journal*, 30(15), 1863–1872. <https://doi.org/10.1093/eurheartj/ehp189>
- Hanft, L. M., Biesiadecki, B. J., & McDonald, K. S. (2013). Length dependence of striated muscle force generation is controlled by phosphorylation of cTnI at serines 23/24. *The Journal of Physiology*, 591(18), 4535–4547. <https://doi.org/10.1113/jphysiol.2013.258400>
- Henze, M., Patrick, S. E., Hinken, A., Scruggs, S. B., Goldspink, P., de Tombe, P. P., ... Solaro, R. J. (2013). New insights into the functional significance of the acidic region of the unique N-terminal extension of cardiac troponin I. *Biochimica et Biophysica Acta - Molecular Cell Research*, 1833(4), 823–832. <https://doi.org/10.1016/j.bbamcr.2012.08.012>
- Hidaka, Hiroyoshi, Asano, M., Iwadare, S., Matsumoto, I., Totsuka, T., & Aoki, N. (1978). A Novel Vascular Relaxing Agent, N-(6-Aminohexyl)-5-Chloro-1-Naphthalenesulfonamide Which Affects Vascular Smooth Muscle Actomyosin. *The Journal of Pharmacology and Experimental Therapeutics*, 207(1), 8–15.
- Hidaka, HIROYOSHI, Yamaki, T., Naka, M., Tanaka, T., Hayashi, H., & Kobayashi, R. (1980). Calcium-regulated modulator protein interacting agents inhibit smooth muscle calcium-stimulated protein kinase and ATPase. *Molecular Pharmacology*,

17(1), 66–72.

- Hinken, A. C., Hanft, L. M., Scruggs, S. B., Sadayappan, S., Robbins, J., Solaro, R. J., & McDonald, K. S. (2012). Protein kinase C depresses cardiac myocyte power output and attenuates myofilament responses induced by protein kinase A. *Journal of Muscle Research and Cell Motility*, 33(6), 439–448. <https://doi.org/10.1007/s10974-012-9294-9>
- Hoffman, R. M. B., Li, M. X., & Sykes, B. D. (2005). The binding of W7, an inhibitor of striated muscle contraction, to cardiac troponin C. *Biochemistry*, 44(48), 15750–15759. <https://doi.org/10.1021/bi051583y>
- Hoffman, R. M. B., & Sykes, B. D. (2009). Structure of the Inhibitor W7 Bound to the Regulatory Domain of Cardiac Troponin C. *Biochemistry*, 48(24), 5541–5552. <https://doi.org/10.1021/bi9001826>
- Houdusse, A., Love, M. L., Dominguez, R., Grabarek, Z., & Cohen, C. (1997). Structures of four Ca²⁺-bound troponin C at 2.0 Å resolution: further insights into the Ca²⁺-switch in the calmodulin superfamily. *Structure*, 5(12), 1695–1711. [https://doi.org/10.1016/S0969-2126\(97\)00315-8](https://doi.org/10.1016/S0969-2126(97)00315-8)
- Howarth, J. W., Meller, J., Solaro, R. J., Trehwella, J., & Rosevear, P. R. (2007). Phosphorylation-dependent conformational transition of the cardiac specific N-extension of troponin I in cardiac troponin. *Journal of Molecular Biology*, 373(3), 706–722. <https://doi.org/10.1016/j.jmb.2007.08.035>
- HUXLEY, H., & HANSON, J. (1954). Changes in the Cross-Striations of Muscle during Contraction and Stretch and their Structural Interpretation. *Nature*, 173(4412), 973–976. <https://doi.org/10.1038/173973a0>
- Hwang, P. M., Cai, F., Pineda-Sanabria, S. E., Corson, D. C., & Sykes, B. D. (2014). The cardiac-specific N-terminal region of troponin I positions the regulatory domain of troponin C. *Proceedings of the National Academy of Sciences of the United States of America*, 111(40), 14412–14417. <https://doi.org/10.1073/pnas.1410775111>
- Hwang, P. M., Pan, J. S., & Sykes, B. D. (2012). A PagP fusion protein system for the expression of intrinsically disordered proteins in Escherichia coli. *Protein Expression and Purification*, 85(1), 148–151.

<https://doi.org/10.1016/j.pep.2012.07.007>

- Hwang, P. M., & Sykes, B. D. (2015). Targeting the sarcomere to correct muscle function. *Nat Rev Drug Discov*, *14*(5), 313–328. <https://doi.org/10.1038/nrd4554>
- Hyberts, S. G., Arthanari, H., & Wagner, G. (2011). Applications of Non-Uniform Sampling and Processing. In *Topics in Current Chemistry* (Vol. 316, pp. 125–148). https://doi.org/10.1007/128_2011_187
- Iakoucheva, L. M. (2004). The importance of intrinsic disorder for protein phosphorylation. *Nucleic Acids Research*, *32*(3), 1037–1049. <https://doi.org/10.1093/nar/gkh253>
- Johnson, B. A., & Blevins, R. A. (1994). NMR View: A computer program for the visualization and analysis of NMR data. *Journal of Biomolecular NMR*, *4*(5), 603–614. <https://doi.org/10.1007/BF00404272>
- Julien, O., Mercier, P., Allen, C. N., Fiset, O., Ramos, C. H. I. I., Lagüe, P., ... Lagu, P. (2011). Is there nascent structure in the intrinsically disordered region of troponin I? *Proteins*, *79*(4), 1240–1250. <https://doi.org/10.1002/prot.22959>
- Kampourakis, T., Yan, Z., Gautel, M., Sun, Y.-B., & Irving, M. (2014). Myosin binding protein-C activates thin filaments and inhibits thick filaments in heart muscle cells. *Proceedings of the National Academy of Sciences of the United States of America*, *111*(52), 18763–18768. <https://doi.org/10.1073/pnas.1413922112>
- Kass, D. A., & Solaro, R. J. (2006). Mechanisms and use of calcium-sensitizing agents in the failing heart. *Circulation*, *113*, 305–315. <https://doi.org/10.1161/CIRCULATIONAHA.105.542407>
- Kato, K. (1997). Clinical Efficacy and Safety of Pimobendan in Treatment of Heart Failure – Experience in Japan. *Cardiology*, *88*(2), 28–36. <https://doi.org/10.1159/000177482>
- Kleerekoper, Q., Liu, W., Choi, D., & Putkey, J. A. (1998). Identification of binding sites for bepridil and trifluoperazine on cardiac troponin C. *Journal of Biological Chemistry*, *273*(14), 8153–8160. <https://doi.org/10.1074/jbc.273.14.8153>
- Klein, B. A., Reiz, B., Robertson, I. M., Irving, M., Li, L., Sun, Y.-B. B., & Sykes, B. D. (2018). Reversible Covalent Reaction of Levosimendan with Cardiac Troponin C in Vitro and in Situ. *Biochemistry*, *57*(15), 2256–2265.

<https://doi.org/10.1021/acs.biochem.8b00109>

- Klein, B. A., Robertson, I. M., Reiz, B., Kampourakis, T., Li, L., & Sykes, B. D. (2019). Thioimidate Bond Formation between Cardiac Troponin C and Nitrile-containing Compounds. *ACS Medicinal Chemistry Letters*, *10*(6), 1007–1012. <https://doi.org/10.1021/acsmchemlett.9b00168>
- Kleywegt, G. J. (1995). Dictionaries for Heteros. *CCP4/ESF- EACBM Newsletter on Protein Crystallography*, *31*, 45–50. Retrieved from http://xray.bmc.uu.se/usf/factory_5.html
- Kobayashi, T., Jin, L., & de Tombe, P. P. (2008). Cardiac thin filament regulation. *Pflügers Archiv - European Journal of Physiology*, *457*(1), 37–46. <https://doi.org/10.1007/s00424-008-0511-8>
- Li, M. X., Hoffman, R. M. B., & Sykes, B. D. (2006). Interaction of Cardiac Troponin C and Troponin I with W7 in the Presence of Three Functional Regions of Cardiac Troponin I †. *Biochemistry*, *45*(32), 9833–9840. <https://doi.org/10.1021/bi060779a>
- Li, M. X., & Hwang, P. M. (2015). Structure and function of cardiac troponin C (TNNC1): Implications for heart failure, cardiomyopathies, and troponin modulating drugs. *Gene*, *571*(2), 153–166. <https://doi.org/10.1016/j.gene.2015.07.074>
- Li, M. X., Saude, E. J., Wang, X., Pearlstone, J. R., Smillie, L. B., & Sykes, B. D. (2002). Kinetic studies of calcium and cardiac troponin I peptide binding to human cardiac troponin C using NMR spectroscopy. *European Biophysics Journal : EBJ*, *31*(4), 245–256. <https://doi.org/10.1007/s00249-002-0227-1>
- Li, M. X., Spyrapoulos, L., & Sykes, B. D. (1999a). Binding of Cardiac Troponin-I 147-163 Induces a Structural Opening in Human Cardiac Troponin-C † , ‡. *Biochemistry*, *38*(26), 8289–8298. <https://doi.org/10.1021/bi9901679>
- Li, M. X., Spyrapoulos, L., & Sykes, B. D. (1999b). Binding of cardiac troponin-I147-163 induces a structural opening in human cardiac troponin-C. *Biochemistry*, *38*(26), 8289–8298. <https://doi.org/10.1021/bi9901679>
- Li, M. X., Wang, X., & Sykes, B. D. (2004). Structural based insights into the role of troponin in cardiac muscle pathophysiology. *Journal of Muscle Research and Cell*

- Motility*, 25(7), 559–579. <https://doi.org/10.1007/s10974-004-5879-2>
- Li, Q., & Kang, C. B. (2020). A practical perspective on the roles of solution NMR spectroscopy in drug discovery. *Molecules*, 25(13), 1–19. <https://doi.org/10.3390/molecules25132974>
- Li, Y., Love, M. L., Putkey, J. A., & Cohen, C. (2000). Bepridil opens the regulatory N-terminal lobe of cardiac troponin C. *Proceedings of the National Academy of Sciences of the United States of America*, 97(10), 5140–5145. <https://doi.org/10.1073/pnas.090098997>
- Lindert, S., Li, M. X., Sykes, B. D., & McCammon, J. A. (2015). Computer-Aided Drug Discovery Approach Finds Calcium Sensitizer of Cardiac Troponin. *Chemical Biology & Drug Design*, 85(2), 99–106. <https://doi.org/10.1111/cbdd.12381>
- Lindert, S., Zhu, W., Liu, Y.-L., Pang, R., Oldfield, E., & McCammon, J. A. (2013). Farnesyl diphosphate synthase inhibitors from in silico screening. *Chemical Biology & Drug Design*, 81(6), 742–748. <https://doi.org/10.1111/cbdd.12121>
- Lindhout, D. A., & Sykes, B. D. (2003). Structure and Dynamics of the C-domain of Human Cardiac Troponin C in Complex with the Inhibitory Region of Human Cardiac Troponin I. *Journal of Biological Chemistry*, 278(29), 27024–27034. <https://doi.org/10.1074/jbc.M302497200>
- Linge, J. P., Habeck, M., Rieping, W., & Nilges, M. (2003). ARIA: automated NOE assignment and NMR structure calculation. *Bioinformatics (Oxford, England)*, 19(2), 315–316. <https://doi.org/10.1093/bioinformatics/19.2.315>
- Lipari, G., & Szabo, A. (1982). Model-free approach to the interpretation of nuclear magnetic resonance relaxation in macromolecules. 1. Theory and range of validity. *Journal of the American Chemical Society*, 104(17), 4546–4559. <https://doi.org/10.1021/ja00381a009>
- Lubsen, J., Just, H., Hjalmarsson, A. C., La Framboise, D., Remme, W. J., Heinrich-Nols, J., ... Seed, P. (1996). Effect of pimobendan on exercise capacity in patients with heart failure: main results from the Pimobendan in Congestive Heart Failure (PICO) trial. *Heart*, 76(3), 223–231. <https://doi.org/10.1136/hrt.76.3.223>
- Lugnier, C., Follenius, A., Gerard, D., & Stoclet, J. C. (1984). Bepridil and flunarizine

- as calmodulin inhibitors. *European Journal of Pharmacology*, 98(1), 157–158.
[https://doi.org/10.1016/0014-2999\(84\)90128-6](https://doi.org/10.1016/0014-2999(84)90128-6)
- Malik, F. I., Hartman, J. J., Elias, K. A., Morgan, B. P., Rodriguez, H., Brejc, K., ... Morgans, D. J. (2011). Cardiac Myosin Activation: A Potential Therapeutic Approach for Systolic Heart Failure. *Science*, 331(6023), 1439–1443.
<https://doi.org/10.1126/science.1200113>
- Marieb, E. N., & Hoehn, K. (2013). *Human Anatomy and Physiology Ninth Edition*. Pearson Education.
- Marion, D. (2013). An introduction to biological NMR spectroscopy. *Molecular and Cellular Proteomics*, 12(11), 3006–3025.
<https://doi.org/10.1074/mcp.O113.030239>
- Mateja, R. D., & de Tombe, P. P. (2012). Myofilament length-dependent activation develops within 5 ms in guinea-pig myocardium. *Biophysical Journal*, 103(1), L13-5. <https://doi.org/10.1016/j.bpj.2012.05.034>
- McKay, R. T., Tripet, B. P., Hodges, R. S., & Sykes, B. D. (1997). Interaction of the Second Binding Region of Troponin I with the Regulatory Domain of Skeletal Muscle Troponin C as Determined by NMR Spectroscopy. *Journal of Biological Chemistry*, 272(45), 28494–28500. <https://doi.org/10.1074/jbc.272.45.28494>
- McKillop, D. F., & Geeves, M. A. (1993). Regulation of the interaction between actin and myosin subfragment 1: evidence for three states of the thin filament. *Biophysical Journal*, 65(2), 693–701. [https://doi.org/10.1016/S0006-3495\(93\)81110-X](https://doi.org/10.1016/S0006-3495(93)81110-X)
- Mebazaa, A., Nieminen, M. S., Packer, M., Cohen-Solal, A., Kleber, F. X., Pocock, S. J., ... A, B. (2007). Levosimendan vs Dobutamine for Patients With Acute Decompensated Heart Failure. *JAMA*, 297(17), 1883.
<https://doi.org/10.1001/jama.297.17.1883>
- Memo, M., Leung, M.-C., Ward, D. G., dos Remedios, C., Morimoto, S., Zhang, L., ... Messer, A. E. (2013). Familial dilated cardiomyopathy mutations uncouple troponin I phosphorylation from changes in myofibrillar Ca²⁺ sensitivity. *Cardiovascular Research*, 99(1), 65–73. <https://doi.org/10.1093/cvr/cvt071>
- Michaels, A. D., McKeown, B., Kostal, M., Vakharia, K. T., Jordan, M. V., Gerber, I.

- L., ... Chatterjee, K. (2005). Effects of Intravenous Levosimendan on Human Coronary Vasomotor Regulation, Left Ventricular Wall Stress, and Myocardial Oxygen Uptake. *Circulation*, *111*(12), 1504–1509. <https://doi.org/10.1161/01.CIR.0000159252.82444.22>
- Mittag, T., Orlicky, S., Choy, W.-Y., Tang, X., Lin, H., Sicheri, F., ... Forman-Kay, J. D. (2008). Dynamic equilibrium engagement of a polyvalent ligand with a single-site receptor. *Proceedings of the National Academy of Sciences of the United States of America*, *105*(46), 17772–17777. <https://doi.org/10.1073/pnas.0809222105>
- Morgan, B. P., Muci, A., Lu, P. P., Qian, X., Tochimoto, T., Smith, W. W., ... Morgans, D. J. (2010). Discovery of omecamtiv mecarbil the first, selective, small molecule activator of cardiac myosin. *ACS Medicinal Chemistry Letters*, *1*(9), 472–477. <https://doi.org/10.1021/ml100138q>
- Narita, A., Yasunaga, T., Ishikawa, T., Mayanagi, K., & Wakabayashi, T. (2001). Ca²⁺-induced switching of troponin and tropomyosin on actin filaments as revealed by electron cryo-microscopy¹ Edited by A. Klug. *Journal of Molecular Biology*, *308*(2), 241–261. <https://doi.org/10.1006/jmbi.2001.4598>
- Neri, D., Szyperski, T., Otting, G., Senn, H., & Wüthrich, K. (1989). Stereospecific Nuclear Magnetic Resonance Assignments of the Methyl Groups of Valine and Leucine in the DNA-Binding Domain of the 434 Repressor by Biosynthetically Directed Fractional ¹³C Labeling. *Biochemistry*, *28*(19), 7510–7516. <https://doi.org/10.1021/bi00445a003>
- Nieminen, M. S., Fruhwald, S., Heunks, L. M. A., Suominen, P. K., Gordon, A. C., Kivikko, M., & Pollesello, P. (2013). Levosimendan: current data, clinical use and future development. *Heart, Lung and Vessels*, *5*(4), 227–245. Retrieved from <https://pubmed.ncbi.nlm.nih.gov/24364017/>
- Oleszczuk, M., Robertson, I. M., Li, M. X., & Sykes, B. D. (2010). Solution structure of the regulatory domain of human cardiac troponin C in complex with the switch region of cardiac troponin I and W7: The basis of W7 as an inhibitor of cardiac muscle contraction. *Journal of Molecular and Cellular Cardiology*, *48*(5), 925–933. <https://doi.org/10.1016/j.yjmcc.2010.01.016>

- Olson, C. B., & Waud, D. R. (1970). On Looking at Electrical Activity of Heart Muscle. *Anesthesiology*, 33(5), 520–533. <https://doi.org/10.1097/00000542-197011000-00015>
- Opie, L. H. (2003). *Heart Physiology: From Cell to Circulation Fourth Edition*. Lippincott Williams & Wilkins.
- Orts, J., & Gossert, A. D. (2018). Structure determination of protein-ligand complexes by NMR in solution. *Methods*, 138–139, 3–25. <https://doi.org/10.1016/j.ymeth.2018.01.019>
- Papp, Z., Agostoni, P., Alvarez, J., Bettex, D., Bouchez, S., Brito, D., ... Édes, I. (2020). Pharmacological Therapy Levosimendan Efficacy and Safety : 20 years of SIMDAX in Clinical Use Pharmacological Therapy.
- Papp, Z., Édes, I., Fruhwald, S., De Hert, S. G., Salmenperä, M., Leppikangas, H., ... Follath, F. (2012). Levosimendan: molecular mechanisms and clinical implications: consensus of experts on the mechanisms of action of levosimendan. *International Journal of Cardiology*, 159(2), 82–87. <https://doi.org/10.1016/j.ijcard.2011.07.022>
- Parry, D. A. D., & Squire, J. M. (1973). Structural role of tropomyosin in muscle regulation: Analysis of the X-ray diffraction patterns from relaxed and contracting muscles. *Journal of Molecular Biology*, 75(1), 33–55. [https://doi.org/10.1016/0022-2836\(73\)90527-5](https://doi.org/10.1016/0022-2836(73)90527-5)
- Parvatiyar, M. S., Pinto, J. R., Dweck, D., & Potter, J. D. (2010). Cardiac Troponin Mutations and Restrictive Cardiomyopathy. *Journal of Biomedicine and Biotechnology*, 2010, 1–9. <https://doi.org/10.1155/2010/350706>
- Pellecchia, M., Bertini, I., Cowburn, D., Dalvit, C., Giralt, E., Jahnke, W., ... Siegal, G. (2008). Perspectives on NMR in drug discovery: a technique comes of age. *Nature Reviews Drug Discovery*, 7(9), 738–745. <https://doi.org/10.1038/nrd2606>
- Pineda-Sanabria, S. E., Julien, O., & Sykes, B. D. (2014). Versatile Cardiac Troponin Chimera for Muscle Protein Structural Biology and Drug Discovery. *ACS Chemical Biology*, 9(9), 2121–2130. <https://doi.org/10.1021/cb500249j>
- Pineda-Sanabria, S. E., Robertson, I. M., Sun, Y.-B. B., Irving, M., & Sykes, B. D. (2016). Probing the mechanism of cardiovascular drugs using a covalent

- levosimendan analog. *Journal of Molecular and Cellular Cardiology*, 92, 174–184. <https://doi.org/10.1016/j.yjmcc.2016.02.003>
- Pollesello, P., Papp, Z., & Papp, J. G. (2016). Calcium sensitizers: What have we learned over the last 25 years? *International Journal of Cardiology*, 203, 543–548. <https://doi.org/10.1016/j.ijcard.2015.10.240>
- Pollesello, P., Ovaskas, M., Kaivolai, J., Tilgmanns, C., Lundstroms, K., Kalkkinenn, N., ... Taskinens, J. (1994). Binding of a new Ca²⁺ sensitizer, levosimendan, to recombinant human cardiac troponin C. *The Journal of Biological Chemistry*, 269(46), 28584–28590. Retrieved from <http://www.ncbi.nlm.nih.gov/pubmed/7961805>
- Porumb, T., Yau, P., Harvey, T. S., & Ikura, M. (1994). A calmodulin-target peptide hybrid molecule with unique calcium-binding properties. *Protein Engineering*, 7(1), 109–115. Retrieved from <http://www.ncbi.nlm.nih.gov/pubmed/8140087>
- Potter, J. D., & Gergely, J. (1975). The calcium and magnesium binding sites on troponin and their role in the regulation of myofibrillar adenosine triphosphatase. *The Journal of Biological Chemistry*, 250(12), 4628–4633. Retrieved from <http://www.ncbi.nlm.nih.gov/pubmed/124731>
- Reina-Doreste, Y., Stern, J. A., Keene, B. W., Tou, S. P., Atkins, C. E., DeFrancesco, T. C., ... Meurs, K. M. (2014). Case-control study of the effects of pimobendan on survival time in cats with hypertrophic cardiomyopathy and congestive heart failure. *Journal of the American Veterinary Medical Association*, 245(5), 534–539. <https://doi.org/10.2460/javma.245.5.534>
- Rezvanpour, A., Phillips, J. M., & Shaw, G. S. (2009). Design of high-affinity S100-target hybrid proteins. *Protein Science: A Publication of the Protein Society*, 18(12), 2528–2536. <https://doi.org/10.1002/pro.267>
- Rieping, W., Habeck, M., Bardiaux, B., Bernard, A., Malliavin, T. E., & Nilges, M. (2007). ARIA2: Automated NOE assignment and data integration in NMR structure calculation. *Bioinformatics*, 23(3), 381–382. <https://doi.org/10.1093/bioinformatics/btl589>
- Robertson, I. M., Baryshnikova, O. K., Li, M. X., & Sykes, B. D. (2008). Defining the binding site of levosimendan and its analogues in a regulatory cardiac troponin C-

- troponin I complex. *Biochemistry*, 47(28), 7485–7495. <https://doi.org/10.1021/bi800438k>
- Robertson, I. M., Boyko, R. F., & Sykes, B. D. (2011). Visualizing the principal component of ^1H , ^{15}N -HSQC NMR spectral changes that reflect protein structural or functional properties: application to troponin C. *Journal of Biomolecular NMR*, 51(1–2), 115–122. <https://doi.org/10.1007/s10858-011-9546-9>
- Robertson, I. M., Li, M. X., & Sykes, B. D. (2009). Solution structure of human cardiac troponin C in complex with the green tea polyphenol, (-)-epigallocatechin 3-gallate. *Journal of Biological Chemistry*, 284(34), 23012–23023. <https://doi.org/10.1074/jbc.M109.021352>
- Robertson, I. M., Pineda-Sanabria, S. E., Yan, Z., Kampourakis, T., Sun, Y.-B. B., Sykes, B. D., & Irving, M. (2016a). Reversible Covalent Binding to Cardiac Troponin C by the Ca^{2+} -Sensitizer Levosimendan. *Biochemistry*, 55(43), 6032–6045. <https://doi.org/10.1021/acs.biochem.6b00758>
- Robertson, I. M., Pineda-Sanabria, S. E., Yan, Z., Kampourakis, T., Sun, Y.-B., Sykes, B. D., & Irving, M. (2016b). Reversible Covalent Binding to Cardiac Troponin C by the Ca^{2+} -Sensitizer Levosimendan. *Biochemistry*, 55(43), 6032–6045. <https://doi.org/10.1021/acs.biochem.6b00758>
- Robertson, I. M., Sevrieva, I., Li, M. X., Irving, M., Sun, Y.-B. B., & Sykes, B. D. (2015). The structural and functional effects of the familial hypertrophic cardiomyopathy-linked cardiac troponin C mutation, L29Q. *Journal of Molecular and Cellular Cardiology*, 87, 257–269. <https://doi.org/10.1016/j.yjmcc.2015.08.017>
- Robertson, I. M., Sun, Y.-B. B., Li, M. X., & Sykes, B. D. (2010). A structural and functional perspective into the mechanism of Ca^{2+} -sensitizers that target the cardiac troponin complex. *Journal of Molecular and Cellular Cardiology*, 49(6), 1031–1041. <https://doi.org/10.1016/j.yjmcc.2010.08.019>
- Rüegg, J. C., Pfitzer, G., Eubler, D., & Zeugner, C. (1984). Effect on contractility of skinned fibres from mammalian heart and smooth muscle by a new benzimidazole derivative, 4,5-dihydro-6-[2-(4-methoxyphenyl)-1H-benzimidazol-5-yl]-5-methyl-3(2H)-pyridazinone. *Arzneimittel-Forschung*, 34(12), 1736–1738. Retrieved

- from <http://www.ncbi.nlm.nih.gov/pubmed/6543308>
- Russell, A. J., Hartman, J. J., Hinken, A. C., Muci, A. R., Kawas, R., Driscoll, L., ... Malik, F. I. (2012). Activation of fast skeletal muscle troponin as a potential therapeutic approach for treating neuromuscular diseases. *Nature Medicine*, *18*(3), 452–455. <https://doi.org/10.1038/nm.2618>. Activation
- Satyshur, K. A., Rao, S. T., Pyzalska, D., Drendel, W., Greaser, M., & Sundaralingam, M. (1988). Refined structure of chicken skeletal muscle troponin C in the two-calcium state at 2-Å resolution. *The Journal of Biological Chemistry*, *263*(4), 1628–1647. Retrieved from <http://www.ncbi.nlm.nih.gov/pubmed/3338985>
- Schüttelkopf, A. W., & van Aalten, D. M. F. (2004a). PRODRG: a tool for high-throughput crystallography of protein–ligand complexes. *Acta Crystallographica Section D Biological Crystallography*, *60*(Pt 8), 1355–1363. <https://doi.org/10.1107/S0907444904011679>
- Schüttelkopf, A. W., & van Aalten, D. M. F. (2004b). PRODRG: a tool for high-throughput crystallography of protein–ligand complexes. *Acta Crystallographica Section D, Biological Crystallography*, *60*(Pt 8), 1355–1363. <https://doi.org/10.1107/S0907444904011679>
- Schwieters, C. D., Kuszewski, J. J., Tjandra, N., & Clore, G. M. (2003). The Xplor-NIH NMR molecular structure determination package. *Journal of Magnetic Resonance*, *160*(1), 65–73. [https://doi.org/10.1016/S1090-7807\(02\)00014-9](https://doi.org/10.1016/S1090-7807(02)00014-9)
- Severs, N. J. (2000). The cardiac muscle cell. *BioEssays*, *22*(2), 188–199. [https://doi.org/10.1002/\(SICI\)1521-1878\(200002\)22:2<188::AID-BIES10>3.0.CO;2-T](https://doi.org/10.1002/(SICI)1521-1878(200002)22:2<188::AID-BIES10>3.0.CO;2-T)
- Sharma, K., & Kass, D. A. (2014). Heart failure with preserved ejection fraction: mechanisms, clinical features, and therapies. *Circulation Research*, *115*(1), 79–96. <https://doi.org/10.1161/CIRCRESAHA.115.302922>
- Shen, Y., & Bax, A. (2012). Identification of helix capping and b-turn motifs from NMR chemical shifts. *Journal of Biomolecular NMR*, *52*(3), 211–232. <https://doi.org/10.1007/s10858-012-9602-0>
- Shen, Y., Delaglio, F., Cornilescu, G., & Bax, A. (2009). TALOS+: A hybrid method for predicting protein backbone torsion angles from NMR chemical shifts. *Journal*

- of Biomolecular NMR*, 44(4), 213–223. <https://doi.org/10.1007/s10858-009-9333-z>
- Sia, S. K., Li, M. X., Spyropoulos, L., Gagné, S. M., Liu, W., Putkey, J. A., & Sykes, B. D. (1997). Structure of Cardiac Muscle Troponin C Unexpectedly Reveals a Closed Regulatory Domain. *Journal of Biological Chemistry*, 272(29), 18216–18221. <https://doi.org/10.1074/jbc.272.29.18216>
- Sisakian, H. (2014). Cardiomyopathies: Evolution of pathogenesis concepts and potential for new therapies. *World Journal of Cardiology*, 6(6), 478–494. <https://doi.org/10.4330/wjc.v6.i6.478>
- Slupsky, C. M., & Sykes, B. D. (1995). NMR solution structure of calcium-saturated skeletal muscle troponin C. *Biochemistry*, 34(49), 15953–15964. <https://doi.org/10.1021/bi00049a010>
- Solaro, R. J., Moir, A. J. G., & Perry, S. V. (1976). Phosphorylation of troponin I and the inotropic effect of adrenaline in the perfused rabbit heart. *Nature*, 262(5569), 615–617. <https://doi.org/10.1038/262615a0>
- Solaro, R J, Bousquet, P., & Johnson, J. D. (1986). Stimulation of cardiac myofilament force, ATPase activity and troponin C Ca⁺⁺ binding by bepridil. *The Journal of Pharmacology and Experimental Therapeutics*, 238(2), 502–507. Retrieved from <http://www.ncbi.nlm.nih.gov/pubmed/2942677>
- Solaro, R J, Fujino, K., & Sperelakis, N. (1989). The positive inotropic effect of pimobendan involves stereospecific increases in the calcium sensitivity of cardiac myofilaments. *Journal of Cardiovascular Pharmacology*, 14 Suppl 2, S7-12. Retrieved from <http://www.ncbi.nlm.nih.gov/pubmed/2478795>
- Solaro, R John, Henze, M., & Kobayashi, T. (2013). Integration of troponin I phosphorylation with cardiac regulatory networks. *Circulation Research*, 112(2), 355–366. <https://doi.org/10.1161/CIRCRESAHA.112.268672>
- Solaro, R John, & van der Velden, J. (2010). Why does troponin I have so many phosphorylation sites? Fact and fancy. *Journal of Molecular and Cellular Cardiology*, 48(5), 810–816. <https://doi.org/10.1016/j.yjmcc.2010.02.014>
- Sonnenblick, E. H., Frishman, W. H., & LeJemtel, T. H. (1979). Dobutamine: a new synthetic cardioactive sympathetic amine. *The New England Journal of Medicine*,

- 300(1), 17–22. <https://doi.org/10.1056/NEJM197901043000105>
- Sorsa, T., Pollesello, P., Permi, P., Drakenberg, T., & Kilpeläinen, I. (2003). Interaction of levosimendan with cardiac troponin C in the presence of cardiac troponin I peptides. *Journal of Molecular and Cellular Cardiology*, 35(9), 1055–1061. [https://doi.org/10.1016/S0022-2828\(03\)00178-0](https://doi.org/10.1016/S0022-2828(03)00178-0)
- Sorsa, Tia, Heikkinen, S., Abbott, M. B., Abusamhadneh, E., Laakso, T., Tilgmann, C., ... Kilpeläinen, I. (2001). Binding of Levosimendan, a Calcium Sensitizer, to Cardiac Troponin C. *Journal of Biological Chemistry*, 276(12), 9337–9343. <https://doi.org/10.1074/jbc.M007484200>
- Spyracopoulos, L., Li, M. X., Sia, S. K., Gagné, S. M., Chandra, M., Solaro, R. J., & Sykes, B. D. (1997). Calcium-induced structural transition in the regulatory domain of human cardiac troponin C. *Biochemistry*, 36(40), 12138–12146. <https://doi.org/10.1021/bi971223d>
- Strynadka, N. C., Cherney, M., Sielecki, A. R., Li, M. X., Smillie, L. B., & James, M. N. (1997). Structural details of a calcium-induced molecular switch: X-ray crystallographic analysis of the calcium-saturated N-terminal domain of troponin C at 1.75 Å resolution. *Journal of Molecular Biology*, 273(1), 238–255. <https://doi.org/10.1006/jmbi.1997.1257>
- Sundaralingam, M., Bergstrom, R., Strasburg, G., Rao, S. T., Roychowdhury, P., Greaser, M., & Wang, B. C. (1985). Molecular structure of troponin C from chicken skeletal muscle at 3-angstrom resolution. *Science (New York, N.Y.)*, 227(4689), 945–948.
- Szilágyi, S., Pollesello, P., Levijoki, J., Kaheinen, P., Haikala, H., Édes, I., & Papp, Z. (2004). The effects of levosimendan and OR-1896 on isolated hearts, myocyte-sized preparations and phosphodiesterase enzymes of the guinea pig. *European Journal of Pharmacology*, 486(1), 67–74. <https://doi.org/10.1016/j.ejphar.2003.12.005>
- Takeda, S., Yamashita, A., Maeda, K., & Maéda, Y. (2003). Structure of the core domain of human cardiac troponin in the Ca²⁺-saturated form. *Nature*, 424(6944), 35–41. <https://doi.org/10.1038/nature01780>
- Tang, X., Orlicky, S., Mittag, T., Csizmok, V., Pawson, T., Forman-Kay, J. D., ...

- Tyers, M. (2012). Composite low affinity interactions dictate recognition of the cyclin-dependent kinase inhibitor Sic1 by the SCFCdc4 ubiquitin ligase. *Proceedings of the National Academy of Sciences of the United States of America*, *109*(9), 3287–3292. <https://doi.org/10.1073/pnas.1116455109>
- Teerlink, J. R., Clarke, C. P., Saikali, K. G., Lee, J. H., Chen, M. M., Escandon, R. D., ... Wolff, A. A. (2011). Dose-dependent augmentation of cardiac systolic function with the selective cardiac myosin activator, omecamtiv mecarbil: A first-in-man study. *The Lancet*, *378*(9792), 667–675. [https://doi.org/10.1016/S0140-6736\(11\)61219-1](https://doi.org/10.1016/S0140-6736(11)61219-1)
- Teerlink, J. R., Diaz, R., Felker, G. M., McMurray, J. J. V., Metra, M., Solomon, S. D., ... Honarpour, N. (2020). Omecamtiv Mecarbil in Chronic Heart Failure With Reduced Ejection Fraction: Rationale and Design of GALACTIC-HF. *JACC: Heart Failure*, *8*(4), 329–340. <https://doi.org/10.1016/j.jchf.2019.12.001>
- Teerlink, J. R., Felker, G. M., McMurray, J. J. V., Ponikowski, P., Metra, M., Filippatos, G. S., ... Wasserman, S. M. (2016). Acute Treatment with Omecamtiv Mecarbil to Increase Contractility in Acute Heart Failure: The ATOMIC-AHF Study. *Journal of the American College of Cardiology*, *67*(12), 1444–1455. <https://doi.org/10.1016/j.jacc.2016.01.031>
- Teerlink, J. R., Felker, G. M., McMurray, J. J. V., Solomon, S. D., Adams, K. F., Cleland, J. G. F., ... Honarpour, N. (2016). Chronic Oral Study of Myosin Activation to Increase Contractility in Heart Failure (COSMIC-HF): a phase 2, pharmacokinetic, randomised, placebo-controlled trial. *The Lancet*, *388*(10062), 2895–2903. [https://doi.org/10.1016/S0140-6736\(16\)32049-9](https://doi.org/10.1016/S0140-6736(16)32049-9)
- Thompson, B. R., Martindale, J., & Metzger, J. M. (2016). Sarcomere neutralization in inherited cardiomyopathy: small-molecule proof-of-concept to correct hyper-Ca²⁺-sensitive myofilaments. *American Journal of Physiology. Heart and Circulatory Physiology*, *311*(1), H36-43. <https://doi.org/10.1152/ajpheart.00981.2015>
- Tikunova, S. B., Cuesta, A., Price, M., Li, M. X., Belevych, N., Biesiadecki, B. J., ... Davis, J. P. (2019). 3-Chlorodiphenylamine activates cardiac troponin by a mechanism distinct from bepridil or TFP. *Journal of General Physiology*, *151*(1),

- 9–17. <https://doi.org/10.1085/jgp.201812131>
- Tripet, B., Van Eyk, J. E., & Hodges, R. S. (1997). Mapping of a second actin-tropomyosin and a second troponin C binding site within the C terminus of troponin I, and their importance in the Ca²⁺-dependent regulation of muscle contraction. *Journal of Molecular Biology*, 271(5), 728–750. <https://doi.org/10.1006/jmbi.1997.1200>
- van der Velden, J. (2011). Diastolic myofilament dysfunction in the failing human heart. *Pflugers Archiv: European Journal of Physiology*, 462(1), 155–163. <https://doi.org/10.1007/s00424-011-0960-3>
- van der Velden, J., Narolska, N. A., Lamberts, R. R., Boontje, N. M., Borbély, A., Zaremba, R., ... Stienen, G. J. M. (2006). Functional effects of protein kinase C-mediated myofilament phosphorylation in human myocardium. *Cardiovascular Research*, 69(4), 876–887. <https://doi.org/10.1016/j.cardiores.2005.11.021>
- van Eerd, J.-P., & Takahashi, K. (1975). The amino acid sequence of bovine cardiac troponin-C. Comparison with rabbit skeletal troponin-C. *Biochemical and Biophysical Research Communications*, 64(1), 122–127. [https://doi.org/10.1016/0006-291X\(75\)90227-2](https://doi.org/10.1016/0006-291X(75)90227-2)
- van Weerd, J. H., & Christoffels, V. M. (2016). The formation and function of the cardiac conduction system. *Development*, 143(2), 197–210. <https://doi.org/10.1242/dev.124883>
- Vassilyev, D. G., Takeda, S., Wakatsuki, S., Maeda, K., & Maeda, Y. (1998). Crystal structure of troponin C in complex with troponin I fragment at 2.3-Å resolution. *Proceedings of the National Academy of Sciences*, 95(9), 4847–4852. <https://doi.org/10.1073/pnas.95.9.4847>
- Vinogradova, M. V, Stone, D. B., Malanina, G. G., Karatzaferi, C., Cooke, R., Mendelson, R. A., & Fletterick, R. J. (2005). Ca²⁺-regulated structural changes in troponin. *Proceedings of the National Academy of Sciences of the United States of America*, 102(14), 5038–5043. <https://doi.org/10.1073/pnas.0408882102>
- Walter, M., Liebens, I., Goethals, H., Renard, M., Dresse, A., & Bernard, R. (1988). Pimobendane (UD-CG 115 BS) in the treatment of severe congestive heart failure. An acute haemodynamic cross-over and double-blind study with two different

- doses. *British Journal of Clinical Pharmacology*, 25(3), 323–329.
<https://doi.org/10.1111/j.1365-2125.1988.tb03310.x>
- Wang, D., Robertson, I. M., Li, M. X., McCully, M. E., Crane, M. L., Luo, Z., ... Regnier, M. (2012). Structural and Functional Consequences of the Cardiac Troponin C L48Q Ca²⁺-Sensitizing Mutation. *Biochemistry*, 51(22), 4473–4487.
<https://doi.org/10.1021/bi3003007>
- Wang, X., Li, M. X., & Sykes, B. D. (2002). Structure of the regulatory N-domain of human cardiac troponin C in complex with human cardiac troponin I147-163 and bepridil. *The Journal of Biological Chemistry*, 277(34), 31124–31133.
<https://doi.org/10.1074/jbc.M203896200>
- Wang, X., Mercier, P., Letourneau, P.-J., & Sykes, B. D. (2005). Effects of Phe-to-Trp mutation and fluorotryptophan incorporation on the solution structure of cardiac troponin C, and analysis of its suitability as a potential probe for in situ NMR studies. *Protein Science : A Publication of the Protein Society*, 14(9), 2447–2460.
<https://doi.org/10.1110/ps.051595805>
- Wang, Y., Pinto, J. R., Solis, R. S., Dweck, D., Liang, J., Diaz-Perez, Z., ... Potter, J. D. (2012). Generation and functional characterization of knock-in mice harboring the cardiac troponin I-R21C mutation associated with hypertrophic cardiomyopathy. *The Journal of Biological Chemistry*, 287(3), 2156–2167.
<https://doi.org/10.1074/jbc.M111.294306>
- Ward, D. G., Brewer, S. M., Calvert, M. J., Gallon, C. E., Gao, Y., & Trayer, I. P. (2004). Characterization of the interaction between the N-terminal extension of human cardiac troponin I and troponin C. *Biochemistry*, 43(13), 4020–4027.
<https://doi.org/10.1021/bi036128l>
- Ward, D. G., Brewer, S. M., Gallon, C. E., Gao, Y., Levine, B. A., & Trayer, I. P. (2004). NMR and mutagenesis studies on the phosphorylation region of human cardiac troponin I. *Biochemistry*, 43(19), 5772–5781.
<https://doi.org/10.1021/bi036310m>
- Ward, D. G., Cornes, M. P., & Trayer, I. P. (2002). Structural consequences of cardiac troponin I phosphorylation. *The Journal of Biological Chemistry*, 277(44), 41795–41801. <https://doi.org/10.1074/jbc.M206744200>

- Wattanapernpool, J., Guo, X., & Solaro, R. J. (1995). The unique amino-terminal peptide of cardiac troponin I regulates myofibrillar activity only when it is phosphorylated. *Journal of Molecular and Cellular Cardiology*, 27(7), 1383–1391. <https://doi.org/10.1006/jmcc.1995.0131>
- Waudby, C. A., Ramos, A., Cabrita, L. D., & Christodoulou, J. (2016). Two-Dimensional NMR Lineshape Analysis. *Scientific Reports*, 6(1), 24826. <https://doi.org/10.1038/srep24826>
- Wexler, R., Elton, T., Pleister, A., & Feldman, D. (2009). Cardiomyopathy: An overview. *American Family Physician*, 79(9), 778–784. <https://doi.org/10.1016/j.nurpra.2007.01.015>
- WHO. (2017). *World Health Statistics 2017: Monitoring health for the SDGs*.
- Wijnker, P. J. M., Sequeira, V., Foster, D. B., Li, Y., Dos Remedios, C. G., Murphy, A. M., ... van der Velden, J. (2014). Length-dependent activation is modulated by cardiac troponin I bisphosphorylation at Ser23 and Ser24 but not by Thr143 phosphorylation. *American Journal of Physiology. Heart and Circulatory Physiology*, 306(8), H1171-81. <https://doi.org/10.1152/ajpheart.00580.2013>
- Wijnker, P. J. M., Sequeira, V., Witjas-Paalberends, E. R., Foster, D. B., dos Remedios, C. G., Murphy, A. M., ... van der Velden, J. (2014). Phosphorylation of protein kinase C sites Ser42/44 decreases Ca²⁺-sensitivity and blunts enhanced length-dependent activation in response to protein kinase A in human cardiomyocytes. *Archives of Biochemistry and Biophysics*, 554, 11–21. <https://doi.org/10.1016/j.abb.2014.04.017>
- Williamson, M. P. (2013). Using chemical shift perturbation to characterise ligand binding. *Progress in Nuclear Magnetic Resonance Spectroscopy*, 73, 1–16. <https://doi.org/10.1016/j.pnmrs.2013.02.001>
- Willott, R. H., Gomes, A. V., Chang, A. N., Parvatiyar, M. S., Pinto, J. R., & Potter, J. D. (2010). Mutations in Troponin that cause HCM, DCM AND RCM: What can we learn about thin filament function? *Journal of Molecular and Cellular Cardiology*, 48(5), 882–892. <https://doi.org/10.1016/j.yjmcc.2009.10.031>
- Wishart, D. S., Sykes, B. D., & Richards, F. M. (1991). Relationship between nuclear magnetic resonance chemical shift and protein secondary structure. *Journal of*

Molecular Biology, 222(2), 311–333. [https://doi.org/10.1016/0022-2836\(91\)90214-Q](https://doi.org/10.1016/0022-2836(91)90214-Q)

World Health Organization. (2014). Global Status Report On Noncommunicable Diseases 2014.

Yamada, Y., Namba, K., & Fujii, T. (2020). Cardiac muscle thin filament structures reveal calcium regulatory mechanism. *Nature Communications*, 11(1), 153. <https://doi.org/10.1038/s41467-019-14008-1>

Yuan, T., Ouyang, H., & Vogel, H. J. (1999). Surface Exposure of the Methionine Side Chains of Calmodulin. *Journal of Biological Chemistry*, 274(13), 8411–8420. <https://doi.org/10.1074/jbc.274.13.8411>

Zhang, J., Guy, M. J., Norman, H. S., Chen, Y.-C., Xu, Q., Dong, X., ... Ge, Y. (2011). Top-down quantitative proteomics identified phosphorylation of cardiac troponin I as a candidate biomarker for chronic heart failure. *Journal of Proteome Research*, 10(9), 4054–4065. <https://doi.org/10.1021/pr200258m>